University of Alberta

Friction Stir Processing (FSP) of Thermal-sprayed Tungsten Carbide-Nickel (WC-Ni) MMC Coating

By

Vinayak Vasudeo Narulkar

A thesis submitted to the Faculty of Graduate Studies and Research

in partial fulfillment of the requirements for the degree of

Master of Science

Department of Mechanical Engineering

Fall 2013

Edmonton, Alberta

Abstract

Tungsten carbide-Nickel (WC-Ni) metal matrix coating with fixed powder composition was deposited using low pressure cold gas dynamic spraying (LPCGDS) and High velocity oxy-fuel (HVOF) spraying. These coatings were subsequently treated with friction stir processing (FSP) as post-deposition heat treatment. The non-FSP and FSP-treated cold-sprayed and HVOF-sprayed WC-Ni MMC coatings were wear test using the standard ASTM G65 dry abrasion test. The aim of this thesis was to investigate the effect of FSP treatment on improvement in wear performance of WC-Ni MMC coating. The results displayed that FSP treatment showed homogeneity and uniformity in microstructure which ensued to improved wear resistance, hardness and toughness of the coating. Scanning electron microscope (SEM) analysis was conducted on the wear-tested samples showed change in wear mechanism from delaminated sheet wear to indentation and scratching due to improved coating toughness.

Acknowledgement

Through this medium, I wish to thank everyone who played active role in accomplishment of my endeavour. I wish to offer special thanks and gratitude to my Supervisor, Dr. A. McDonald, Associate Professor, who played active role in accomplishment of my project. I learnt lessons of time management and professionalism while practising my skills. His unflinching support during difficult phase of project will always remain cradle of inspiration for me in my professional life. The chapters of life which I experienced while working with him will remain indelible part of my life and will be assimilated in my personality.

I wish to offer special thanks to Dr. A. Gerlich, Associate Professor, University of Waterloo for providing timely feedback and guidance on critical aspects related to project. Apart from playing active role in successful execution of the project, his much needed support in carrying out experimental task is equally creditable.

I wish to offer sincere thanks to Mr. Natanael Melendez, whose experimental results paved way for my project. His experimental results laid successful foundation of not only mine but also many upcoming projects in this field.

Equally commendable are efforts of Mr. George Braybrook, and Dr. Nathan Gerein for SEM and EDS results and Mr. Shiraz Merali for XRD results during times of pressure.

Also, laudable are the under graduate and graduate students of MecE 6-25 lab who provided much needed conducive environment for studying and research.

Worth mentioning names are of my colleagues and friends Shantanu Shukla, Prafful Mangal, Nirlipt Mahapatra, Uma Rani, Sahil Bangar and many people who provided mental support in difficult times, who were not only my motivational source However with whom I learnt that life is more than class rooms and degrees.

Of all the people whom I am highly indebted for my success is my family. Their relentless and untiring support remained constant source of inspiration through this phase of life. I will always be indebted for their sacrifices. The lessons of virtue, truth and hard work taught by my parents have remained basic chapters of

my life. I offer my sincere gratitude and obeisance for their efforts in shaping mine and my sister's life to date.

Last but never the least, my sincere inclination towards my faith always developed optimism in me even after several set-back in my endeavours.

Table of Contents

1. Introduction

1.1 Background

1.1.1	Abrasive wear	1
1.1.2	Different techniques to tackle wear	5
1.1.3	Wear resistant materials	10
1.1.4	Thermal spraying	11
1.1.5	High velocity oxy-fuel thermal spraying	12
1.1.6	Cold gas dynamic spraying (CGDS)	14
1.1.7	Limitations of thermal spraying	17
1.1.8	Post-deposition treatment techniques	17
1.1.9	Friction stir processing	18
1.1.10	Superplastic deformation	21
1.1.11	Dynamic recrystallization	21

1.2	Previous Studies	22
1.3	Research Objectives	25

2 Wear mechanisms and Wear theories

2.1	Abrasive wear theories	27
2.2	The delamination theory of wear	31
2.3	Mean free path between reinforcing particles and mechanical properties	45
2.4	Effect of grain size on the toughness of the composite	47

2.5 Wear theories for composites 48

3 Experimental Methods

3.1 Feedstock powder and substrates 54
3.2 Cold spray and High velocity Oxy-fuel deposition 56
3.3 Parameters for friction stir processing 58
3.4 Coating characterization 60
3.5 Dry abrasion testing 66

4. Wear Performance of As-sprayed cold-sprayed WC-Ni MMC Coatings

4.1 The difference in the WC content in the powder and coating compositions of cold-sprayed WC-Ni MMC coating 70
4.2 Correlation among mechanical properties of cold-sprayed pure nickel and WC-Ni MMC coatings 71
4.3 Toughness measurement for cold-sprayed pure nickel and different WC-Ni MMC coating 73
4.4 Wear analyses of as-sprayed cold-sprayed pure nickel and WC-Ni MMC coating 78
4.5 Wear theory to define wear rate of WC-Ni MMC coatings 103
4.6 Coating composition 112

5. Wear Performance of FSP-treated thermal-sprayed WC-Ni MMC Coatings

5.1 Finding parameters for FSP treatment 114
5.2 Wear Analyses of FSP and non-FSP treated 126

thermal-sprayed WC-Ni MMC coating
5.3 EDS and XRD results for different WC-Ni MMC coating 128
5.4 Wear result of non-FSP and FSP-treated thermal-sprayed WC-Ni coating 136
5.5 Wear mechanism 145
6. Conclusion 162
7. Future work and recommendations 164
Bibliography 166
8. Appendix
1 Wear theories calculation 185
2 Calculation of clamping force to hold the coated sample during FSP treatment 193
3 Maximum heat during FSP heat treatment 197

List of tables

Table No.	Table title	Page No.
3.1	WC-12Co content for cold-sprayed pure nickel as well as different WC-Ni MMC coating [2]	54
3.2	Cold spray deposition parameters	57
3.3	HVOF spray deposition parameters for pure nickel coating	57
3.4	HVOF spray deposition parameters for WC-Ni coating	57
3.5	Composition of Alloy HX	58
3.6	Composition of Tungsten carbide grade C1	59
3.7	Sets of parameters used for FSP parameter optimization	59
3.8	ASTM G-65 parameters	68
4.1	WC content in coating for respective mechanical blend used to fabricate cold-sprayed WC-Ni MMC coating [1].	70
4.2	Porosity content for different mechanical blend used to fabricate cold sprayed pure nickel and WC-Ni MMC coating [1].	72
4.3	Crack generation percentage in the various coatings and the respective *c/a* ratios.	77
4.4	Wear rate for different WC-Ni MMC coating using equal pressure and equal wear rate theory.	105
4.5	Wear rate for different WC-Ni MMC using modified wear rate theory	107
5.1	Comparison of mechanical properties of FSP-treated cold-sprayed WC-Ni MMC coating treated with two different tool rotational speeds	124
5.2	Comparison of mechanical properties of FSP-treated	125

	HVOF-sprayed WC-Ni MMC coating treated with two different tool rotational speeds	
5.3	Effect of FSP treatment on mechanical properties of cold-sprayed WC-Ni MMC coating	135
5.4	Effect of FSP treatment on mechanical properties of HVOF-sprayed WC-Ni MMC coating.	136
7.1	Properties of pure nickel and FSP tool	200

List of figures

Figure No.	Figure title	Page No.
1.1	Different types of wear [1]	2
1.2	Schematic of High Velocity Oxy-Fuel (HVOF) spraying process [39]	13
1.3	Schematic of low pressure cold spraying process [66]	16
1.4	Schematic of friction stir processing[77]	19
1.5	Schematic of different reactions of in-flight WC-Co powder with surrounding atmosphere while spraying [39].	24
2.1	Cross-sectional image of material showing annealed surface and work hardened sub-surface zone [108]	29
2.2	Schematic of flatting of asperities and spreading on material's surface during wear [176].	33
2.3	Flattened and spread-out asperities under action of wear [176].	34
2.4	Graph depicting maximum strain in material in sub-surface zone [167]	47
2.5	(a)Application of resultant stress on material surface resulting n generation of tensile and compressive zones in sub-surface of material [179] (b)Sub-surface crack geometry under action of movement of asperities during wear [142] (c)Sub-surface crack expansion in trailing edge of crack [179]	42
2.6	Depiction of crack propagation in sub-surface zone due to uplifting of material in tensile stress region of crack [121]	45
2.7	Representation of composite as per Equal pressure	48

	theory	
2.8	Representation of wear of composite as per Equal pressure theory	49
2.9	Representation of composite as per Equal wear theory	50
2.10	Representation of wear of the composite as per Equal wear theory	50
3.1	Schematic of dry abrasion wear test [6]	67
4.1	Graph of (a) wear rate verses mean free path between WC-12Co particles and (b) wear rate verses hardness of WC-Ni MMC coating [71].	71
4.2	SEM image of cold-sprayed (a) pure nickel coating, (b) WC-Ni MMC containing 7 wt.% WC, (c) WC-Ni MMC containing 19 wt.% WC, (d) WC-Ni MMC containing 56 wt.% WC, and (e) WC-Ni MMC containing 66 wt.% WC, with indents generated by 1000 gf load.	76
4.3	SE-SEM image of surface of wear-tested cold-sprayed pure nickel coating showing presence of ploughing and scratching on the surface.	79
4.4	Cross-sectional BSE- SEM images of wear-tested cold-sprayed pure nickel coating at low magnification,	81
4.5	Cross-sectional BSE- SEM images of wear-tested cold-sprayed pure nickel coating at high magnification,	82
4.6	BSE-SEM surface image of WC-Ni coating fabricated from 50 wt.% WC- 50wt.%Ni.	84
4.7	BSE-SEM cross-sectional images of WC-Ni MMC coating fabricated from powder composition of 50 wt% WC - 50 wt.% Ni at low magnification.	86
4.8	BSE-SEM cross-sectional images of WC-Ni MMC	87

	coating fabricated from powder composition of 50 wt% WC - 50 wt.% Ni at high magnification displaying delaminated wear sheet.	
4.9	Surface image of coating fabricated from powder composition of 75wt.% WC - 25wt.% Ni. (a) BSE-SEM image and (b) SE-SEM image.	89
4.10	BSE-SEM cross-sectional image of worn out coating fabricated from 75 wt.% WC – 25 wt.% Ni at low magnification indicating fragmented wear sheets	91
4.11	BSE-SEM cross-sectional image of worn out coating fabricated from 75 wt.% WC – 25 wt.% Ni at high magnification.	92
4.12	Surface image of wear-tested as-sprayed WC-Ni coating fabricated from the powder composition of 92 wt.% WC - 8 wt.% Ni. (a)and (b) BSE-SEM image and (c) SE-SEM image	94
4.13	Cross-sectional BSE-SEM image of coating fabricated from powder composition of 92 wt.% WC – 8 wt.% Ni (a) at low magnification and (b), (c) and (d) at high magnification.	96
4.14	SE-SEM surface image of WC-Ni MMC coating fabricated from powder composition of 96 wt.% WC - 4 wt.% Ni..	97
4.15	Cross-sectional BSE-SEM image of WC-Ni MMC coating fabricated from powder composition of 96 wt.% WC - 4 wt.% Ni (a) and (c) at low magnification and (b) at high magnification.	100
4.16	Graphical representation of wear rate plotted using different "*C*" values against experimental wear rate.	108
4.17	Graphical representation of wear rate plotted using two close "*C*" values against experimental wear rate.	109

4.18	Representation of the experimental wear rate values and wear rate values of pure nickel and WC-Ni MMC coating using all the wear theories.	110
4.19	Representation of the experimental wear rate values and wear rate values of different WC-based MMC coating using the equal wear rate and modified wear theories.	110
5.1	Cross-sectional BSE-SEM image of FSP-treated cold-sprayed WC-Ni MMC coating showing (a) microstructure and (b) different zones along coating thickness.	115
5.2	FSP-treated cold-sprayed WC-Ni MMC coating (a) at low magnification and (b) at high magnification.	117
5.3	Cross-sectional BSE-SEM image of FSP-treated HVOF-sprayed WC-Ni MMC coating with tool rotational speed of 1400 RPM.	118
5.4	Cross-sectional BSE-SEM image of FSP-treated HVOF-sprayed WC-Ni MMC coating showing un-processed portion of MMC coating	119
5.5	Cross-sectional BSE-SEM image of friction stir processed zone of FSP-treated HVOF-sprayed WC-Ni MMC coating showing uniform and homogenous microstructure.	119
5.6	Cross-sectional BSE-SEM image of as-sprayed cold-sprayed WC-Ni MMC coating showing presence of numerous pores in microstructure (dark spots in nickel binder are pores).	122
5.7	Cross-sectional BSE-SEM image of FSP-treated cold-sprayed WC-Ni MMC coating treated with tool rotational speed of 900 RPM.	123
5.8	Cross-sectional SEM image of FSP-treated cold-	124

	sprayed WC-Ni MMC coating treated with tool rotational speed of 1400 RPM.	
5.9	FSP-treated WC-Ni MMC coating (a) cold-sprayed WC-Ni MMC and (b) HVOF-sprayed WC-Ni MMC coating.	126
5.10	Wear-tested FSP-treated cold-sprayed WC-Ni MMC coating.	126
5.11	Wear-tested FSP-treated HVOF-sprayed WC-Ni MMC coating.	127
5.12	Back side of FSP-treated cold-sprayed WC-Ni MMC coating indicating burnt zone.	128
5.13	Back side of FSP-treated HVOF-sprayed WC-Ni MMC coating indicating burnt zone.	128
5.14	EDS result of cold-sprayed WC-Ni MMC coating.	129
5.15	XRD result of as-sprayed cold-sprayed WC-Ni MMC coating [5].	130
5.16	(a) Cross-section of the FSP-treated cold-sprayed WC-Ni MMC coating for EDS and (b) EDS result of the region under consideration.	132
5.17	XRD result of FSP-treated cold-sprayed WC-Ni MMC coating.	133
5.18	XRD result of as-sprayed HVOF-sprayed WC-Ni MMC coating.	134
5.19	XRD result of FSP-treated HVOF-sprayed WC-Ni MMC coating.	134
5.20	Cross-sectional BSE-SEM images of wear tested FSP-treated cold-sprayed WC-Ni MMC coating (a) at low magnification and (b), (c), (d) and (e) at high magnification.	137
5.21	Cross-sectional BSE-SEM images of wear tested FSP-treated cold-sprayed WC-Ni MMC coating at	138

high magnification.
5.22 Cross-sectional BSE-SEM images of wear-tested HVOF-sprayed WC-Ni MMC coating at low magnification. 139
5.23 Cross-sectional BSE-SEM images of wear-tested HVOF-sprayed WC-Ni MMC coating at high magnification. 140
5.24 Cross-sectional BSE-SEM images of wear-tested FSP-HVOF-sprayed WC-Ni MMC coating showing cracked and delaminated wear sheet. 142
5.25 Cross-sectional BSE-SEM images of wear-tested FSP-HVOF-sprayed WC-Ni MMC coating showing shallow indents of abrasives during wear. 143
5.26 Cross-sectional BSE-SEM images of wear-tested FSP-HVOF-sprayed WC-Ni MMC coating showing deep indents of abrasives during wear. 144
5.27 Cross-sectional BSE-SEM images of wear-tested FSP-HVOF-sprayed WC-Ni MMC coating showing cracked wear sheet. 144
5.28 Cross-sectional BSE-SEM image of cold-sprayed WC-Ni MMC coating fabricated from powder composition of 96 wt.% WC - 4 wt.% Ni (a) at low magnification and (b) at high magnification. 146
5.29 Schematic representation of cold-sprayed WC-Ni MMC coating fabricated from powder composition of 96 wt.% WC – 4 wt.% Ni. 147
5.30 Schematic representation of wear-tested cold-sprayed WC-Ni MMC coating fabricated from powder composition of 96 wt.% WC - 4wt.% Ni. 148
5.31 Cross-sectional BSE-SEM image of as-sprayed cold-sprayed WC-Ni MMC coating showing presence of 149

numerous pre-existing voids in the microstructure.

5.32 Schematic representation of (a) FSP-treated cold-sprayed WC-Ni MMC coating, (b) wear testing, (c) and (d) wear-tested FSP-treated cold-sprayed WC-Ni MMC coating. 151

5.33 Cross-sectional SEM image of wear-tested FSP-treated cold-sprayed WC-Ni MMC coating showing presence of equiaxed and uniform distribution of individual carbides in the composite (a) with flow lines visible, (b) friction stir processed zone visible. 152

5.34 Cross-sectional BSE-SEM image of FSP-treated cold-sprayed WC-Ni MMC coating showing reduced content of pre-existing voids in the microstructure. 153

5.35 Schematic of HVOF-sprayed WC-Ni MMC coating showing islands of nickel scattered in WC-Ni MMC microstructure. 155

5.36 Cross-sectional BSE-SEM image of HVOF-sprayed WC-Ni MMC coating showing presence of numerous pre-existing voids in the microstructure. 155

5.37 Cross-sectional BSE-SEM image of wear-tested HVOF-sprayed WC-Ni MMC coating showing presence of elongated voids and cracks oriented in sliding direction. 156

5.38 Cross-sectional BSE-SEM image of wear-tested HVOF-sprayed WC-Ni MMC coating showing presence of elongated voids and cracks oriented in sliding direction. 156

5.39 Schematic of FSP-treated HVOF-sprayed WC-Ni MMC coating showing islands of nickel scattered in WC-Ni MMC microstructure. 157

5.40 Cross-sectional BSE-SEM image of wear tested FSP- 158

	HVOF-sprayed WC-Ni MMC coating showing presence of (a) no sub-surface cracking and (b) limited sub-surface cracking, in the composite.	
5.41	Cross-sectional SE-SEM image of wear tested FSP-treated HVOF-sprayed WC-Ni MMC coating showing presence of indents and subs-surface cracks.	159
5.42	Cross-sectional SEM image of FSP-treated HVOF-sprayed WC-Ni MMC coating showing presence of homogenous and uniform microstructure in FSP-treated zone.	160
5.43	Cross-sectional BSE-SEM image of FSP-treated HVOF-sprayed WC-Ni MMC coating showing presence of nickel binder uniformly distributed in the microstructure.	161
7.1	Depiction of weld bead at substrate base to provide effective clamping during FSP treatment of WC-Ni MMC coating	194

Nomenclature and Abbreviations

1.1.1 List of Abbreviation

Co	Cobalt
Ni	Nickel
WC	Tungsten carbide
Al_2O_3	Alumina
SiO_2	Silica
NiCr-	Nickel-chromium based
NiO	Bunsenite
Co_3W_3C	Cobalt tungsten carbide
Co_6W_6C	Cobalt tungsten carbide
W_2C	Di-tungsten carbide
$CoWO_4$	Cobalt tungstate
Co_2W_4C	Cobalt tungsten carbide
$Co_3W_9C_4$	Cobalt tungsten carbide
WC-Ni	Tungsten carbide-nickel based MMC
WC-12 Co	Tungsten carbide- 12 wt. % cobalt
WC-10 Co	Tungsten carbide- 10 wt. % cobalt
RWAT	Rubber wheel abrasive test
ASTM	American society for testing of materials
HVOF	High velocity oxy-fuel spraying
LPCGDS	Low pressure cold gas dynamic spraying
HPCGDS	Low pressure cold gas dynamic spraying
CS	Cold spraying
SEM	Scanning electron microscopy
SE-SEM	Secondary electron scanning electron microscopy
BSE-SEM	Back scattered electron scanning electron microscopy
FSP	Friction stir processing

HV	Hardness value
MMC	Metal matrix composite
EDS	Energy dispersive X-ray spectroscopy
XRD	X-ray diffraction

1.1.2 List of symbols

H_a	Hardness of abrasive (HV)
H_s	Hardness of the material (HV)
C	Specific heat of the material (J/kg-ºC)
ΔT	Difference in melting point and temperature of the material during wear (K)
V_{WC}	Volume of tungsten carbide in the WC-Co MMC
N_{WC}	Number of tungsten carbide particles intersected by line of interest
W_c	Wear rate of composite (mm^3/N-m)
W_m	Wear rate of matrix (mm^3/N-m)
W_r	Wear rate of reinforcement (mm^3/N-m)
V_m	Volume of matrix
V_r	Volume of reinforcement
C	Contribution coefficient
W	Wear rate of the material (mm^3/N-m)
Δm	Coating mass difference before and after the wear test (g)
P	Normal load applied on the coating during the wear test (N)
S	Total sliding distance during the wear test (m)
V	Volume of material removed (mm^3)
E	Young's Modulus of material (GPa)
l	Sliding distance (m)
K_{IC}	Fracture toughness (MPa-$m^{1/2}$)

H	Material Hardness (kg/mm^2)
l_o	Length of the reinforcement (μm)
r_o	Radius of the reinforcement (μm)
F_t	Tangential force (N)
L	Weld length (m)
a	Weld bead width (m)
N	Normal force or vertical thrust force on tool (N)
Q*	Non-dimensional heat input
σ_G	Yield stress of nickel at 0.8 times of solidus temperature (T_s) (MPa)
A_W	Cross-sectional area of the FSP tool (m^2)
f	Ratio of heat generated at work piece to heat generated in tool
K	Thermal conductivity of the work piece (W/m-ºC)
v	Linear velocity of the tool on work piece (m/s)
ρ_{WC-Co}	Density of WC-Co (kg/m^3)
$\rho_{(WC-Ni)CS}$	Density of cold-sprayed WC-Ni MMC coating (kg/m^3)
$\rho_{(WC-Ni)HVOF}$	Density of HVOF-sprayed WC-Ni MMC coating (kg/m^3)
C_{WC-Co}	Specific heat of WC-Co (J/kg-ºC)
$C_{(WC-Ni)CS}$	Specific heat of CS-sprayed WC-Ni MMC coating (J/kg-ºC)
$C_{(WC-Ni)HVOF}$	Specific heat of HVOF-sprayed WC-Ni MMC coating (J/kg-ºC)
K_{WC-Co}	Thermal conductivity of WC-Co (W/m-ºC)
$K_{(WC-Ni)CS}$	Thermal conductivity CS-sprayed WC-Ni MMC coating (W/m-ºC)
$K_{(WC-Ni)HVOF}$	Thermal conductivity of HVOF-sprayed WC-Ni MMC coating (W/m-ºC)

T*	Non-dimensional peak temperature
T_P	Peak temperature (K)
T_A	Ambient temperature (K)
Ts	Solidus temperature (K)

1.1.3 List of Greek symbols

ρ	Density of the composite coating (g/mm^3)
ω	Rotational speed of tool (RPM)
ζ	Shear stress acting on each side weld bead (MPa)
μ	Coefficient of friction between tool and coating
λ	Mean free path between reinforcing particles (μm)

Chapter 1: Introduction

1.1 Background

1.1.1 Abrasive Wear

For bodies in surface contact and under relative motion, wear is imminent. Tribology is the field that deals with the study of interactions among bodies in surface contact and under relative motion. This interaction may either involve two or more solids or solids and fluids in motion. In fluids, usually, the wear is performed by liquids or gases entrained with small particles that impact the surface of the material and eventually contribute to its loss [1, 2]. Interaction among bodies involves friction and eventual wear, hence understanding the correlation among factors responsible for wear is essential to resolve this problem successfully. Wear is a broad term and is defined as the loss of material due to the interaction among different solids or solids and fluids. Usually, wear is a function of the surrounding environment, the contact pressure, the relative motion between two or more bodies in contact and the material properties like hardness and toughness, to name a few [1 - 5].

Wear is classified into four basic types depending on the mechanism they exhibit for material removal [1 - 4]. The types of wear are:

a) Surface fatigue,

b) Adhesive wear,

c) Abrasive wear, and

d) Tribochemical reactions

Figure 1.1 presents the schematic representation of different types of wear.

In *surface fatigue*, the continuous and repeated impacts of one material (usually harder than the other) on the other material's surface result in cracking and delamination of the material [1 - 4].

In *adhesion wear*, the two materials under the action of pressure come into surface contact. The ensuing pressure results in deformation and subsequent

fusion of two materials at the asperities. The fused zone is usually harder compared to the parent material. If the two materials are set in relative motion, cracking is generated usually in the softer parent material which results in detachment of the fused zone or its clinging to the hard parent material. Thus, wear will occur in the form of loss of materials due to cracking in the fused zone [1 - 4].

In *abrasive wear*, the wear happens due to the difference in hardness between two materials in relative motion. The material's surface shows asperities projecting from it. The asperities of the harder material will result in wearing away of the softer material. In two body abrasion, the worn out debris exits after abrasion while in three body abrasion, the worn out debris may remain in spaces between two abrading surfaces which eventually contributes to the wear of the softer parent material along with wear done by the hard parent material [1 - 3].

In *tribochemical wear*, the wear happens due to the reaction of either or both materials' surfaces. The reacted surface is hard and often brittle, which during wear, may chip-off under the action of stress during interaction [1 - 4].

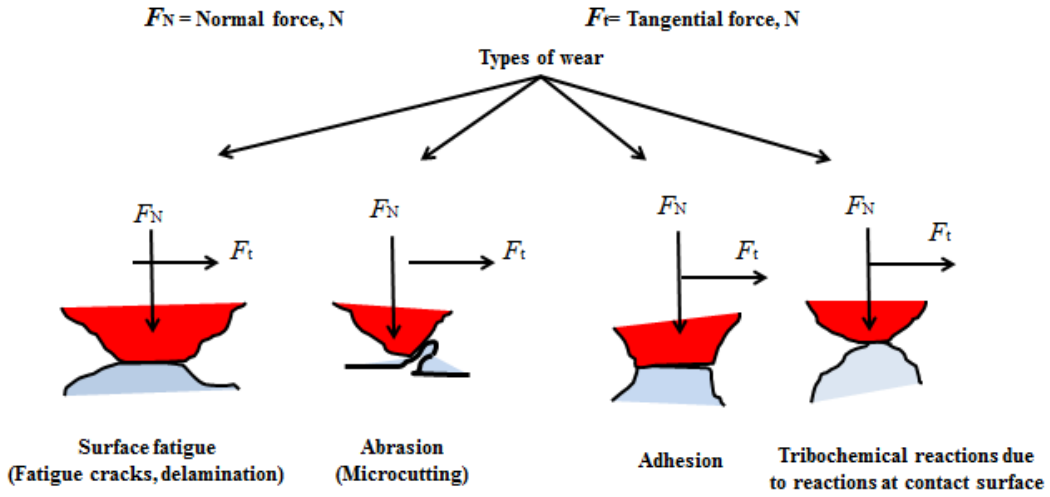

Figure 1.1. Different types of wear [1].

Wear of material seldom acts alone as per the types mentioned above. Usually, it is combined effect of different types mentioned above acting in tandem to result in cumulative destruction of any material. Some prominent examples are: failure of pump impellers in hydro power plants which is combination of abrasive and tribochemical wear; failure of ball and needle bearing between shaft and rotor, which is combination of adhesive, surface fatigue and abrasive wear; failure of drill tool which is combination of abrasive and tribochemical wear (here it appears as erosion-corrosion of drill tool material); cracking of rails of railroad which is combined action of surface fatigue, abrasive and tribochemical wear and so on[1 – 5].

Of all the types of wear mentioned above, abrasive wear is a common type of wear found in materials under surface contact. The wear mechanism defining destructive action of abrasive wear is complex combination of many sub-mechanisms. In abrasive wear, the cutting action of sharp grits or asperities protruding from the material's surface also accompanies other wear mechanisms like micro-cutting, ploughing or digging in the material, micro-fracture (in the form of slicing or cracking of hard phases in the material), pullout of hard reinforcing particles or the phases of the materials, accelerated fatigue (in the form of cracking or micro-pit formation on the surface), which can act as a crack initiation site too. The micro-pits generated due to the pullout or removal of particular phases act as solution reservoir, which will eventually contribute to galvanic, crevice or pitting corrosion. The micro-pits or cavities on the surface are also generated due to the cavitation corrosion, especially seen in pipes, impellers, pumps, and turbine parts like turbine blades and draft tubes. [3].

Abrasive wear is classified into two sub-types depending on the wear mechanism they exhibit [1 - 4]:

a) Two body abrasive wear

In two body abrasive wear, the asperities from hard parent material wear out soft parent material. The worn out debris leave the spaces between two materials. Common examples of this wear are found in grinding, machining, drilling.

b) Three body abrasive wear

In this type of wear, the asperities of the hard parent material as well as the debris generated during wear contribute to the wearing of soft parent material. Here, third body is debris However in few cases, it can be any other material like abrasives, sand, which will entrain the space between two parent materials and be responsible for wear. The debris generated during wear may or may not have high hardness, However usually it contributes to the wear of softer parent material under the action of load. Common examples of this type of wear are found in polishing operation, bearings, [4, 5].

Compared to two body abrasive wear, three body abrasive wear is common in many industrial applications. In most industrial applications, the third body is abrasives like sand, grit, which accelerate the wearing of softer parent material [1 - 3].

To measure abrasive wear performance of materials, rubber wheel abrasion test (RWAT) or ASTM G-65 abrasive wear test [6] is commonly used. This is a common test to rank material as per their abrasive resistance for numerous applications like mining and excavation equipment, construction equipment. In this test, the material to be wear tested is loaded against the rotating rubber wheel while sand as abrasives fall from the hopper in the spaces between wheel and the specimen under test. The working principle of this test is discussed in experimental section of thesis. The application of constant force ensures continuous contact between specimen material and the wheel during test. Numerous attempts to modify this test set-up has resulted in widespread acceptance of test results and are deciding factor for validation of any material for test field conditions [7 - 11].

1.1.2 Different techniques to tackle abrasive wear

The successful way to tackle wear is to understand the root cause of it. Wear is in fact material property dependent; hence effective solution for this lies in

determining the factors responsible for it. The factors responsible for wear of any material are:

a) Abrasive size and hardness,
b) Abrasive shape,
c) Material hardness,
d) Material fracture toughness,
e) Material's resilience,
f) Surface roughness of the material,
g) Sliding speed and sliding force.

Abrasive size and hardness is known to have pronounced effect on the wear of the material. It is found that higher hardness of the abrasives show high wear rate of the material. The reason for this is weak and friable abrasives on striking material's surface cannot maintain their integrity. They fracture easily to small particles on impact and lose their effectiveness. The shattered pieces do not have required weight to transfer the destructive force needed for wear. The hard abrasives have ability to maintain their shape and contribute to the wear. Hence, it is found that wear rate is a strong function of the abrasive hardness [12]. Also, the shape of the abrasive is known to play crucial role in wear of the material. The angular and sharp edge abrasives are able to provide more concentrated force needed for the wear. Thus, bigger abrasive with high hardness and angular shape are known to cause more damage to the material during wear [12, 13].

Also, abrasive size is important factor in wear. For particle size less than 100 μm, the wear efficiency is reduced drastically [13]. Abrasive velocity is also important factor in wear. Higher abrasive velocity results in more kinetic energy to be transferred to the impacting material which results in higher wear rate [13]. The wear rate is higher at acute angle of attack and decreases as this impingement attack moves close to 90^{o} [13 - 16].

The hardness of the material is important factor when deciding the intensity of the damage generated due to abrasive. The wear intensity is determined using ratio of hardness of abrasive (H_a) to hardness of the material (H_s).

If $H_a/ H_s > 1.2$, plastic indents are produced on the surface by abrasives. This means that abrasives are successful to create damage to the surface of material in form of indents. These indents result in material removal and contribute to wear.

If $H_a/ H_s < 1.2$, no plastic indents are produced in the material.

Thus, it means that more the hardness of the parent material in comparison with the hardness of the abrasive, less will be its wear rate [17].

Fracture toughness is another property of material which affects its wear rate. Usually, crack propagation happens due to action of tensile stress on the material ahead of crack. Hence, material weaker in tensile strength will easily fracture resulting in easy crack propagation in the material. Fracture toughness indicates the resistance offered by the material to crack propagation, and crack propagation is easier if weak phases (phases with low tensile strength) or cavities are present ahead of crack front. Thus, fracture toughness of the material will be improved by increasing phases, which has high tensile strength [22 - 24].

Material's resilience indicates the resistance offered by the material to plastic deformation. Resilience depends on yield strength of the material. Lower yield strength, lower is the resilience. Material with low resilience will easily deform and result in plastic deformation. Hence, higher resilience indicates material can absorb high energy before deforming plastically. Thus, presence of highly resilient phases or material with higher yield strength improves overall resistance to plastic deformation [22 - 25].

Wear is surface phenomenon. Hence, rough surface will have lot of surface undulation, which will be easily vulnerable to the attack of the abrasives. Thus, smooth surface will offer less debris during wear due to fewer asperities on it [22 - 25].

Sliding speed and sliding force both influence wear phenomena. Hence, higher the sliding speed and force more will be the wear. Also, higher sliding force will result in more sub-surface effect in form of increased cracking and delamination of the material. Thus, lower sliding speed and force, lower will be the wear of any material [22].

Some of the prominent ways to inhibit or restrict the destructive effects of the wear are [2, 17]:

a) Change in design,

b) Material replacement,

c) Surface engineering, which includes surface modification techniques,

A change in design or material replacement is not feasible in many industrial installations. For example, if the wear in the form of cavitation is happening to pipe bends or in pump impellers, it cannot be tackled by replacement of pipe bends.

Wear of any material is material property dependent; so, better material should be used as per the service conditions or the surrounding environment. Hence, use of materials designed to withstand wear conditions is the easiest and the most effective way to deal with wear. However material replacement is also the least popular option, considering the high cost and limited availability in market as the biggest constraint acting in its acceptance. For example, replacing low carbon steel with special grade stainless steel for marine application is not only the most costly option However raises questions on its availability in the market during times of replacement. Also, cost of products is vulnerable to fluctuating market prices, which makes them unreliable option. Other factors like weight, processing as per the application requirements, also rule out the applicability of this method to tackle wear [17].

The last technique of surface engineering is not only easy However has proved to be an effective technique to tackle the ensuing wear problem. Surface properties and features of any material have a major role to play in the wear of any material. The ostensibly smooth looking surface of any material involves lot of complex features which play active role in wear. The surface of any material under microscope shows lot of asperities and valleys protruding from the surface. These surface undulations contribute to the wear of the material under the action of pressure and relative motion between different materials in surface contact. These surface undulations are defined as surface roughness and play collective role in wear along with material properties like hardness, toughness, to name a few. The

destructive effect of wear always start from the surface of any material, so to improve wear resistance, the material properties like hardness, toughness and wear resistance, of the surface has to be improved. Hence, if surface undulations are corrected and surface properties improved by using suitable surface modification techniques, then wear resistance is also improved. Surface modification techniques include surface deposition of wear resistant materials and surface processing techniques [21 - 23]. The improvement of wear resistance of any material's surface is achieved either by deposition of wear resistant material or by induction of elements into the surface making it hard and tough, and ultimately resulting in improved wear resistance of the surface. Deposition of wear resistant materials is achieved by using conventional deposition techniques like thermal spraying, vapor deposition techniques, electrodepositon, and so on. The induction of hard elements like carbon or nitrogen is achieved by using surface treatment techniques like carburizing, nitriding, carbonitriding, and parkerizing The deposition techniques offer lot of advantages compared to induction techniques, some of them are [18 – 21]:

- Easy application with little or negligible modification of the core material properties,
- Easy replacement with wide choice of materials to be deposited and
- Less dependency on factors like surrounding environment, composition and crystal structure of the base material, chemical affinity between base material and diffusing constituents, and so on
- Also, the material deposited as coating introduces negligible change in fluid dynamic properties since small coating thickness does not affect the flow of fluids over material even after surface treatment.

Thus, among all the techniques, the most easy, effective and popular technique is surface deposition of wear resistant materials.

There are different surface deposition techniques, some of which are mentioned below [18 - 21]:

a) Electrodeposition technique,

b) Chemical and physical vapor deposition,

c) Weld overlays and laser cladding,

d) Surface hardening techniques and,

e) Thermal spraying

The electrodeposition techniques include electroplating and electroless plating; and vapor deposition techniques include physical and chemical vapor deposition techniques. The electrodeposition and vapor deposition techniques deposit materials with thickness in tens of micrometer. The process is not only time consuming and expensive, However also involves dependency on the chemical environment. Also, depositions of hard and wear resistant materials are difficult by these techniques [18].

The techniques like weld overlay and laser cladding although successful in terms of the coating thickness and versatility in terms of the materials to be deposited, however it involves lot of deposition problems. Some of them are generation of weld spatter, slow deposition rate and high process cost (especially for laser cladding), generation of toxic fumes, high heat and chances of electric shock (for weld overlay). The excess heat generated during deposition may result in work piece distortion and the generation of the residual stresses in the substrate. Also, diffusion of coating constituents into the substrate and metallurgical changes in the substrate due to the high heating temperature, are other unfavorable aspects of these techniques. These issues restrict their applicability and limit its acceptance rate [18 - 21].

Surface hardening techniques include carburizing and nitriding, which involves induction of hard elements like carbon, nitrogen, into surface of material which results in increase in surface hardness and toughness. It also includes techniques like flame and induction hardening, high power lamp hardening, wherein material is heated to above austenitizing temperature (for steels), held for some time for homogenization and then quickly quenched in suitable coolant. Depending on cooling rate, surface hardness improvement will be decided. This method is successful mostly for small size, simple shape, steel and its alloys only. Also, work piece distortion and heat cracks can affect substrate life span [18].

Compared to the above techniques, thermal spraying is cheap, easy to apply, portable, offers good adaptability in terms of the material(s) to be deposited, less distortion and less metallurgical changes in the substrate and can be easily automated for mass production. Hence, this technique of surface deposition is the most suitable technique for surface modification of any material [18, 20, 21].

1.1.3 Wear resistant materials

As discussed earlier, the easy and assured way to deal with wear problem is through the deposition of wear resistant materials [18]. The common wear resistant materials used are alumina (Al_2O_3), tungsten carbide (WC), silica (SiO_2) and nickel-chromium based alloys (NiCr-)[25 - 36]. Among all these materials mentioned above, the material which has high hardness and wear resistance (after diamond) with satisfactory mechanical properties like corrosion resistance, ability to blend with soft binder to generate coating with required toughness, and easy to thermal spray, is tungsten carbide (WC) [25 – 36, 38, 39].

Usually, the coating materials are applied as metal matrix composites. In metal matrix composites (MMCs), the hard particles are mixed with soft binder in proper proportion [29, 30, 36, 38, 39]. Among the different types of MMC, the common type used as coating for wear and corrosion applications is particle reinforced metal matrix composite. Here, hard reinforcing particles are distributed in soft binder. The hard reinforcing particles withstand the compressive stress and provide compactness needed to withstand fluctuating stresses in cyclic loading. The presence of soft and ductile binder results in improved toughness, wear and corrosion resistance along with improved binding tendency of the coating with the substrate. The binder helps in distribution of the compressive stress by plastically deforming under stress. Also, its effective wetting of hard reinforcement provides necessary cushioning effect against the impact of abrasives and protection against aqueous corrosion [29 - 32, 36, 37]. Usually, fine distribution of reinforcing particles in binder results in better mechanical properties like hardness, toughness, in composite [33, 35, 37, 39].

Many metal matrix composite (MMC) coatings with hard reinforcing particles are successfully used in rigorous wear and corrosion conditions [25 - 36]. The common reinforcing material used in MMCs for wear applications is tungsten carbide (WC) [25 - 27, 32, 34 - 36]. The tungsten carbide alone in powder or wire form are difficult to deposit using normally available high temperature thermal spraying with less microstructural changes. This is because of its high reactivity with surrounding atmosphere under high spraying temperature conditions and extremely low plastic deformation ability even at high temperature [40, 41, 43]. The tungsten carbide in powder form is usually sintered with relatively soft and ductile binder element like cobalt or nickel. Cobalt is more popular element used in sintering since it dissolves some amount of carbide during high temperature sintering, resulting in a complex bonded structure which improves its adhesiveness with surrounding carbide grains. The improvement in corrosion resistance is provided by inclusion of nickel. Also, carbide as binder offers good combination of hardness and toughness to whole mixture [30, 32 - 36].

1.1.4 Thermal spraying

Thermal spraying is a material deposition technique wherein feed stock material in wire, rod or powder form are heated or partially melted by the energy source during its transit through the spraying system. The heat for spraying is either electrical or through combustion flame. The heated or partially melted material is then expelled through system at high velocity by the process gases, to deposit on the material's surface as a coating [20, 21]. Thermal spraying is considered to offer lot of advantages over other deposition techniques [21]:

- Virtually, any material can be heated or partially melted to deposit as coating,
- Deposition of material with relatively insignificant effect on the substrate is possible,
- Material depositon can be controlled, resulting in coating thickness varying from 20 micrometer to several hundred micrometers depending on

the parameters like material(s) to be deposited, heat supplied to the feedstock, material feed rate and torch travel velocity over the substrate.

Some of the prominent and popular thermal spraying variants are [21]:

a) Flame spraying,

b) Plasma spraying,

c) Detonation spraying,

d) Wire arc spraying,

e) High velocity oxy-fuel spraying,

f) Cold spraying.

In all the above spraying techniques except wire arc spraying, powder as feedstock material is used. Plasma spraying can also be operated using coating material in powder as well as wire form.

The thermal spraying techniques like flame, plasma, detonation and high velocity oxy-fuel spraying techniques use high temperature (usually > 2700°C) sources to heat and partially melt the feedstock material to deposit as a coating. In the wire arc spraying, there is an electric arc struck between anode and cathode resulting in melting of the feedstock wire, which is then propelled by high velocity gases to deposit as a coating. The cold spraying uses relatively low temperature (less than 900°C) and high pressure (0.5 - 5.0 MPa) to expel feedstock at high velocity (300 to 600 m/s) to coat on the substrate [21].

1.1.5 High velocity Oxy-fuel (HVOF) spraying

Compared to high temperature thermal spraying variants like plasma, flame and detonation spraying, high velocity oxy-fuel spraying is successful and popular due to the properties of the coatings that it produces. The high spraying temperature in flame and plasma spraying, results in melting and fusion of the powder particles which increases its chemical reactivity with the surrounding atmospheric gases and substrate along with other phases in the powder. The high spraying temperature introduces porosity and results in distortion of the substrate and generation of the residual stresses [21].

In order to control or reduce the disastrous effects mentioned above during spraying, high velocity oxy-fuel spraying is sometimes used. In high velocity oxy-fuel spraying, the mixture of gaseous or liquid fuels like kerosene, propane, or other ignitable fluid fuel, enters the combustion chamber along with oxygen, which is ignited to undergo combustion (Fig. 1.2). The heat of combustion results in high temperature during spraying, which heats and propels incoming powder particles through a converging-diverging (de-Laval) nozzle at high velocity (usually ≥1000 m/s) to deposit as a coating on the surface. The high spraying velocity results in plastic deformation of the softened and partially melted powder particles, resulting in a tight bonding of different phases, which provides good cohesive toughness in the coating and good adhesion of the coating to the substrate. Various composite coating fabricated using this spraying technique showed good mechanical properties in terms of hardness, wear resistance and high density [20, 21, 36, 38, 39]. Also, lower residual stresses and good retention of chemical properties of the feedstock powder can be obtained by optimizing the parameters assisted by low in-flight time during spraying [40, 41, 44].

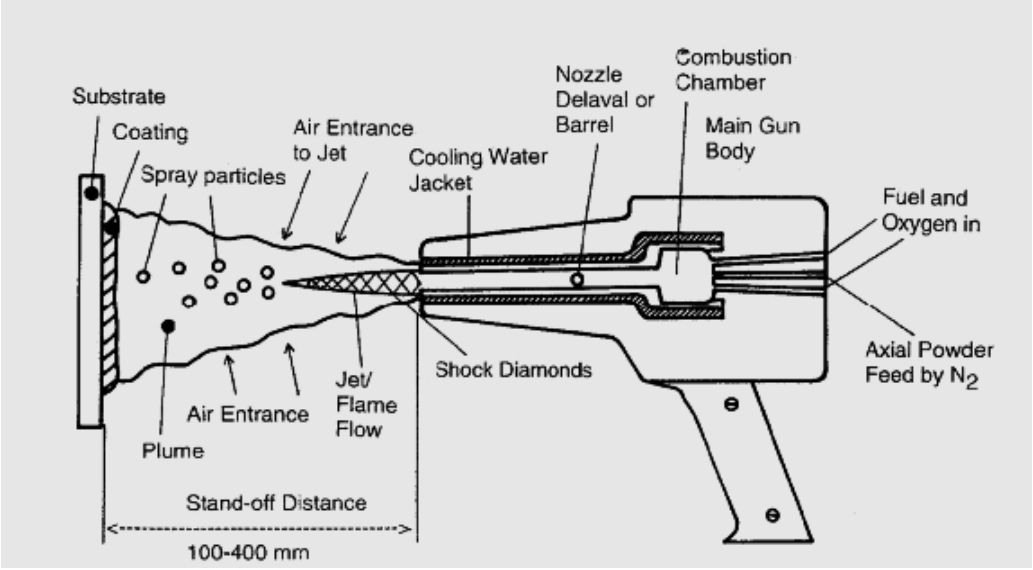

Figure 1.2. Schematic of High Velocity Oxy-Fuel (HVOF) spraying process [40]

1.1.6 Cold gas dynamic spraying (CGDS)

Although high velocity oxy-fuel spraying boasts of many advantages compared to other thermal spraying techniques, there still exist several issues which are peculiar for any high temperature thermal spraying techniques. Some of these are [40 - 53]:

- Oxidation, decarburization, formation of intermetallic compounds and amorphous phases,
- Diffusion of constituents along powder diameters resulting in chemical heterogeneity,
- Entrapment of gases and volatile constituents between different layers generating pores and voids; also, lowering of the cohesive strength of the coating due to the formation of pores,
- Reaction of the coating constituents with the substrate; distortion of substrate and generation of residual stresses in the coating and the substrate,
- The formation of complex carbides, oxides and other compounds during spraying results in increased brittleness.
- The entrapped gases may expand and result in embrittlement cracking if the coating is to be used for high temperature applications. Such brittle structure is more prone to corrosion fatigue and stress corrosion cracking which will be assisted by the pores present in the coating. The formation of different and unexpected chemical constituents may initiate and accelerate galvanic corrosion in aqueous solution.
- Substrate heating and warping are common problem for high temperature processes.

Hence, a coating deposition process needs to be used, which can produce coatings devoid of all the defects. To mitigate the issues raised due to the high spraying temperature, a relatively new variant of thermal spraying is being introduced called as cold gas dynamic spraying or cold spraying (CS) [21]. In this thermal spraying process, the MMC mixture particles are heated close to 900°C

(maximum) while non-combustible carrier gas like helium, nitrogen or even air is used during spraying [54 – 71, 82]. The velocity during spraying is usually above critical velocity value which is material dependent and is closely associated with the supply pressure [54 - 58]. In this spraying technique, the powder particles intercept high pressure hot gases (maximum temperature ≈ 900 °C) which are directed towards converging-diverging (de-Laval) nozzle. The maximum supply pressure is around 4 MPa [55, 56]. The pressure energy of the gas mixture is converted into kinetic energy to propel them at high velocity to deposit as coating on the substrate. The gases used are helium, nitrogen, air or a combination of these, which act as a carrier medium and transfer heat to powder to assist in deposition. Due to the low spraying temperature and high spraying velocity (300 – 1000 m/s), the powder particles are devoid of all the high temperature issues raised in coatings deposited by other high temperature thermal spraying techniques. This spraying technique has shown beneficial features generally absent in HVOF-sprayed coating like lower porosity, no oxidation, decarburization and degradation of in-flight powder particles [55 - 57]. The coating obtained is also dense with less cracking due to less residual tensile stresses in the coating [55, 56, 71]. All this ultimately contributes to the improved mechanical properties of MMC like hardness, improved toughness (due to lowered porosity) and brittleness, as shown by numerous authors [66 - 71]. The shortcoming of particle softening due to high temperature is overcome by deformation of powder due to the high spraying velocity which also provides good cohesive and adhesive strength to the coating [56, 57]. The porosity is essentially reduced, which improves wear resistance, and limited thermal stresses are generated in the substrate [56, 71].

The cold spraying process is classified into two variants depending on the spraying pressure [55]:

a) High pressure cold gas dynamic spraying (HPCGDS) or high pressure cold spraying and

b) Low pressure cold gas dynamic spraying (LPCGDS) or low pressure cold spraying

In high pressure cold gas dynamic spraying (HPCGDS), the spraying pressure varies in the range of 1.5 to 5 MPa and the spraying temperature is close to 900°C. The carrier gas(es) used are helium, nitrogen or a mixture of both. The use of high spraying temperature and pressure provides high deposition efficiency compared to low pressure cold spraying which makes it suitable to deposit hard reinforcing composites. However, high spraying pressure demands costly equipment and control devices which add to the overall process cost [55, 67, 71].

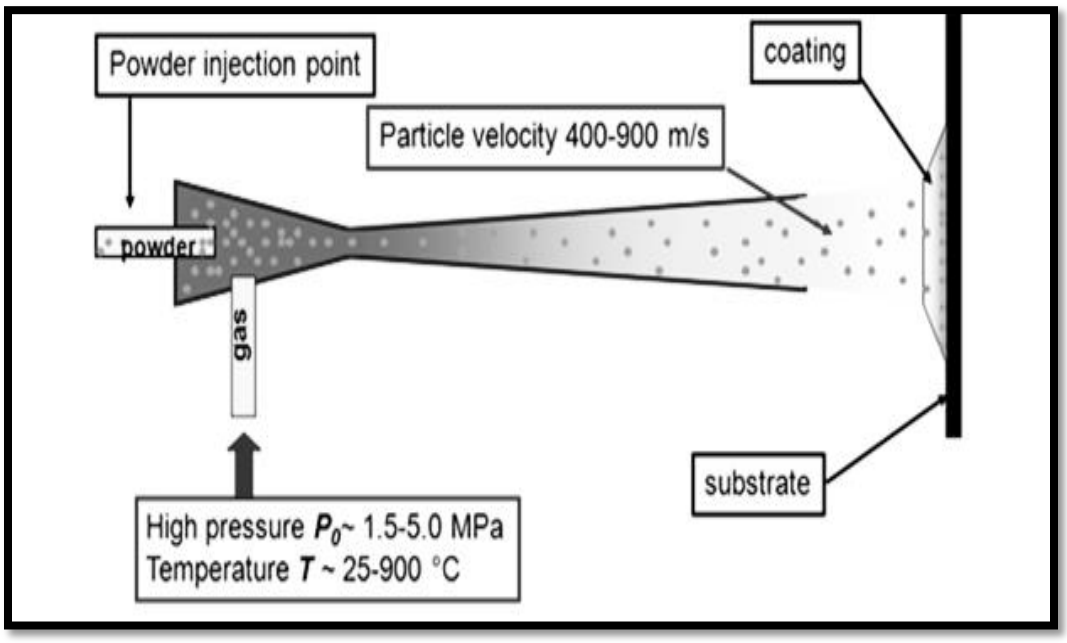

Figure 1.3. Schematic of low pressure cold spraying process [67]

In low pressure cold gas dynamic spraying (LPCGDS), the spraying pressure is less than 1 MPa while spraying temperature is less than 550°C. The carrier gas is low cost, easily available medium: air. Figure 1.3 shows schematic of low pressure cold spraying process. Although it has low deposition efficiency, coatings deposited using this technique can show mechanical properties like hardness, toughness, comparable to those obtained using HPCGDS. The use of relatively simple and low cost equipment, accessories, and low cost gas(es) results in lowering of the overall coating cost. Also, the process can be made in modular form which makes it portable [54, 55, 67 - 71, 82].

1.1.7 Limitations of thermal spraying

Although thermal spraying claims of providing so many benefits to coating in terms of hardness, wear and corrosion resistance, none of the above mentioned techniques can guarantee a coating devoid of detrimental issues generated after spraying along with its visible side effects on substrate: residual stresses, warping and distortion [40 - 52]. Apart from the high temperature defects discussed in above paragraph which are common in many high temperature thermal spraying techniques, many other issues exist even in low temperature spraying technique like cold spraying [54 – 71, 79]:

- Non-uniform and non-homogenous microstructure,
- Loss of reinforcement during spraying results in different coating composition compared with powder while affects coating proerties,
- Low hardness and toughness (due to lower content of hard phases in coating),
- Low melting temperature with no reactivity among different phases results in improper packing of powder during spraying resulting in porosity and
- Comparatively low mechanical properties like hardness, wear resistance, in comparison with high temeprature thermal-sprayed coating.

1.1.8 Post-deposition treatment techniques

Considering the limitations of thermal spraying mentioned above, there exist many post-deposition treatment techniques to overcome these issues. Different post-deposition techniques are used depending on the requirements of the final coating. Removal of residual stresses along with homogenization of the microstructure is the primary purpose behind many techniques. In fact, these characteristics results in improvement in other mechanical properties like toughness, corrosion and wear resistance along with reduction in porosity and induction of uniformity in the microstructure. Diffusion of chemical species also

results in reduction of chemical heterogeneity, which adds to uniformity in microstructure [72 – 75].

There are number of post-deposition techniques, some of which are mentioned below:

a) Laser heating,

b) Furnace heating in air or inert atmosphere,

c) Induction heating,

d) Friction stir processing,

1. Laser heating as post-deposition technique is a costly and slow process. The heat used during heating is a function of many parameters like work piece-torch gap and voltage, apart from coating thermal parameters like thermal conductivity, [14].
2. Furnace and induction heating although popular post-deposition techniques, However long heating and cooling cycle time restrict its applicability for mass production only. The furnace heating of the coated substrate restricts the size of the sample to be treated using this technique. Also, heating effect of the substrate is unavoidable which further adds to the complexity of these techniques [16].
3. Friction stir processing is relatively new and emerging post-deposition technique. In this, the thermal and mechanical stresses generated during treatment results in the fragmentation of hard reinforcement particles. Also, mechanical stirring results in homogenization and uniform distribution of reinforcement in the coating. The thermal stresses also assist in chemical diffusion of constituent species which further aids in chemical homogeneity. The advantage of this technique over others is its low cost, reliable, effective technique with fast application rate and less thermal effects on the substrate [79, 80].

1.1.9 Friction stir processing

Friction stir processing is a variant of friction stir welding and friction stir spot welding [76 - 85]. In friction stir processing, a non-consumable rotating tool under the action of the vertical axial force, travels over the material's surface with fixed linear velocity (Fig. 1.4). The friction between the tool and material's surface results in generation of the excessive heat, while the action of tool rotation results in generation of the mechanical stresses in the material [79, 80]. The tool used must withstand the heat generated during processing. Hence, it should have the high softening temperature and the ability to retain mechanical properties like hardness, toughness, wear resistance, even at high temperature. Tool material depends on the material to be processed, hence usually hard, wear resistant and high temperature resistant materials like martensitic steel, tungsten carbide, nickel based alloys, are choices [79, 80, 83 - 85].

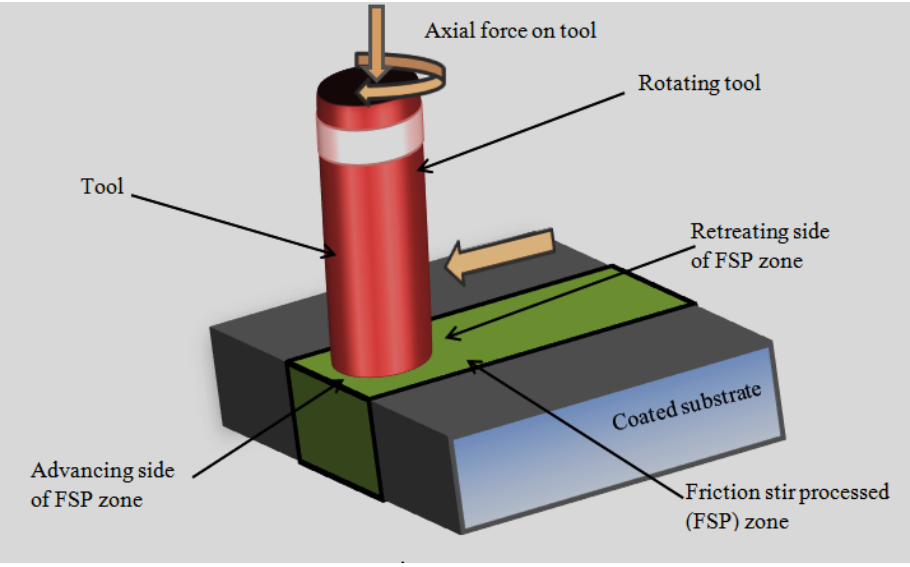

Figure 1.4. Schematic of friction stir processing [76].

Friction stir processing produces uniform and homogenous microstructures, resulting in improved mechanical properties like decreased dislocation density, reduction of porosity and inter-lamellar cracking, reduction of chemical inhomogeneity (due to the diffusion of chemical species and reactions triggered by high temperature). The reason for decreased dislocation density is the

annealing effect generated due to high friction heat which relieves the material of augmented dislocation density due to mechanical stressing during processing [76]. Improvements in toughness, wear and corrosion resistance, reduction of hardness are some of the possible attriHoweveres of this post-deposition process. The reduction of intermetallic phases along with the inducement of homogeneous composition with uniform thermal properties assisted by controlled heating and cooling cycle ultimately results in reduction or removal of residual stresses in the coating. The heat generated during friction stir processing can be easily controlled by the use of suitable coolant. Also, thermal stirring results in proper wetting of reinforcement with a binder and compressive stresses of the tool ultimately improve adhesive and cohesive strength of the coating [79, 80].

The friction stir processing of any material is a function of many process parameters like [80]:

a) Tool travel velocity, m/s

b) Axial force on the tool, kN

c) Tool rotational speed, RPM

d) Number of passes of the tool on the substrate.

It was found that the increasing the value of parameters like axial force on the tool, tool rotation speed, number of passes of the tool on the substrate, and decreasing tool travel velocity leads to generation of more heat which is being transferred onto the substrate. Lower tool travel velocity assisted by the high tool rotational speed and number of passes results in more incidence time of heat at any location (localized heating); while, more axial force results in more penetration of this heat and induction of more mechanical stresses in the microstructure. Higher axial force results in increased material density due to closing of pores and promote bonding between binder and the substrate, ultimately contributing to improved adhesive and cohesive strength. The higher axial force along with high tool rotational speed assists in fragmentation of the reinforcement and wider and deeper friction stir zone, due to more reach of thermal and mechanical stresses in the material [76 - 81].

The application of FSP to various thermal-sprayed coating showed that there is wide scope for improvement in mechanical properties like hardness, lowering of porosity, lowering of mean free path, fragmentation of carbides with subsequent improvement in toughness [79, 82 – 85]. To date, no studies have been conducted to quantify mechanical properties such as wear resistance of friction stir processed thermal-sprayed coatings.

1.1.10 Superplastic deformation

Friction stir processing belongs to a category of deformation technique called superplastic deformation. This method of deformation process differs from normal plastic deformation processes. In this, the material is progressively deformed with subsequent application of heat. The heat is either frictional heat generated during the process or it is externally supplied. The heat results in continuous softening and dissolution of the dislocation, due to which the material receives less resistance during deformation. Hence, materials can undergo appreciable deformation at high temperature compared to their deformation at room temperature under same stress conditions. There are various theories to support this claim. One of such theory says that this feature in any material is exhibited due to dynamic recrystallization phenomena. The arrangements of grains take place in such a way that they offer less resistance to the motion of dislocations. Also, the existing dislocations get annihilated during process, due to which continuous application of mechanical stress is possible with fewer efforts [86, 87].

Superplastic deformation is a common characteristic of microstructures exhibited by the following processes [86 - 93]:

a) Friction stir processing,

b) Equal channel Angle processing,

c) Superplastic forming,

d) Annealing and hot tensile straining

1.1.11 Dynamic recrystallization

In dynamic recrystallization, the material undergoes crystallization during application of the mechanical stress. The recrystallization happens due to the application of sufficient heat either externally or due to friction during processes. The heat generated results in softening and heating of the material to temperature beyond recrystallization temperature which results in the annihilation of dislocations and formation of equiaxed, strain free grain. The new grain formed has a low dislocation density which offers less resistance to the plastic deformation. Although the grains undergo refinement during plastic deformation, However the defects like grain boundary, dislocations, does not offer resistance to the motion of dislocation. Hence, the material as such has a favorable microstructure for deformation. Such structure has a fine grain structure with uniform distribution of grains and phases and more homogeneity. The homogenous nature of microstructure is due to accelerated diffusion of chemical species during dynamic recrystallization. The dynamic recrystallization is thus function of heat and mechanical stresses generated during or applied during the process [76 - 93].

1.2 Previous Studies

The tungsten-carbide-cobalt-nickel (WC-Co-Ni) coating fabricated using HVOF spraying process showed numerous reactions with surrounding atmosphere as well as with other constituents in the powder at high temperature. Some of these reactions confirm the phenomena of decarburization, oxidation and formation of intermetallic phases during spraying. The formation of various unexpected and undesirable phases hamper mechanical properties like ductility, wear resistance, toughness, by inducing residual stresses, increased porosity content, reaction with substrate, warping and cracking of substrate and coating [40, 41, 43, 44, 50 - 53].

Reaction of contents (WC-Co-Ni) with oxygen [40]:

$4WC + O_2(g) \rightarrow 2W_2C + 2CO(g)$ $\Delta_r G^o_{1273K} = -362kJ/mol$

$2WC + O_2(g) \rightarrow 2W + 2CO(g)$ $\Delta_r G^o_{1273K} = -378kJ/mol$

$WC + O_2(g) \rightarrow W + CO_2(g)$ $\Delta_r G^o_{1273K} = -360kJ/mol$

$\frac{2}{3}\ WC + O_2(g) \rightarrow \frac{2}{3} WO_2 + \frac{2}{3} CO(g)$ $\Delta_r G^o_{1273K} = -366kJ/mol$

$\frac{2}{3} WC + O_2(g) \rightarrow \frac{1}{4} W_2O_6(g) + \frac{1}{2} CO(g)$ $\Delta_r G^o_{1273K} = -306kJ/mol$

$\frac{2}{3} WC + O_2(g) \rightarrow \frac{1}{6} W_3O_9(g) + \frac{1}{2} CO(g)$ $\Delta_r G^o_{1273K} = -327kJ/mol$

$2W_2C + O_2(g) \rightarrow 4W + 2CO(g)$ $\Delta_r G^o_{1273K} = -393kJ/mol$

$W_2C + O_2(g) \rightarrow 2W + CO_2(g)$ $\Delta_r G^o_{1273K} = -338kJ/mol$

$2W + O_2(g) \rightarrow 2WO(g)$ $\Delta_r G^o_{1273K} = -582kJ/mol$

$\frac{2}{3} W + O_2(g) \rightarrow \frac{2}{3} WO_3(g)$ $\Delta_r G^o_{1273K} = -346kJ/mol$

$2C + O_2(g) \rightarrow 2CO(g)$ $\Delta_r G^o_{1273K} = -448kJ/mol$

Reactions with H_2O and CO_2 [39]

$C + H_2O \rightarrow CO(g) + H_2(g)$ $\Delta_r G^o_{1273K} = -46\ kJ/mol$

$2WC + CO_2(g) \rightarrow W_2C(g) + 2CO(g)$ $\Delta_r G^o_{1273K} = -9.2kJ/mol$

$W_2C + CO_2(g) \rightarrow 2W + 2CO(g)$ $\Delta_r G^o_{2073K} = -141kJ/mol$

$2Co + O_2(g) \rightarrow 2CoO$ $\Delta_r G^o_{1273K} = -290kJ/mol$

$2WC + CoO \rightarrow W_2C + Co + CO(g)$ $\Delta_r G^o_{2073K} = -185kJ/mol$

$$WO_3\,(g) + 3WC\,(s) \rightarrow 4W + 3CO\,(g) \qquad \Delta_r G^o_{1273K} = -344\ \text{kJ/mol}$$

$$Ni + \frac{1}{2}O_2(g) \rightarrow NiO \qquad \Delta_r G^o_{1273K} = -250\ \text{kJ/mol}$$

Thus, it is clear that WC-Co powder gets severely affected while its flight through surrounding atmosphere (Fig. 1.5). The high spraying temeprature also results in heavy reactivity among different constitutents which affects mechanical properties in finally fabricated coating.

To counter the issues raised during HVOF spraying process, a comparatively low temperature thermal spraying process is used for fabrication of WC-Co based MMC coating. Many studies on application of WC-based MMC coating using high-temperature cold spraying (HPCS) and low-temperature cold spraying (LPCS) has shown positive result in terms of fabricating coating with no after effects [59 – 66, 68 - 72].

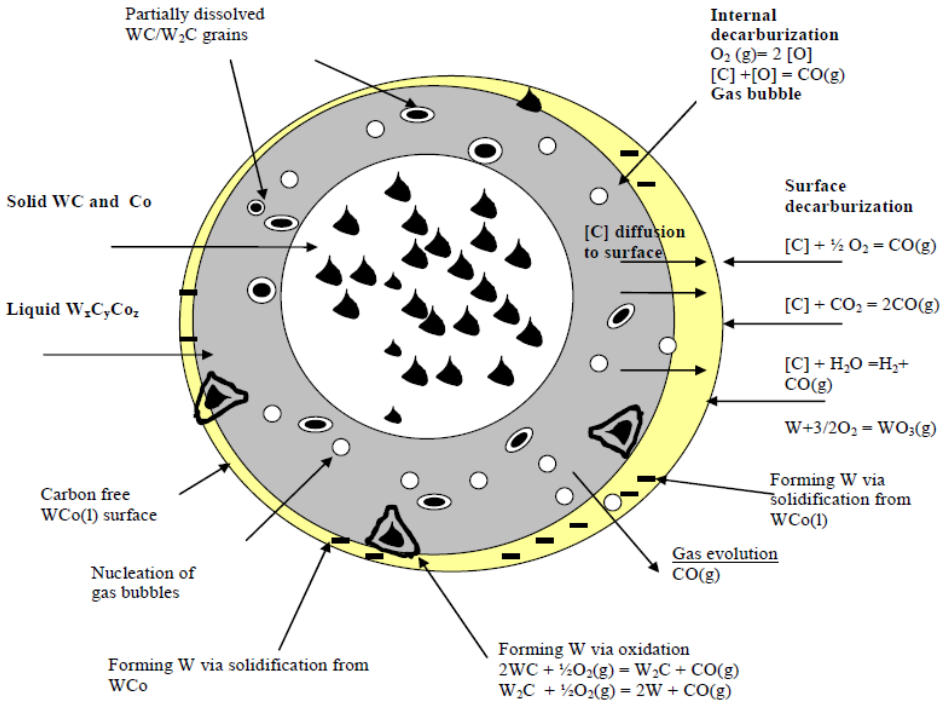

Figure 1.5. Schematic of different reactions of in-flight WC-Co powder with surrounding atmosphere while spraying [40].

The numerous studies on WC-based MMC coating fabricated using HPCS showed that higher hardness with coating thickness close to the value obtainable by HVOF process is possible [59 - 65]. The works of Kim [60, 62], Gao [63, 64], and Li [65] proved that nano-structured WC-based MMC coating can be successfully fabricated using HPCS. However, costly gases along with high equipment cost, makes this process uncompetitive in the market. To compensate for this, a LPCS process using cheap gas like air with spraying pressure less than 1.5 MPa is suggested [55, 67]. The low spraying pressure results in use of small, portable and cheap spraying accessories, lowering the overall coating cost. Besides having all the advantages of high pressure cold spraying like lower porosity and no degradation of powder material during spraying, the lower coating cost makes it an attractive option for simple wear applications [69 – 71, 82]. Although there are limited research articles on WC-based coating deposited using LPCS, few papers on fabrication of other MMCs and pure metals reflects benefits of this technique [69, 70, 82]. The work on LPCS WC-based MMC coating by few authors showed hardness comparable to those obtainable by HPCS [71]. The absence of any undesirable compounds in such WC-based MMC coating will definitely reduce corrosion problems [59 - 66, 71]. However in spite of all these positive aspects, the WC-based MMC coating fabricated using low pressure cold spraying (LPCS) showed mechanical properties like hardness, wear resistance, comparatively lower than high temperature thermal spraying techniques like high velocity oxy fuel (HVOF) spraying technique [71]. To counter this problem successfully, a post-deposition technique called friction stir processing (FSP) is proposed. The successful studies on various materials and alloys like Al-alloys have shown tremendous scope for improvement of mechanical properties of WC-based MMC coating [79, 83]. The application of FSP treatment on WC-based MMC coating showed success in terms of improved hardness [84, 85]. The biggest challenge is to date, no study have been ever carried out on wear analyses of friction stir processed high velocity oxy-fuel (HVOF) sprayed and low pressure cold-sprayed (LPCS) WC-based MMC coating. It is expected that the mechanical properties like hardness, toughness,

wear resistance, of thermal-sprayed WC-based MMC coating will be improved by application of friction stir processing treatment.

1.3 Research objectives

The research in this thesis study is concentrated on conducting optimization of low pressure cold-sprayed tungsten carbide-cobalt-nickel coating and improvement in wear resistance of cold-sprayed as well as HVOF-sprayed WC-Ni MMC coating after friction stir processing.

The research objectives are to:

i) Define wear resistance of low pressure cold-sprayed tungsten carbide –cobalt-nickel (WC-Co-Ni) coating in the compositional range of 0 - 65 wt.% WC-12Co in WC-Ni MMC coating,

ii) Study the influence of friction stir processing (FSP) on the wear resistance of cold-sprayed and HVOF-sprayed conventional WC-Ni coating,

iii) Describe wear mechanism of cold-sprayed and HVOF-sprayed WC-Ni MMC coatings on the basis of experimental and theoretically generated results.

iv) Study the mechanism for improvement in mechanical properties like hardness, toughness, and wear resistance, due to FSP treatment on various coatings.

Chapter 2. Wear mechanisms and wear theories for composites

2.1 Abrasive wear theories

For a long time, wear and erosion of material by abrasives were considered to be material properties dependent phenomena. Numerous work of researchers in the past have shown that attack of abrasives at oblique angle on the surface results in transfer of its energy to the material's surface [13, 93 - 99]. Heavy plastic deformation of material happens with result that it creates crater on the surface, subsequently followed by material removal in large lip [13, 93 - 102]. The volume of the lip is always less than the volume of the crater formed due to large plastic deformation of the material happening during wear. It is also predicted that this deformation is aided by the frictional heat generated during wear which assists in material deformation prior to failure. Numerous studies have shown that volume of material removed during wear is function of factor: $C \times \rho \times \Delta T$

Where,

C = specific heat of the material,

ρ = density of wear tested material, and

ΔT is the difference in melting point and temperature of the material during wear.

It is found that high temperature during wear lowers flow stress and increases material removal. Thus, volume of material removed is found to be inversely proportional to the factor: $C \times \rho \times \Delta T$ [101, 102].

Wear of material due to impacting or flowing solid particles seems to be influenced by two forces. The forces normal to the material surface result in deformation of the material which is seen as depressions or craters in the surface. The material is plastically deformed due to this force, hence wear due to this is known as deformation wear. The other component of the force is cutting force and is parallel to the surface. This force results in shearing of the material, due to

which crack generated at the surface propagate sub-surface and result in shearing of the material [104].

The wear of the ductile material under the action of the abrasives result in formation of micro machined chips which depending on the hardness of the material will decide the next course of action. Sometimes, the action of the abrasives result in continuous deformation and extrusion of the material till overhanging lips are formed which are subsequently removed by the flowing abrasives [13, 93 – 104]. It is found that for soft materials, the chips remain intact with the parent material indicating that it will undergo plastic deformation until failure while for hard materials, they break away easily from the surface. It was postulated that the attack of abrasives at high velocity results in generation of heat which is transferred to chips and quick heat dissipation results in its hardening [102, 103]. The chips formed have more hardness than parent material, due to which for hard material, they separate easily during wear [105].

Wear of the material is considered to be steady-state phenomena wherein continuous impact of abrasives result in plastically deformed and work hardened sub-surface zone. The frictional heat generated during wear results in softening, probably annealing of the surface zone with lower flow stress value than the sub-surface zone and is easily amenable to wear. The wear of the surface occurs in form of platelets due to continuing abrasive impact which are progressively removed when their critical fracture strain limit is reached [104].

Wear of soft material happens due to the shearing action while hard materials are abraded due to inherent surface and material defects like pores, inter lamellar cracks. Also, loosening and progressive removal of the cementing binder between hard reinforcing particles in composite result in subsequent removal of them [106].

Numerous papers discussing wear of ductile material has been published in the past. It is seen that during wear, the impacting abrasives on the material surface result in formation of depressed zone on the surface. The material immediately below the surface undergoes continuous plastic deformation and subsequent work hardening. The work hardening of the material results in conversion of the

material behavior from ductile to brittle. The wear of the ductile material happens due to the formation of three different zones in any material. The three zones are as follows:

a) First zone is the surface zone. At surface, there is thin layer of thickness 5-15 μm (Fig. 2.1). This zone recieves maximum heat during deformation due to friction. The frictional heat results in annelaing and softening of the material layer due to which, there is increase in ductility even after progressive plastic deformation during wear. The softened surface is vulnerable region and is easily prone to the attack of the abrasives. Deep indents and craters are common in this zone due to lowered hardness. The surface shows heavy material loss due to impact of the abrasives. The attack and travel of the abrasives in this zone results in smearing and ploughing action on it. The occurrence of indents and craters in this zone is a clear indicaton of lowered mechanical properties like hardness and toughness.

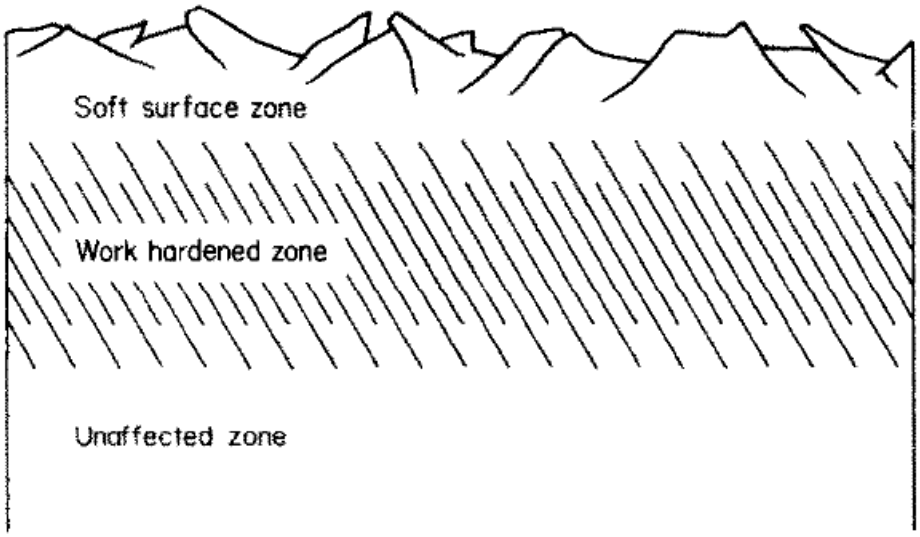

Figure 2.1. Cross-sectional image of material showing annealed surface and work hardened sub-surface zone [108].

b) Second zone is the sub-surface zone. This zone extend just below zone 1 and extends to greater depth compared to zone 1 (Fig. 2.1). This zone ensues due to large plastic deformation of the abraisves. The continous action of the abrasives result in improved mechanical properties like hardness and work hardening which increase as we move further deep into the material. The region close to the zone 1 has lower hardness due to softening effect from the heat transfered during wear. The hardness increase reaches a peak value at certain depth below the surface and then recedes till it reaches properties of parent material [22, 121, 154, 155].

c) The third zone is the unaffected zone of original parent material (Fig. 2.1). This zone lies exactly below zone 2 when considered from the top surface of the material subjected to wear.

During wear, the digging abrasives result in crack propagation in zone 1. The extrusion of the top portion of the material is seen as platelets [98, 104, 108]. It is found that the angles of attack of abrasives play distinct role in wear. Even if the angle of attack of abrasive is low, However sufficient play between the hard abrasive and the material surface result in change in actual angle of attack. The abrasives with sharp edges have more contribution to the wear. At a shallow angle of attack of abrasives, the wear is influenced by the horizontal component of the velocity and smear craters are generated on the surface. At higher impingement angle, the attack of abrasives results in ploughing type of crater. Thus, attack of abrasives is severe at higher impingement angle. It is seen that there is peak in wear at particular angle of attack and beyond that, it recedes [93, 97, 105, 108]. The wear of ductile material starts from the surface and is accelerated due to softening of the material. As the zone 1 is removed and zone 2 comes in contact, the frictional heat results in softening and annealing of portion of zone 2 to some depth. This results in conversion of zone 2 to zone 1. Wear happens in same way as it happened for all previous layers which formed part of zone 1. The region close to the crater is progressively forged–extruded as platelets which separate

easily under the action of flowing abrasives. The region below zone 1 shows progressive increase in hardness again due to plastic deformation; and continues till it gets transformed to zone 1[107].

The wear of the hard and brittle material happens due to cracking and separation of material in form of flakes. Ploughing is also seen as a form of mechanism of wear for few materials containing soft cementing binder [108].

The sub surface cracking is also commonly seen in many materials. There were two possible explainations for such cracking phenomena being discussed:

a) Low cycle fatigue phenomena: As per this theory, the alternating normal component of the force acting on the material surface results in localization of the stress to some depth below the surface. The tensile component of the force results in accumulation of the strain and when this strain reaches the local fracture strain limit, the fracture of the material happens [110, 111].
b) Delamination theory (Suh's theory[121]): As per this theory, the continuing plastic deformation by the slider on the surface results in accumulation of the dislocations in sub-surface zone. At surface or zone close to surface, the dislocations has free surface where they can travel without entanglement and thus less work hardening is observed in the surface zone. However in sub-surface zone, the moving dislocations are obstructed by the presence of hard obstacles like second phase particles and inclusion which result in dislocation entanglement and progressive work hardening. The accumulation of such dislocation around any inclusion or hard reinforcing particle result in void nucleation which under the action of tensile stress elongate to micro cracks. Linking of numerous such cracks result in large sub-surface crack [110] .

2.2 The delamination theory of wear

The delamination theory proposed by Suh and Jahanmir [103, 121, 138] in the 1970s is a modification of the fretting wear previously proposed by many

researchers [23, 24, 113, 121, 122, 129, 130, 137 - 140, 153, 157, 161, 166, 171, 180]. An excellent paper describing fretting wear is given by Hurricks in 1970 [112]. Fretting involves continuously changing amplitude or repeated attack of one surface over the other. The changing amplitude happens due to surface undulations or surface roughness. The crest region of surface will undergo plastic deformation while trough region making slight contact will undergo elastic deformation. The changing amplitude waves results in generation of normal stresses on the material surfaces during momentarily material contact which then ensue in material transfer and finally removal of scalp of material. The final damage to the material is in form of steady state wear, wherein layers or areas of material is progressively removed [111 - 114]. The delamination theory proposed by Suh and co-workers [22 - 24, 121, 130, 138, 157, 161, 174, 175, 178, 179] has features which resembles close to as has been discussed for fretting wear. Wear is not purely just material contact or rubbing of one material's surface over other However it also involves material loading and stress transfer [121]. Depending on the value of the stress and its frequency which indicates its fluctuations, the wear damage varies. For material surface under load and with relative motion of one surface with respect to other, the wear happens due to delaminated wear sheet or layer formation [121]. There are few stages in delamination wear sheet formation which will describe its correlation with the fretting wear.

The formation of the Beilby layer

Machined or unmachined surface of any material is never perfect in terms of surface roughness. Depending on the type of machining process used, the surface roughness can be defined. Even for fabricated or cast material, surface irregularities exist and it is estimated using surface roughness and waviness. Surface roughness plays crucial role in wear of any material. Asperities on the surface define the surface roughness. Rough surface always has higher number and varying height of the asperities, which influence the wear mechanism. The asperities look like hills and valleys under the microscope.

During wear, the asperities on the surface contact each other and the forces from one body are transferred to other. It is found that asperities deform under the action of applied load (Fig. 2.2). The material properties affect and define the deformation characteristics of the material. It is found that hard material can easily deform the asperities of the softer material. In some cases, these asperities deform and spread over the surrounding areas on the surface while in other cases, they fracture and contribute to the wear by being trapped in spaces between the material's surfaces [23, 121, 125, 126, 130, 138, 152, 153, 174, 175]. The size of these asperities is usually smaller than the wear particles separated during the delamination process. Hence it is easier to distinguish the fractured asperities from the wear particles on the surface. The wear of any material always start with deformation and proceeds with facture of the asperities. It means that the asperities act as retarder of wear rate.

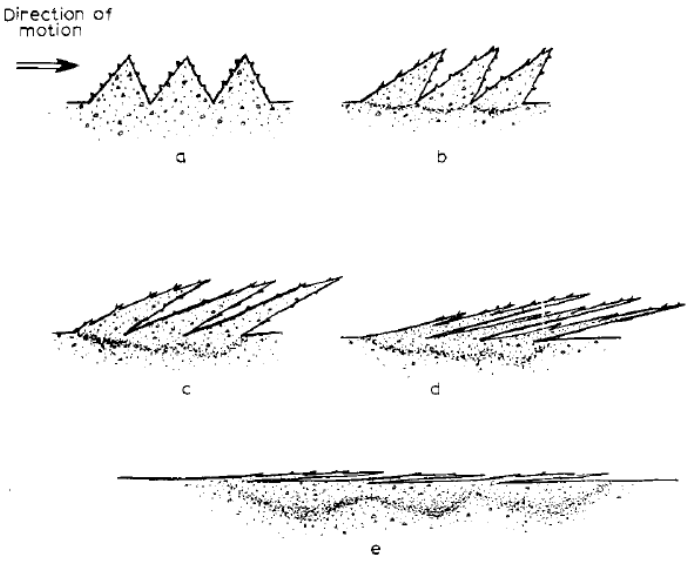

Figure 2.2. Schematic of flattening of asperities and spreading on material's surface during wear [176].

A close look at Fig. 2.2 explains the phenomena of flattening of wear which is supported by image shown in Fig. 2.3. During wear, the deformed asperities spread over the adjoining areas covering the lower height asperities. This is followed by deformation of lower height asperities, which spreads over the

surface and may form cohesive bonding with the surrounding materials. If the asperities continue to deform this way, a limit comes when there are no more asperities projecting from the surface, since they have either tear out due to fracture or they must have plastically deformed under the action of compressive force and has spread over the surface. The surface becomes flat and looks more uniform in terms of asperities' distribution. The spread out of deformed asperities in the neighbouring areas is the weakest region where the crack propagation is probable during early stages of wear. The wear of this material now takes place due to delamination failure [22 – 24, 94, 96 - 100, 114, 106 - 110, 113 - 118, 126 - 131, 137 - 140, 145 – 154, 157, 169 – 175, 176].

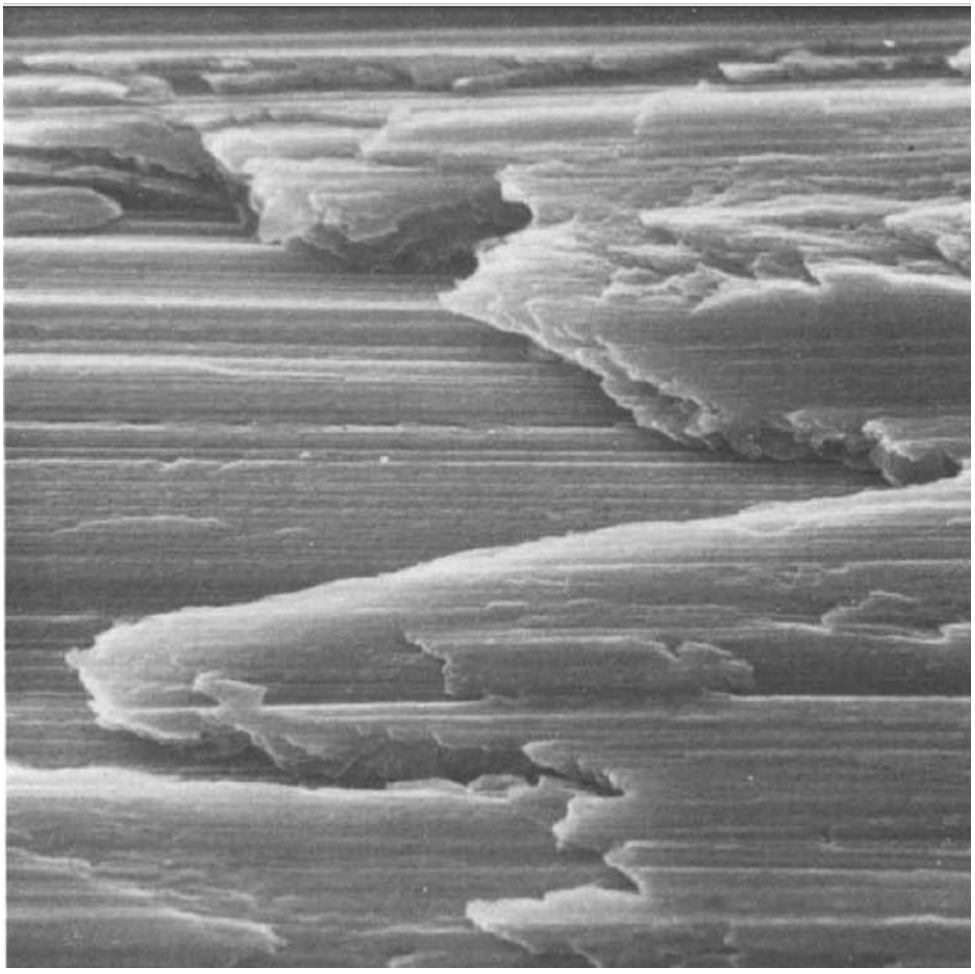

Figure 2.3. Flattened and spread-out asperities under action of wear [176].

During wear deformation of the asperities, the bonding with the surrounding material plays important role. The bonding happens due to keying or locking of the spread out material with surrounding areas. If the cohesive bonding is insufficient to hold the deformed material under the attack of abrasives, then it will spall or be lifted over and will be carried away as wear particle. Spalling happened due to varying amplitude of stress transferred during wear. This varying amplitude happens due to asperities of varying height projecting from the surface as well as abrasives and wear debris trapped in the space between the surfaces. Thus the stress fluctuates as surface contact happens [22 - 24, 121, 130, 138, 153, 154, 156, 157, 161, 169, 174, 175, 178].

Usually, the spreading of material as flow layer happens in forward direction as well as on sides. The spread out film sometimes occupy gaps between the asperities and crack at corners due to bending stress. In few cases, continuous extrusion of spread out film results in accumulation of strain and when it crosses critical strain limit, cracks begin to permeate in such films. Such films separates as thin layers which are not representative of delamination process [22, 23, 119, 129, 139, 149 - 152, 175, 176]. Due to this, they cannot represent the wear layers or particles generated during wear. For layers which are removed due to the formation of sub-surface cracks under the action of normal and shear stress, the asperities will indicate excessive deformation and elongation especially in the direction of wear. The elongation will indicate the effect of stress; and asperities will elongate to indicate a lamellar structure. Such layers are called Bielby layer [22 - 24, 121, 122, 130, 136, 138, 140, 152, 153, 157, 161, 174, 178].

For hard material with low strain hardening exponent or for dispersion hardened composite, the asperities deformation is localised and elongation is negligible. The worn delamination layer would not show lamellar structure indicating its fewer tendencies for plastic deformation. Hence, such materials crack due to void nucleation [23, 118, 121, 124, 130 - 132, 148, 159, 161, 173, 178]. The wear of the material is also dependent on the waviness of the material. Waviness indicates surface irregularity with large deviation compared to surface roughness. A surface roughness will represent asperities with varying height However waviness will

represent surface irregularity which has strong influence on the tangential as well as the shear stress. For large variation waviness, the tangential component of the stress will have pronounced effect on the wear of the material [24, 121, 150, 152, 153, 157].

Deformation of the surface layer

The plastic deformation of the material under the action of stress results in incremental progressive wear of the material. With cycle of asperities passing on the surface (which means that as the sliding distance increases), the shear strain continue to accumulate in the material in the form of progressive plastic deformation. As the material gets strained under the action of stress, the material loses its capacity to strain harden more. In fact, the strain hardening capacity after progressive cycles of stress would not resemble unstrained material. During stressing of the material, the material after plastic deformation will spring back after release of stress or lowering of stress, however springing back would not revert it to its original shape. The continuous effect of compressive stress results in plastically deformed zone in the form of depression at the wear location. The hardened material with accumulation of strain energy progresses towards fracturing stage [23, 24, 115, 117 - 122, 125, 126, 128 - 131, 136, 138 - 141, 150 – 153, 157, 158, 162, 167, 174, 176, 178]. Suh, *et al*.[23, 24, 121, 122, 130, 138, 153, 157, 161, 174, 178, 179] have mentioned that the strain gets accumulated with progression of sliding distance and is a function of the traction force. The accumulating stress will eventually end up as crack and finally as delaminated layer. Thus increasing the resistance to delamination tendency is through increasing the flow stress of the material. This is possible by using ductile material as well as using particles in material which will offer resistance to crack initiation and propagation. It is found that plastically deformed zone is a function of flow stress; hence higher flow stress means more deformation under stress. It is found that higher the sliding distance, higher is the wear strain accumulation [23, 24, 118, 121, 122, 129, 136, 149 - 151, 155, 165 - 167, 170, 171, 174].

Crack nucleation

The crack nucleation in material during wear is a strong function of stress: both, tangential as well as normal stress [23, 118, 121, 127, 130, 138, 141, 143, 161, 180, 182, 183]. Also, crack has the tendency to concentrate sub-surface than at the surface since the effect of the load results in deformation of the material to some depth below the surface. Thus, it is not the surface where they may be nucleated but in subsurface areas where they are nucleated. The surface will undergo enough plastic deformation However it will transfer all the normal load acting on it to the material located deep below the surface. Also, sub-surface has more stress zones due to accumulation of dislocation since friction heat relieves surface of dislocation accumulation. Thus, sub-surface will indicate relatively high stress zone and binder is more stressed than surface.

Figure 2.4 depicts higher surface traction indicating highly stressed compared to surface. Hence, surface although may have some discontinuity However void nucleation may rarely happen on it [23, 24, 121, 122, 127 - 131, 136 - 138, 140 - 143, 153, 160, 161, 171, 173 - 175, 178, 9]. However damage in form of ploughing or scratching on the surface may contribute to the delaminated layer formation. In few cases, these damaged surfaces may help in provision of sites for lateral crack nucleation which will meet the sub-surface crack, parallel to the surface [121]. Cracking on surface usually happens due to indentation or digging of abrasives into the surface. During wear, these hard and sharp edges will scrap the surface resulting in uplifting. Owing to this, sub-surface crack nucleation or crack initiation tendency increases as the load increases. Higher normal as well as tangential load will result in more probability of crack nucleation at higher depth below the surface. It means higher load will result into more crack nucleation sites along the thickness of the material. Thus, below the surface along the thickness, there will be number of layers which will be separated due to crack nucleation. As the void nucleation tendency increased with increasing load, the delamination layer formation tendency will also be increased [23, 121, 127, 129 - 132, 140, 161]. Hence, wear of such material is strongly accelerated under the action of

higher loads. Now, nucleation in material is usually dependent on the void as well inclusion content in the material. Numerous theories support the claim that void nucleation is considered to occur under the action of residual stresses at the inclusion sites [116, 121, 123, 124, 127, 132, 134, 135, 148, 159, 178, 179]. The adhesion between inclusion and the surrounding binder plays important role for void nucleation. If the overall stress at the inclusion-binder interface is higher than adhesive strength of the material, crack is eminent. In such case, the interface surrounding the inclusion loosens under the action of tensile stress, which pulls away the binder from the inclusion. Pulling away of the binder will result in formation of void between binder and inclusion which is a crucial phase for void nucleation and crack generation [142, 164, 165]. The stress acting on the material results in progressive plastic deformation of the material. If the flowability of the inclusion or reinforcement, and the binder is different under the influence of stress, then binder may plastically deform in such a way that it would not conform to the shape of the inclusion. The areas of inclusion or reinforcement which remained uncovered by binder completely will be reflected as void. These voids under the application of stress will elongate and will continue to envelope whole reinforcement or inclusion.

Another reason for void nucleation is that under the action of stress, the material surrounding the inclusion are strained which result in loosening of the material cover around it and this will be reflected as gap at the interface of inclusion and binder material [121, 123, 124, 131, 132, 134, 135, 142 - 144, 146, 148, 161, 163 - 165, 171, 173, 175, 178, 179, 181 - 183]. The void formation is more pronounced as the inclusion size increases. The increased inclusion size offer more resistance on the binder material around corners when strained. Thus, at large diameter section in the inclusion, the binder will experience more deviation in the flow of the binder fibre. Hence, large size inclusion will offer more strain as binder fibre passes around it. Hence in tension, they will be under triaxial state of stress due to which, it is likely that binder tearing is easier and binder will lose contact with the inclusion. The cohesive strength between the inclusion and binder will be lower for big size inclusion than for small size since binder has to

conform to the shape of the inclusion which results in more strain it. Reinforcing the matrix with hard, rigid component will increase the overall hardness, due to which there will be less effect of stresses at the higher depth. Hence void formation and crack initiation tendency will be reduced. The cohesive toughness between reinforcement and binder is important parameter since lower the value, more easy is the tendency of the reinforcement to separate from the binder resulting in void nucleation. Also, reinforcement should be uniform in shape and homogenously distributed in the composite [116, 117, 123, 124, 132, 134, 135, 144, 148, 161].

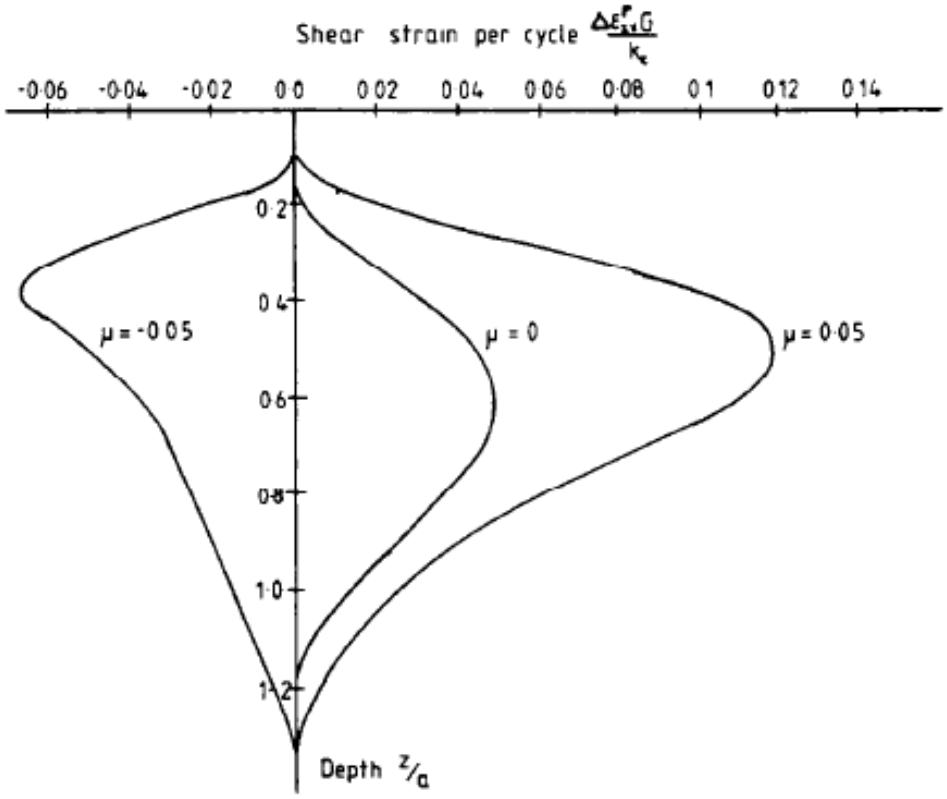

Figure 2.4. Graph depicting maximum strain in material in sub-surface zone [167].

Sub-surface crack nucleation

The sub-surface crack formation and propagation is discussed in this paragraph. As mentioned earlier, crack initiation occurs due to void initiation. Hence, when

these voids collapse to form cracks, the cracks have two fronts where their propagation can happen (see Fig. 2.5). It is indicated by Jahanmir and Suh [22, 121, 130] that when there is moving surface with crack located in the material, assume that crack is parallel to the surface and has two fronts from which propagation can happen. The crack front with orientation in direction of movement of asperities on surface, is called the leading edge of crack while the crack front with orientation opposite to the direction of movement of asperities on the surface, will be called as trailing edge of the crack. During wear, when the load on the surface is substantial, it will generate normal hydrostatic pressure which will induce compressive stress in the material below it. With movement of asperities, this stress will be spread over in that region. Thus crack at leading edge of the material will be under compressive stress while the crack in trailing edge of the material will be under tension (Fig. 2.5 a) [121, 142, 179].

With progression of cycles of stress, the plastic deformation and strain hardening of material under compressive as well as tensile stress will happen. The section of the surface under compressive loading will undergo deformation to result in depression while the section of material under tensile loading will result in elongation or pulling out of the material (Fig. 2.5 c). In fact, the depression in compressive loading will result in increased tensile loading, due to which material will be under intense strain. The void nucleation and void coalescence will happen in tensile section more. In the compressive section, void nucleation may happen but the tendency is less. Void nucleation in tensile section will happen especially in two phase materials and composite material or materials containing second phase particles distributed in matrix. The tensile loaded zone will result in elongation and progressive straining of the material which will result in void nucleation at the interface of the inclusion and binder. The void nucleation will result in necking of the section of the material between the void formed zones. Thus, under strain, fracture is fast in such necked zone and void coalescence is faster in tensile loaded zone [116, 121, 123, 124, 130, 132, 148]. Such tensile loaded zone will fracture and this fracture will be either lateral crack emanating from the surface and will propagate inside to join the already existing sub-surface

crack front or sub-surface crack front may propagate to reach the surface due to tensile loading. The crack front showing propagation in the direction of shear stress will be under compressive stress while the crack front which has propagation direction opposite to the direction of shear stress will be in tension (Fig. 2.5 (b) and (c)). It is found that this compressive stress as well as the tensile stress generated during wear is restricted to few layers below surface, hence the wear layer generated are thin. Although the stress effect is limited and is restricted to thickness of few microns but increased stress may enhance this effect even further deep into the material. Hence, higher loading on the surface during wear may result in the formation of damaged material even further deep below the surface. Also, fluctuating loading on the surface due to varying size of abrasive as well as the formation of the depression zone during wear results in formation of varying compressive stress wave which travel all the way and are reflected from the bottom surface as tension stress wave front. These waves when they meet the compression stress front will result into net tensile or compressive stress at different points along the depth of the material. The location where the net stress wave is tensile will result in opening of the crack in compressive zone. It may perhaps result into void nucleation especially at the inclusion-binder interface. However at the trailing side of crack front where tensile stress is acting, this tensile stress wave reflected from the bottom of the material will result in an additive effect. Due to this, it will accelerate the opening of crack front and void nucleation. The void coalescence is accelerated in this zone. Due to this, the material will fracture early and will result in uplifting of the material once it is fractured. Also, as the material continues to depress more in the compressive stressed zone, it will result in more tensile stress effect in trailing section with easy propagation of crack and fracturing of the material. The fractured section will open up more and will be lifted further. This will result in bending stress being exerted on the material section in compressive stress zone. Now, further action of tensile stress in trailing zone will result in further opening of the sub-surface crack and further lifting of the material [23, 24, 116 - 124, 126 - 132, 134 - 145, 146 - 151, 153 - 155, 159, 161, 162, 164, 165, 167 - 179].

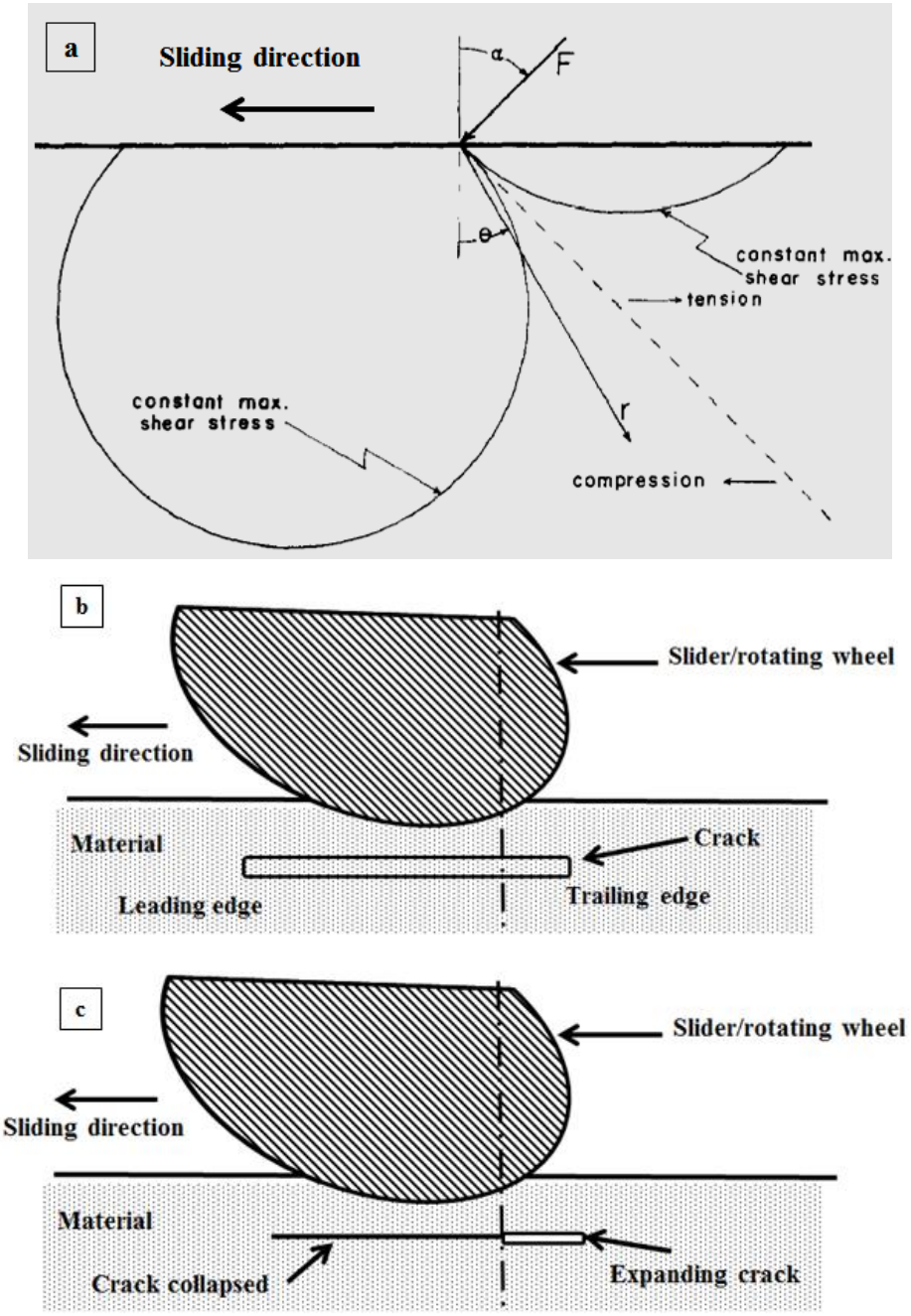

Figure 2.5 (a) Application of resultant stress on material surface resulting n generation of tensile and compressive zones in sub-surface of material [179]

(b) Sub-surface crack geometry under action of movement of asperities during wear [142]

(c) Sub-surface crack expansion in trailing edge of crack [179]

Crack propagation

The delamination crack will propagate close to the region just below the end where the bending stress is a maximum. When the stress due to bending cross the critical stress to failure, surface will crack which will eventually meet with the sub-surface crack resulting in completion of the delaminated layer. The final delaminated material will be separated from the surface which will be carried away by the flowing abrasives. It is found that the travel of the sub-surface crack is accelerated under the action of the shear stress during wear. The shear stress will help in propagation of the crack in the direction of the asperities movement. This way, the crack front in the leading edge will propagate while crack front in trailing edge will meet the fracture generated at the surface. Also, the friction coefficient is known to play important role in wear. The higher the friction coefficient value, higher is the surface traction resulting in friction force. It is found that along the depth of the material, the stress varies However at particular depth below the surface, the stress reaches a critical stress value which will result into crack initiation. Thus, higher the stress more will be the tendency for crack initiation at higher depth below the surface [23, 24, 121, 129 – 131, 136, 138, 140, 142, 153, 161, 164, 165, 171, 174, 175, 178].

The crack always experiences cyclic stress fluctuations from tension to compression as each asperities pass over the surface, which helps in its propagation. It is found that in case of material with absence of defects like inclusion, voids, crack will be generated on the surface due to abrasive particle digging or indentation damage to the surface [115, 117, 119, 122, 129, 136, 152, 157, 166, 170, 171]. These cracks then follow the path which is oriented and guided by the resultant stresses. These stress help to propagate the crack deep into the material which then follow the path of least resistance in such way that crack may result in formation of layer which has serrated surface. This surface indicates that crack had to travel a path which could result in zone which provided a favourable condition for its travel. The crack resulted in serrations which will finally end up uplifting of the layered material. This layered material will result

into bending stress being generated at the extreme edge of the raised section and when the stress due to this bending crosses the critical stress which corresponds to fracture limit, then cracking will be generated at that section (Fig. 2.6). This lateral crack will then travel along the thickness of the material and will meet the sub-surface crack. The final delaminated material will be removed as wear layer which will be representative of the wear process prominently observed for brittle material [121, 130, 131, 140, 142, 143, 164, 165].

Hence, it is found that the material failure starts with void formation or crack nucleation, void coalescence or cracks bridging and finally void collapse to crack and crack propagation into final fractured surface.

Thus wear is modified form of fretting wear wherein the effect of cyclic loading along with material defects play combined role in material fracture. The wear is simple process and it is found that cracks may initiate from the surface or they may develop sub-surface and may propagate till it reaches the surface. Surface of any material is rough and has various location where crack can ensue, hence wear is type of fretting failure; here too the surface discontinuities result in wear of the material.

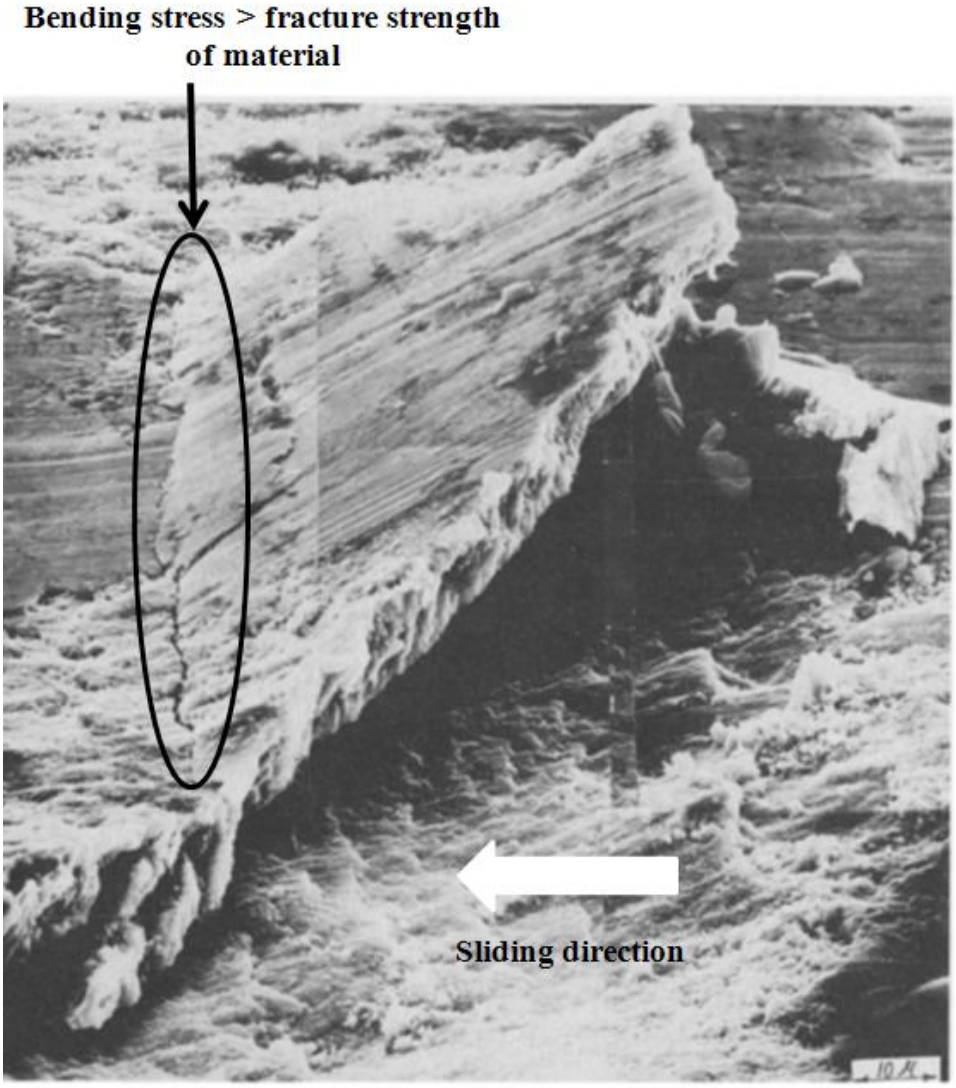

Figure 2.6. Depiction of crack propagation in sub-surface zone due to uplifting of material in tensile stress region of crack [121].

2.3 Mean free path between reinforcing particles and mechanical properties

The mean free path between reinforcing hard particles in a metal matrix composite is an important factor affecting mechanical properties like hardness, toughness, tensile strength, and wear and corrosion resistance of any composite material [184 - 190]. In any composite material, the mean free path defines the proximity of the reinforcement particles to each other in the composite.

For WC-Co based composite, mean free path (λ) is given by [184, 186, 188]:

$$\lambda = \frac{(1 - V_{WC})}{N_{WC}} \qquad (2.1)$$

Where,

V_{WC} = Volume of tungsten carbide in the WC-Co MMC,

N_{WC} = Number of tungsten carbide particles intersected by line of interest

In any composite, binder as well as reinforcement plays an equally important role. The contribution to mechanical properties like hardness, wear resistance, is taken care by reinforcement in the composite while toughness, corrosion resistance, modulus of elasticity, is taken care by the binder. If the mean free path is small value wherein the reinforcing particles are close, then reinforcement content in whole composite will increase. It means, that if reinforcement content continues to increase, then composite will exhibit properties close to as shown by reinforcement like: high hardness and wear resistance, low plastic deformation, low toughness, high brittleness [191 - 195]. However it is found that, higher reinforcement content induces brittleness in the composite and makes it unable to withstand the fluctuating stresses to which material is subjected. Such composite cracks easily due to low fatigue toughness; and crack travels unhindered due to absence of tough phase in the material. Also, if the binder does not bond and wet completely the reinforcing particles, then it will be observed as porosity which will further contribute to the brittleness of the composite [22, 121]. If the mean free path between reinforcing particles is higher and if binder content is higher than the reinforcement in the composite, then composite will be softer and will exhibit properties close to as shown by pure binder itself like low hardness, poor wear resistance, good toughness, Such material will be easily worn out in wear environment since soft binder will offer less resistance to hard abrasives. The abrasives will dig and scrap-off the reinforcing particles. Once the binder is removed to appreciable amount, then it would not be able to hold remaining reinforcement and it will be dislodged by flowing abrasives [94 - 105]. Thus, reinforcement will be unable to impart necessary properties like hardness, wear resistance, to the composite. It means the mean free path between reinforcement

should maintain balance of a binder and reinforcement content in the composite in such a way that the composite is hard and wear resistant along with good toughness and corrosion resistance.

2.4 Effect of grain size on the toughness of the composite

Grain size in any composite has a peculiar effect on its mechanical properties. The grain size of reinforcement plays a prominent role than the grain size of binder. This is because reinforcement offers significant improvement in mechanical properties like hardness, wear resistance, corrosion resistance, of the composite. The bigger the reinforcement size, or more agglomerated the reinforcement are, inferior will be the properties of composites. The main reason for this is that, the bigger reinforcement particle in the composite result in large variations in the flow of binder around it. The binder is like sea in which reinforcement particles act like island. The bigger reinforcement particles result in straining of the binder around it, especially at locations where the variation of binder flow is large, usually at the corners. The bigger reinforcement particles or an agglomerated particle has a complex shape compared to single and small reinforcement particles whose shape is close to a sphere. Due to this, the flowability of binder around big reinforcement particles or agglomerated particle is limited. The limited flowability of binder results in binder not reaching to intricate corners; hence there is incomplete wetting of the binder around the reinforcement particles. This improper wetting of hard reinforcing particles lowers the adhesive bonding of the reinforcement particle to the binder. Thus void nucleation is probable in such structure and wear rate is higher for such material [121, 189, 190].

Also, non-homogenous distribution of reinforcement phases in the microstructure results in inferior mechanical properties like hardness, wear rate. The random distribution of reinforcements results in non-uniform zones on composite surface such that areas with high content of soft, ductile binder will be more vulnerable to attack of flowing abrasives during wear resulting in high wear rate [71].

2.5 Wear theories for composites

The attack of abrasives results in wear. Different wear models and theories are quantified for wear of materials, however for composites three theories are widely accepted and applied. The three theories are:

a) Equal pressure theory,
b) Equal wear theory,
c) Modified equal wear rate theory.

The underlying principles of all the three theories are different, such that they relate overall wear rate to the wear rate of the individual constituents. Usually the effects of individual constituent on the wear rate are dealt and their basic rule discussed.

A) Equal pressure theory:

In equal pressure theory, it is assumed that the binder and the reinforcing particles are distributed in the overall composite in such a manner that the pressure or normal stress on each constituent remains same as if they are laid as layers one above the other (Fig. 2.7). Thus, there will be a layered arrangement of binder and reinforcing particles one above the other in the composite with load normal to the surface of the layers.

Figure 2.7. Representation of composite as per Equal pressure theory

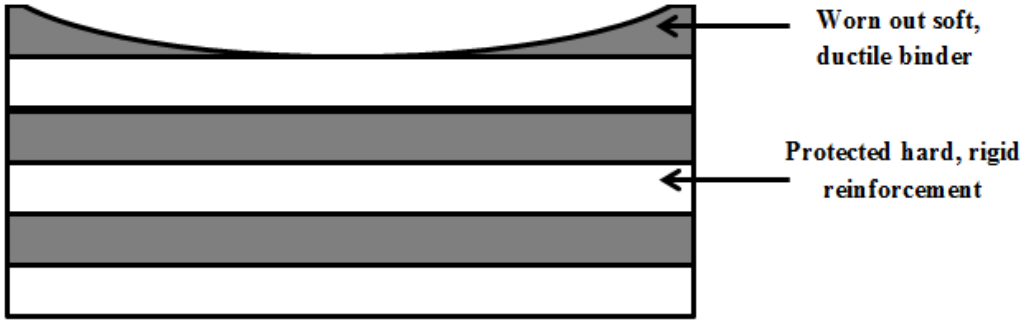

Figure 2.8. Representation of wear of composite as per Equal pressure theory.

Hence, overall load remains constant and it is assumed that the wear rate is a function of pressure/normal load and individual wear rate per unit load. Thus, it is postulated that for purely ductile material, the wear rate will be higher, However as the content of the hard reinforcing particles increases, the wear rate starts to regress. The underlying principle behind this theory is: initially, the soft binder will be removed, and then the hard phase will be removed (Fig. 2.8). The hard reinforcing particle has low wear rate, hence it will retard overall wear rate of the composite. Depending on the distribution of hard reinforcing material in the form of layers in the composite, wear rate will be decided. As the content of hard phase increases, overall wear rate will continue to decrease in proportion. Thus, it means that the fall in wear rate is directly proportional to the rise in the content of overall hard phase(s) in the composite. Thus, this theory states that the wear rate is directly proportional to the content of the soft phase(s) in the overall composite [191, 192, 195 -197].

The wear rate of composite (W_c) as per equal pressure theory is given by Eq. 2.2 as [196]

$$W_c = (V_m W_m) + (V_r W_r) \qquad (2.2)$$

Where,

W and *V* are the wear rates and volume fractions of individual constituents in the composite, respectively. The subscripts c, m, and r in the equation designate the composite, matrix, and reinforcement, respectively.

B) Equal wear theory:

A second wear theory is 'Equal Wear Theory'. In this theory, the basic underlying principle is: the wear of all the constituents (hard reinforcement and soft binder) remains constant. This means that for two phases in the composite, the overall load is divided into two parts in such a way that the mass loss will remain same for all the phases irrespective of their wear rate (Fig. 2.9). This means that the soft binder will share low load while the hard reinforcement will share high load to get equal mass loss even with unequal wear rate. When the content of the reinforcement is less and the binder is more in the composite, wear of the soft binder will be initiated. The distributed load will cause wear of the soft binder to such a depth that hard reinforcement will be the visible phase on the surface (Fig. 2.10). The hard phase will take the overall load and will wear out to the amount of the soft binder. The hard reinforcement phase in the composite being wear resistant, will be the wear retarding phase in the composite. The lower wear rate of the reinforcement will ensue in longer period to generate the same amount of mass loss alike softer binder phase.

Figure 2.9. Representation of composite as per Equal wear theory.

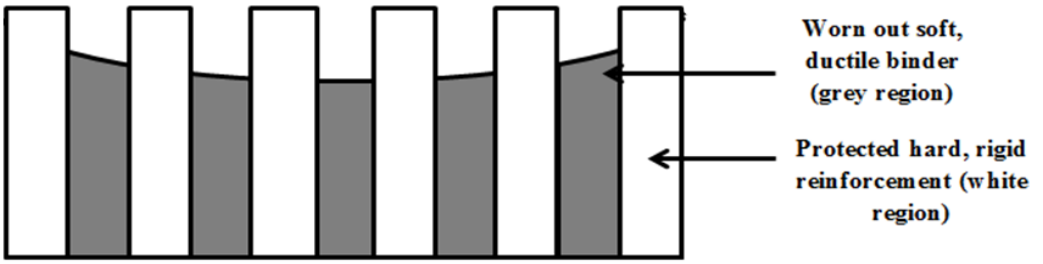

Figure 2.10. Representation of wear of the composite as per Equal wear theory.

Thus, within a stipulated duration, unless same amount of mass loss of hard phase happens, the wear of soft phase would not be initiated. Thus, the wear rate of the overall composite is reduced.

Hence, according to this wear theory, even a small amount of hard reinforcement will lower the overall wear rate of the composite substantially compared to wear rate value indicated by individual ductile phase in the composite when tested under the same experimental conditions. This theory indicates that the wear rate of composite containing small content of reinforcement will be close to the wear rate of composite containing large content of reinforcement. Thus, the postulate that the wear rate of composite containing any content of reinforcement will be close in numerical value seems impractical and unreasonable. The main reason for its limited acceptance is its less emphasis on the role of ductile binder. It does not signify the role of the binder as cementing material and overestimates the role of reinforcement. It does not consider the loss of reinforcement when the content of the binder as cementing material is less. Also, role of adhesive toughness, uniformity, distribution of load, are some of the prominent aspects which are unclear in this theory [198 – 201].

The wear rate of composite (W_c) as per equal wear theory is given by eq. 2.3 as [200]:

$$\frac{1}{W_c} = \frac{V_m}{W_m} + \frac{V_r}{W_r} \qquad (2.3)$$

Where, subscripts have same meaning as defined for equal pressure theory.

C) Modified Wear Theory:

The next theory of wear is called as modified wear theory. This theory is specifically modified equal wear theory since equal wear theory underestimates the role of binder and failure of reinforcement due to cracking, chipping, it can predict wear rate value for composite containing reinforcement in mid-range satisfactorily. This means that, when the reinforcement content is low or high, there exists a different phenomenon which needs consideration. It is noted that when the reinforcement content in the composite is low, then it is likely that

during the fabrication process there will be a random distribution of reinforcement in the composite. So it is likely to influence the wear rate of the reinforcement; and during wear, along with the binder, reinforcement will be plowed or dug away from the composite. Also, the difference in flow strength of the ductile binder and hard reinforcement will influence the pore formation tendency under the action of compressive stress. During wear under the action of compressive stresses or normal load, the soft binder surrounding the reinforcement will spread and/or will deform plastically. Due to this, it will lose bonding with the reinforcement and will form pores between reinforcement and the binder. Hence the overall wear rate of the composite will be close to the wear rate of the pure ductile binder under same wear conditions. Similarly, for composite containing high content of reinforcement, wear rate will be higher since there is less amount of binder as cementing material between the reinforcements. Due to this, the composite would not be able to withstand the shear stress applied during wear and wear will be accelerated due to easy removal of the reinforcement. In such composite, the binder content would not be enough to fill the spaces between carbides and applied stress will result in easy generation of pores. The toughness of such composite will be less and crack propagation will happen easily, assisted by the presence of pores between carbides. Thus, the wear rate of the composite during low and high reinforcement contact would not follow the trend as depicted by the 'equal wear rate theory' [121, 201].

The cracking of composite in wear conditions can happen due to many reasons. Some of the reasons which were discussed in above mentioned theories are: void nucleation at reinforcement-binder interface, sub-surface crack propagation, elongation of pre-existing void in the composite along with cracking and chipping of reinforcement. To take care of all the uncertainties mentioned above, a correction factor should be introduced in the equal wear theory [201]. Hence, a factor called "contribution coefficient" is included in equal wear theory. This modifies the theory to the "Modified wear theory".

Thus Modified wear theory is described using formula as given in Eq. (2.4) [201]:

$$\frac{1}{W_c} = \frac{V_m}{W_m} + C\frac{V_r}{W_r}, \text{ for } V_r \leq 0.5. \qquad (2.4)$$

Here, "*C*' is the contribution coefficient and is dimensionless quantity defining cracking, chipping and pull-out of reinforcement from binder during wear process. All the other terms have same meaning as described in equal pressure theory.

Chapter 3. Experimental Method

3.1 Feedstock powder and substrates

Various powders were used in this study. For cold-sprayed WC-Ni MMC coating, a sintered and crushed, WC-12 wt.% Co powder (referred to as "WC" for simplicity) (72F-NS, Sulzer Metco, Westbury, NY, USA), with a size distribution of -45+15 μm, was mechanically blended with a specially designed nickel powder for cold spraying (SST-N5001, Centerline, Ltd., Windsor, ON, Canada) to fabricate the WC-based MMC coatings. For HVOF–sprayed WC-Ni MMC coating, a sintered and crushed WC-12wt.% Co (same powder as used for cold spraying of WC-Ni coating) was mixed with precipitated, nickel powder (56C-NS, Sulzer Metco, Westbury, NY, USA) with a size distribution of -75 + 45 μm and with 99.3 % purity. The powder morphology of WC and nickel powder used in cold spraying has already been shown and discussed in a previous study [71]. For this study the optimized powder composition (the parameters used for optimization where hardness, mean free path, porosity and wear rate) obtained for cold-sprayed WC-Ni MMC coating was selected. The procedure used for optimization has been discussed in a previous work [71].

Table 3.1. WC-12Co content for cold-sprayed pure nickel as well as different WC-Ni MMC coating [71]

Powder composition	Coating composition vol.% of WC-12Co	Coating composition wt. % of WC-12Co
Pure nickel	0	0
50 wt.% WC- 50 wt.% Ni	4 ± 2 (n = 9)	7 ± 3 (n = 9)
75 wt.% WC- 25 wt.% Ni	11 ± 2 (n = 10)	19 ± 3 (n = 10)
92 wt.% WC- 8 wt.% Ni	42 ± 4 (n = 12)	56 ± 4 (n = 12)
96 wt.% WC- 4 wt.% Ni	52 ± 2 (n = 12)	66 ± 2 (n = 12)

Although powder preparation of different composition to arrive at an optimized powder composition was not dealt with this study, but wear phenomena for cold-sprayed and HVOF-sprayed pure nickel and different WC-based MMC coatings are being discussed in this study.

Table 3.1 shows the powder composition of different WC-based MMC for optimization of the cold-sprayed MMC. The table also displays the coating composition in terms of amount of WC content in WC-based MMC. The "n" in table 3.1 indicates number of images assessed with Image Pro software towards determination of WC content in the WC-Ni MMC coating. In advanced stage of research, the wear mechanism for friction stir processed thermal-sprayed coating is also studied. For all the characterization as well as wear studies of the thermal-sprayed coating, the sample size and material used as substrate was constant. The substrate used for all studies was 1018 mild steel. For wear test, the rectangular cross-sectional blocks with coated area of 75 mm × 25 mm and thickness of 25mm were used. The characterization of all the coatings was also carried on the same substrate with change in sample dimensions to 13 mm × 13 mm and 3 mm thick. For characterization, the coated area is usually 13 mm × 10 mm. The coating of material to be characterized as well as wear tested is applied on one side of the sample only. Prior to spraying, the substrates were cleaned, degreased using ethanol and then wiped with paper to remove any traces of oil or dust remaining on the surface. After that, the surface to be coated using thermal spraying were roughened using #24 alumina grit medium (Manus Abrasive Systems, Inc., Edmonton, AB, Canada) to remove traces of moisture, oxide layer, dirt, dust or greasy layer remaining on the surface and to impart good adhesion of MMC coating with the substrate surface by providing keying zone for the powder in the substrate. To assure removal of abrasives after grit blasting, a blow of compressed air is directed towards the surface. The substrate preparation step is followed by the powder preparation for thermal spraying.

3.2. Cold spray and High velocity Oxy-fuel deposition

The study involved a comparison of mechanical properties of cold-sprayed as well as HVOF-sprayed pure nickel and WC-Ni MMC coating. The cold spraying system (SST series P, Center Line, Ltd., Windsor, ON, Canada) was tuned to the optimized operating condition for fabrication of pure nickel and WC-Ni MMC coating. The cold spray system was controlled using an optimized robot (HP-20, Motoman, Yaskawa Electric Corp., Waukegan, IL, USA) which was operated using programmable pendant.

To provide supersonic speed to the powder mixture, the converging–diverging de-Laval nozzle is provided at the exit of the cold spray torch. The cold spray torch is a low pressure system using a mixture of argon as a secondary gas while helium and nitrogen mixture as the primary carrier gas. The nozzle is 120 mm in length with an entrance diameter of 4.46 mm, and an exit diameter of 6.40 mm. The nozzle is designed in such a way that sub-sonic speed of the mixture is converted to sonic in throat section and finally to supersonic speed in the diverging section of the nozzle. The transport of the powder and the compressed air from the de-Laval nozzle to the substrate at high speed, imparts sufficient adhesive strength for bonding of the coating to the substrate. A volumetric powder feeder (5MPE, Sulzer Metco, Westbury, NY, USA) delivered the powder mixture to the cold spray unit using argon as the carrier gas.

The spray parameters used for deposition of the coatings are shown in Table 3.2.

The substrate was preheated to a temperature of 500 - 550ºC with two passes of the torch over its surface keeping the nozzle travel speed twice than as used during normal spraying to improve coating adhesion. There was no modification to other spraying parameters, and care was taken to switch off the powder feeder during spraying.

Table 3.2. Cold spray deposition parameters.

Pressure of compressed air (kPa)	634
Temperature of compressed air (°C)	550
Stand-off distance (mm)	5
Gun velocity (mm/s)	5
Pressure of argon carrier gas for powder (kPa)	483
Volumetric flow rate of argon carrier gas (SCFH)	15
Powder FMR (flow meter reading)	60
Number of passes	2

The spray parameters used for the deposition of pure nickel coating and WC-Ni MMC coating by HVOF spraying are given in Tables 3.3 and 3.4.

Table 3.3: HVOF spray deposition parameters for pure nickel coating

Oxygen (scfh)	1950
Fuel (gph)	6.5
Carrier (scfh)	26
Feeder speed (rpm)	180
Stand-off distance (mm.)	375
Barrel (mm.)	100

Table 3.4: HVOF spray deposition parameters for WC-Ni MMC coating

Oxygen (scfh)	1800
Fuel (gph)	6.0
Carrier (scfh)	25
Feeder speed (rpm)	220
Stand-off distance (mm)	375
Barrel (mm)	100

The substrate was grit blasted to sufficient surface roughness for better adhesion of coating and removing traces of oil, dirt, grease, from the surface. The HVOF spraying was initially tried with same nickel powder (as used in cold spraying) to obtain pure nickel as well as WC-Ni MMC coating; However frequent clogging of the hose generated technical difficulties while spraying. Hence, to resolve this problem, a bigger size nickel powder (with 99.3% purity and bigger size compared to previous nickel powder) was used. The HVOF spraying after initial trials were finally tuned up to the parameters for spraying pure nickel and WC-Ni MMC coating. The spray torch used for HVOF spraying (TAFA JP 5000, Praxair, Tafa, USA) used kerosene as the fuel.

3.3. Parameters for friction stir processing

To understand the effect of post-deposition treatment on thermal-sprayed coating, a relatively new technique called friction stir processing is used. The pure nickel and WC-Ni MMC coating obtained through cold spraying and HVOF spraying was treated with friction stir processing. The tool for friction stir processing was decided as Alloy HX (Ni based superalloy) considering that it will be able to withstand temperature and thermal stresses generated at 1000 - 1500ºC since it has high melting point. The brief calculation indicating maximum possible heat generated and temperature rise during FSP treatment of WC-Ni MMC coating is given in Appendix 4. The composition of this alloy is given in Table 3.5. However, an inability to withstand the thermal and mechanical stresses generated during processing, led to the softening and eventual deformations of the tool.

Table 3.5. Composition of Alloy HX

Elements	**Content (wt. %)**
Nickel	Rest
Iron	17- 20.0
Chromium	20.5- 23.0
Molybdenum	8- 10.0
Copper, Cobalt, Tungsten, Titanium	Traces

Table 3.6. Composition of Tungsten carbide grade C1

Elements	**Contents (wt. %)**
Tungsten Carbide	90- 94%
Cobalt	6- 10%

This was subsequently replaced with new tool material to take care of the high thermal and mechanical stresses generated due to the friction during processing. The new tool material selected was Tungsten carbide grade C1 (WC with 6-10 wt.% Co). The composition of this tool material is given in Table 3.6. The tool used for FSP treatment was a cylindrical rod with no pin at its base. The dimension of the rod was 12 mm diameter and 50 mm length. After finalization of the tool material, the next task was the selection of the process parameters. The selection of the parameters were done in such a way that the thermal and mechanical stresses could generate a friction stir processed zone to a depth of 200 – 300 μm in cold-sprayed WC-Ni MMC coating so that it can be tested with maximum possible sliding distance of wear conditions.

Two sets of parameters were used for friction stir processing of both the thermal-sprayed WC-Ni MMC coatings (Table 3.7).

Table 3.7. Sets of parameters used for FSP parameter optimization

Parameters	**Set 1**	**Set 2**
Tool travel velocity over thermal-sprayed WC-Ni MMC coating	33 mm/min	33 mm/min
Tool rotational speed	900 RPM	1400 RPM

In friction stir processing, the axial force on the tool and the tool travel velocity over the coatings were kept constant while the tool rotational speed was changed. Thus the change in tool rotational speed defined the change in the processing parameters. The selection of tool rotational speed was decided on the basis of the

heat and the mechanical stresses which will be sufficient enough to generate thermal as well as mechanical stresses in the coating. The two different tool rotational speed values used are: 900 RPM and 1400 RPM. Both the thermal-sprayed WC-based MMC coatings were treated with both the sets of parameters.

The parameters used for FSP treatment of thermal-sprayed coatings:

- Tool travel velocity over the coating 33 mm/min.
- Tool rotational speed 1400 RPM

The friction stir processing treatment was carried out only on thermal-sprayed WC-Ni MMC coatings, since it required use of different processing parameters for pure nickel coating.

3.4 Coating characterization

The characterization of the coatings involved lot of features which will be discussed in this chapter. The coatings obtained from cold spraying and HVOF spraying were initially characterized to decide the effectiveness of using defined powder composition. The characterization of coating included measurement of hardness, porosity, mean free path and toughness. Also, cross-sectional images of the coating obtained using microscopy were extensively checked to measure porosity and cracks in the coating. For HVOF-sprayed pure nickel as well as WC-Ni MMC coating, the finalization of the parameters were done on the basis of the image which will give completely crack-free image after deposition. This involved finding the lateral and longitudinal cracks in the thermal-sprayed coating which are generated due to the warping and generation of residual stresses from use of high spraying temperature.

The thickness measurement of the cold-sprayed coatings was done with use of micrometer screw gauge (Thread Check Inc., New York, U.S). The micrometer is outside diameter (Mitutoyo-outside micrometer-series 101-105, accuracy = ± 0.0001 in, with carbide tipped measuring faces).

To do weight measurement of samples, Ohaus Scout Pro Balance SP2001 (Ohaus Corporation, NJ, US). The specification of weighing balance is: Maximum capacity = 2000g, least count = 0.1g, Stabilization time = 3 sec. The instrument is battery operated and provided with digital LCD display screen to display readings to six digits.

To do hardness and toughness measurement as well as to do microscopic analyses of the coatings, the coating was sectioned along its thickness. The sectioning is done using diamond or abrasive wheel under copious flow of coolant and at low rotating speed so that heat generated during sectioning should be expended as much as possible. This is necessary since it is expected that heat generated during sectioning of sample may raise coating temperature to sufficient value which may burn and create microstructural changes in the coating. After sectioning, the coatings are ground to remove any sharp burrs projecting from the sectioned surface. The sectioned samples were then held under flowing water to remove traces of coolant, debris; and finally cleaned with ethanol to remove water remaining on it. Afterwards, the sample surface is cleaned with paper to wipe out solvent remaining on it. This is followed by directing a jet of high pressure air to remove any traces of solvent. The coatings to be viewed under microscope or for hardness and toughness measurement are mounted in epoxy resin.

The epoxy mount is prepared by mixing resin to hardener in the weight ratio of 5:1. After uniformly mixing the mounting medium, taking care that few bubbles are generated after mixing; it is then poured around the sample in the mount. The curing time for epoxy mixture is 4 to 6 hours, after which the mounted sample is removed from the mount. The mounted samples are then polished on the sand blaster to remove thin layer of epoxy formed on the surface of interest. The rough polishing of the mounted samples usually start with 180 grit paper followed by 400, 800 and 1200 grit paper (LECO, Mississauga, ON, Canada). The numerical value for each paper indicates the average number of grits that can be accommodated in one square inch area of the paper. Thus, higher number indicates fine polishing paper. Fine polishing involved polishing samples on

polishing cloth under copious flow of diamond solution (LECO, Mississauga, ON, Canada). The fine polishing starts with use of 9 μm polishing solution followed by 6μm and 3μm polishing solution. The polishing paper remained same when changing polishing solution from 9 to 3 μm. Last step in polishing process involved use of 1 μm diamond solution on specially designated polishing cloth (LECO, Mississauga, ON, Canada). During each polishing stage using particular polishing paper like 180, 400 grit, care should be taken that polishing should be carried out till scratches are seen on the surface in particular direction and no scratch marks in other direction from previous process are visible. For moving on to next polishing stage, the sample should be rotated by 90° so that they cut the scratches generated by previous process and scratches generated in that direction are visible. Final fine polishing should result in completely flat, mirror polished surface. This indicates that there exist no scratches from previous operations which will obstruct the reflection of the light. After polishing, the sample surface is cleaned with running water and finally with ethanol to remove traces of water sticking to it. Also, the layer of ethanol protects surface from further oxidation in open atmosphere.

For hardness measurement, there is no requirement of completely mirror polished surface, However surface should be free from visible scratches, since they may affect the hardness readings due to peculiarities of the unevenness in the rough surface. The hardness measurement involved application of load on the sample's surface. The top and the base of the sample should be flat and parallel, so that sample does not move during application of the load. The micro Vickers hardness tester (MVK-H1, Mitutoyo, Aurora, IL, USA) uses diamond indenter which is pyramid in shape with angle between opposite faces of 136° [202]. The load is applied on the sample for specific duration of 10 seconds and then load is retracted. The indent generated on the sample is viewed through the optical microscope provided in the hardness tester. The measurement of two mutually perpendicular diagonals results in determination of the hardness value. All hardness measurements were done at 300gf load for all thermal-sprayed as well as FSP-treated thermal-sprayed coatings. The purpose of using 300gf load for

hardness measurement is with consideration that higher load would generate cracking in the softer coatings like pure nickel and WC-Ni MMC coatings containing higher content of nickel in the composition. For measuring hardness value of the cold-sprayed WC-Ni MMC coating, a total of 40 hardness measurements were done on three different samples while for HVOF-sprayed pure nickel and WC-Ni MMC coating, a total of 72 hardness readings were taken on three samples. The hardness measurements on HVOF-sprayed samples were carried out till optimized parameters were determined. For FSP-treated thermal-sprayed WC-Ni MMC coatings, the hardness measurements were integral part of parameter optimization process. A total of 15 hardness readings for each FSP-treated thermal-sprayed WC-Ni MMC coating treated with different processing parameters were carried out. Along with parameter optimization, hardness measurements played important role in determination of homogenous distribution of carbides in the WC-Ni MMC coating. For carrying out hardness indent on the coating, the procedure as specified by ASTM E384 standard is followed [203]. Precaution was taken that indent should be located at least four diagonals away from each edge of the sample as well as from the neighbouring indent as per ASTM C1327 standard [202]. The purpose of space between two neighbouring indents is to avoid influence of strain hardening effects on hardness readings. The standard deviation in the hardness value indicates the degree of homogeneity in the coating. For FSP-treated thermal-sprayed coatings, the standard deviation from the mean hardness value were less compared to those indicated by non-FSP-treated thermal-sprayed WC-Ni coatings.

Wear resistance of the coating is also function of its toughness. To measure toughness of the coating, the Vickers indentation technique is used [204 - 208]. Toughness measurement was done on micro Vickers hardness tester (MVK-H1, Mitutoyo, Aurora, IL, USA). Toughness measurement was done on cross-sectional surface of coating similar to those done in hardness test. All the precautions as prescribed for hardness test were equally applicable for this test also [202, 203]. In Vickers indentation technique, sufficiently high load was applied on the coating surface resulting into generation of the cracks at the indent

edges and corners. The test involved generation of indent (usually square, rhombus or kite shaped) using traditional micro Vickers hardness tester, with crack(s) generated at the corners being taken into consideration. The cracks with orientation parallel to the top surface were taken into consideration. For toughness measurement, the test load of 1000g was used which could generate cracking of the tough WC-Ni MMC coating especially fabricated using powder composition of 96 wt.% WC - 4wt.% Ni and 92 wt.% WC - 8wt.% Ni. The toughness of the coating is a function of applied load, crack length from the centre of the square based indent, half length of the diagonal in the direction of the crack and the hardness value of the coating at that load [204, 205]. The inability to predict Young's modulus for WC-Ni MMC coating due to non-homogenous microstructure resulted in restricting toughness prediction using *'c/a'* ratio. The ratio of the crack length to half diagonal length was finally used in deciding relative coating toughness as was done by Lopez and Mellor [208]. Here '*c*' is the average crack length value measured from the centre of the indent while '*a*' is the half length of the diagonal measured in the direction of the crack [204, 205].

The high magnification microscopic images of pure nickel and WC-Ni MMC coating were captured using scanning electron microscope (SEM). A SEM (EVO MA 15, Zeiss, Cambridge, UK) fitted with energy dispersive X-ray spectroscopy (EDS) was used for microscopy examination and analyses of the coatings. The Zeiss EVO scanning electron microscope can provide image magnification in range of 20 X to 100 KX. The Bruker Silicon Drift Detector used for Energy Dispersive X-Ray analysis/ mapping in EDS can reach peak resolution of 125 eV. The EDS assisted in rough quantification of elemental analyses of the coating which was clarified later on using X-ray diffraction analyses. To avoid charging of epoxy mounted coated samples during SEM examination, a thin layer of carbon film is pasted on substrate of the sample for effective carbon conductivity. Seldom use of unit sputter coater (EM SCD005, Leica [Baltec Instrument], Balzers, Liechtenstein) with provision of a carbon evaporation accessory is made. The SEM magnification involved examination of surface as well as cross-sectional areas of coated sample using secondary electron as well as back

scattered electron mode. The surface features were reflected in secondary electron (SE) images while determination of coating inhomogeneity and other phases was possible in back scattered electron (BSE) images.

After rough elemental analyses using EDS in SEM machine, the determination of different phases in the coatings was done using X-ray diffraction technique. The negative impact of oxidation, decarburization and increased carbide content can be ascertained by finding phases generated in them by X-ray diffraction analyses. The X-ray diffraction was done on X-ray diffracting equipment with following specification: Instrument = Rigaku Ultima IV – XRD with elemental copper as X-ray Source (Anode), Power = 40 kV / 44 mamps. For X-ray diffraction on coated samples, the samples were run with advancing thin film stage with glancing incidence angle of 1° while 2-theta angle ranged from 10 to 110°. The divergence slit for X-ray emitter was 0.1 while receiving and scatter slit were kept at open mode. Flat graphite crystal was used as mono-chromator to reduce fluorescence in back ground.

To measure other coating features like porosity, mean free path between carbides (which help to determine the homogeneity and distribution of the carbides in the composite) and the carbide size, the extensive use of image analysis software program (ImagePro, Media Cybernetics, Bethesda, MD, USA) was done.

The image analysis software used micrographs along the cross-sectional portion of the coating obtained using scanning electron microscopy (SEM). The presence of different elements in the coating was confirmed using elemental chemical analyses through energy dispersive X-ray spectral analyses (EDS) facility. For the image analyses of all the coatings, low magnification with 350X scale was used so that the whole cross-sectional thickness of the coating can be accommodated in the image. The measurement of mean free path between carbides in the coating involved measurement of the number of carbides at any section along the coating thickness. The fractioning of the number of carbides by total coating thickness at that section will indicate the number of carbides per unit length. At least six to seven sections were carried for each sample of the thermal-sprayed coating and

the average value defined the final mean free path between the carbides. The discussion on measurement of mean free path values for different cold-sprayed WC-Ni MMC coating was already elaborated in the following papers [71].

To measure WC-content in the WC-Ni MMC coating using Image analyses software, the binary colour combination method was used. The BSE-SEM mode of cross-sectional image of the WC-Ni MMC coating displayed nickel as dark/black entity while WC-based carbides as white entity. The area under scanner is selected by marking its boundaries and then the Image Pro software marks the carbide (WC-12Co) zones with marker. After adjusting the slider so that marker selects as many carbides as possible in demarcation area, the area is measured. The ratio of area of white zone with respect to the overall scanned area gives the percentage of WC-12Co content in the coating. Numerous such readings of cross-sectional images along the length of the sample were taken and the average of these reading will decide the final WC content in the coating. Same procedure is used while measuring porosity content in the WC-Ni MMC coating, only difference that porosity is darker in colour than nickel binder and BSE-SEM image used for identifying it should make difference in colour of nickel and porosity properly visible.

3.5 Dry abrasion testing

The main purpose of this research was to conduct qualitative and quantitative wear measurement of the non-FSP treated and FSP-treated thermal-sprayed coating. Fig. 3.1 shows schematic of dry abrasive wear test used to find wear rate of the coatings that were explored in this study.

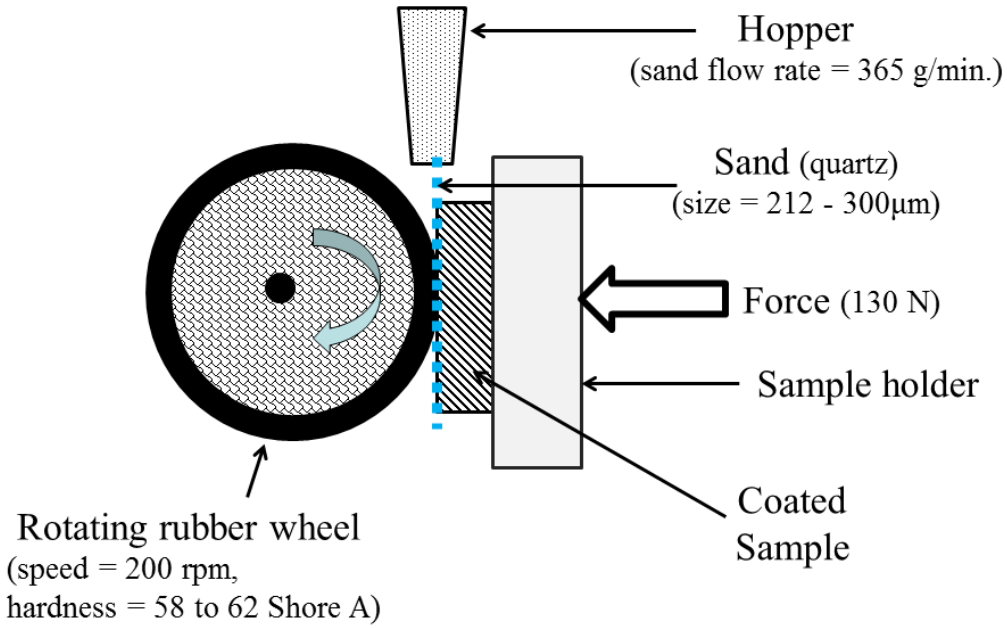

Figure 3.1: Schematic of dry abrasion wear test [6]

The wear tests for different cold-sprayed WC-Ni MMC coating were carried out on the basis of the rough estimate of wear rate using its hardness and estimated toughness value. For all the coating, wear rate was obtained using dry abrasive wear test (ASTM G-65 (04) test) [6]. Although the wear test was same, However lower hardness and toughness value prompted use of different wear procedures for cold sprayed pure nickel and different WC-Ni MMC coatings. The use of same procedure resulted into digging or wearing out of the coating as well as the substrate resulting in erroneous wear rate readings. For pure cold-sprayed nickel coating, 'Procedure C' (total wheel revolutions during test = 100 and duration = 30 sec./0.5 min.) is used. For WC-Ni MMC coatings fabricated from powder composition of 50 wt.% WC - 50 wt.% Ni, 75 wt.% WC - 25 wt.% Ni and 92 wt.% WC - 8wt.% Ni, 'Procedure E' (total wheel revolutions during the test = 1000 and duration = 5 min.) while for WC-Ni MMC coating fabricated from powder composition of 96 wt.% WC - 4wt.% Ni , ASTM G-65(04) test with 'Procedure B' (total wheel revolutions during the test = 2000 and duration = 10 min.) is used. Except wheel revolutions during the test, all the parameters in ASTM G-65 test were kept constant. The wheel material used for wear test was

neoprene derivative due to unavailability of chlorobutyl rubber. Same hardness of wheel material as specified in ASTM standard was maintained here i.e. 60 shore A durometer. The parameters of ASTM G-65 (04) test are as mentioned in Table 3.8.

Table 3.8. ASTM G-65 parameters

Parameters	**Values**
Load (N)	130
Wheel speed (rpm)	200
Abrasive used	AFS 50/70 Silica (Quartz) (US Silica, Ottawa, IL, USA)
Abrasive size (μm)	212 - 300
Abrasive flow rate (g/min)	365
Test duration (min)	10 (for total wheel revolution of 2000)
Wheel material	Neoprene

For HVOF-sprayed pure nickel coating, ASTM G-65 (04) test with 'Procedure C' while for WC-Ni MMC coating fabricated from optimized powder composition (96 wt.% WC – 4 wt.% Ni), 'Procedure B' is used. For FSP-treated cold-sprayed as well as HVOF-sprayed WC-Ni MMC coating fabricated from optimized powder composition, ASTM G-65 test with 'Procedure B' to calculate the wear rate for individual coatings was proposed. To calculate the wear rate, two samples per composition (n = 2) is used. The sample count of two was also selected instead of one to account for repeatability and to take care of any discrepancy introduced during powder mixing or fabrication process as per the principle of replication [209].

The wear rate of the coating (Eq. 3.1) is carried out by using the Archard's formula as mentioned below [210]:

$$W = \frac{\Delta m}{(\rho \times P \times S)}, \qquad (3.1)$$

where,

W = wear rate of the coating, mm^3/N-m

Δm = coating mass difference before and after the wear test, g

ρ = density of the composite coating, g/mm^3

P = normal load applied on the coating during the wear test, N

S = total sliding distance during the wear test, m

The wear tested coatings were sectioned across the thickness to understand the wear mechanism of the coating. After sectioning the samples, depending on the length of the sectioned piece, it is either mounted in the resin or used as it. The sectioned samples are then polished using same procedure as mentioned above while doing hardness test. After polishing the sample surface to "mirror polish" finish, it is then viewed under the scanning electron microscope to get back scattered electron (BSE) and secondary electron (SE) images.

The wear tested non-FSP as well as FSP-treated thermal-sprayed pure nickel as well as WC-Ni MMC coatings were examined using SEM in both backscattering electron (BSE) and secondary electron (SE) modes to determine the chemical composition, topography, wear damage, as pre-requisite for wear mechanism determination. A detailed description of the preparation of the cross-sectional samples can be found elsewhere [71].

Chapter 4. Wear Performance of As-sprayed cold-sprayed WC-Ni MMC Coatings

Cold-sprayed pure nickel and WC-Ni MMC coating containing varying content of WC is obtained. After characterization, the coatings were wear-tested using dry abrasive wear test (ASTM G-65 test). Various aspects of this study are covered in different sub-sections mentioned below.

4.1. The difference in the WC content in the powder and coating compositions of cold-sprayed WC-Ni MMC coating

Various cold-sprayed WC-Ni MMC coating containing varying content of WC is obtained. It is found that the powder used for depositing cold-sprayed WC-Ni MMC coating has a different composition compared with coating composition (see Table 4.1). In table 4.1, the '*n*' stands for number of images that were studied to calculate WC content in WC-Ni MMC coating. The main reason for this is the difference in the density of the WC-12Co and Ni powder. Before spraying, the powders of agglomerated WC-Co and nickel were blended mechanically to get uniform and homogeneous mixture. However, during spraying, it was difficult to maintain a constant powder composition due to density differences in the components of the powder.

Table 4.1. WC content in coating for respective mechanical blend used to fabricate cold-sprayed WC-Ni MMC coating [71].

Mechanical Blend	**WC content in coating (wt.%)**
50 wt.% WC – 50 wt. % Ni	7 ± 3 (n = 9)
75 wt.% WC – 25wt. % Ni	19 ± 3 (n = 10)
92 wt.% WC – 8 wt. % Ni	56 ± 4 (n = 12)
96 wt.% WC – 4 wt. % Ni	66 ± 2 (n = 12)

4.2. Correlation among mechanical properties of cold-sprayed pure nickel and WC-Ni MMC coatings

Cold spraying was used to fabricate WC-Ni MMC coatings for wear applications. The performance of the coatings was quantified by investigating the wear rate as a function of mean free path between the reinforcing hard WC particles and the overall hardness of the coating. The Fig. 4.1(a) shows graph of mean free path between reinforcing WC-12Co particles versus wear rate plotted for cold-sprayed WC-Ni MMC coating fabricated with the varying powder composition of WC-12Co in the mechanically blended mixture. In graph, the numerical value at each co-ordinate indicates WC-12Co content in the powder while numerical value in parenthesis indicate wt. % of WC-12Co content in the WC-Ni MMC coating. It can be seen from the graph (Fig. 4.1(a)) that with progressive increase in the content of hard reinforcement, WC-12Co, in the mixture results in a progressive decrease in wear rate and mean free path.

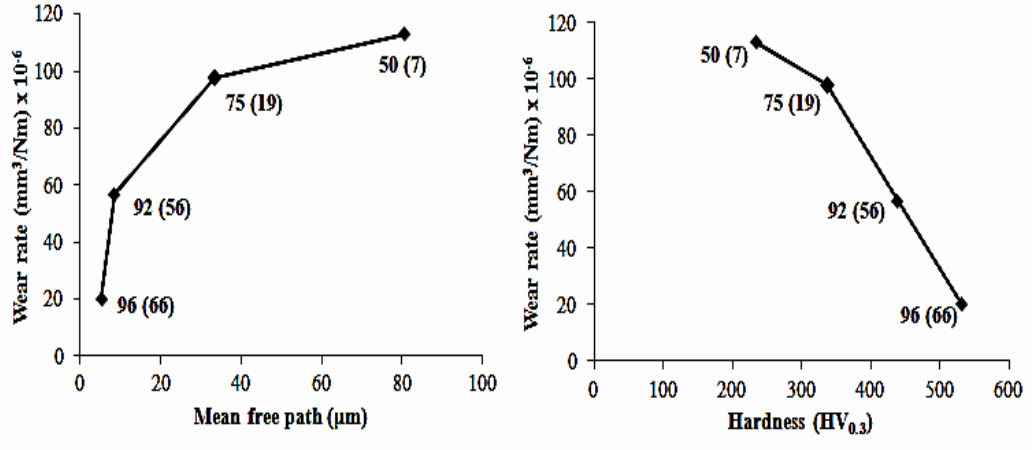

Figure 4.1. Graph of (a) wear rate verses mean free path between WC-12Co particles and (b) wear rate verses hardness of WC-Ni MMC coating [71].

It is clear from Fig. 4.1(b) that as the hardness is increasing due to the progressive increase in the WC-content in the WC-Ni MMC coating, the wear rate is also lowering [71]. The increased WC-12Co content in the MMC coating results in lowering of the mean free path. This reduces the content of soft, ductile nickel binder trapped between carbide particles. The impact of WC-12Co particles during spraying results in reduced coating porosity (see Table 4.2). The lowering of mean free path results in more content of WC-12Co in coating resulting in increased rigidity and compactness. The increased WC-12Co content in the MMC coating results in overall increase in coating's hardness although it is heterogeneous in composition. Such high WC-content WC-Ni MMC coating when subjected to wear results in load sharing between hard reinforcing particles and soft binder. The soft binder will undergo deformation. However, hard reinforcement will transfer load to surrounding binder. The hard WC-12Co particles being wear resistant will result in lowering of the wear rate as their content in the MMC coating is increased [71]. This phenomenon has been elaborated in upcoming section 4.4.

Table 4.2 also shows porosity for cold-sprayed pure nickel coating and different WC-Ni coating with varying content of WC-12Co in the mixture. In Table 4.2, '*n*' indicates number of samples taken to arrive at mentioned value. It is clear that porosity is also showing a decreasing trend as the content of the WC-12Co in the mixture is increased.

Table 4.2. Porosity content for different mechanical blend used to fabricate cold sprayed pure nickel and WC-Ni MMC coating [71].

Mechanical Blend	**Porosity in MMC coating**
Nickel control	$7 \pm 0.2(n=3)$
50 wt.% WC – 50 wt. % Ni	2 ± 0.7 ($n = 9$)
75 wt.% WC – 25wt. % Ni	$0.8 \pm 0.2(n = 10)$
92 wt.% WC – 8 wt. % Ni	0.002 ± 0.005 ($n = 9$)
96 wt.% WC – 4 wt. % Ni	0.3 ± 0.1 ($n =12$)

4.3. Toughness measurement for cold-sprayed pure nickel and different WC-Ni MMC coating

It has been mentioned in many papers that wear of any material is function of hardness as well as interfacial toughness. One such formula relating wear rate to hardness and toughness is as follows [212]:

$$V = \frac{(P^{9/8} \times E^{4/5} \times l)}{K_{IC}^{1/2} \times H^{1/2}} \qquad (4.1)$$

Where,

V = volume of material removed, mm^3

E = Young's Modulus of material, GPa

P = Applied load during wear, N

l = sliding distance, m

K_{IC} = Fracture toughness, MPa-$m^{1/2}$

H = Material Hardness, kg/ mm^2

For cold-sprayed WC-Ni MMC coating, it is clear from Fig. 4.1 that increase in hardness has contributed to increase in wear rate. As per Eq. (4.1), toughness is also important quality influencing wear rate. Toughness indicates energy absorbed by the material during fracture. Hence, toughness measurement of cold-sprayed pure nickel and WC-Ni MMC was conducted.

Toughness measurement in cold-sprayed pure nickel and WC-Ni MMC coating is a difficult task. The main reason for this is due to the presence of large content of voids for pure nickel coating and non-homogenous distribution of carbides for WC-Ni MMC coating. The presence of large content of voids results in non-uniform distribution of load during toughness measurement. This results in material spreading and occupying the void space during deformation resulting in erroneous toughness reading. It showed same phenomena when toughness measurement was tried for cold-sprayed pure nickel coating (Fig. 4.2 (a)). The application of 1000 gf load on nickel coating resulted into sinking of coating, However no distinct cracking at edges or corners was visible. The cracks even if present were difficult to distinguish from the inter-layer splats present in the coating. Also, it is postulated that application of load by hardness tester resulted in material spreading out and filling the pre-existing voids. Due to this, it is less likely for coating to fracture; and may give wrong prediction of high toughness.

For cold-sprayed WC-Ni MMC coating, the cracking was distinct; indicating that material has shown progressive improvement in toughness with increasing content of WC in the coating (Fig. 4.2 (b) – (e)). The addition of WC to the coating would surely affect the overall toughness, since WC is hard and tough material. Also, toughness indicates the adhesive toughness between carbides and nickel binder. If the adhesion is incomplete resulting in voids or pores between the phases, then cracking will occur easily. The main reason for this is the incomplete bonding indicating loosely held carbides in the binder of the composite. So application of load will result in easy breaking off of the bonds, ultimately cracking the composite. The cracking will also be motivated under the presence of pores which will offer least resistance for crack propagation. Thus, crack propagation will be faster in composite containing higher porosity content [22].

For WC-Ni MMC coating fabricated from powder composition of 50 wt.% WC - 50 wt.% Ni, the toughness measurement using Vickers hardness tester showed clear cut cracking with numerous cracks on sides as well as at the corners of the indent (Fig. 4.2 (b)). Since the coating contained more than 95 wt.% of Ni in its

composition, it is expected that coating will be soft and indent size will be bigger in comparison to visible indents in other WC-Ni MMC coating. For toughness measurement, the cracks located at the corner of the indent are taken into consideration [205]. It is found that the cracks at the indent corners seem to follow path of least resistance. Cracks are found to propagate usually in the soft, ductile nickel binder zone only. On confronting hard rigid WC-12Co agglomerated particles, crack would either by-pass them or they would break the soft cementing cobalt binder present between individual WC particles. Toughness being function of Young's modulus of the material; hence suitable Young's modulus value was suggested for the coating. However non-homogenous distribution of carbides in the coating increased uncertainty in prediction of Young's modulus value. Hence, Young's modulus value was discarded and toughness measurement was cancelled. Instead of quantitative prediction of toughness value, the ratio of crack length (*c*) to half diagonal length of the indent (*a*) was taken into the consideration. The toughness measurement procedure was used by Lopez – Mellor [208]. Thus, the higher value of '*c*/*a*' will indicate that toughness is less and coating will wear out faster.

For WC-Ni MMC coating fabricated from powder composition of 75 wt.% WC - 25 wt.% Ni, the coating did not showed much content of WC in the MMC coating (Fig. 4.2 (c)). The cracking tendency was less compared to coating fabricated from powder composition of 50 wt.% WC - 50 wt.% Ni. This coating showed numerous cracks at the sides as well as at the corners of the hardness indent, indicating that coating has low toughness value. The crack width was narrow when compared with cracks in coating fabricated from powder composition of 50 wt.% WC - 50 wt.% Ni.

Same procedure was continued for WC-Ni MMC coating fabricated from powder composition of 92 wt.% WC - 8 wt.% Ni and 96 wt.% WC - 4 wt.% Ni (Fig. 4.2 (d) and (e)). It is seen that as coating with powder composition changed from 75 wt.% WC - 25 wt.% Ni to 92 wt.% WC - 8 wt.% Ni, the cracking tendency reduced dramatically (Fig. 4.2 (c) and (d)). In fact, cracking, if observed, were usually at the corners, indicating effect of triaxial state of stress. The indent size

was small and even crack length was small. Crack width was thin and difficult to see at the magnification used for WC-Ni MMC coating containing lower content of WC. This indicates that radial and penny shaped cracks have not travelled so deep into the microstructure. The cracking tendency reduced significantly (see Table 4.3) as we moved from coating fabricated from powder composition of 92 wt.% WC - 8 wt.% Ni to 96 wt.% WC - 4 wt.% Ni. This indicates substantial improvement in toughness even with slight change in WC content in the content. This was attributed to the uniformity and homogeneity of the carbides in the coating. Also, increased content of WC-12 Co particles reduced mean free path between them. Thus, the amount of soft, ductile nickel binder distributed between carbides is reduced. Thus, crack tip will be offered strong resistance for its propagation due to increased content of WC in the coating. Table 4.2 indicates the number of times hardness indents that were taken ('*n'* value) and the percentage of indents which showed cracks for respective coating.

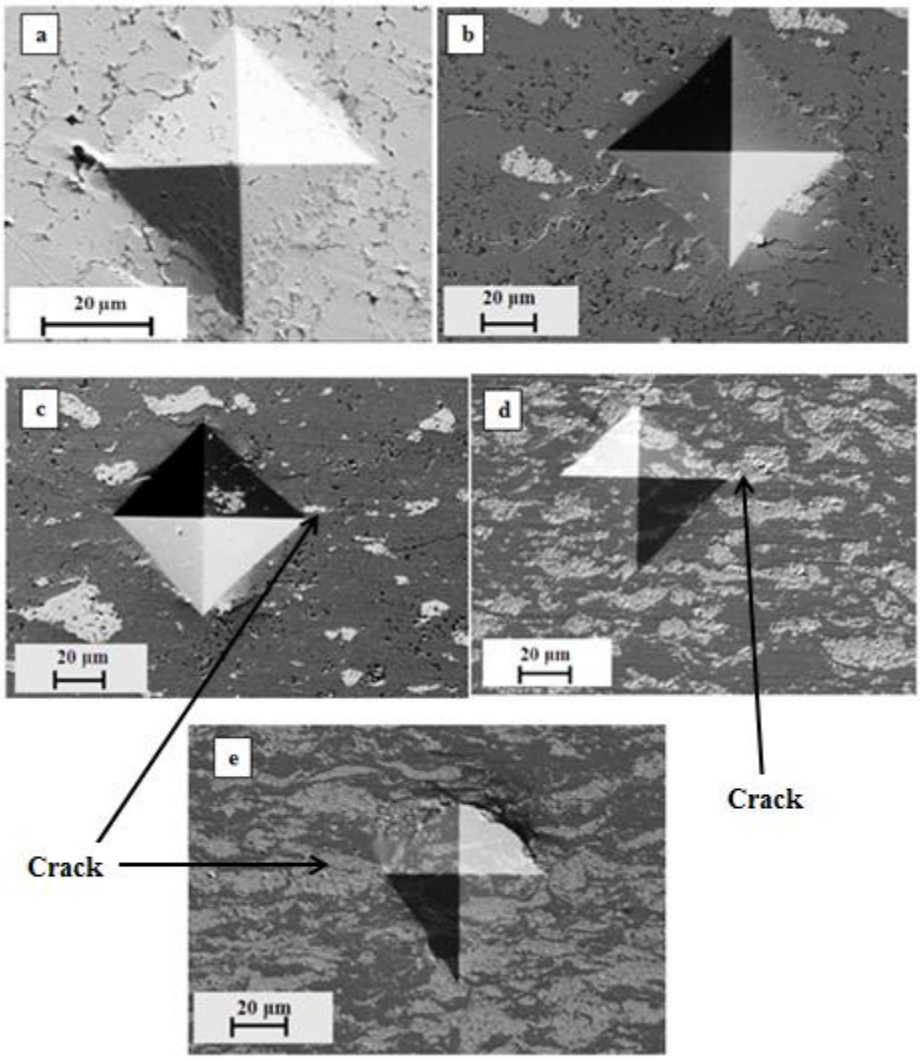

Figure 4.2. SEM image of cold-sprayed (a) pure nickel coating, (b) WC-Ni MMC containing 7 wt.% WC, (c) WC-Ni MMC containing 19 wt.% WC, (d) WC-Ni MMC containing 56 wt.% WC, and (e) WC-Ni MMC containing 66 wt.% WC, with indents generated by 1000 gf load.

Thus, from qualitative representation of toughness measurement, it is clear that toughness value of the WC-Ni MMC coating increased progressively as the content of WC-12Co is increased.

The '*c/a*' ratio for WC-Ni MMC coating fabricated from powder composition of 50 wt.% WC - 50 wt.% Ni and 75 wt.% WC - 25 wt.% Ni was not taken into consideration. The reason for this lies in presence of numerous cracks at sides as

well as at the corners. It means that load exerted during toughness measurement resulted into fracturing of material at sides as well as at corners. Thus, load applied during test have been distributed and resulted into fracturing of material all around the indent. Hence, crack length at corner would not exactly correspond to the load applied during toughness measurement.

Table 4.3. Crack generation percentage in the various coatings and the respective *c/a* ratios.

WC Content in Coating (wt.%)	**Percentage of Indents with Cracks (%)**	***c/a* ratio**
0	100 (n = 10)	n/a
7	100 (n = 16)	n/a
19	100 (n = 15)	n/a
56	82 (n = 22)	1.7 ± 0.5 (n = 18)
66	22 (n = 9)	1.9 (n = 2)

4.4. Wear analyses of as-sprayed cold-sprayed pure nickel and WC-Ni MMC coating

The cold-sprayed pure nickel and WC-Ni MMC coating were wear-tested using the ASTM G-65 wear abrasion test procedure. The wear result of cold sprayed coating showed complete ductile behavior for pure nickel coating and a combination of ductile behavior and fragmented wear debris for WC-Ni MMC. The wear mechanism of pure nickel and different WC-Ni MMC is discussed in coming sub-sections.

a) Cold-sprayed pure nickel coating

The wear of the cold-sprayed pure nickel coating showed heavy scratching and ploughing on the surface (see Fig. 4.3). The surface had cracks and delaminated cracks were seen on the surface. The heavy ploughing and ridge formation on the surface indicated that the wear of the nickel coating must have happened due to the combination of ploughing and delamination cracks.

A close look at Fig. 4.3 will indicate straight scratches on the surface. This indicates that ploughing of surface due to abrasives must have happened unabated to long distance. The material removal in such soft material usually happens in the form of continuous chips. The volume of chips will be less than that of the volume of material removed due to progressive plastic deformation of chip ahead of abrasive.

The final breaking of chips happens due to increased hardening at the section which is holding it with parent material [13, 14, 97 - 100, 121, 212]. The scratches do not seem to be deep, indicating that the depth of penetration is less. Hence, impingement angle of abrasives on surface is less [14, 211].

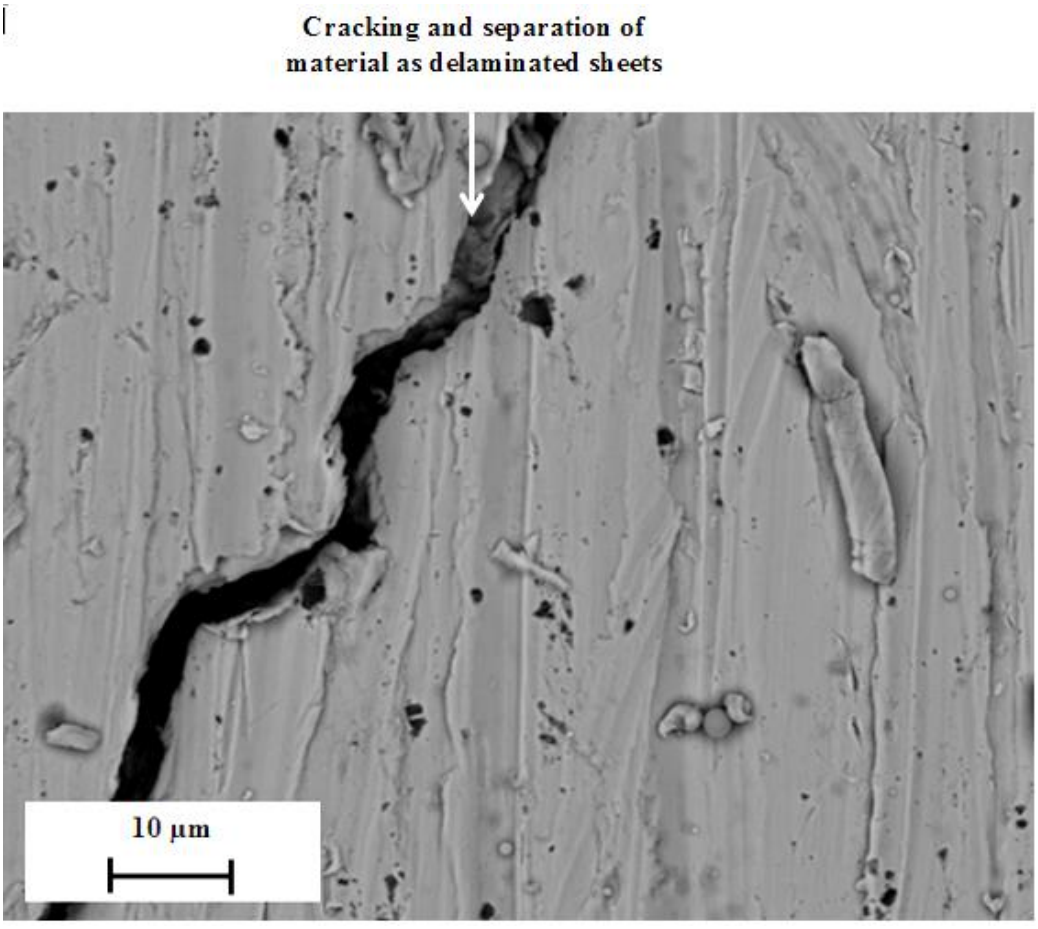

Figure 4.3. SE-SEM image of surface of wear-tested cold-sprayed pure nickel coating showing presence of ploughing and scratching on the surface.

The cross-sectional images of the pure nickel coating indicated presence of numerous lateral and longitudinal cracks (Fig. 4.4 and 4.5). The lateral cracks emanating from the surface travelled all the way through the thickness of the coating and met the longitudinal sub-surface cracks. The sub-surface cracks were mostly straight and parallel to the surface. There was increased presence of pores in the coating, mostly concentrated near the top surface (Fig. 4.4 and 4.5). The increased porosity indicated that loading during wear resulted in the generation of pores or voids; partly due to poor cohesion between the nickel particles and partly due to the elongation of pre-existing voids after cold spraying under the effect of the stress [37, 57, 123, 124, 132, 148]. The main reason for poor cohesive toughness between nickel particles is due to low wettability of nickel particles and low tensile strength of the nickel which is peculiarity of low strength ductile material [37, 57, 132, 148]. During cold spraying, the spraying temperature results in softening and spreading of nickel on the surface. These spread - out nickel coating seem like sheets piled one above the other. The spreading of the nickel results in bonding among nickel particles at the asperities. The strength of the bond formed under compressive stress during spraying, may be slightly more than the parent material [102]. Such bonds when stressed during wear will be easily broken since increase in hardness is accompanied with increased brittleness [103, 142]. The breaking of bonds between these spread-out sheets results in it easy separation. Thus, cold-sprayed nickel coating when wear-tested showed separation of material in the form of delaminated sheets. Also, the bonding is imperfect, resulting in development of porous structure under stress [57, 102]. The existing pores under the action of tensile and shear stress during wear elongates and eventually collapses to form micro cracks [22]. Numerous such micro cracks can be seen scattered all over the material which then coalesced to form major crack. These cracks under the action of stresses join to form a major crack with an orientation parallel to the surface. The main reason for orientation parallel to the surface is due to the direction of movement of wear wheel over the surface [22, 123, 158]. The pores' elongation and orientation is strongly influenced by the sliding direction of abrasives and wheel on the surface [123].

The main reason for such crack instigation is the low tensile strength of the nickel. Also, cold-sprayed nickel has lot of the inherent pores in the microstructure which results in easy crack instigation and pore elongation under the action of the stress. This contributed to the lowering of the cohesive toughness of the coating [37, 57, 123, 124, 132, 148]. The continuous and straight cracks in the cross-sectional images indicate absence of hard, reinforcing particles to obstruct the flow of the cracks. The crack was slanted and travelled straight, indicating that the pores were closely spaced in that zone. The shear stress resulted in the shear loading of the material between pores, which easily fractured to provide a path for the crack propagation. The cracks were seen at the interface of the substrate and coating, indicating that the tensile stress waves generated due to impacting compressive stresses, were able to breach its toughness limit. This is evident in the form of crack being generated there. Thus, this portion is the vulnerable portion of the coating during wear. The travel of the lateral crack from the surface through the coating thickness indicates crushing of the coating under compressive stress which resulted in the fracture of the material [123]. Also, fluctuating load assisted in cracking of the microstructure indicating low fatigue toughness of the coating [123].

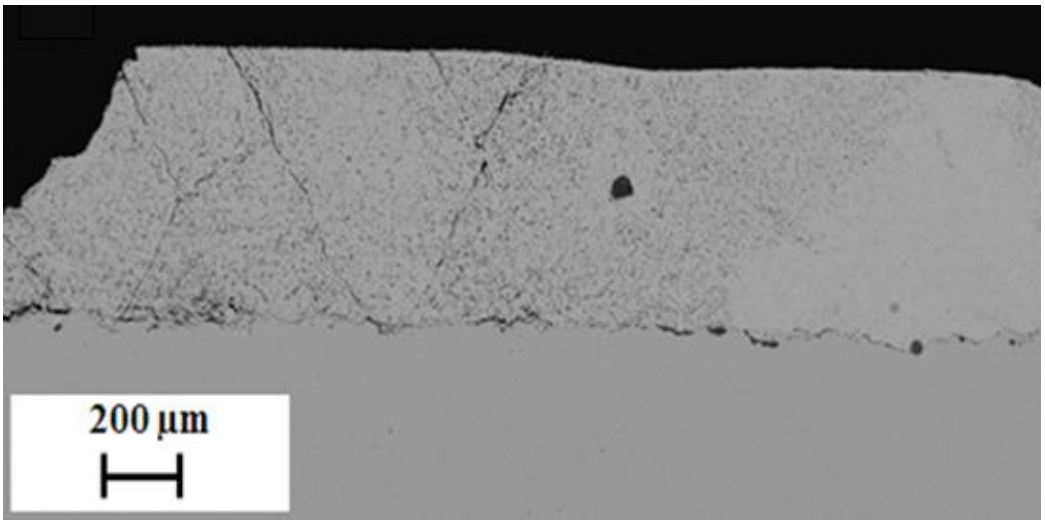

Figure 4.4. Cross-sectional BSE- SEM images of wear-tested cold-sprayed pure nickel coating at low magnification,

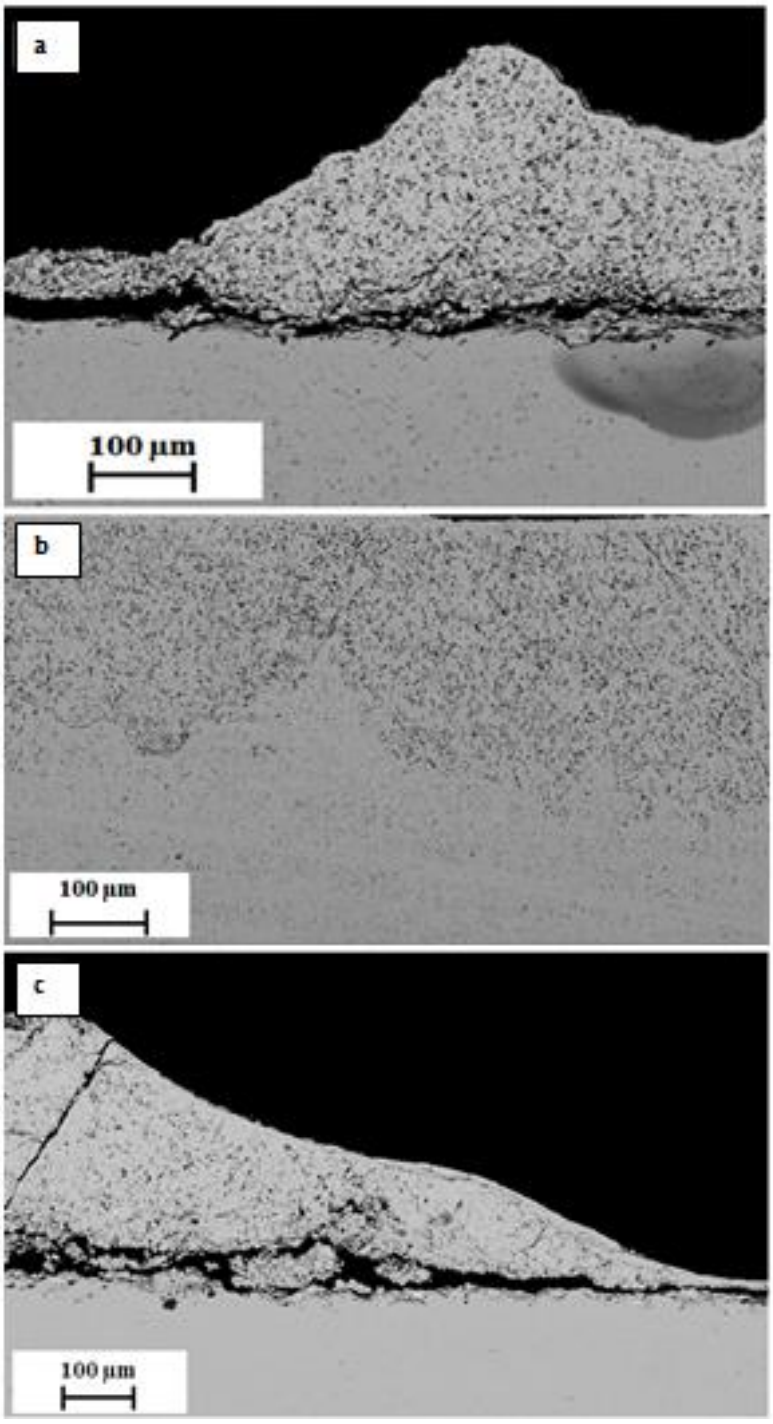

Figure 4.5 (a)-(c). Cross-sectional BSE- SEM images of wear-tested cold-sprayed pure nickel coating at high magnification,

b) Cold-sprayed WC-Ni MMC coating fabricated from powder composition of 50 wt.% WC - 50 wt.% Ni:

Figure 4.6 shows the top surface of wear tested WC-Ni MMC coatings fabricated from powder composition of 50 wt.% WC – 50 wt.% Ni. The surface showed scattered islands of hard, rigid WC-12Co agglomerated particles widely separated by soft, ductile nickel binder. The flowing abrasives induced heavy damage in the nickel region during wear. This is clear in the form of wide scars of abrasives (Fig.4.6 (a)). The impact of abrasives generated deep indents which are clearly seen as dark spots in the nickel region. In some cases, (Fig. 4.6), there were large and deep indents around hard, rigid WC-12Co reinforcement. This indicates that the motion of the flowing abrasives was thwarted by hard WC-12Co particles. Thus, abrasives must have either chipped off or had to change course of its path after striking this rigid portion.

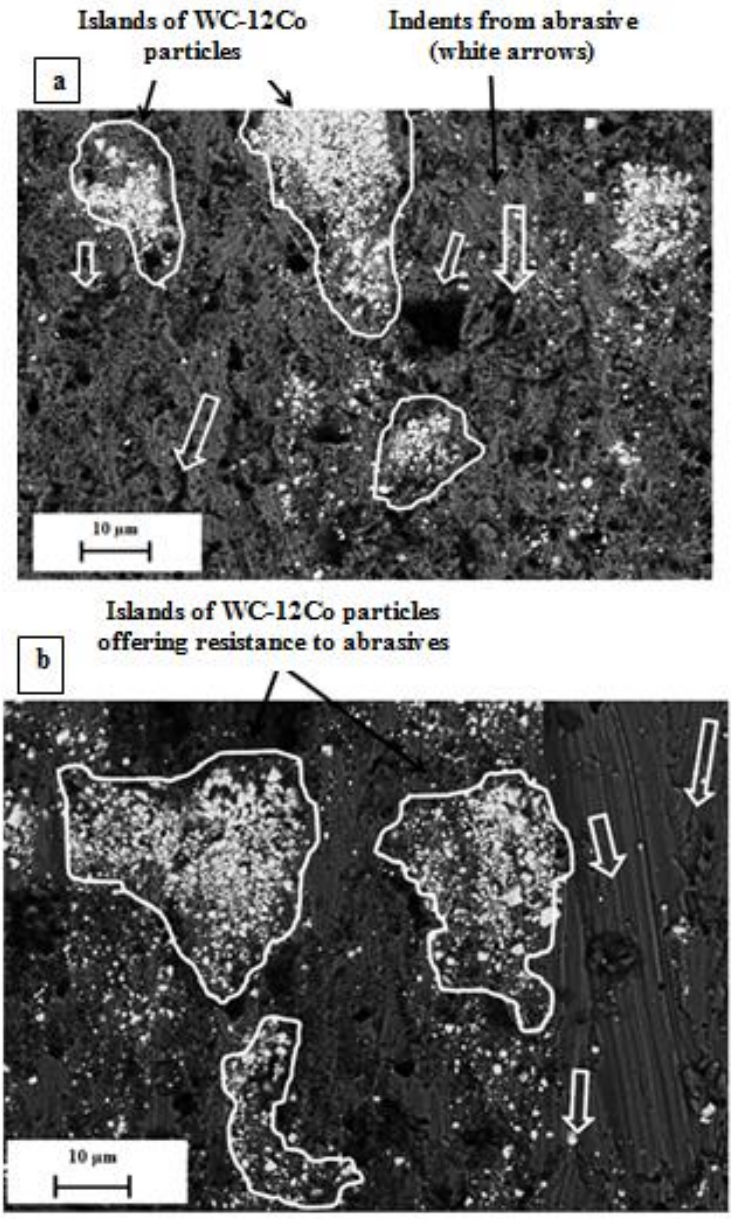

Figure 4.6. BSE-SEM surface image of WC-Ni coating fabricated from 50 wt.% WC- 50wt.%Ni.

Figure 4.7 shows a BSE-SEM cross-sectional image of WC-Ni MMC coating fabricated from powder composition of 50 wt.% WC - 50 wt.% Ni. The cross-sectional image reflected the essence of damage caused during wear. The surface showed initiation and propagation of crack easily in the material (Fig. 4.7 (b) –

(d)). The crack propagation seems to occur unhindered, due to large content of soft, ductile nickel binder. The sub-surface zone showed high pore content which seems to have nucleated under the action of hydrostatic (normal) and shear stress during wear test (Fig. 4.7 and 4.8). This porous structure seems to have contributed to the crack propagation in the microstructure. The carbide content is less and seems to have scattered widely in the sea of nickel binder. Cracking happened straight and seems to travel deep into the structure. It means that the fluctuating stress must have generated fatigue cracks which travelled unhindered deep into the material. Cracks on confronting carbides bypass them by traveling around them (Fig. 4.7 (c) and 4.8). Their drifting around carbide seems to be encouraged by the presence of voids nucleated under the action of compressive and shear stress. The presence of delaminated sheets indicates wear of this composite seems to follow delamination theory of wear (Fig. 4.7 and 4.8) [13].

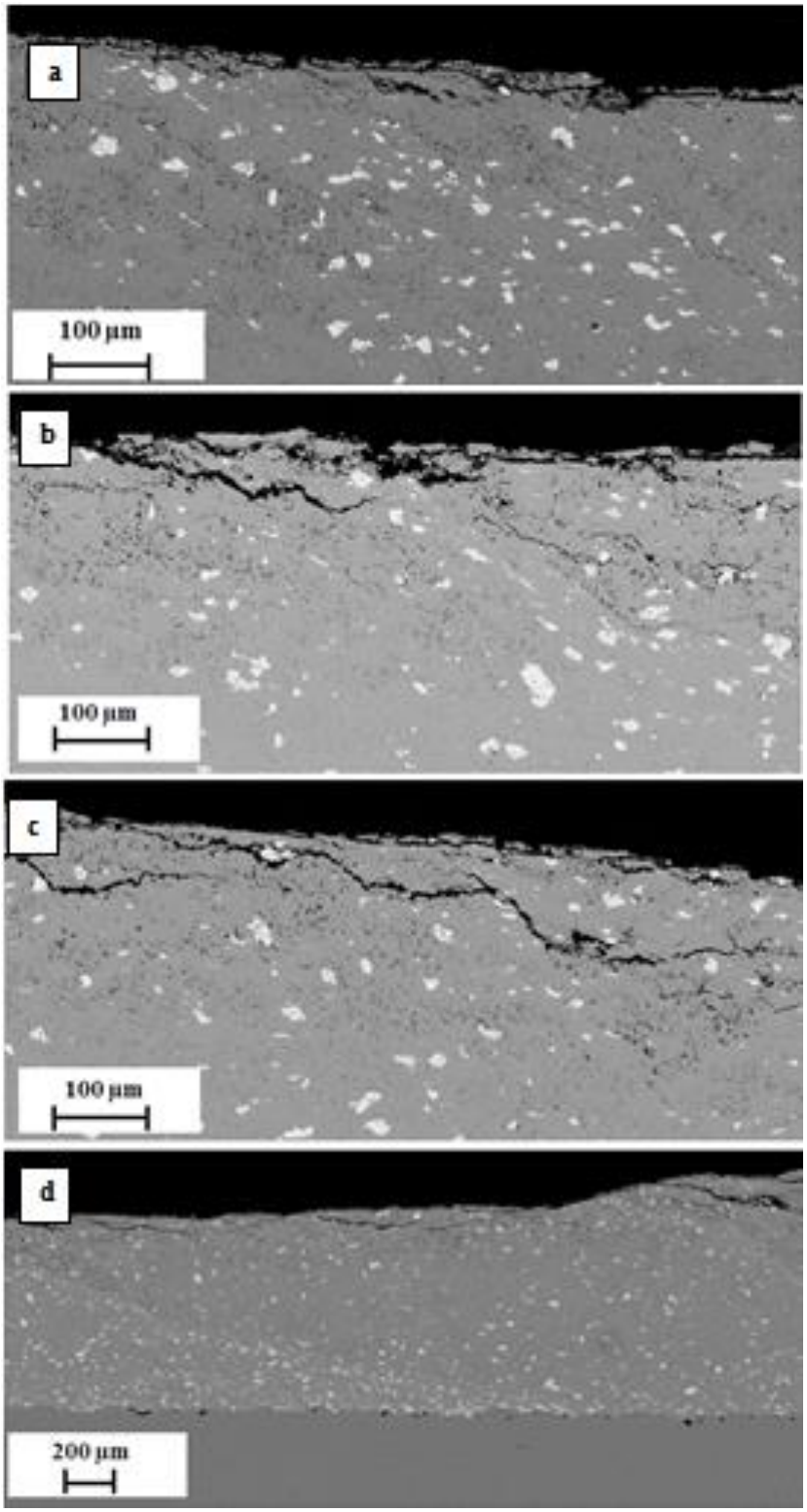

Figure 4.7 (a) - (d). BSE-SEM cross-sectional images of WC-Ni MMC coating fabricated from powder composition of 50 wt% WC - 50 wt.% Ni at low magnification.

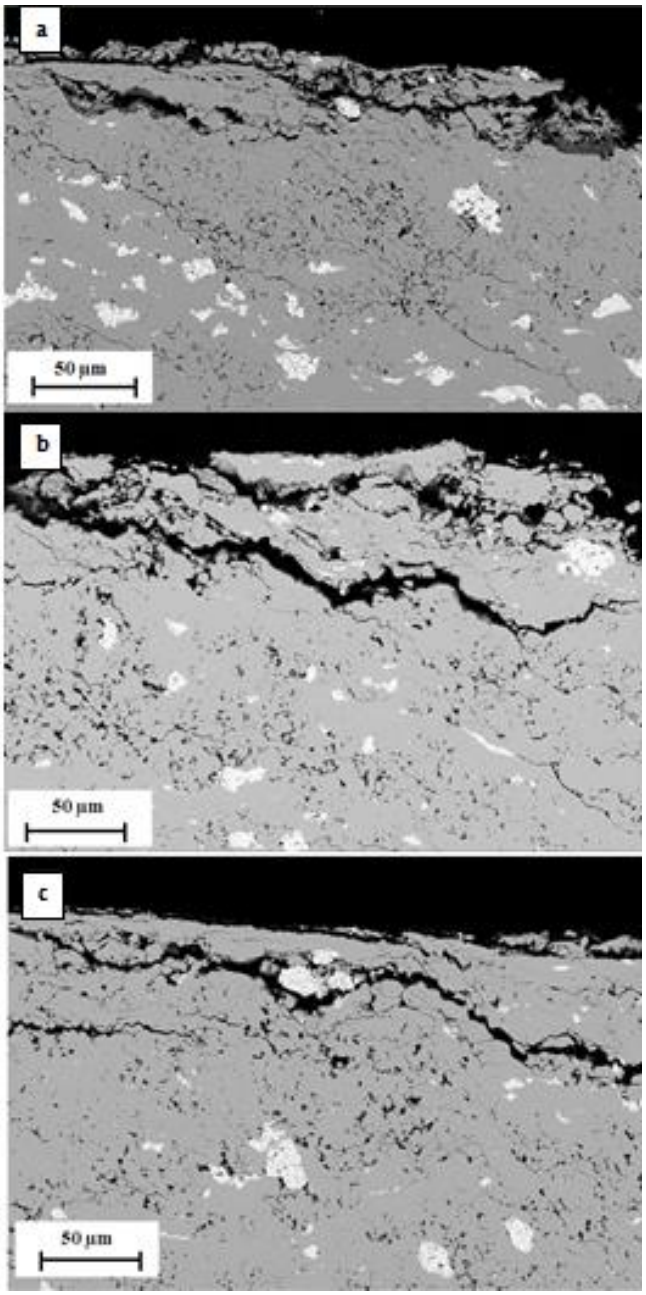

Figure 4.8 (a) – (c). BSE-SEM cross-sectional images of WC-Ni MMC coating fabricated from powder composition of 50 wt% WC - 50 wt.% Ni at high magnification displaying delaminated wear sheet.

c) Cold-sprayed WC-Ni MMC coating fabricated from powder composition of 75 wt.% WC – 25 wt.% Ni

Figure 4.9 shows the surface of the WC-Ni MMC coating fabricated from powder composition of 75wt.% WC - 25wt.% Ni. The wear tested surface showed similar appearance to that of WC-Ni MMC coating fabricated from the powder composition of 50 wt. % WC - 50wt. % Ni. The surface image showed islands of WC scattered (areas marked with white boundaries) in the sea of soft, ductile nickel binder (Fig. 4.9 (b)). The abrasives damaged nickel binder by indentation and scratching (Fig. 4.9 (a)). The impacts of the abrasives in the form of indents were clearly seen as black areas scattered in the microstructure (Fig. 4.9 (b)). The white border arrows indicate the path followed by abrasives on the composite surface (Fig. 4.9 (a)). The scratches are clearly visible on the coating surface indicating that nickel became vulnerable phase during wear. The widely scattered carbides were unable to offer substantial protection to nickel binder. Hence long scratches on the surface are clear indication that action of abrasives was unabated by the presence of carbides in composite. The main reason for this is the higher mean free path between carbides and lower carbide content in the composite [71, 192, 198]. The high value of average mean free path between hard WC-12Co reinforcement meant that they were widely scattered and did not offered sufficient resistance to the flowing abrasives. Also, relatively close value of wear rate of this MMC coating to coating fabricated from powder composition of 50 wt. % WC - 50wt. % Ni indicated that slight increase in carbide content in this coating was not effective in improving wear resistance of the MMC coating. The destructive effect of wear on MMC was also clear from the cross-sectional image of the wear tested coating.

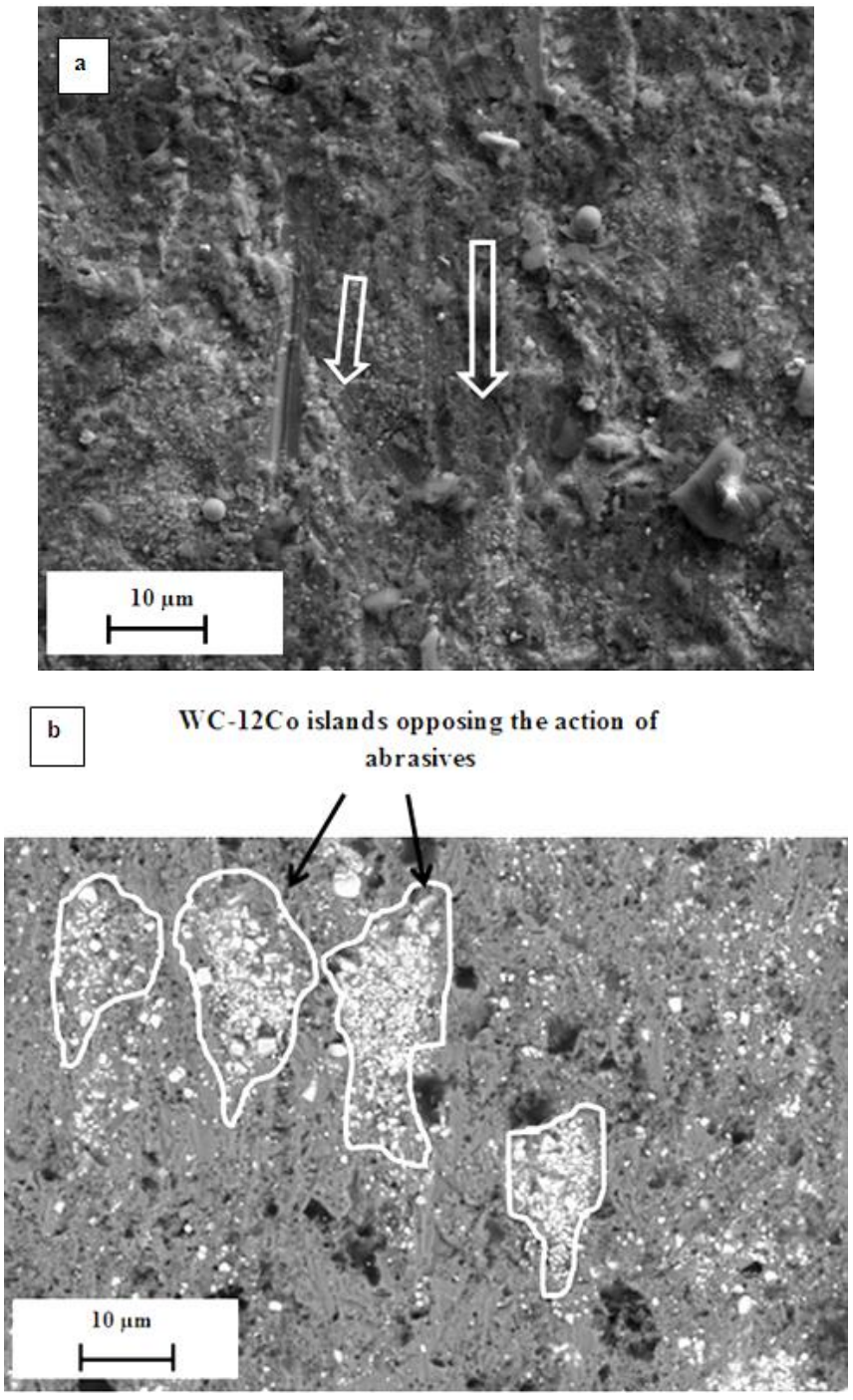

Figure 4.9. Surface image of coating fabricated from powder composition of 75wt.% WC - 25wt.% Ni. (a) BSE-SEM image and (b) SE-SEM image.

Figure 4.10 shows cross-sectional images of WC-Ni MMC coating fabricated from powder composition of 75 wt.% WC - 25 wt.% Ni. The Fig. 4.10 (a) and (b)

shows the cross-sectional image of the coating at lower magnification. It is clear in the image that wear resulted in formation of fragmented thin delaminated sheets which are loosely held together on its base. A close look at these wear sheets at higher magnification reveals typical features of these sheets. Figure 4.11 shows completely cracked zone of delaminated wear sheets. It was seen that there were numerous sub-surface cracks in the composite microstructure as well as in the delaminated wear sheets. The sub-surface cracks were wide and oriented parallel to the surface. The crack propagation seems to be motivated under the action of stresses generated during wear. The cracks travelled around favorable zones like soft nickel binder and voids present in the composite. A close look at images in Fig. 4.11 show presence of large voids in sub-surface zone which appear like they are elongated under the action of shear stress during wear. As per delamination theory, these voids usually nucleate at carbide-binder interface or due to cracking of soft binder under the action of stresses during wear. Such voids may either elongate to form big voids which pressurize surrounding areas and crack them or they may collapse to form microcracks with orientation in the direction of stress [121]. The elongation of voids pressurizes surrounding nickel binder and when this strain crosses fracture strain limit, nickel cracks. Numerous such cracks can be seen emanating from the void boundaries (see Fig. 4.11 (a) and (c)). The cracking is also seen around WC-12Co reinforcing particle as mentioned in Fig. 4.11 (a) which indicates that nickel binder around it has already strained during wear and further straining from void elongation resulted in easy cracking at the interface. The longer crack length on right hand side of the void in Fig. 4.11 (a) indicates that sliding direction is from left to right. Thus, stress orientation seems to motivate crack propagation in microstructure. The joining of the sub-surface crack to surface discontinuity like notches, indents, indicate that crack propagation is motivated by stressed or damaged zone on the surface. Thus, material wear seems to happen as per delamination theory [121].

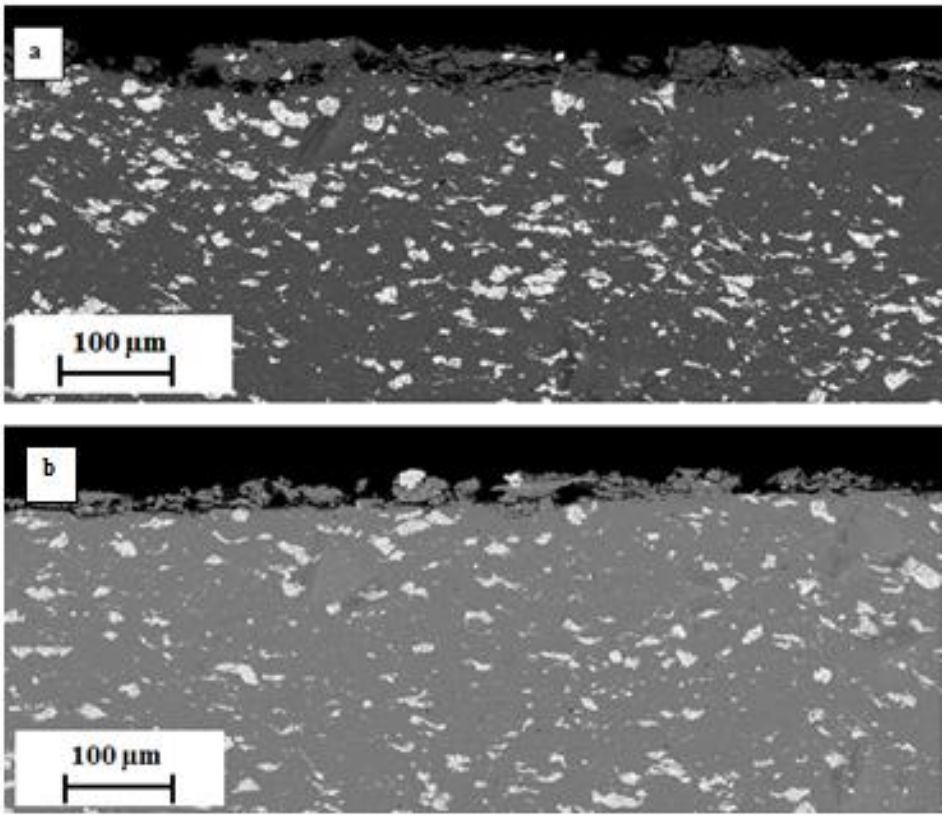

Figure 4.10. BSE-SEM cross-sectional image of worn out coating fabricated from 75 wt.% WC – 25 wt.% Ni at low magnification indicating fragmented wear sheets

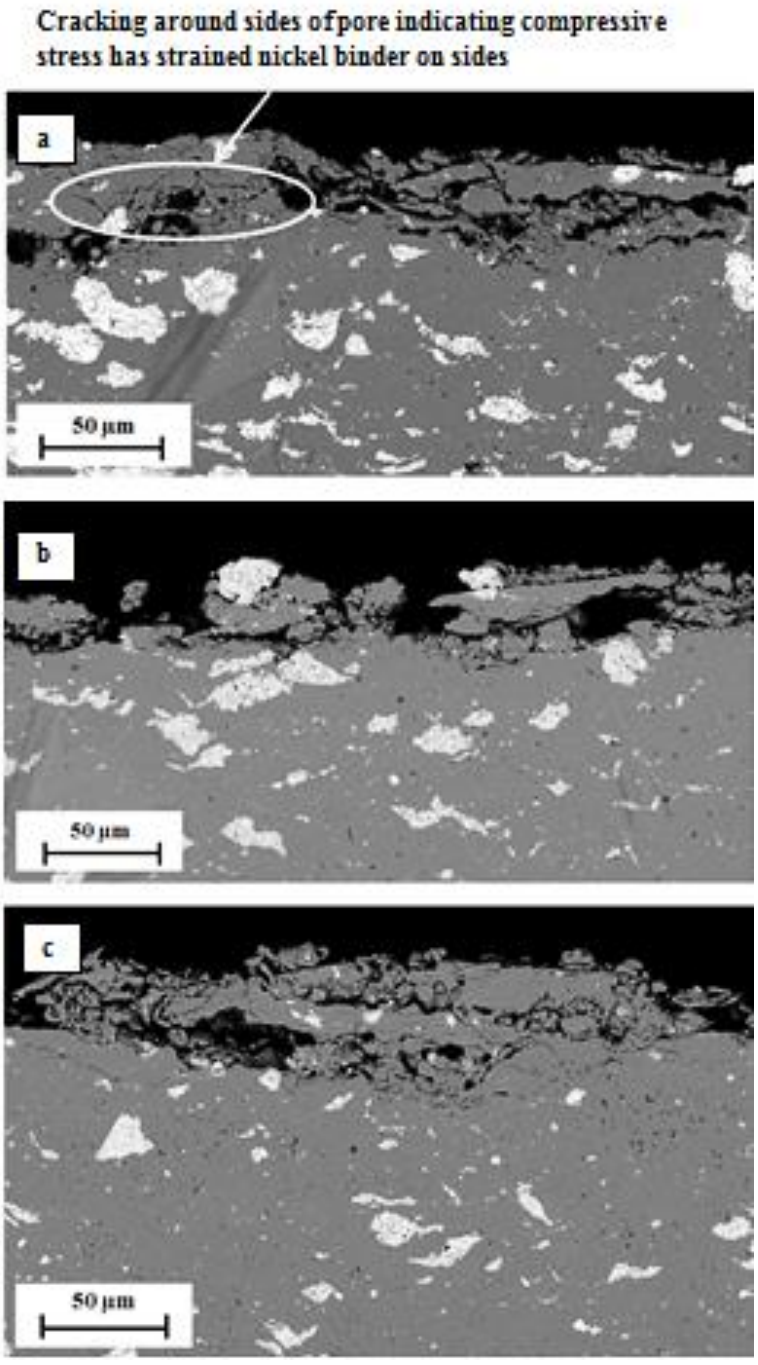

Figure 4.11 (a) – (c). BSE-SEM cross-sectional image of worn out coating fabricated from 75 wt.% WC – 25 wt.% Ni at high magnification.

d) Cold-sprayed WC-Ni MMC coating fabricated from powder composition of 92 wt.% WC – 8 wt.% Ni:

Figure 4.12 shows wear tested surface image of cold-sprayed WC-Ni MMC coating fabricated from powder composition of 92 wt.% WC - 8 wt.% Ni. The surface of this coating showed close resemblance to other WC-Ni MMC coating containing lower content of WC. Digging of abrasives had damaged the nickel binder region, while still protecting the hard, rigid WC-12Co reinforcement. The hard WC-12Co offered resistance to abrasives However they were still successful in scraping off the nickel in between these reinforcement islands. Arrows in Fig. 4.12 indicate the attack of abrasives on the surface. The path followed by the abrasives on the surface was not identical indicating that abrasives must have rolled on the surface during wear.

The Fig. 4.13 shows cross-sectional images for wear tested WC-Ni MMC coating fabricated from powder composition of 92 wt.% WC - 8 wt.% Ni. The total wheel revolutions used for this coating remained similar to that of other WC-Ni MMC coatings containing lower content of WC. The surface of the wear tested coating shows fragments of delaminated wear sheets loosely held together from sides and base. It indicates that attack of abrasives have resulted into crack being concentrated in sub-surface zone to a thickness of 10- 20 µm.

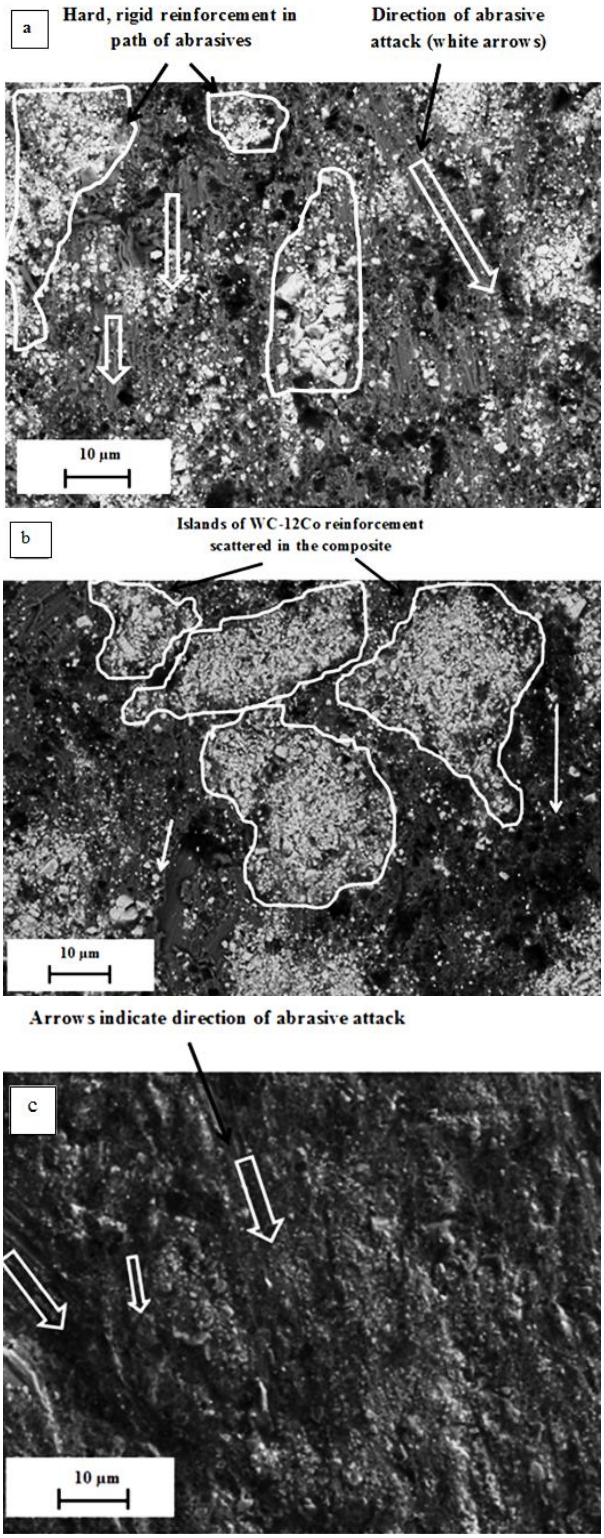

Figure 4.12. Surface image of wear-tested as-sprayed WC-Ni coating fabricated from the powder composition of 92 wt.% WC - 8 wt.% Ni.
(b) and (b) BSE-SEM image and (c) SE-SEM image

The cross-sectional image of wear tested WC-Ni MMC coating fabricated from powder composition of 92 wt.% WC - 8wt.% Ni showed numerous fragmented wear sheets scattered as the top surface of the composite coating. It means that wear of this coating must have followed the same route as mentioned by delamination theory [121]. A close look at these cross-sectional images show presence of numerous minute sub-surface cracks oriented parallel to the top surface (Fig. 4.13 (d)). Their presence around WC reinforcing particles ensured that void nucleation must be prominent reason for its origin. The presence of numerous voids in sub-surface zone indicates that crack propagation will be assisted by them. A clear view of crack branching out from sides of void is visible in Fig. 4.13 (d) which proves the postulate presented by delamination theory. Thus, void nucleation and crack generation are interconnected phenomena and is clearly indicative in cross-sectional image of this coating. The images of Fig. 4.13 (b) and (c) show presence of numerous scattered delaminated sheets on top surface. These sheets are generated during wear test and are clear indication that crack generation and propagation parallel to the surface are a prominent reason for this.

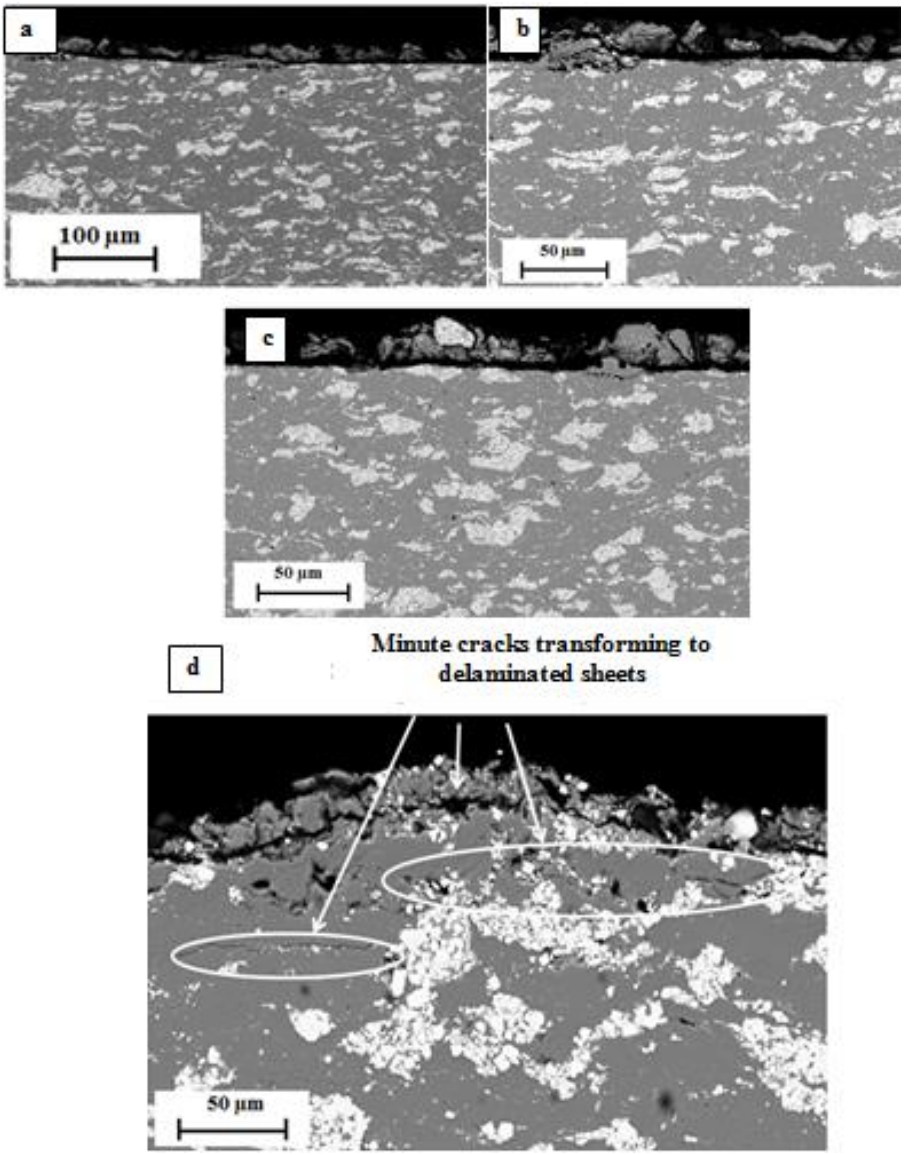

Figure 4.13. Cross-sectional BSE-SEM image of coating fabricated from powder composition of 92 wt.% WC – 8 wt.% Ni (a) at low magnification and (b), (c) and (d) at high magnification.

e) Cold-sprayed WC-Ni MMC coating fabricated from powder composition of 96 wt.% WC – 8 wt.% Ni:

The Fig. 4.14 (a) and (b) indicates the SE-SEM surface image of wear tested cold-sprayed WC-Ni MMC coating fabricated from powder composition of 96 wt.% WC - 4 wt.% Ni.

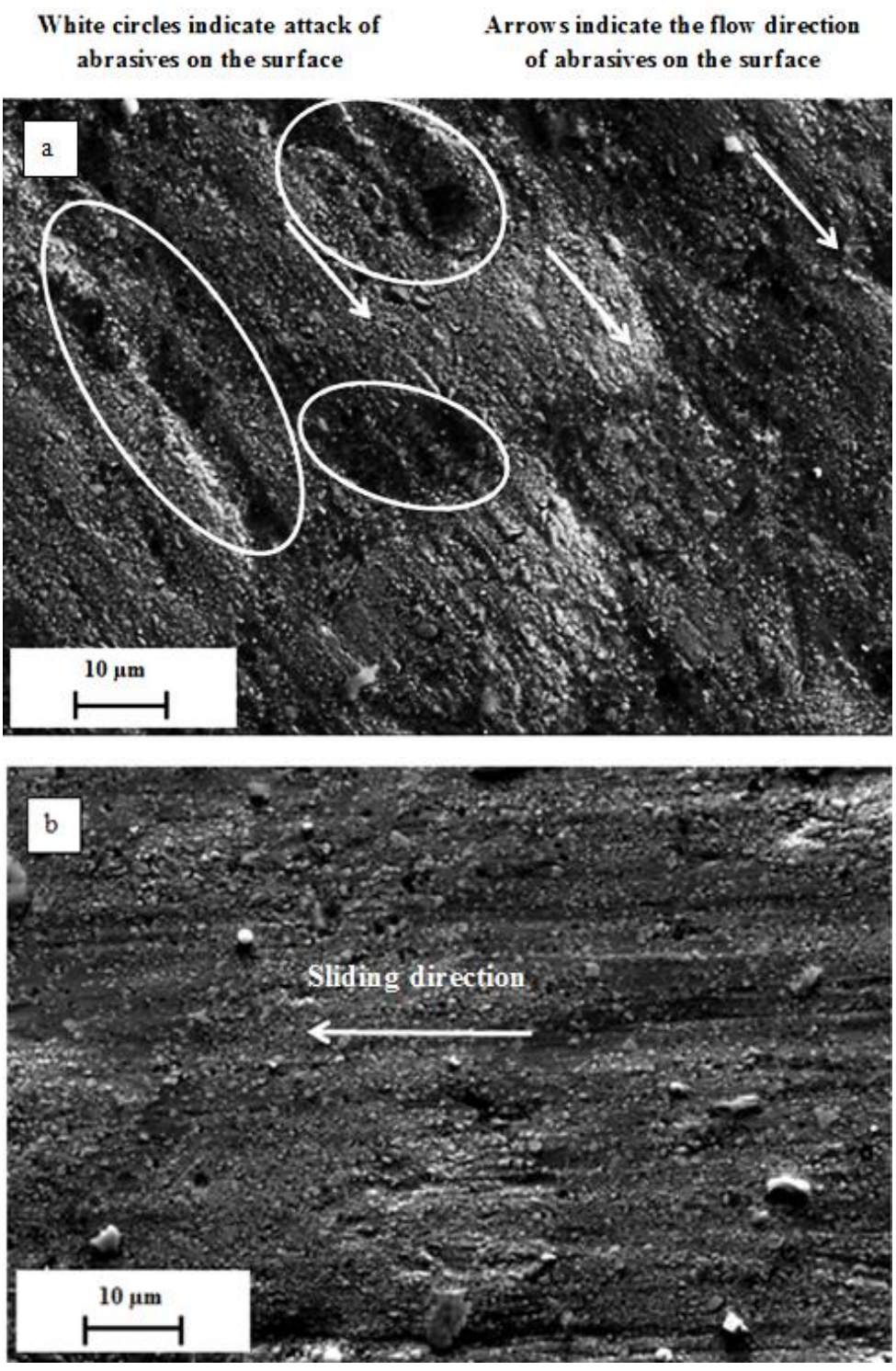

Figure 4.14 (a) and (b): SE-SEM surface image of WC-Ni MMC coating fabricated from powder composition of 96 wt.% WC - 4 wt.% Ni.

Compared to the surface image of cold-sprayed WC-Ni MMC coating containing lower content of WC, the surface image of this coating showed less damage. There were fewer scratches on the surface. The absence of ploughing and digging on the surface indicates that surface is mostly dominated by the WC particles. The role of the nickel is in form of thin layer of cementing material. Hence, it was not directly amenable to the attack of the abrasives. The surface had flow lines indicating orientation of carbides in the composite [158]. These flow lines also stem out from scratching of the nickel binder between the WC particles. Thus, the removal of nickel binder between WC-12Co particles indicates abrasive flow direction during wear. There were minute pits or depressions on the wear tested surface as indicated by white circles in Fig. 4.14 (a).

Figure 4.15 shows cracking in cross-sectional SEM image of WC-Ni MMC coating fabricated from powder composition of 96 wt.% WC - 4 wt.% Ni. The coating showed nearly straight crack However crack propagation seems to be influenced by the presence of weak spots like soft ductile nickel binder. The cracking seemed to be motivated by straining and tearing of nickel binder which provided path for crack propagation. The reason for this is reflected in the microstructure. The cross-sectional image of this coating showed lamellar microstructure. It looked like layered arrangement with alternate layers of soft, ductile nickel binder and hard, rigid WC-12Co. The greyish nickel trapped between hard, rigid WC-12Co reinforcement proved weak zone under fluctuating stress. The action of compressive and shear stress resulted in fracturing of the nickel binder. However crack nucleation seems to be caused due to pre-existing pore in the microstructure. Crack usually started due to the presence of pores which might have nucleated around hard, rigid, non-deforming WC-12Co particle under the action of normal and shear stress [121]. The stress must have torn the soft nickel binder covering the WC particle to result in pore. These pores under the action of stresses must have elongated to micro crack. A close look at Fig. 4.15 showed cracks following path of least resistance, resulting in formation of delaminated sheets. In Fig. 4.15 (b), the cracks close to the top surface have

joined the notch or damaged portion at the surface. The notch or dent seemed like an attack of abrasives which has resulted into lifting of the material from the surface. The abrasives seem to have gouged the surface which created a rift in the material. The crack generated at this location followed the path of least resistance by tearing apart the nickel binder. Crack width is large in this region, indicating that stress during wear resulted in easy fracturing of large content of nickel material with no resistance offered by surrounding hard carbide phase. The crack propagation might had commenced unabated till it encounters hard, rigid WC-12Co particles. At this juncture, the crack propagation was assisted by the bending stress generated due to lifting of the cracked portion. The cracked portion separated as sheet with one end fixed to the base. The flowing abrasives exerted lifting force. This bending stress then acts on the soft, ductile material behind the WC-12Co particles and crack progression happened [121]. Thus, cracks by-passed WC-12Co particles and crack propagation happened unabated even after encounter of hard phases in the composite. If the crack deviates and propagates deep into the material, then crack propagation rate decreased due to large demand of bending stress. Hence, such crack stops after propagating deep into the material. In few cases, crack propagated parallel or close to the surface and met some surface discontinuity or lateral fatigue crack resulting in fractured delaminated sheets as certain in Fig. 4.15 (b).

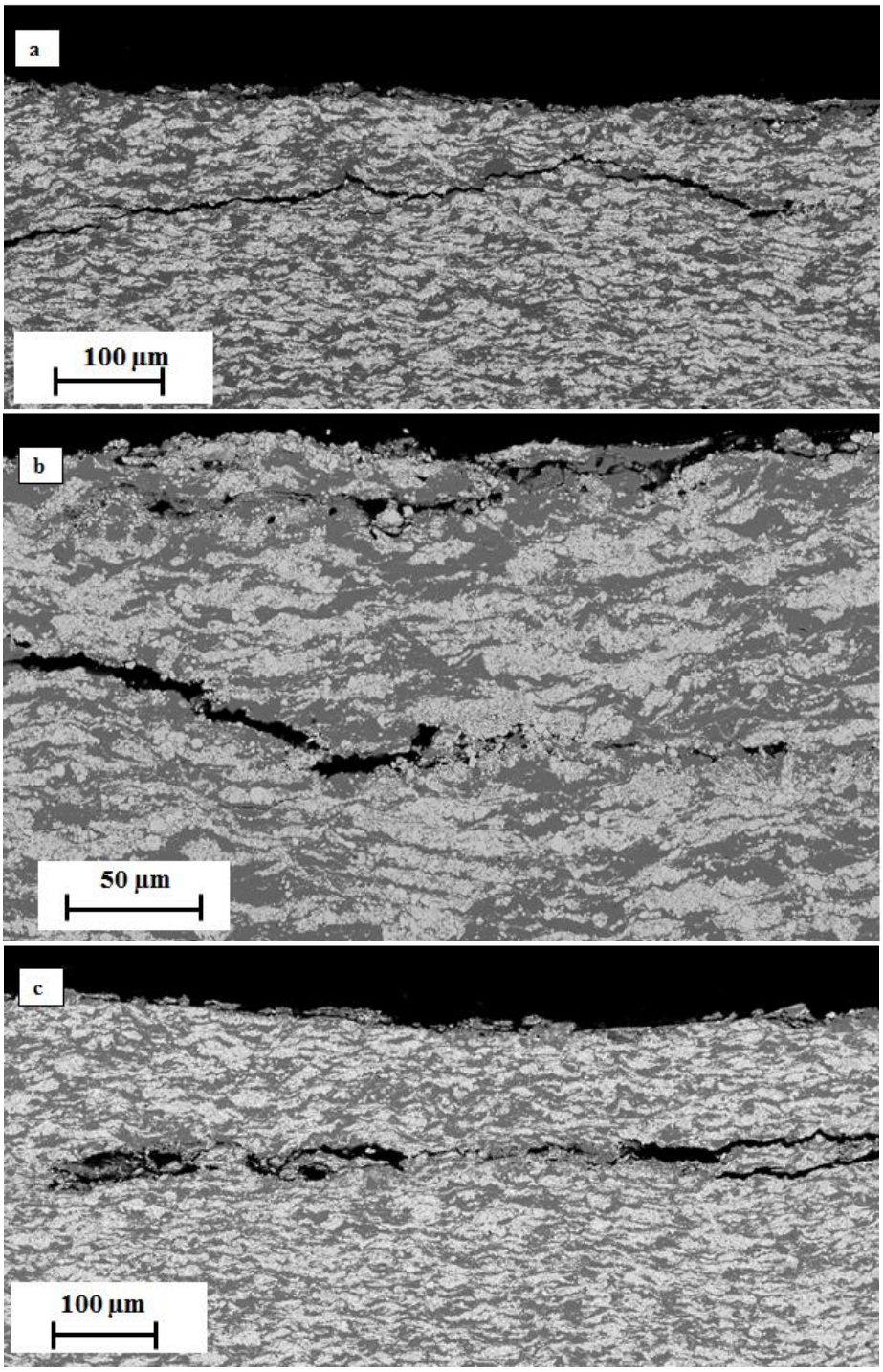

Figure 4.15. Cross-sectional BSE-SEM image of WC-Ni MMC coating fabricated from powder composition of 96 wt.% WC - 4 wt.% Ni (a) and (c) at low magnification and (b) at high magnification.

The cracks mostly travelled around the WC-12Co particles indicating that the pores mostly nucleated at the interface of WC-12Co particles and the surrounding binder. This indicated that under the action of the compressive stress during wear, the wetting of the binder around WC-12Co particle has reduced and uncovered some of the areas which might nucleate as pores. These pores offer an easy path for crack propagation. The subsurface cracks present in MMC coating eventually became parallel to the surface; however the absence of the lateral crack from the surface indicated that the surface had higher fatigue strength. The coating and the surface had higher content of WC; hence, surface was less vulnerable to the attacks of the abrasives. The attack of fluctuating stress resulted in less damage to the surface. The absence or reduction of damage due to abrasives lowered the notch point for initiation of fatigue cracks. Also, improved toughness due to higher content of WC-based carbides offered resistance to the crack initiation and propagation. Also these cracked layers might be eventually raised under the action of the compressive stresses. Also, the crack propagation will take place due to the generation of tensile stress in the tailing zone of the wheel. This might result into the raising of the material which will result in tensile stress and then favor travel of the crack [121, 123].

For coating fabricated from powder composition of 92 wt. % WC - 8wt. % Ni and 96 wt.% WC - 4wt.% Ni, the wear tested surface of the coating showed less damage on the surface in comparison with other WC-Ni MMC. The BSE-SEM images of the wear-tested surface showed presence of numerous white zones of WC-12Co particles. These coatings have more content of WC-12Co compared to coatings fabricated from powder composition of 50 wt.% WC – 50 wt.% Ni and 75 wt.% WC - 25 wt.% Ni.

These indicated that the soft and ductile nickel might had been removed from the surface, revealing hard, rigid WC-12Co phase. The hard WC-12Co particles offered resistance to the travelling abrasives on the surface, which also resulted in less damage to the sub-surface zone of the coating.

This indicates that there might be more content of rigid constituent, and impact of these heavy reinforcing phases at high velocity during spraying on soft nickel

binder resulted into its good adhesion with the binder. Thus the adhesive toughness of these MMC coatings is higher compared to the previous coatings containing lower content of WC-based carbides. Pores were still seen close to the surface However they were few in the count even after higher revolutions of the wheel on the surface during wear test, especially for coatings fabricated from powder composition of 96 wt.% WC - 4wt.% Ni. For this coating, 2000 wheel revolutions were used during wear test which is twice the number of revolutions used for any cold-sprayed WC-Ni MMC coating dealt in this study. These WC-based coating with higher content of WC is more compact; and has higher compressive load bearing capacity compared to coating fabricated from powder with low WC content. The cracks emanating from the surface and then their propagation in the sub-surface indicated that they were encouraged by the existence of the pores in the subsurface [121, 123, 124, 132, 148].

The coatings fabricated from powder composition of 96 wt.% WC – 4 wt.% Ni showed more homogeneity than coating fabricated from powder composition of 92 wt.% WC – 8 wt.% Ni. It means that although carbide content is nearly same, the carbide distribution was more uniform and homogenous in the composite for coating fabricated from powder composition of 96 wt.% WC – 4 wt.% Ni. Such distribution of carbides resulted in equal spacing of nickel binder between them in the composite. Thus, carbides were able to provide protection to the surrounding nickel binder more effectively for homogenous microstructure. The abrasives used had size varying from 212 - 300 μm. Hence, if the mean free path between carbides was less and microstructure had uniform and homogenous distribution of carbides, then less amount of nickel binder will be scraped out from the composite. The width of nickel binder zone was less than abrasives, hence abrasive might be unable to penetrate deep into the composite. Also, nickel in such composite might appear as soft binder zone surrounded by hard carbides. Thus, flowing abrasives might had encountered carbide before meeting nickel binder. The carbides in cold-sprayed WC-Ni MMC coatings were agglomerated particles with width of 25 - 45μm. So they offered strong resistance to the heavy abrasives during wear. The impact energy of the abrasives was not enough to

uproot such big carbides during wear. Hence, removal of the carbides and damage to sub-surface nickel was improbable in such composites. However continuous impact of abrasives generated sufficient stress for crack nucleation in sub-surface zone. Thus, damage to coating happened in form of delaminated sheets separated from the coating [121].

4.5 Wear theory to define wear rate of WC-Ni MMC coatings

To define limits for experimental wear rate, the wear rate values for different WC-Ni MMC coating was calculated using equal wear and equal pressure wear theories [192, 198]. The wear rate of WC-Ni MMC coating can be calculated as per the equations given below. The lower limit of wear rate of MMC is given by equation of equal wear theory which is presented as Eq. (4.2) while upper limit of wear rate of MMC is given by equal pressure theory which is presented as Eq. (4.3) as,

$$\frac{1}{W_c} = \frac{V_m}{W_m} + \frac{V_r}{W_r} \tag{4.2}$$

$$W_c = V_m W_m + V_r W_r \tag{4.3}$$

where W and V are the wear rates and volume fractions of constituents in the MMC, respectively. The subscripts c, m, and r apply to the composite, matrix, and reinforcement, respectively.

The wear rate of any composite can be described in the range defined by these two wear theories. The wear rate values postulated by equal pressure theory indicate that wear rate of composite decreases in linear proportion as reinforcement content is increased in the composite. Similarly, the wear rate values postulated by equal wear theory define lower limit values. They overestimate the effect of addition of reinforcement on the overall wear rate of the composite. These wear rate theories does not take into consideration the effect of

void nucleation at binder-reinforcement boundary, cracking and chipping of reinforcement and removal of composite in the form of delaminated sheets due to sub-surface cracks. It also does not take into consideration the compressive stresses induced in soft binder during spraying which results in improved adhesive toughness and wear resistance. Hence, the actual wear rate of the composite is higher than that predicted by equal wear theory and lower than equal pressure theory [201].

The modified wear theory is a modified form of equal wear theory. It considers the beneficial effects offered to composite due to the presence of reinforcing content in the composite, However it also considers the limitations offered by the reinforcement size, shape and its bonding with binder in the composite. The effect of pre-existing voids and adhesive toughness of binder-reinforcement was taken into consideration while defining wear rate in this theory [201]. These factors are defined using a factor called contribution coefficient "*C*" and the equation defining wear rate of MMC as per modified wear theory is presented by Eq. (4.4)

$$\frac{1}{W_c} = \frac{V_m}{W_m} + C\frac{V_r}{W_r}, \text{ for } V_r \leq 0.5. \qquad (4.4)$$

The contribution coefficient is dimensionless quantity and is a factor defining the discrepancy in experimental and theoretical wear rate considering the effect of inhomogeneity in composite. The limitation of this theory is that it can define the wear rate of composite for reinforcement content less than 50 volume percent only.

In order to use equations (2 - 4), the wear rate of individual phases is desired. For our study, wear rate of pure cold-sprayed nickel was experimentally derived while wear rate of WC-12Co was obtained from past study [212]. Since there was no prior research work on wear of WC-12Co under similar experimental conditions (ASTM G-65 testing conditions), the use of wear rate of WC-Co material with varying content of Co was recommended. To find wear rate of WC-12Co, the wear rate of WC-10 Co wear tested (ASTM G-65 test) using same procedure,

from the literature was used [212]. The wear rate of WC-10Co was validated since sintered powder was used for wear test. Further, the wear rate of WC-12Co was deduced using Li *et al.*'s proposed equation [213] where ratio of wear rate of two different composites was proportional to the ratio of binder (which is cobalt) content and the grain size of their reinforcements (WC in this case). Thus, assuming that grain size remained same for WC-10Co and WC-12Co powder, the wear rate of WC-12Co powder was easily found after substitution of values in the formula.

The wear rate values corresponding to different WC-Ni MMC coating as per equal pressure and equal wear rate theory is given in Table 4.4. Refer to Appendix 1 for calculation of wear rate values for different wear theories.

Table 4.4. Wear rate for different WC-Ni MMC coating using equal pressure and equal wear rate theory.

Powder composition	**Equal pressure theory wear rate (mm^3/Nm) $\times 10^{-6}$**	**Equal wear theory wear rate (mm^3/Nm) $\times 10^{-6}$**
96 wt.% WC - 4 wt.% Ni	595	0.
92 wt.% WC - 8 wt.% Ni	711.6	0.14
75 wt.% WC - 25 wt.% Ni	1092.9	0.53
50 wt.% WC - 50 wt.% Ni	1185.2	1.54
100 wt. % Ni	1232.9	1232.9

A quick glance at wear rate values indicated by equal pressure theory and experimental wear rate values for WC-Ni MMC, it is clear that there is strong deviation between both of them. These deviations were comparatively minute

when experimental wear rate values are compared with wear rate values obtained using equal pressure theory. So it is clear that equal wear theory underestimates wear rate values for all WC-Ni MMC. Hence, a need for wear theory to define wear rate of WC-Ni MMC arises and this can be achieved using 'Modified wear rate theory'. Modified wear rate theory involved obtaining value fo contribution coefficient or "*C*" value. To find this, initially the value of "*C*" is obtained for each WC-Ni MMC coating by substitution of experimental wear rate value of that MMC and individual phases in the composite i.e. wear rate of pure nickel and WC-12Co. The volume content of individual phases was inserted and finally the value of "*C*" corresponding to particular composition of WC-Ni MMC coating was obtained. Thus, for four different WC-Ni MMC coating, four different values of "*C*" will be obtained, each corresponding to its composition. After obtaining value of "*C*", the wear rate for all the four WC-Ni MMC coating was obtained by substitution of wear rate of individual phases in the MMC.

The wear rate corresponding to different WC-Ni MMC coating using different "*C*" value is presented in Table 4.5.

Table 4.5. Wear rate for different WC-Ni MMC coating using modified wear rate theory.

***C* values**	**Wear rates for respective powder composition (mm^3/Nm)**			
	96 wt.% WC - 4 wt.% Ni	92 wt.% WC - 8 wt.% Ni	75 wt.% WC - 25 wt.% Ni	50 wt.% WC - 50 wt.% Ni
12.5×10^{-3}	9.25×10^{-6}	11.3×10^{-6}	41.0×10^{-6}	113×10^{-6}
5.025×10^{-3}	22.9×10^{-6}	27.9×10^{-6}	97.8×10^{-6}	249×10^{-6}
2.426×10^{-3}	47×10^{-6}	56.9×10^{-6}	188×10^{-6}	427×10^{-6}
5.711×10^{-3}	20.2×10^{-6}	24.6×10^{-6}	86.8×10^{-6}	224×10^{-6}
1st Average: 6.411×10^{-3}	18×10^{-6}	21.9×10^{-6}	77.8×10^{-6}	203×10^{-6}
2nd Average: 4.387×10^{-3}	26.2×10^{-6}	31.9×10^{-6}	111×10^{-6}	277×10^{-6}
Volume percent of WC content in the coating	52	42	11	4
Experimental wear rate values	20×10^{-6}	57×10^{-6}	98×10^{-6}	113×10^{-6}

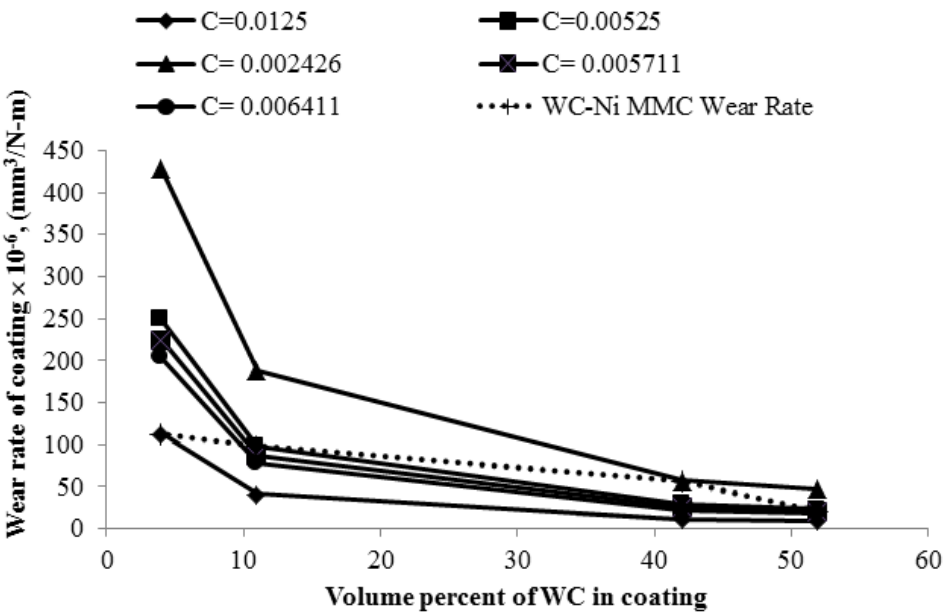

Figure 4.16. Graphical representation of wear rate plotted using different "*C*" values against experimental wear rate.

Thus, each "*C*" value will give four wear rates corresponding to the four different WC-based coatings. To understand the role played by "*C*" value obtained for all four different WC-Ni MMC, we will refer to table 4.5 and Fig. 4.16. In Fig. 4.16, the experimental wear rate values are indicated as "WC-Ni MMC wear Rate". In table 4.5, we will consider top four "*C*" values. The "*C*" values range from the lowest of 2.426×10^{-3} to the highest of 12.5×10^{-3}. The wear rate of composite by modified wear rate is inversely proportional to "*C*" value. Hence, high "*C*" value should lower wear rate and reverse case for low "*C*" value. Thus, the wear rate value for all four WC-Ni MMC obtained using $C = 2.426 \times 10^{-3}$ were higher than the experimental wear rate value of WC-Ni MMC while wear rate values were lower than experimental values for $C = 12.5 \times 10^{-3}$ (Refer Fig. 4.16). Thus, it is clear that $C = 2.426 \times 10^{-3}$ overestimates wear rate of composite while $C = 12.5 \times 10^{-3}$ underestimates wear rate values of composites. Meanwhile, we also obtained average "*C*" value for four "*C*" values, which were representatives of all four WC-Ni MMC. This average "*C*" is 6.411×10^{-3}. The wear rate values obtained using this "*C*" was also lower than experimental wear rate values. Thus, this

average value underestimated wear rates of WC-Ni MMCs. Thus, till this stage, the wear rate value obtained for respective WC-based MMC from four different "*C*" values showed strong deviation from experimentally obtained wear rates. In order to effectively define "*C*" value for WC-based MMC, the statistical principle of regression to the mean is used (Fig. 4.16). As per this principle, if the results show large standard deviation due to particular value, then removal of that can lower the deviation without significant effect on mean [214, 215].

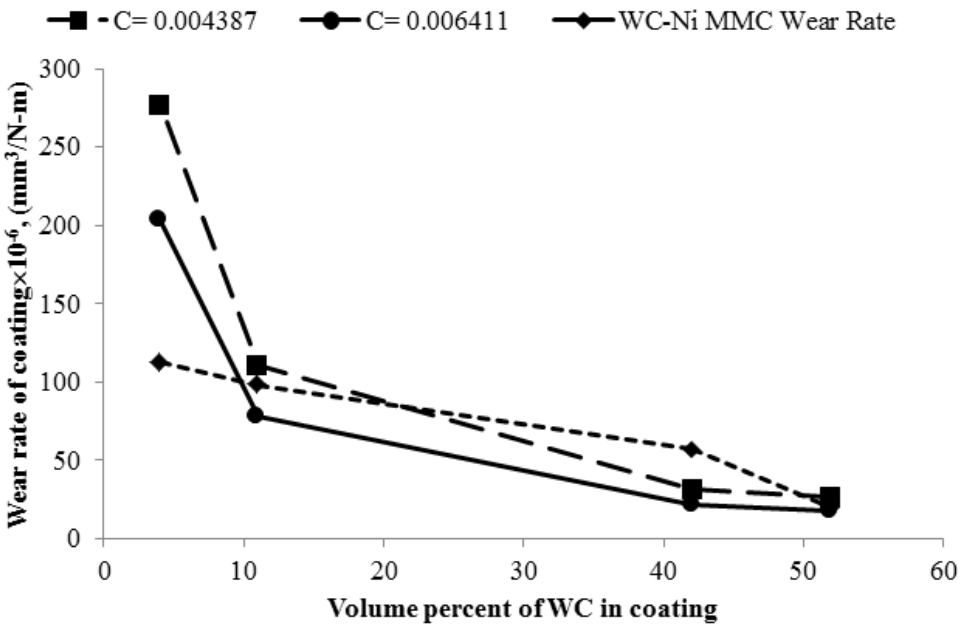

Figure 4.17. Graphical representation of wear rate plotted using two close "*C*" values against experimental wear rate.

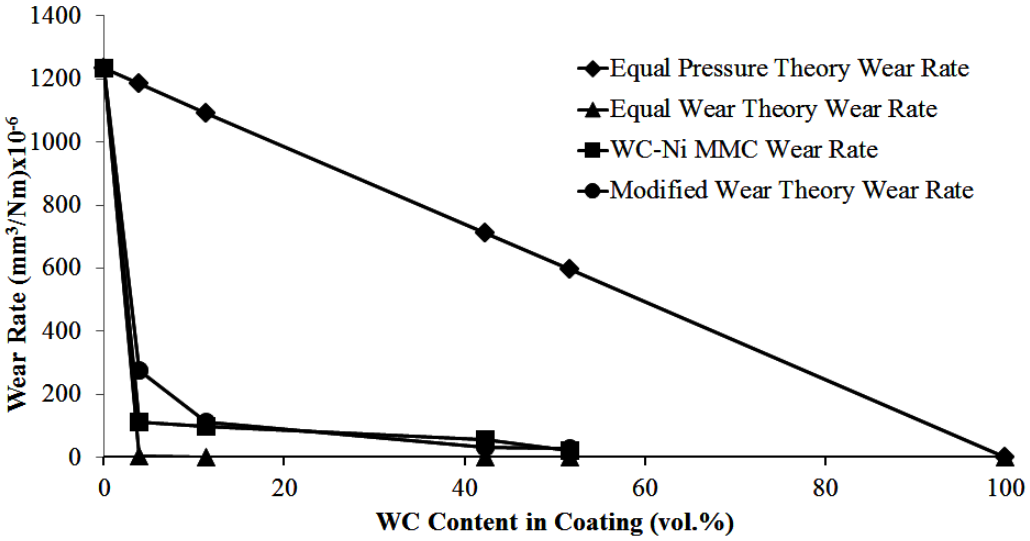

Figure 4.18. Representation of the experimental wear rate values and wear rate values of pure nickel and WC-Ni MMC coating using all the wear theories.

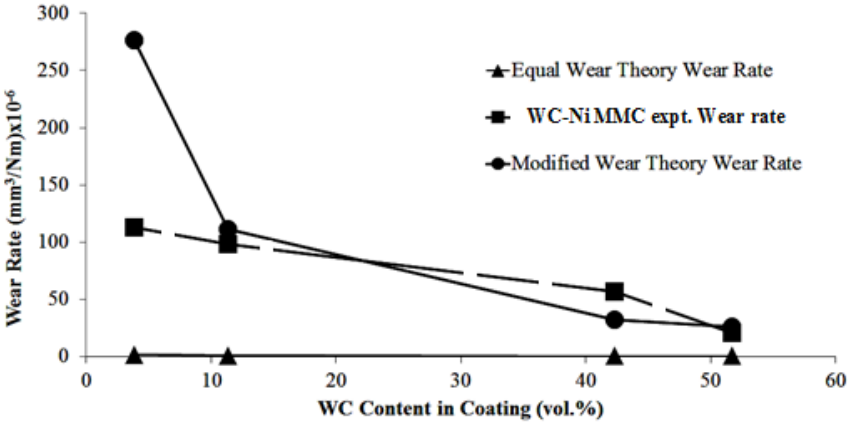

Figure 4.19. Representation of the experimental wear rate values and wear rate values of different WC-based MMC coating using the equal wear rate and modified wear theories.

The value of $C = 6.4155 \times 10^{-3}$ is the average of "*C*" value for all the four WC-Ni MMC coatings. It is found that wear rate values of WC-Ni MMC coatings were close and in acceptable limit for all compositions except coating fabricated from powder compositions of 50 wt. %WC – 50 wt.% Ni. Hence, to define "*C*" which

will predict wear rate close to as depicted experimentally for WC-based MMC, the average value of "*C*" corresponding to WC-based MMCs fabricated from powder composition of 75 wt.% WC - 25 wt.% Ni, 92 wt.% WC - 8 wt.% Ni and 96 wt.% WC – 4 wt.% Ni was calculated. Hence, a new "*C*" value is derived which is average of "*C*" values derived for all WC-Ni MMC coatings except the MMC fabricated from powder composition of 50 wt.% WC – 50 wt.% Ni . This new value of "*C*" is 4.4×10^{-3}. The notion behind this new "*C*" value was consideration of "*C*" range of 2.426 to 5.711×10^{-3}. A new "*C*" value obtained should be representative of "*C*" values of this range. Hence, "*C*" value of 12.5×10^{-3} was considered as outlier as per Chauvenet's criterion. Also, to follow the assumption of a normal distribution, a value of "*C*" needs to be considered which would predict values satisfactorily for other WC-Ni MMC coating [213, 214].

Figure 4.17 shows graphical representation of wear rate for all WC-Ni MMC coatings plotted using both these average "*C*" values. We consider "$C = 6.415 \times 10^{-3}$" as first average while $C = 4.4 \times 10^{-3}$ as second average. In our advancement towards final selection of "*C*" we discarded average value of 6.415×10^{-3}. The reason for discarding "$C = 6.415 \times 10^{-3}$" is due to large standard deviation value. For example, the standard deviation (S.D.) for $C = 6.415 \times 10^{-3}$ is 4.3×10^{-3} while for $C = 4.4 \times 10^{-3}$, the S.D. is 1.732×10^{-3}. The probability of getting more than 1.4 standard deviations is about 0.1. So, the statistic value is 0.1 x 4 (number of data points) = 0.4, which is less than 0.5. So, according to Chauvenet's criterion, the $12.5\ 10^{-3}$ value could be discarded [213]. The wear rate value for all WC-based MMC was deduced using this new "*C*" value and plotted against experimental values. It is clear from Fig. 4.17 - 4.19 that wear rate obtained using this value of "*C*" for all WC-Ni MMC coatings showed closeness except the composite fabricated from powder composition of 50 wt.% WC – 50 wt.% Ni. The value of "*C*" was finalized at 4.4×10^{-3} after consideration that it was able to define wear rate for all WC-Ni MMCs except the one fabricated from powder composition of 50 wt.% WC – 50 wt.% Ni.

The significance of "*C*" is that, it should indicate the role of reinforcement chipping, reinforcement removal due to loosening with binder, in the wear rate. In case of WC-Ni MMC coating, the "*C*" value seems to define its role satisfactorily for MMC fabricated from powder composition of 75 wt.% WC – 25 wt.%. Ni and above or WC-Ni MMC containing WC content higher than 10 vol. %. However, it assumes that MMC coating containing less than 10 vol. % WC content cannot be predicted using this "*C*" value. Thus, value of $C = 4.4 \times 10^{-3}$ was considered as a best possible "C" value to define experimental wear rate values of different WC-Ni MMC in volume range of 10 to 52 vol. %. To understand a deviation between experimental and theoretical wear values, a close look at wear rate value of cold-sprayed pure nickel and WC-based MMC coating fabricated from powder of 50 wt.% WC – 50 wt.% Ni must be done. The wear rate of pure nickel is 1233×10^{-3} mm^3/ N-m while wear rate of WC-Ni MMC coating under consideration is 112×10^{-3} mm^3/N-m. This drastic fall in wear rate definitely shows large deviation in values predicted by wear theory. For other WC-Ni MMC coating, the experimental wear rate values are close. Hence, wear rate values predicted using modified wear theory did not showed much deviation from experimental values. This indicates that wear rate of other WC-Ni MMC coating with WC-content in range from 0 to 10% needs to be included for better quantification of wear rate using modified wear theory. Thus, neglecting wear rate for first WC-Ni MMC coating (i.e. the WC-Ni MMC coating fabricated from powder composition of 50 wt.% WC – 50 wt.% Ni) , the current value of "$C = 4.4 \times 10^{-3}$" gives satisfactory wear rate for other WC-Ni MMC coating.

4.6 Coating composition

The coating deposited using cold spraying was optimized to the powder composition of 96 wt.% (WC-12Co) - 4 wt.% Ni. The optimized powder composition was decided on the basis of comparison of mechanical properties like hardness, porosity, mean free path, toughness, wear rate [71]. As per the principle of replication in experimental design, to find the variation in WC- content in WC-Ni MMC coating composition, the powder composition of cold-sprayed as well as

HVOF-sprayed WC-Ni MMC coating was kept constant [216]. The difference in the coating composition in terms of WC content in the MMC coating will reflect the percentage of loss of reinforcing particles during the thermal spraying process. The coating composition remained constant when testing the effect of friction stir processing on them.

Chapter 5. Wear Performance of FSP-treated thermal-sprayed WC-Ni MMC Coatings

The thermal-sprayed WC-Ni MMC coatings were exposed to a post-deposition treatment called friction stir processing (FSP). The powder composition of WC-Ni MMC coating was the optimized powder composition i.e. 96 wt.% WC – 4 wt.% Ni. This powder composition was kept constant parameter for all FSP study to be carried out on thermal-sprayed WC-Ni MMC coatings. The novelty of this study lies in notion that friction stir processing as post-deposition treatment will improve mechanical properties of WC-Ni MMC coatings. Various sub-sections in this chapter will discuss the steps followed in friction stir processing of thermal-sprayed WC-Ni MMC coatings.

5.1 Finding parameters for FSP treatment

The application of the FSP treatment involved initial step of deciding the FSP parameters which will give satisfactory properties in WC-Ni MMC coating. The decision making material parameters are: depth of friction stir processed zone in the MMC and the hardness of the MMC after FSP treatment. To decide the final FSP parameters to be used for preparing wear test sample, initial FSP treatment was carried out on thermal-sprayed WC-Ni MMC coating and characterization was carried out.

Figure 5.1 shows BSE-SEM cross-sectional image of FSP-treated WC-Ni MMC coating. A close look at Fig. 5.1(a) shows presence of flow lines in the microstructures. These flow lines are generated due to heavy mechanical and thermal stresses generated during FSP treatment which resulted in fragmentation and distribution of carbides in the composite. There was presence of pores in the composite microstructure. This might generated due to incomplete fusion of nickel binder. It seems that the heat generated during FSP treatment was not able to properly fuse the cavities, hence seen as pores.

Figure 5.1 (b) shows different zones in FSP-treated cold-sprayed WC-Ni MMC coating. It is clear from figure that there are three distinct zones in any FSP

treated material: friction stir processed zone, transition zone and parent material zone. Any FSP-treated material is divided into three zones.

The upper most zone close to surface where FSP treatment was applied is called as friction stir processed (FSP) zone. This zone showed maximum effect of FSP treatment like improved homogeneity, improved mechanical properties like hardness, toughness.

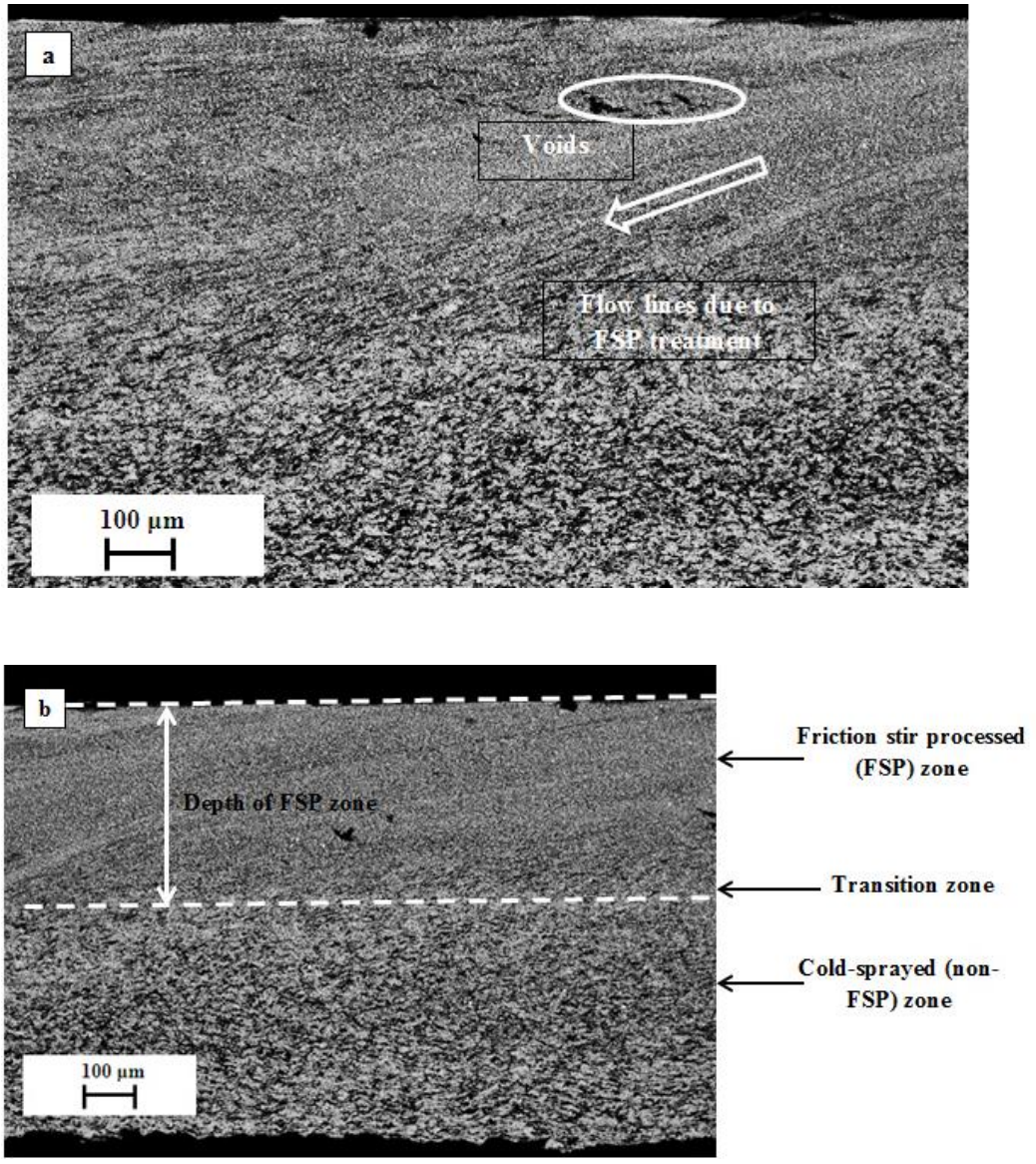

Figure 5.1. Cross-sectional BSE-SEM image of FSP-treated cold-sprayed WC-Ni MMC coating showing (a) microstructure and (b) different zones along coating thickness.

The middle portion was that region which showed mixture of microstructure of FSP-treated as well as un-processed parent material. This zone was comparatively thin and was difficult to distinguish.

At sufficient depth below the top surface of the FSP-treated WC-Ni MMC coating, the microstructure showed unaffected zone of cold-sprayed WC-Ni MMC coating. The microstructure showed same microstructure as seen for cold-sprayed WC-Ni MMC coating wherein there was distribution of agglomerated WC-12Co reinforcing particles (white zones) dispersed in soft, ductile nickel binder (grey zone). The microstructure showed numerous small spots which indicated presence of numerous small voids generated during fabrication process. The cold spraying of WC-Ni powder might not impart sufficient compressive stress for efficient binding of nickel around WC-12Co particles. Also, minute voids in the nickel binder indicate poor cohesion between individual nickel particles.

The third portion was the unaffected parent material zone. This zone showed no effect of FSP treatment on microstructural changes [80].

Figure 5.2 showed BSE-SEM image displaying cross-sectional view of FSP-treated cold-sprayed WC-Ni MMC coating with set of parameters containing tool rotational speed of 1400 RPM. The FSP-treated WC-Ni MMC coating showed thick friction stir processed layer. This layer varied in thickness from 390 µm to 405 µm. The friction stir processed zone, transition zone and unprocessed parent material zone were clearly and distinctly visible in the microstructure. The fragmented carbides in the friction stir zone indicated effect of thermal and mechanical stress on agglomerated carbides of cold-sprayed coating (Fig. 5.2 (b)). The carbide distribution was uniform with homogeneity reflected in form of constant binder gap. The absence of pores indicated efficient distribution combined with effective wetting of carbides with nickel binder.

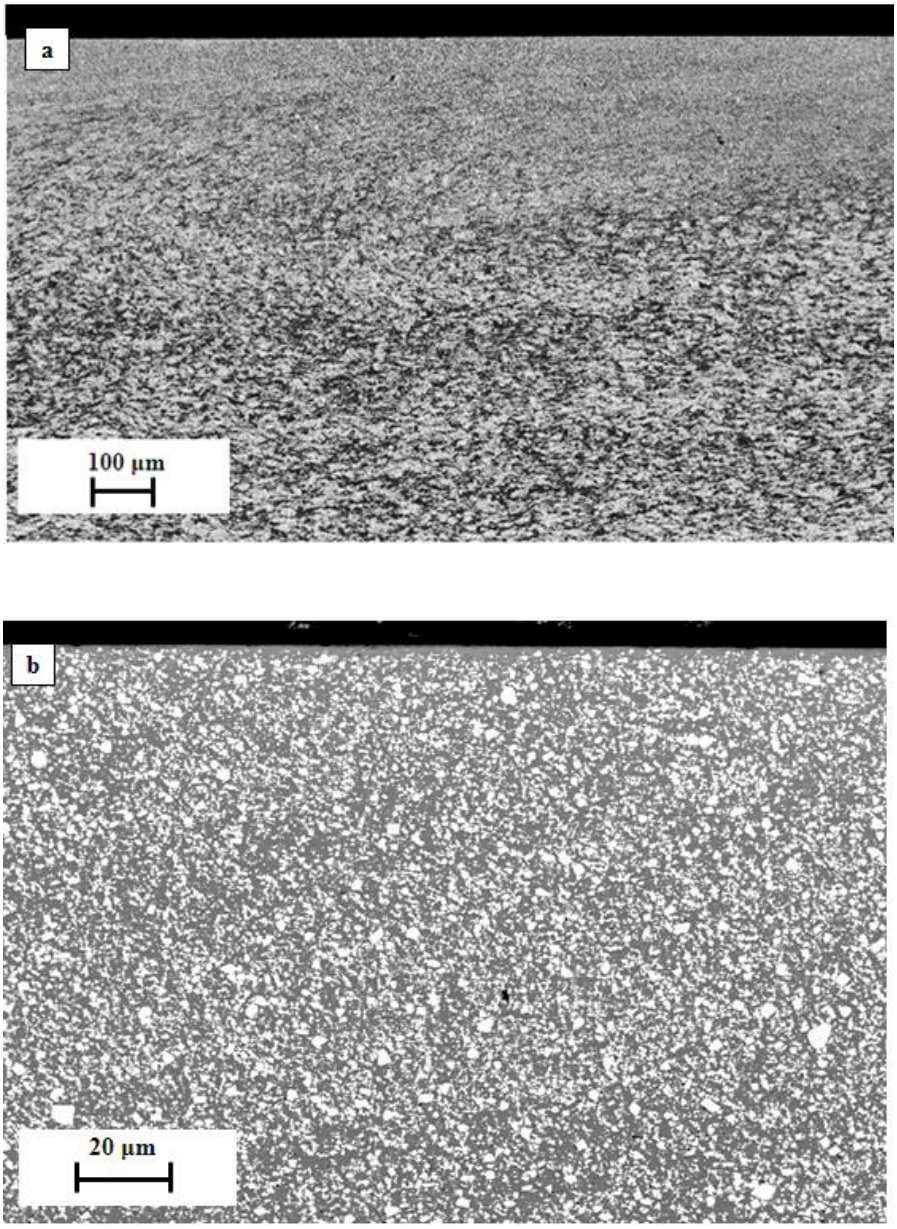

Figure 5.2. FSP-treated cold-sprayed WC-Ni MMC coating (a) at low magnification and (b) at high magnification.

Figure 5.3 showed BSE-SEM image displaying cross-sectional view of FSP-treated HVOF-sprayed WC-Ni MMC coating with set of parameters containing tool rotational speed of 1400 RPM. The FSP-treated WC-Ni MMC coating showed thin friction stir processed layer. This layer varied in thickness from 71 µm to 85 µm. At sufficient depth below the surface, there existed non-affected parent material zone. Its microstructure is similar to HVOF-sprayed WC-Ni

MMC coating. There was distribution of soft nickel binder islands separated by different carbides, oxides and intermetallic compounds (Fig. 5.4). The microstructure of FSP zone was uniform and homogenous compared to unaffected parent material zone (Fig. 5.5). The microstructure showed distribution of nickel binder between carbides with absence of voids and pores in the microstructure.

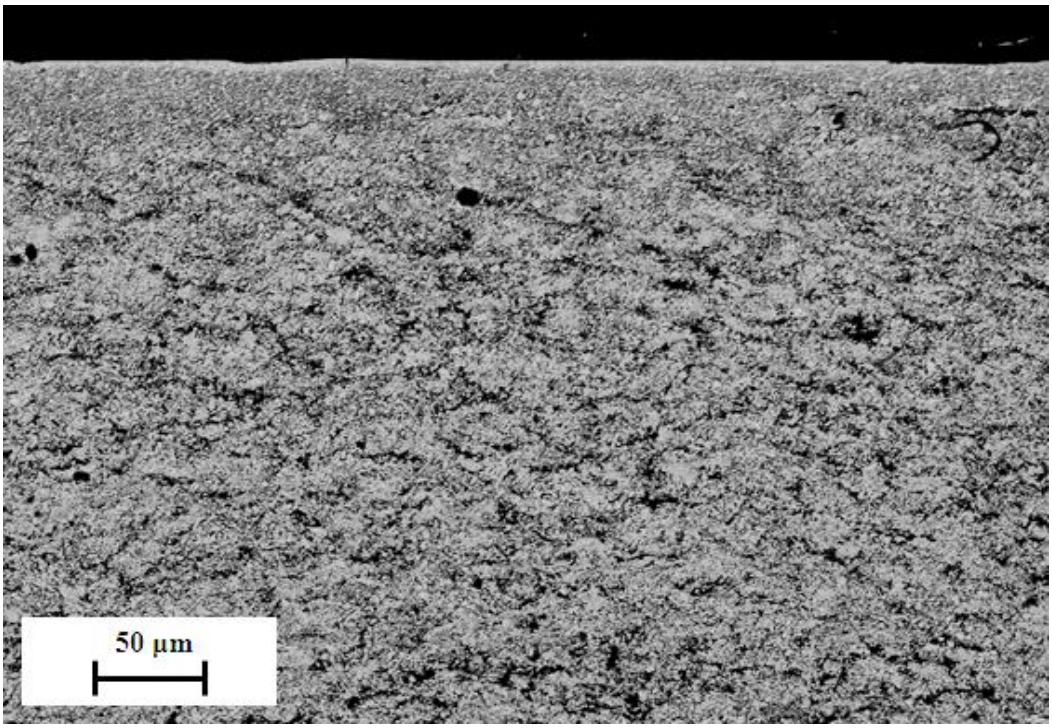

Figure 5.3. Cross-sectional BSE-SEM image of FSP-treated HVOF-sprayed WC-Ni MMC coating with tool rotational speed of 1400 RPM.

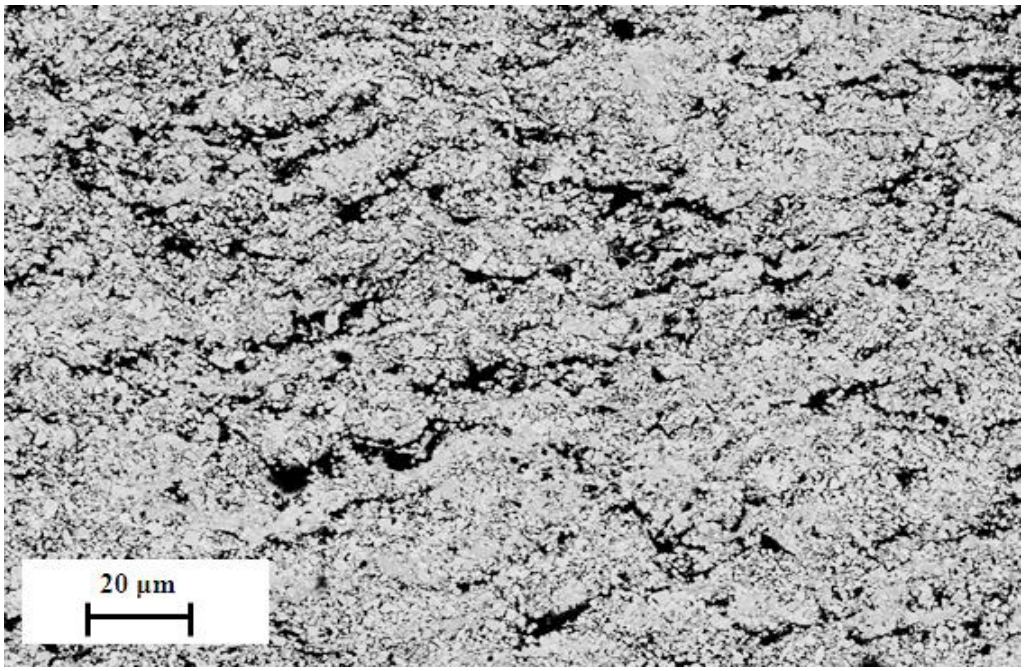

Figure 5.4. Cross-sectional BSE-SEM image of FSP-treated HVOF-sprayed WC-Ni MMC coating showing un-processed portion of MMC coating.

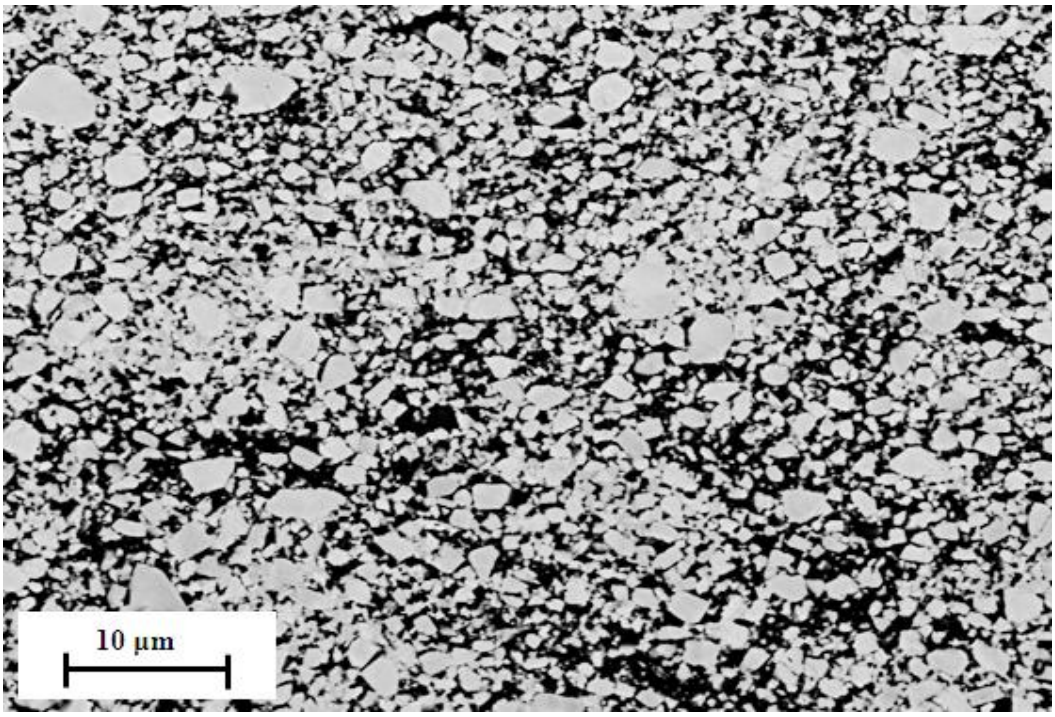

Figure 5.5. Cross-sectional BSE-SEM image of friction stir processed zone of FSP-treated HVOF-sprayed WC-Ni MMC coating showing uniform and homogenous microstructure.

Two sets of parameters were used for friction stir processing of both the thermal-sprayed coatings. In friction stir processing, three important parameters define the process: axial force on the tool, tool rotational speed and tool travel velocity over the coating surface [80]. In friction stir processing, the axial force on the tool and the tool travel velocity over the coatings were kept constant while the tool rotational speed was changed. Thus the change in tool rotational speed defined the change in the processing parameters. The selection of tool rotational speed was decided on the basis of the heat and the mechanical stresses generated in the coating material. This value will be dependent on coating composition which should be sufficient enough to generate thermal as well as mechanical stresses in the coating. The two different tool rotational speed values used were: 900 RPM and 1400 RPM.

Both the thermal-sprayed WC-Ni MMC coatings were treated with both the sets of parameters followed by characterization. The characterization of the FSP-treated thermal-sprayed WC-Ni MMC coatings involved measurement of the material parameters: hardness, toughness, mean free path between WC carbides, carbide shape and the depth of the friction stir processed zone in the coating. The coatings were checked for distribution of binder around the reinforcing WC-12Co particles to find traces of voids. The presence of voids indicated poor adhesion which may translate to higher wear rate. The FSP treated-coatings were sectioned longitudinally (along the direction of travel of FSP tool on the surface) and laterally (along the direction, perpendicular to the travel of FSP tool on the surface); and viewed under the scanning electron microscope for characterization. The characterization of the FSP-treated cold-sprayed WC-Ni MMC coating, showed that the set of parameters containing tool rotational speed of 1400 RPM gave better mechanical properties in terms of hardness, porosity, compared to set containing tool rotational speed of 900 RPM. This markedly difference in the porosity content in FSP-treated cold-sprayed WC-Ni MMC coating treated with two sets of parameters is clear in Fig. 5.7 and Fig. 5.8.

The Fig. 5.6 shows cross-sectional image of cold-sprayed WC-Ni MMC coating. The microstructure showed numerous voids which are clear even at lower

magnification. It is found that as per delamination theory, voids in microstructure are main precursor for crack nucleation and driving force for their propagation [22]. The microstructure of FSP-treated thermal-sprayed WC-Ni MMC coating was relatively homogenous and less faulty when compared with non-FSP treated coating. As example, the FSP-treated cold-sprayed WC-Ni MMC coating is considered. The Fig. 5.7 and 5.8 shows cross-sectional image of FSP-treated cold-sprayed WC-Ni MMC coating treated with tool rotational speed of 900 RPM and 1400 RPM, respectively. A close look at Fig. 5.7 displayed presence of numerous voids in the nickel binder. Voids still existed in WC-Ni MMC FSP-treated with tool rotational speed of 1400 RPM but their count were higher in WC-Ni MMC FSP-treated with 900 RPM. At some locations in Fig. 5.7, the voids had angular shape indicating that they might have been generated during sectioning or polishing stage of sample preparation. But their effect should also be reflected in Fig. 5.8. But void counts were still the lower in count even if this aspect was considered. It also means that if carbides are easily dislodged during polishing stage of sample preparation, the interfacial toughness between reinforcing carbide particles and nickel binder is lower. The absence or reduction in count of such voids in the microstructure of WC-Ni MMC coating FSP-treated with tool rotational speed of 1400 RPM asserts the statement that this microstructure has less microstructural faults than the microstructure of WC-Ni MMC coating treated with tool rotational speed of 900 RPM. It was clear that the tool rotational speed of 900 RPM might not generate sufficient stresses during processing which resulted in incomplete wetting and enveloping of nickel binder around WC-12Co particle. The stresses generated during FSP treatment were enough to fragment agglomerated WC-12Co However were insufficient for uniform distribution of nickel binder around carbide particles. The nickel binder was not offered enough stress for flowing around the WC-12Co particles. The pre-existing voids play detrimental role in lowering of material properties like toughness, hardness and wear resistance by contributing to catastrophic failure of the material. These voids under wear conditions may elongate and result in cracking of the surrounding binder [2, 37, 217]. The presence of numerous voids in the microstructure also

indicates poor adhesion between different phases of the coating. Thus FSP-treatment of HVOF-sprayed WC-Ni MMC coating with 900 RPM tool rotational speed depicted poor adhesive toughness of the coating.

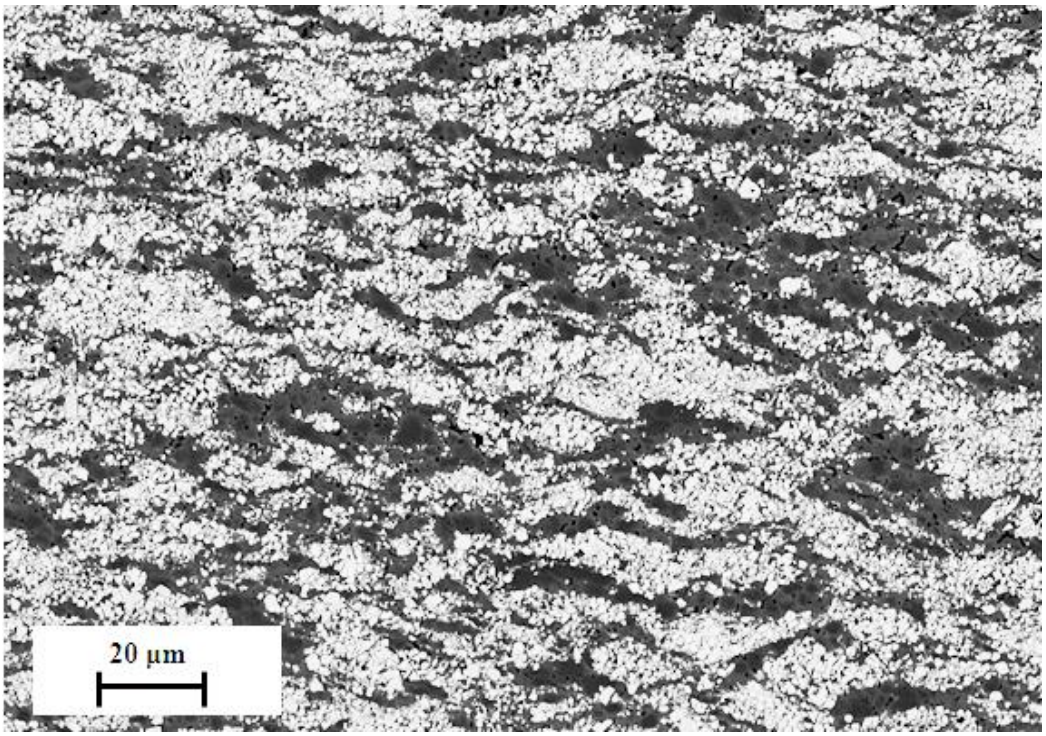

Figure 5.6. Cross-sectional BSE-SEM image of as-sprayed cold-sprayed WC-Ni MMC coating showing presence of numerous pores in microstructure (dark spots in nickel binder are pores).

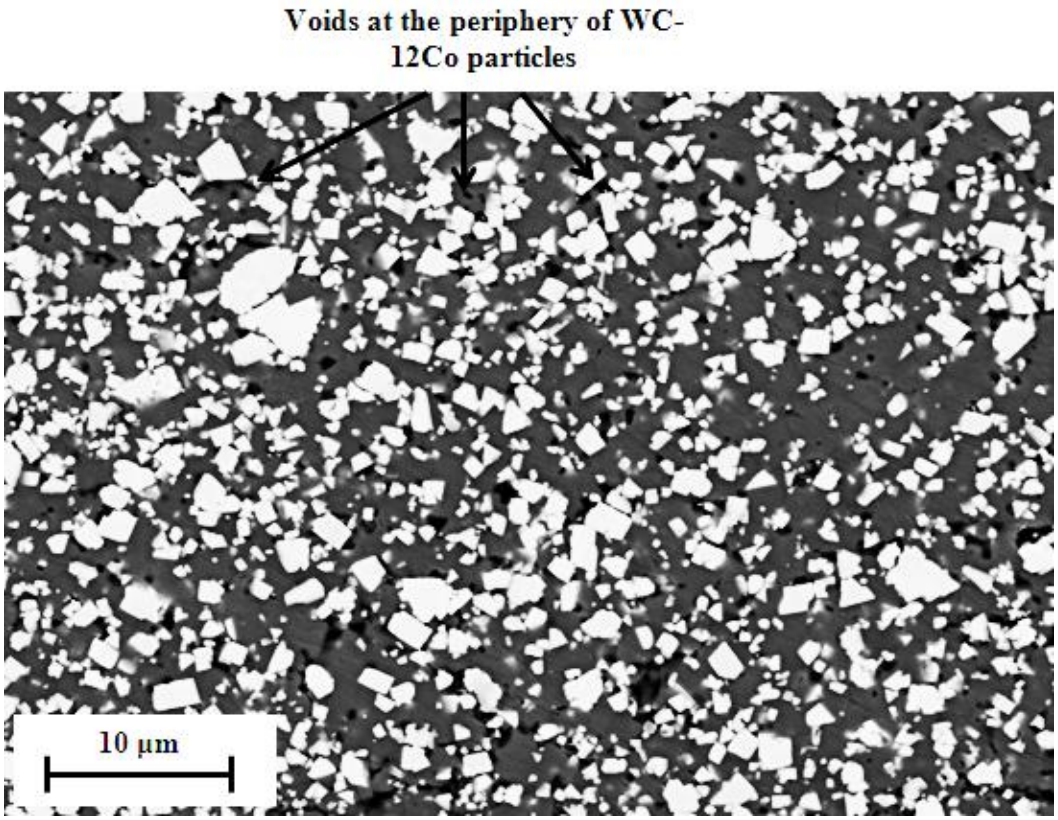

Figure 5.7. Cross-sectional BSE-SEM image of FSP-treated cold-sprayed WC-Ni MMC coating treated with tool rotational speed of 900 RPM.

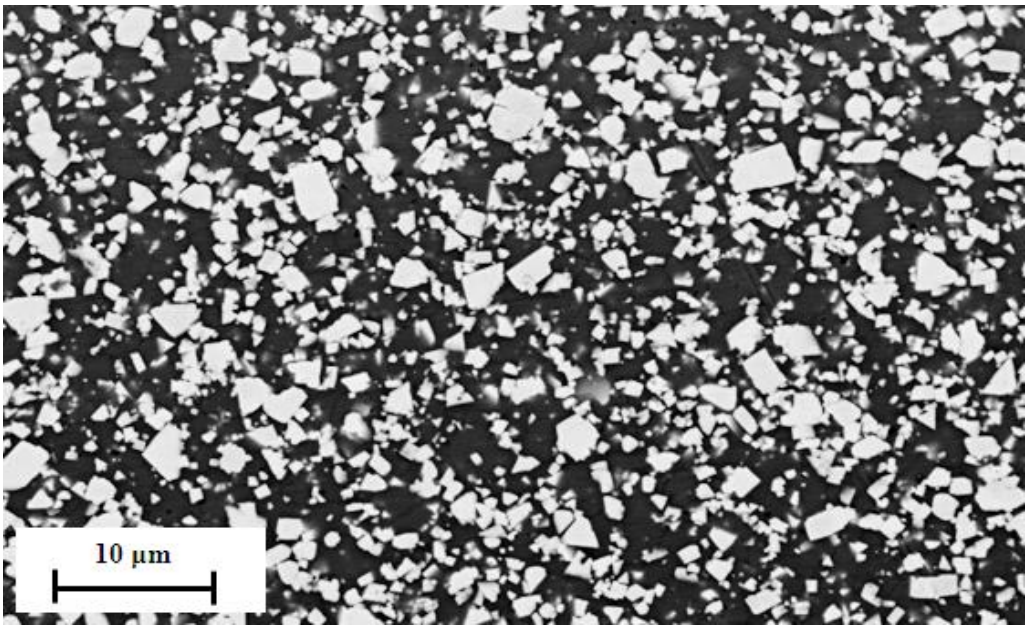

Figure 5.8. Cross-sectional SEM image of FSP-treated cold-sprayed WC-Ni MMC coating treated with tool rotational speed of 1400 RPM.

The comparisons of coating microstructure in terms of parameters after FSP treatment are shown in Table 5.1 for cold-sprayed and Table 5.2 for HVOF-sprayed WC-Ni MMC coating.

Table 5.1. Comparison of mechanical properties of FSP-treated cold-sprayed WC-Ni MMC coating treated with two different tool rotational speeds.

Parameters	**FSP parameters with 900 RPM tool speed**	**FSP parameters with 1400 RPM tool speed**
Hardness	416.15 ± 39 $HV_{0.3}$ (n = 13)	420 ± 20 $HV_{0.3}$ (n = 20)
Depth of friction stir zone	~ 380.5 µm (n = 4)	~ 400 µm (n = 4)
Porosity	High	Low
Carbide distribution	Uniform and homogenous	Uniform and homogenous
Carbide size range	0.5 – 3 µm	0.5 – 2.5 µm

Table 5.2. Comparison of mechanical properties of FSP-treated HVOF-sprayed WC-Ni MMC coating treated with two different tool rotational speeds.

Parameters	**FSP parameters with 900 RPM tool speed**	**FSP parameters with 1400 RPM tool speed**
Hardness	893 ± 98 $HV_{0.3}$ ($n = 43$)	990 ± 69 $HV_{0.3}$ ($n = 56$)
Depth of friction stir zone	~ 56 µm	~ 80 µm
Carbide distribution	Uniform and homogenous	Uniform and homogenous

Thus, from Tables 5.1 and 5.2, it is clear that FSP treatment to both the thermal-sprayed WC-Ni MMC coating will give better mechanical properties when treated with set of parameters containing tool rotational speed of 1400 RPM.

The wear assessment of FSP-treated cold-sprayed as well as HVOF-sprayed WC-Ni MMC coating was finally done with following FSP parameters:

Tool travel velocity over MMC coating = 33 mm/min,

Tool rotational speed = 1400 RPM.

5.2 Wear Analyses of FSP and non-FSP treated thermal-sprayed WC-Ni MMC coating

Figure 5.9 shows FSP-treated thermal-sprayed WC-Ni MMC coating. The coatings were wear tested in ASTM G-65 wear test. Fig. 5.10 and 5.11shows wear scar on FSP-treated cold-sprayed and FSP-treated HVOF-sprayed WC-Ni MMC coating. The wear rate values of non-FSP treated and FSP-treated thermal-sprayed WC-Ni MMC coating is shown in Table 5.3. The coating composition of as-sprayed HVOF WC-Ni MMC coating is 87 wt.% WC – 13 wt.% Ni.

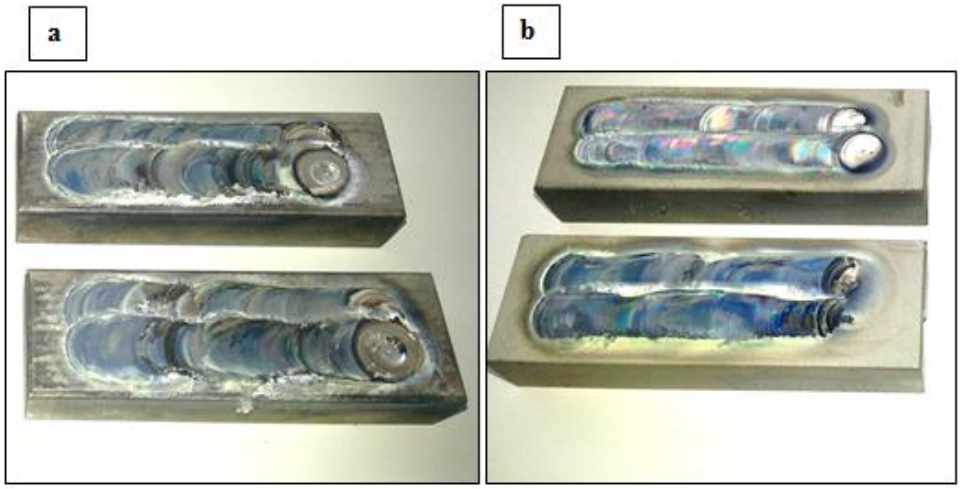

Figure 5.9. FSP-treated WC-Ni MMC coating (a) cold-sprayed WC-Ni MMC and (b) HVOF-sprayed WC-Ni MMC coating.

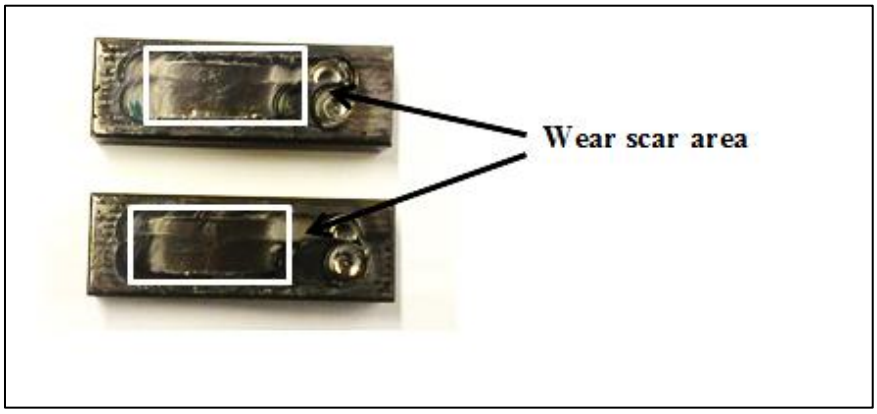

Figure 5.10. Wear-tested FSP-treated cold-sprayed WC-Ni MMC coating.

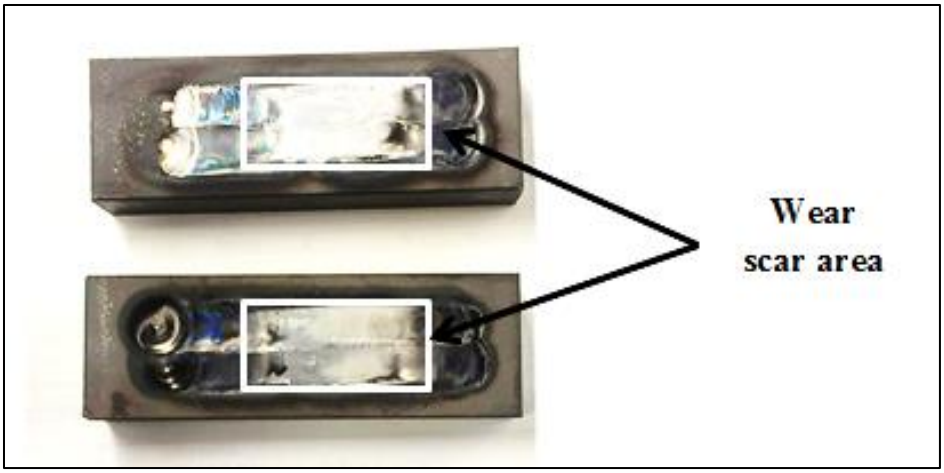

Figure 5.11. Wear-tested FSP-treated HVOF-sprayed WC-Ni MMC coating.

During FSP treatment, coated samples were firmly clamped to its base. See Appendix 2 for calculations regarding minimum clamping force required to fix sample to the base while treating it with FSP. A close look at calculation showed that (See Appendix 3) maximum temperature during FSP treatment of thermal sprayed (i.e. cold-sprayed as well HVOF-sprayed) WC-Ni MMC coating may reach to 1000ºC. It means that high temperature might have resulted in surface reaction of thermal-sprayed WC-Ni coating with surrounding atmosphere. A close look at back side of FSP-treated cold-sprayed WC-Ni MMC coating showed presence of blackened region indicating migration of heat along substrate thickness (Fig. 5.12). For FSP-treated HVOF-sprayed WC-Ni MMC coating, the 'heat tinted' region is small in area since there was lower content of nickel (19 vol. %) compared to its content in cold-sprayed coating (48 vol. %). The WC-12Co being poor conductor of heat compared to nickel, hence, sufficient heat was not transferred through the substrate along its thickness (Fig. 5.13). It means heat might have remained in the coating for long time resulting in deleterious effect on the microstructure. To understand the effect of heat on coating microstructure, XRD analyses of FSP-treated thermal-sprayed WC-Ni MMC coating was carried out.

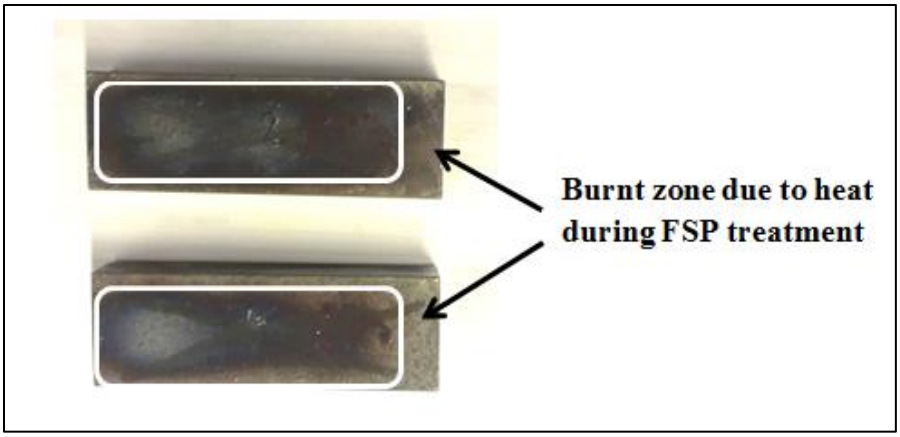

Figure 5.12. Back side of FSP-treated cold-sprayed WC-Ni MMC coating indicating 'heat tinted' zone.

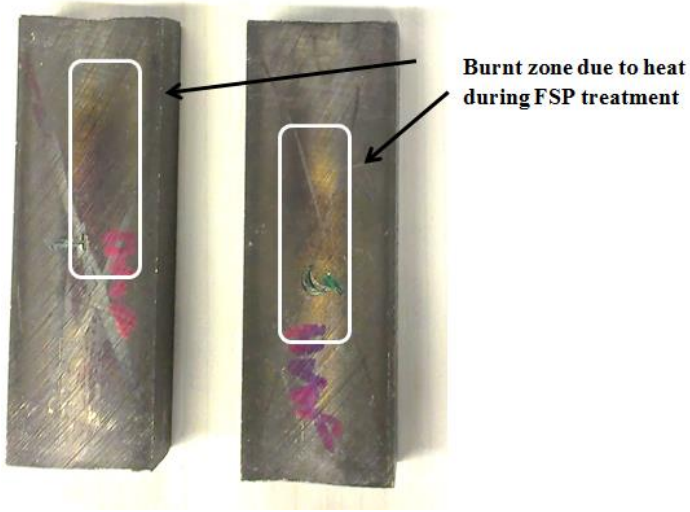

Figure 5.13. Back side of FSP-treated HVOF-sprayed WC-Ni MMC coating indicating 'heat tinted' zone.

5.3 EDS and XRD results for different WC-Ni MMC coating

Figure 5.14 shows Energy dispersive X-ray analyses (EDS) result for cold-sprayed WC-Ni MMC coating fabricated from optimized composition. The coating showed absence of any oxidation and decarburization which is speciality of cold-spraying. This is confirmed from the XRD result shown in Fig. 5.15.

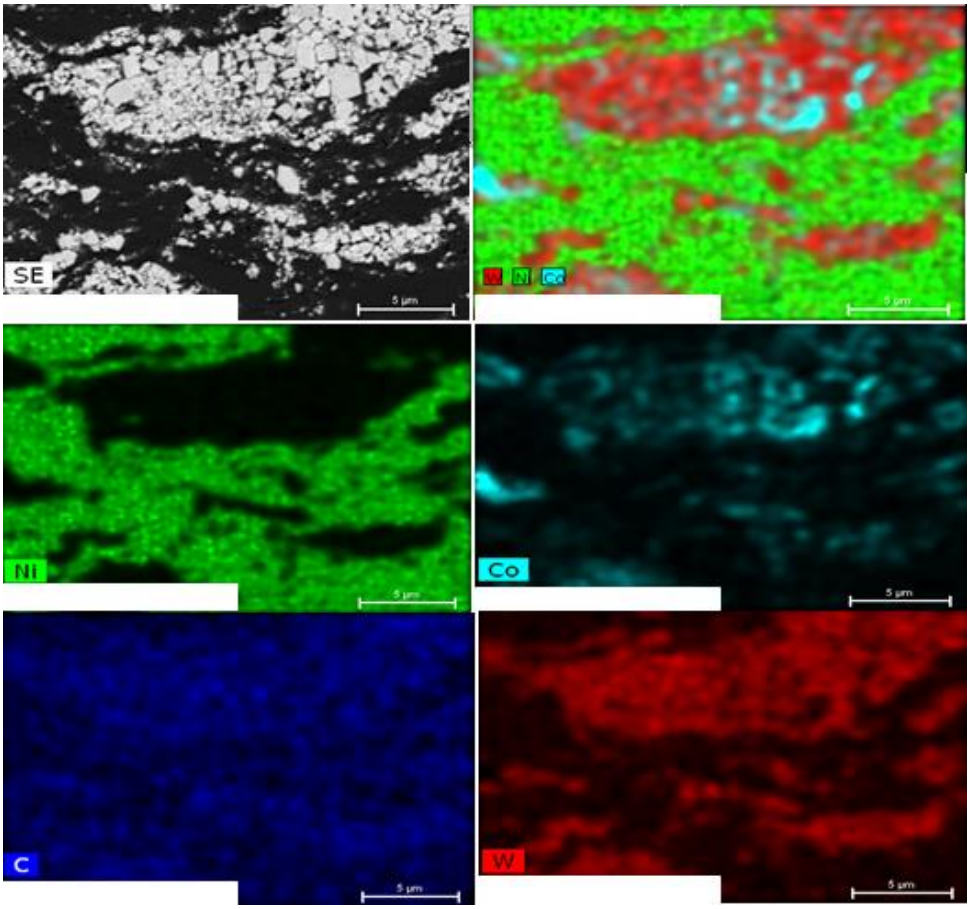

Figure 5.14. EDS result of cold-sprayed WC-Ni MMC coating.

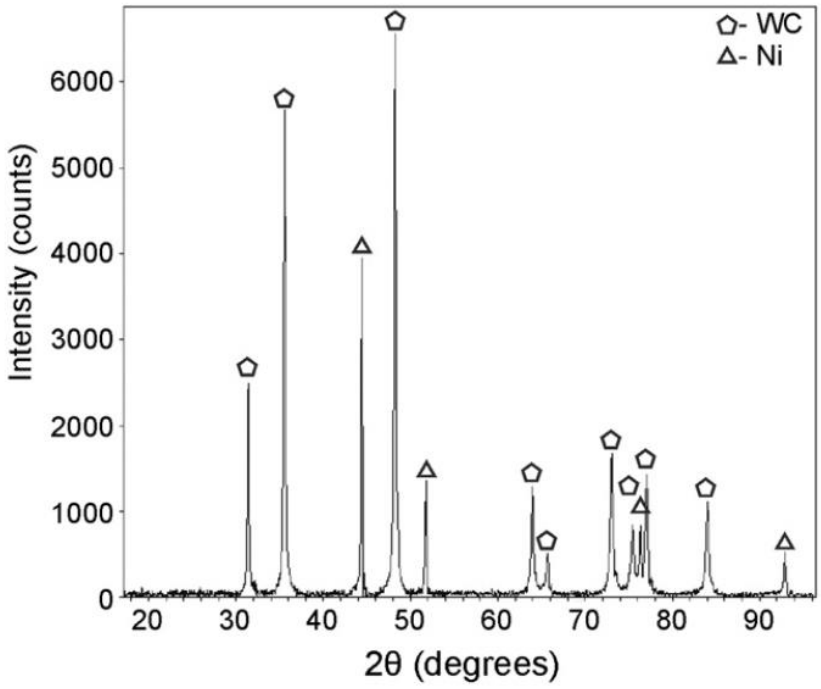

Figure 5.15. XRD result of as-sprayed cold-sprayed WC-Ni MMC coating [71].

The EDS analyses of FSP-treated cold-sprayed WC-Ni MMC coating showed presence of elemental oxygen (Fig. 5.16). The oxygen content though minute in comparison to other elements' content, confirmed the notion of oxidation and decarburization. This was strongly supported by XRD results (Fig. 5.17). The XRD analyses of FSP-treated cold-sprayed WC-Ni MMC coating showed presence of phases like NiO, W_2C and Co_3W_3O in the microstructure along with the presence of conventional phases like WC, Co, Ni. The overlapping of NiO and Co_3W_3O may cast doubt on presence of these phases in WC-Ni MMC. Also, their count and intensity being lower in XRD results indicate that these phases may not be significant in amount in MMC. But temperature for formation and energy of reaction for formation of these phases is lower than that required for formation of W_2C. Hence, if W_2C has shown presence in XRD result, then it can be speculated that these phases might co-exist with it. This suggests that the heat generated during FSP treatment might have raised the temperature to sufficient value for the formation of these phases. The oxidation of nickel, cobalt, and decarburization of WC to W_2C indicates spontaneous reaction of different phases with atmosphere.

The occurrence of these phases at 1000ºC is probable as shown by numerous studies [40 – 43, 218]. The presence of these phases indicates that there might be sufficient supply of heat of reaction for generation of these phases. It indicated that oxygen from surrounding atmosphere might have reacted with elements from the coating.

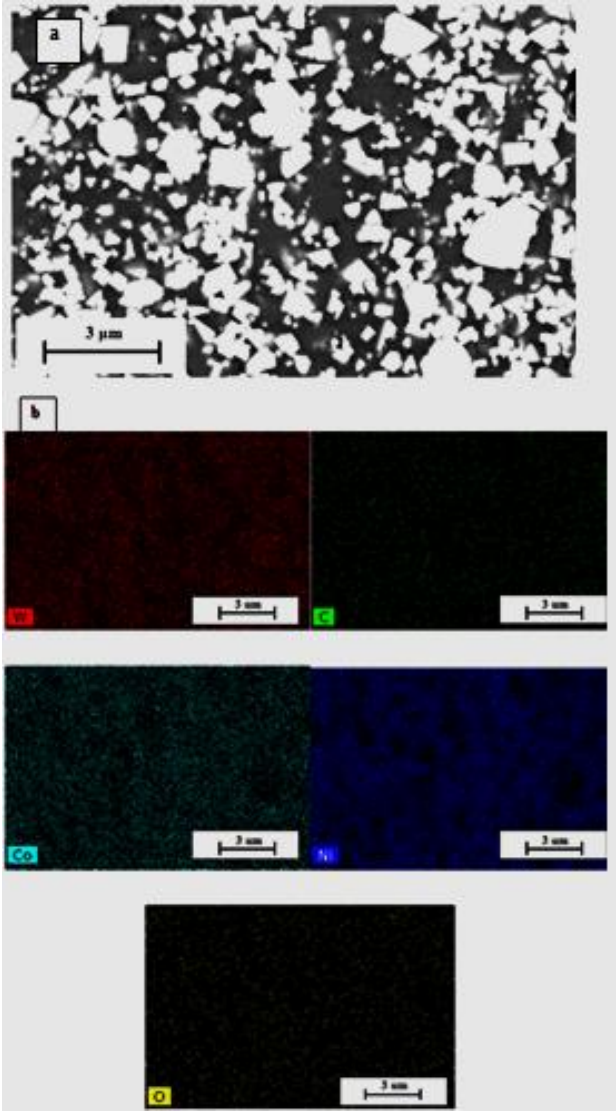

Figure 5.16. (a) Cross-section of the FSP-treated cold-sprayed WC-Ni MMC coating for EDS and (b) EDS result of the region under consideration.

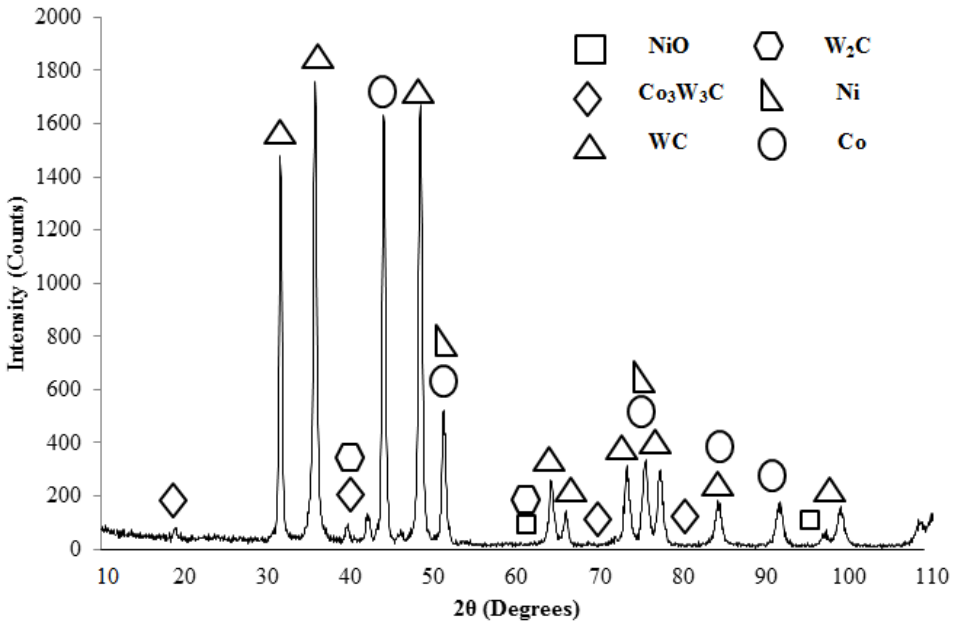

Figure 5.17. XRD result of FSP-treated cold-sprayed WC-Ni MMC coating.

The XRD result for HVOF-sprayed WC-Ni MMC coating showed presence of numerous carbides along with powder constituents (Fig. 5.18). The presence of these carbides indicates that heavy oxidation and decarburization of powder might have occurred during spraying. Numerous papers have supported the presence of these chemical compounds in WC-based MMC coating during spraying and have mentioned their deleterious effect on mechanical properties of the coating [40 – 43, 218].

The XRD analyses of FSP-treated HVOF-sprayed WC-Ni MMC coating showed presence of all the chemical constituents present in the HVOF-sprayed coating (Fig. 5.19). The presence of $CoWO_4$ and Co_3W_3C in XRD result of FSP-treated coating does not indicate that they were absent in HVOF–sprayed coating. They were over-shadowed by significant content of other phases. Usually, formation of any extraneous phases during spraying results in increased porosity and generation of residual stresses ultimately reducing mechanical properties like toughness, resilience, etc. in the WC-Ni MMC coating [40 – 43, 218].

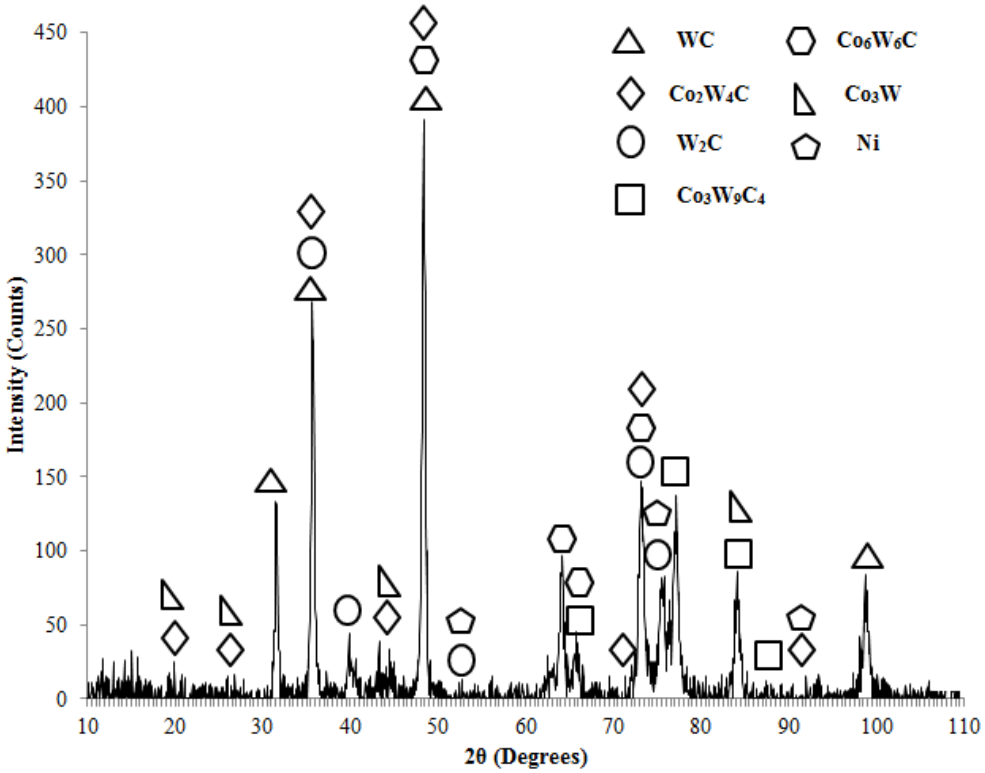

Figure 5.18. XRD result of as-sprayed HVOF-sprayed WC-Ni MMC coating.

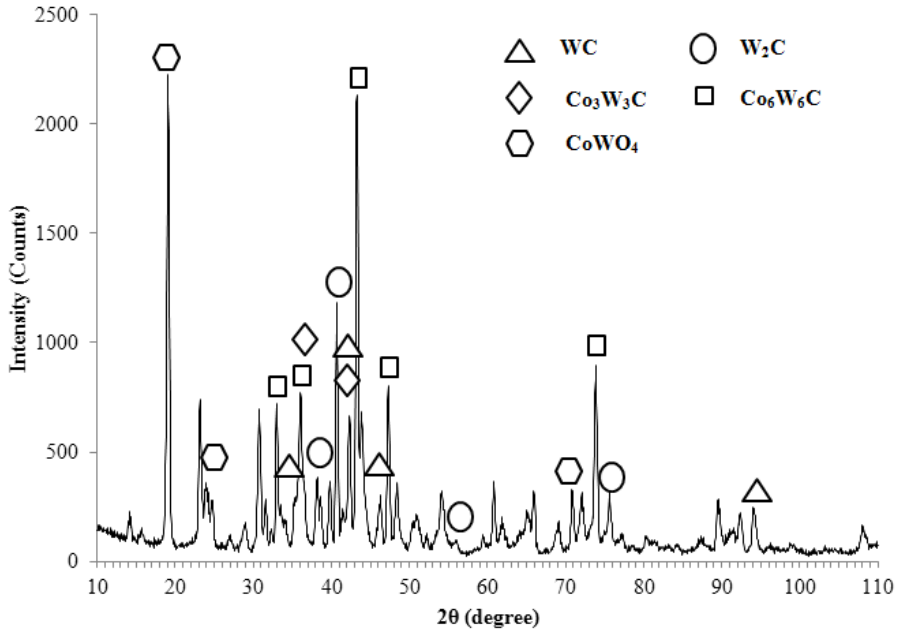

Figure 5.19. XRD result of FSP-treated HVOF-sprayed WC-Ni MMC coating.

The effect of FSP treatment on mechanical properties of thermal-sprayed WC-Ni MMC coating is represented in Table 5.3 and 5.4. Seeing the wear result, it is clear that the effect of presence of these phases on mechanical properties of MMC coating is negligible and FSP treatment has resulted in improved homogeneity and uniformity in the microstructure.

Usually, the presence of intermetallic phases and compounds in the microstructure resulted in lowering of ductility and toughness due to depletion of useful constituents like Ni, Co [40 – 43, 218]. However wear results of FSP treated coating indicated that the presence of these phases does not have a detrimental effect on the mechanical properties of the composite. To understand the reason behind improvement in wear resistance, images of the wear tested FSP-treated thermal-sprayed WC-Ni coatings will be analyzed.

Table 5.3. Effect of FSP treatment on mechanical properties of cold-sprayed WC-Ni MMC coating.

Parameters	**Cold-sprayed WC-Ni MMC coating**	**FSP-treated cold-sprayed WC-Ni MMC coating**
Wear rate (mm^3/N-m)	20.2×10^{-6}	5.0×10^{-6}
Carbide distribution	Agglomerated islands of WC-12Co distributed in a sea of nickel binder	Uniform and homogenous distribution of individual WC-12Co in nickel binder
Carbide size range	25 - 45 µm	0.5 - 2.5 µm
Hardness	410 ± 50 $HV_{0.3}$	420 ± 20 $HV_{0.3}$
Mean free path	9.7 µm	1.6 µm
Toughness measurement at 1000 gf load	Coating cracked, hence lower toughness	No cracks in coating, hence higher toughness

Table 5.4. Effect of FSP treatment on mechanical properties of HVOF-sprayed WC-Ni MMC coating.

Parameters	**HVOF-sprayed WC-Ni MMC coating**	**FSP-treated HVOF-sprayed WC-Ni MMC coating**
Wear rate (mm^3/N-m)	3.1×10^{-6}	0.65×10^{-6}
Hardness	840 ± 97 $HV_{0.3}$	990 ± 69 $HV_{0.3}$
Toughness measurement at 1000gf load	No cracks in coating, hence high toughness	No cracks in coating, hence high toughness

5.4 Wear result of non-FSP and FSP-treated thermal-sprayed WC-Ni coating

For FSP-treated cold-sprayed WC-Ni MMC coating, there were few cracks emanating from the surface and travelling sub-surface with slanted orientation (Fig. 5.20 and 5.21). The FSP-treatment has transformed WC-Ni coating into compact, rigid material due to uniform and homogenous distribution of hard, rigid WC-12Co particles in the MMC (Fig. 5.21 (a)). The surface showed asperities and undulations which had more hardness and toughness than non-FSP treated WC-Ni MMC coatings (refer Table 5.3 and 5.4). These undulations resulted into fluctuating stress during wear. The surface cracks seem to have evolved due to the action of fluctuating stress resulting in fatigue loading on the composite [23, 32, 115, 119, 205]. The path of the cracks seems to be comparatively straight compared to cracks seen in cold-sprayed WC-Ni MMC coating (Fig. 5.21 (b)). Also, these cracks in FSP-treated coating are thin in width and propagate by fracturing soft nickel binder (see Fig. 5.20 (a)). This indicated that their path of travel was motivated by the presence of soft, ductile nickel binder. Since, the thickness of the nickel trapped between carbides was thin, hence crack width was also less. Cracks seem to by-pass hard reinforcing carbides, which indicate that energy at the crack tip was not enough to crack carbides.

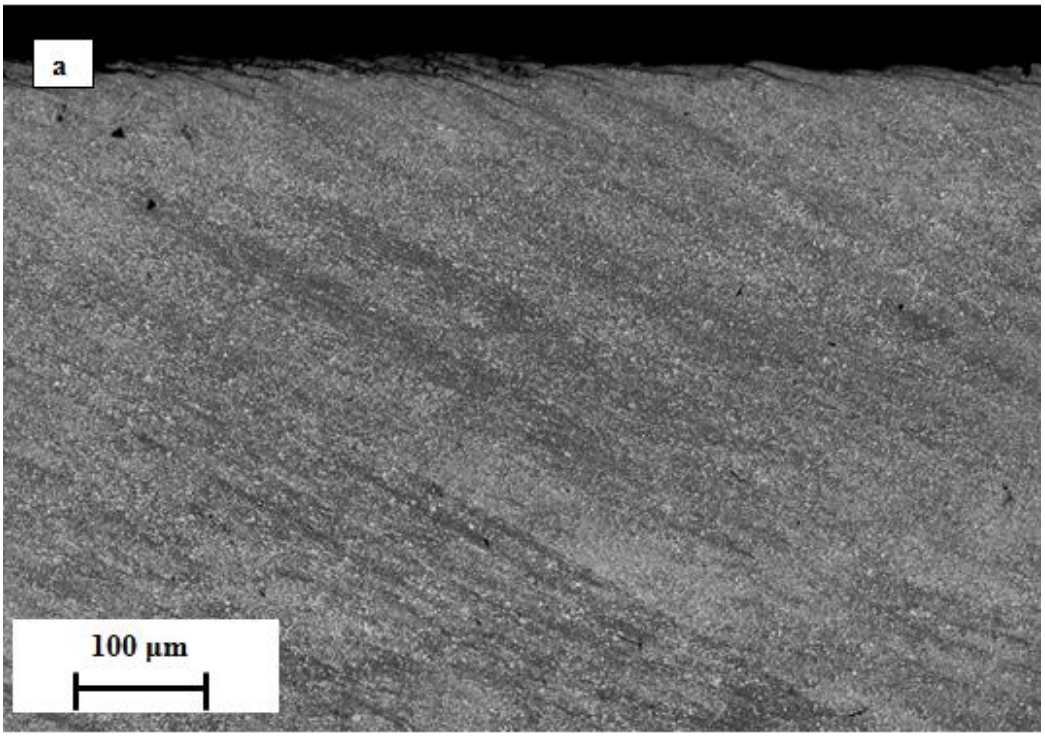

Figure 5.20 (a). Cross-sectional BSE-SEM images of wear tested FSP-treated cold-sprayed WC-Ni MMC coating at high magnification.

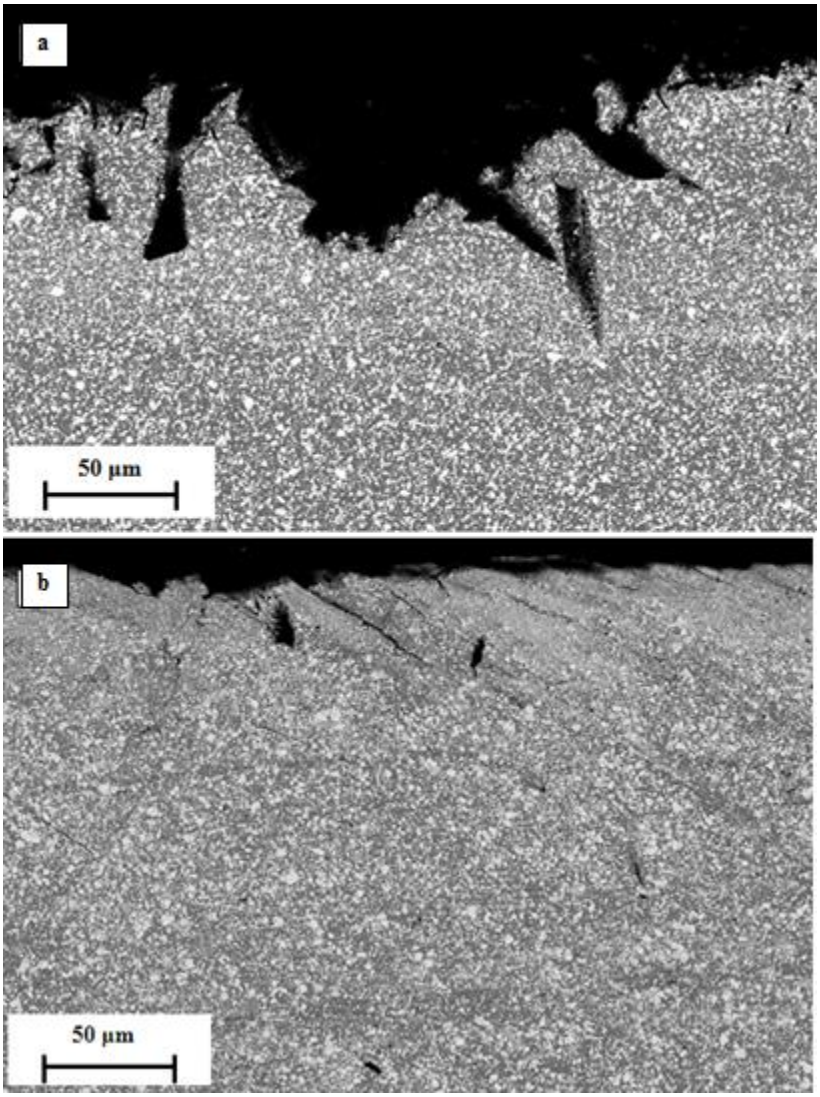

Figure 5.21 (a) and (b). Cross-sectional BSE-SEM images of wear tested FSP-treated cold-sprayed WC-Ni MMC coating at high magnification.

For HVOF-sprayed WC-Ni MMC coating, the cracking was completely evident in the form of fatigue and delamination cracks (Fig. 5.22). As seen in Fig. 5. 22, the top surface of the coating showed several indents due to the attack of abrasives. As seen in Fig. 5.23 (b), the attack of abrasives resulted in indents at the surface which created a key location for crack nucleation. The microstructure showed presence of sub-surface cracks with orientation parallel to the surface (Fig. 5.23). The cracks travelled the path of least resistance by fracturing the nickel binder located between carbides.

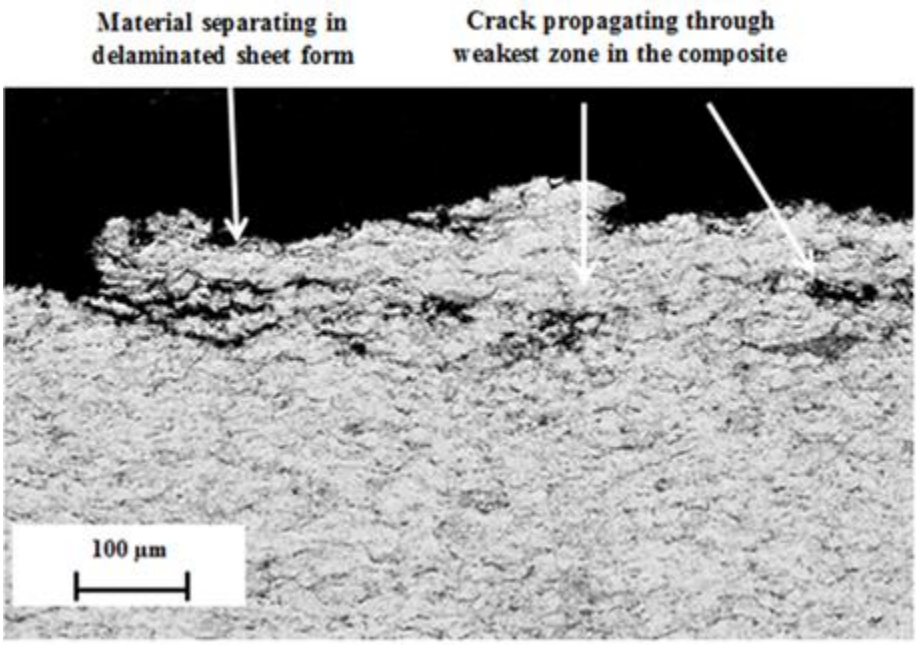

Figure 5.22. Cross-sectional BSE-SEM images of wear-tested HVOF-sprayed WC-Ni MMC coating at low magnification.

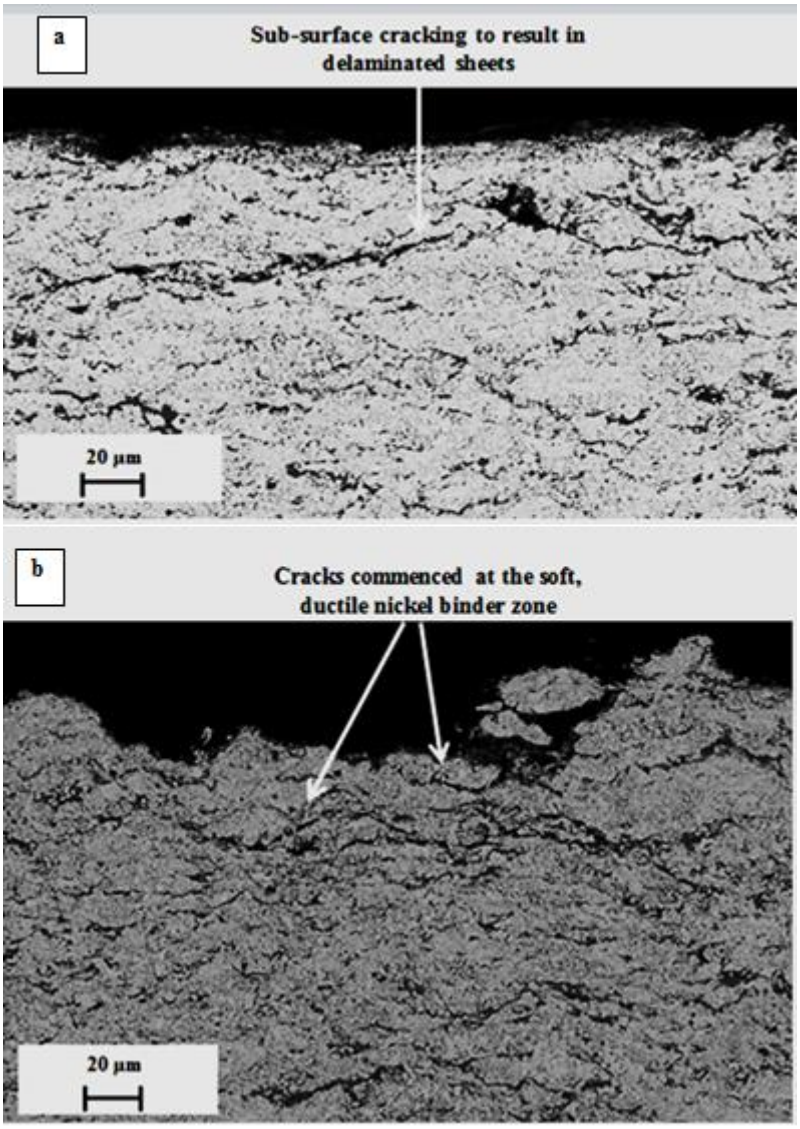

Figure 5.23 (a) and (b). Cross-sectional BSE-SEM images of wear-tested HVOF-sprayed WC-Ni MMC coating at high magnification.

For FSP-treated HVOF-sprayed WC-Ni MMC coating, the cracking was completely minimal (Fig. 5.24 - 5.26), however cross-sectional images of wear-tested FSP-treated WC-Ni MMC coating showed different morphology. Abrasives had damaged the surface which was evident in the form of scratches or indents on the material (Fig. 5.25 – 5.27). The damage was not so severe in the form of cracking or ploughing off of material. It seemed that, adhesion between different phases in the composite was good hence surface was immune to the

attack of fluctuating stress. There was minimal presence of fatigue cracks as well as the sub-surface delamination cracks, indicating that the material was less vulnerable to the effect of hydrostatic (normal) and shear stresses generated during wear. The surface of FSP-treated HVOF-sprayed WC-Ni MMC coating showed ploughing-off as material removal phenomena; however this removal is minute in comparison with the cold-sprayed WC-Ni MMC coating (See Fig. 5.25 and 5.26). The soft nickel binder present between carbides in the FSP-treated HVOF-sprayed WC-Ni MMC coating was distributed in such a way that they occupy less vulnerable position in the coating. The heat generated during FSP treatment resulted in the formation of various oxides and carbides which act as binding agent in the composite. The thermal and mechanical stresses applied during FSP treatment combined with the mechanical mixing vortex resulted in uniform and homogenous coagulation. The microstructure showed improved adhesion assisted by the thermal and mechanical stress which fuses porosity and cracks (if any) generated during HVOF spraying. The vanishing of clearly visible nickel binder in HVOF-sprayed WC-Ni MMC coating after FSP treatment indicated that the structure had less vulnerable phases for crack initiation and propagation. Usually, the presence of hard phases like oxides and carbides of the cobalt, nickel and tungsten carbide resulted in an increase in brittleness and lower toughness of the coating. The difference in mechanical properties like hardness, toughness, of these phases might increase chances of vulnerability of coating to cracking during cooling. The presence of these phases will result in residual stresses and will induce brittleness in the composite. It was postulated that the presence of hard phases and transformation of ductile binder to hard, brittle nickel oxides will lower fatigue strength and increase the tendency of generation of fatigue cracks [32, 40 - 43, 218, 115 - 119]. However the absence of any cracks (fatigue cracks, cooling cracks and delaminated cracks) indicates that the structure was immune to the attack of abrasives even after 2000 wheel revolutions.

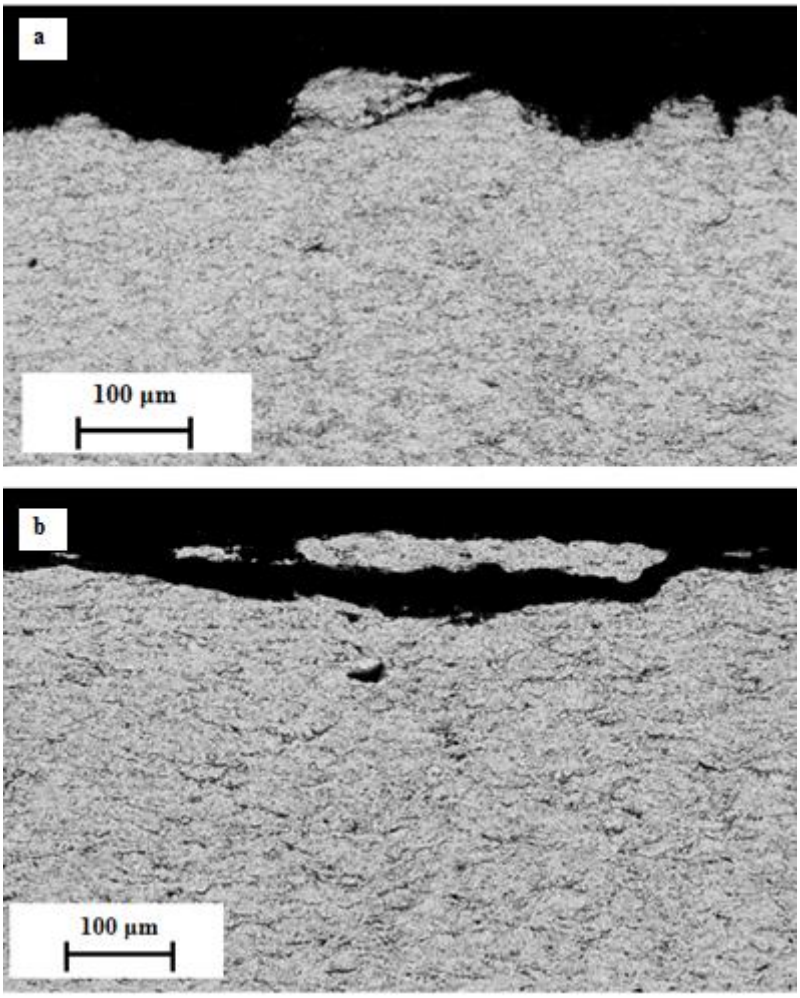

Figure 5.24. Cross-sectional BSE-SEM images of wear-tested FSP-HVOF-sprayed WC-Ni MMC coating showing cracked and delaminated wear sheet.

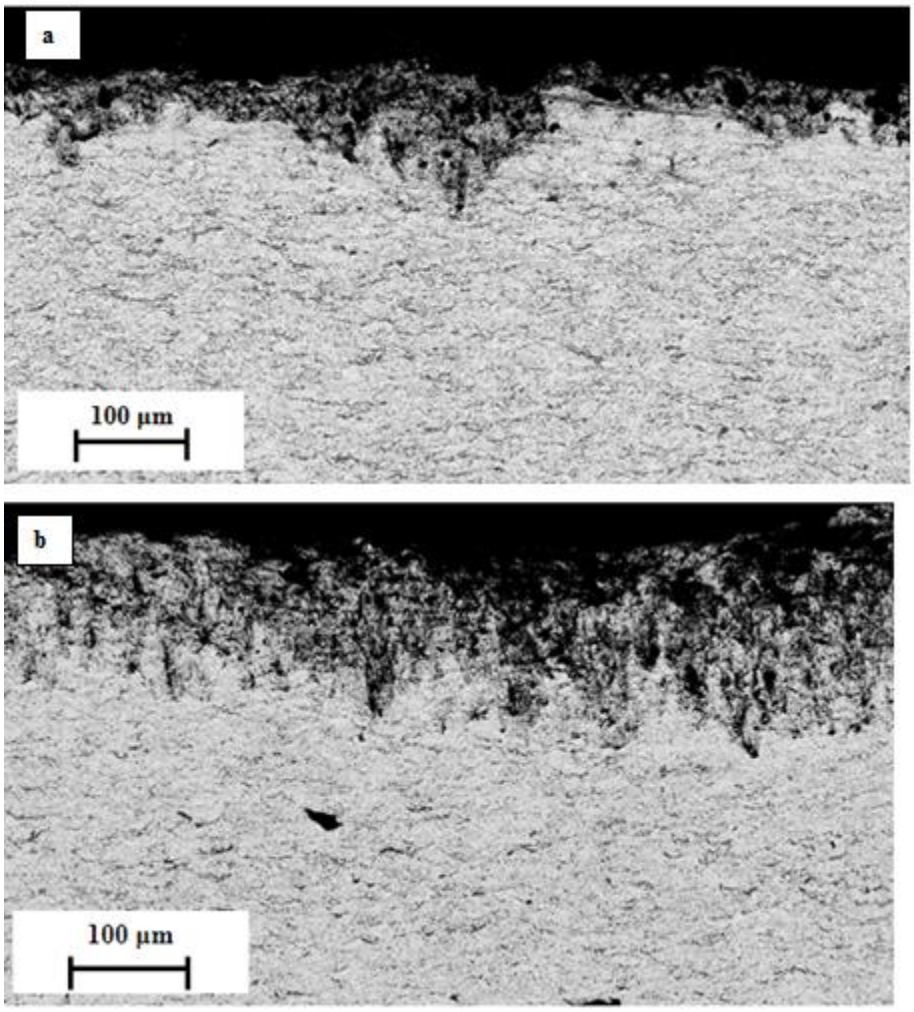

Figure 5.25. Cross-sectional BSE-SEM images of wear-tested FSP-HVOF-sprayed WC-Ni MMC coating showing shallow indents of abrasives during wear.

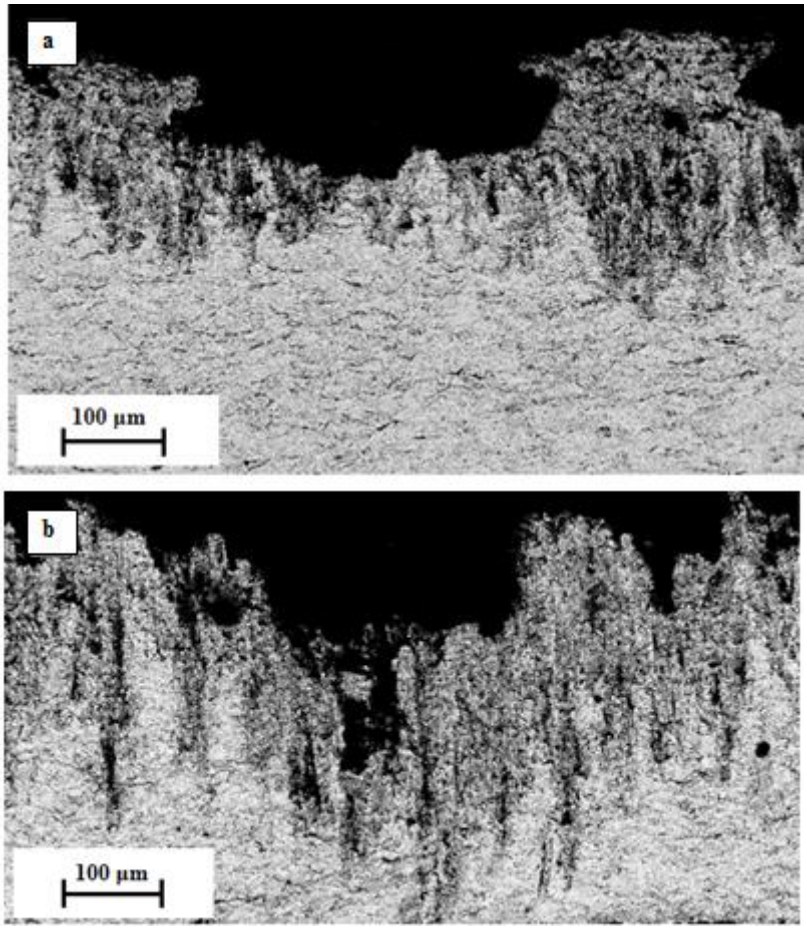

Figure 5.26. Cross-sectional BSE-SEM images of wear-tested FSP-HVOF-sprayed WC-Ni MMC coating showing deep indents of abrasives during wear.

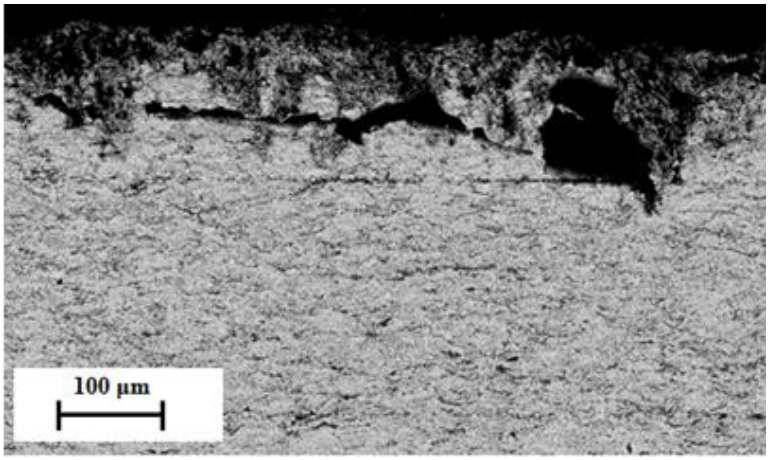

Figure 5.27. Cross-sectional BSE-SEM images of wear-tested FSP-HVOF-sprayed WC-Ni MMC coating showing cracked wear sheet.

5.5 Wear mechanism

To understand the reasoning for improvement in wear resistance of FSP-treated thermal-sprayed WC-Ni MMC coating, it was necessary to understand the wear mechanism defining their wear performance.

Let us consider cross-section of wear-tested cold-sprayed WC-Ni MMC fabricated from optimized composition. As can be seen in Fig. 5.28, there is distinctly visible wide sub-surface crack travelling parallel to the surface. Its propagation was motivated by the presence of soft, ductile nickel binder in the MMC.

The surface cracking was minimal However sub-surface cracks were evident in many images. In few cross-sectional images of wear-tested material, there was substantial removal of material at surface which was evident in form of reduced thickness at that zone. It seems that stress during wear resulted in wear away of material However shear stress in sub-surface zone acts on movement of dislocations which could one of the prominent reason for crack initiation and propagation. The cracking seems to be motivated by pre-existing pores or nucleation of new pores due to action of stress at reinforcement-binder interface. These pores under action of compressive stress collapse to form micro cracks. The propagation of these cracks may be further assisted by the shear stress along with soft nickel binder.

Hence, to understand the behaviour of such material, a model needs to be constructed which will depict the wear behaviour. The model should represent the material before wear and after wear. Effects of pore nucleation, reinforcement shape and size seems to play important role on wear of material. Hence, they should be designed in such way that their presence should reflect pronounced effect of wear of material. The interfacial toughness of reinforcement-binder play crucial role and is strong function of fabrication process also. Hence, development of appropriate model may help to elucidate the wear mechanism of this MM

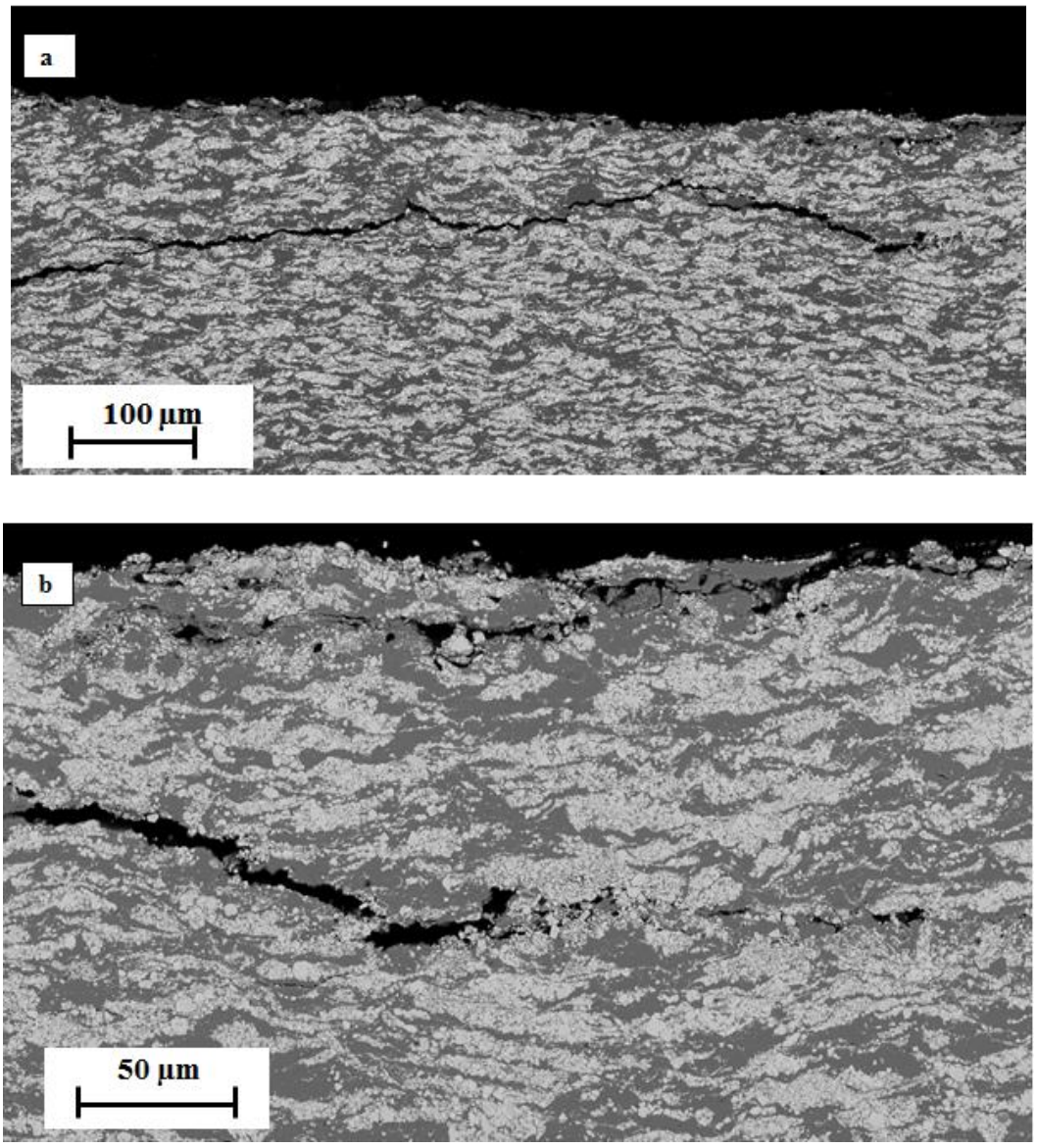

Figure 5.28. Cross-sectional BSE-SEM image of cold-sprayed WC-Ni MMC coating fabricated from powder composition of 96 wt.% WC - 4 wt.% Ni (a) at low magnification and (b) at high magnification.

The microstructure of the cold-sprayed WC-Ni MMC can be represented as shown in schematic diagram below (Fig. 5.29).

Figure 5.29 shows schematic of microstructure of cold-sprayed WC-Ni MMC coating fabricated from powder composition of 96 wt.% WC – 4 wt.% Ni. As can

be seen, there is dispersion of agglomerated WC-12Co reinforcing particles in the soft, ductile nickel binder. The reinforcing particles are widely scattered in the composite indicating that average mean free path between two carbides is high. When such composite is exposed to wear conditions, the abrasives attack the soft, nickel binder easily. The hard reinforcing WC-12Co particles are able to protect nickel surrounding it however areas of nickel widely separated from reinforcing particles remain unprotected (Fig. 5.30). These become an easy target for flowing abrasives. Also, hard reinforcing particles offer resistance to flowing abrasives, due to which they roll on the surfaces. Hence, abrasives spend more time on the surface and travel comparatively longer time before coming to rest. During rolling on surface, they are able to transfer their kinetic energy for wearing away of soft nickel binder. Hence, such composite shows deep depression and wide crater during wear test.

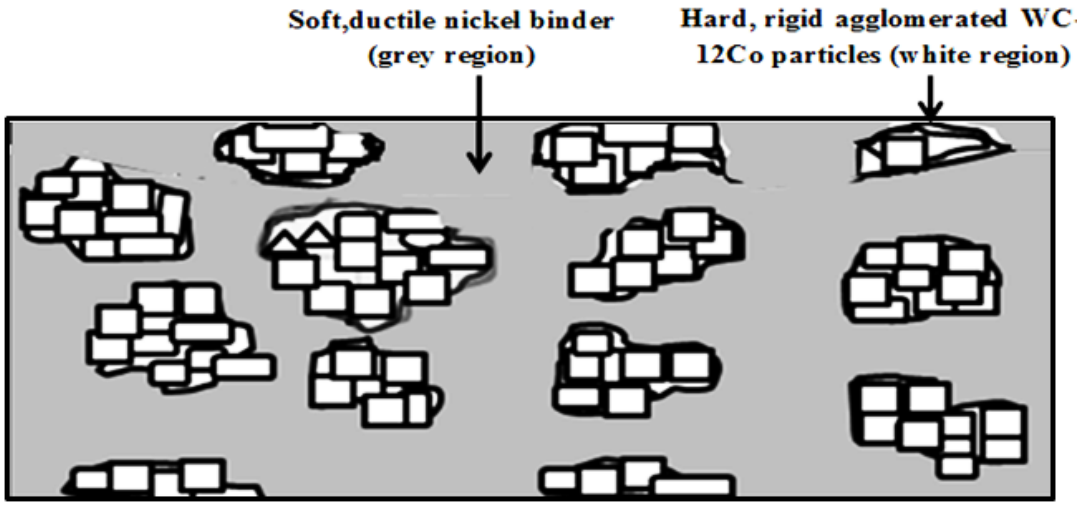

Figure 5.29. Schematic representation of cold-sprayed WC-Ni MMC coating fabricated from powder composition of 96 wt.% WC – 4 wt.% Ni.

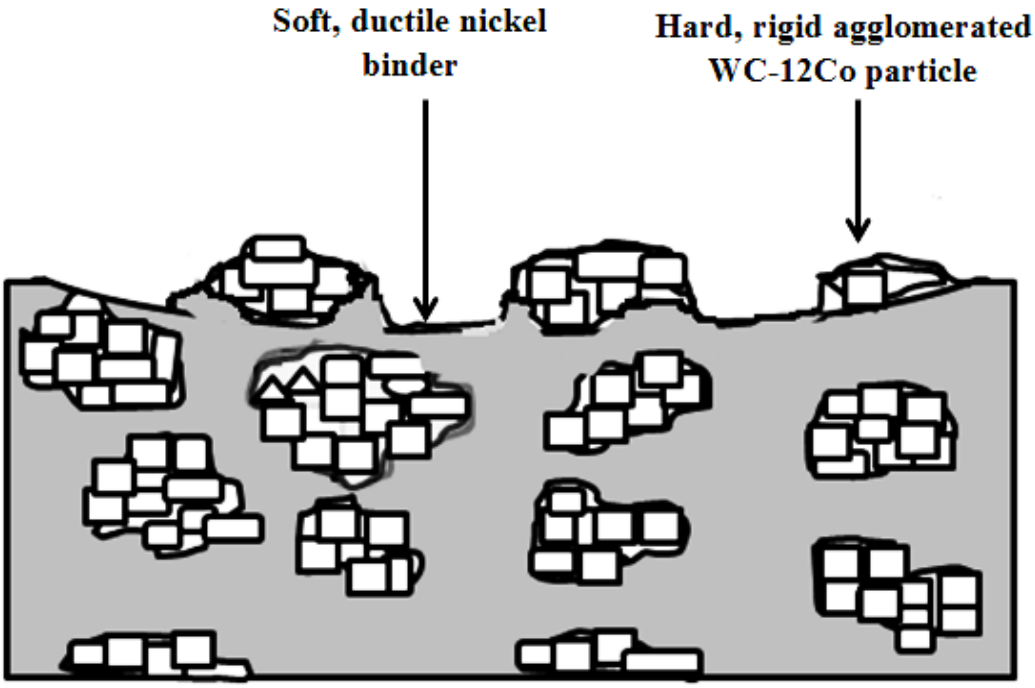

Figure 5.30. Schematic representation of wear-tested cold-sprayed WC-Ni MMC coating fabricated from powder composition of 96 wt.% WC - 4wt.% Ni.

It is seen that reinforcement shape has definite effect on deformation response and void nucleation tendency [23]. Let l_o/r_o be the aspect ratio of the reinforcement where l_o= length of the reinforcement while r_o = radius of the reinforcement. It is found that for reinforcement with $l_o/r_o >> 1$, the flow strength and strain hardening effect is higher. Actually flow strength is. Also, hydrostatic stress at the corner of the reinforcement is higher, resulting in development of plastic strains in the binder material around it. These aspects eventually result in void nucleation [22, 23, 37, 189, 205, 217]. A close look at Table 5.3 indicates that carbide size for cold-sprayed WC-Ni MMC varies in range of 25 - 65µm while for FSP-treated cold-sprayed WC-Ni MMC, it lies in range of 0.5 - 1µm. For large agglomerated carbides, their complete wetting with nickel is improbable. Hence, there will be some areas, which will remain uncovered and will appear as void. Also, widely scattered WC-12Co agglomerated particles indicate that they did not offer compressive stress effectively to surrounding nickel binder during spraying. Thus, loosely packed nickel binder will exhibit pores in it (Fig. 5.31). Numerous such

voids are present in widely scattered nickel in microstructure indicating loose packing of nickel in the composite. Such pores may have contributed to wear by offering easy route for crack nucleation and propagation as per delamination theory [22, 23, 37, 189, 217].

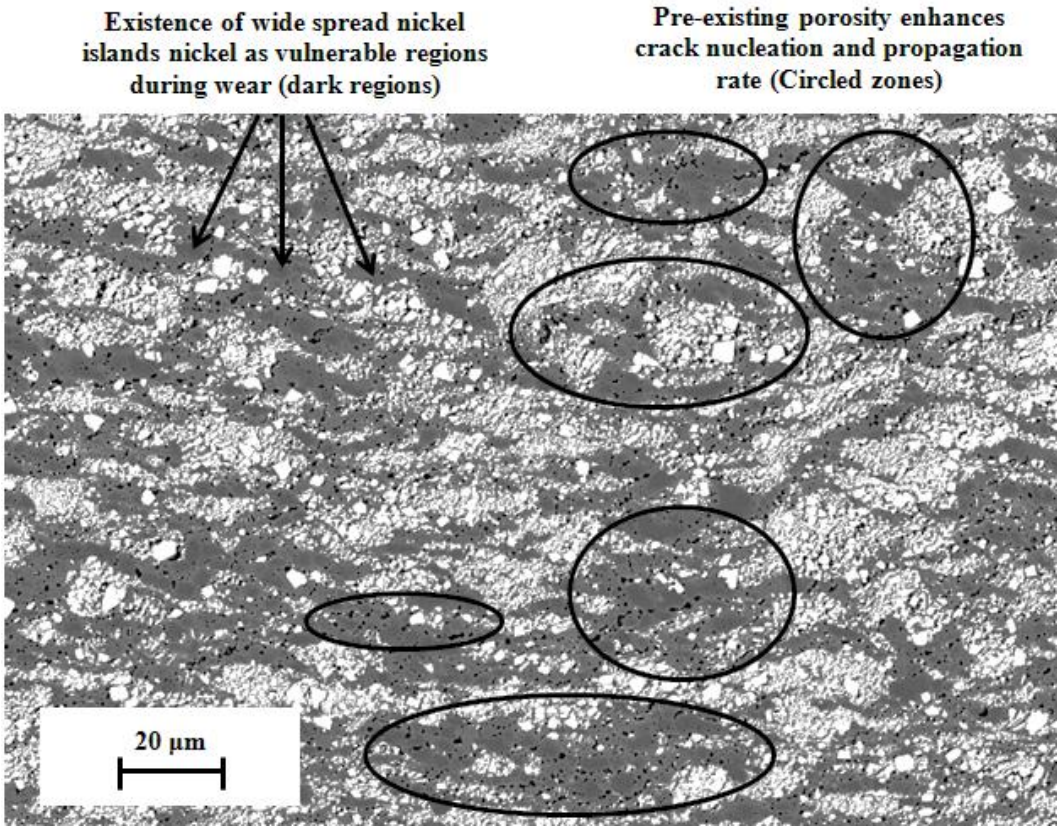

Figure 5.31. Cross-sectional BSE-SEM image of as-sprayed cold-sprayed WC-Ni MMC coating showing presence of numerous pre-existing voids in the microstructure.

For FSP-treated cold-sprayed WC-Ni coating, different wear morphology is seen. This will be explained with use of Fig. 5.32. As can be seen in the figure, the FSP-treated cold-sprayed WC-Ni MMC coating can be represented as chequered arrangement of black and white squares in the matrix. Black regions represent nickel binder while white regions symbolize WC-12Co particles (Fig. 5.32 (a)). The reason for representing them as equal squares is due to uniform and equi-spaced arrangement of WC-12Co reinforcing particles in the nickel binder (Fig. 5.33). Figure 5.33 (a) represents wear-tested FSP-treated cold-sprayed WC-Ni MMC coating displaying strong effect of FSP-treatment in form of flow lines in the microstructure. Fig. 5.33 (b) shows homogenously distributed WC-12Co particles separated by thin layer of nickel binder. This homogenous representation indicates the effect of FSP treatment on distribution of reinforcing particles in the composite. On subjecting FSP-treated cold-sprayed WC-Ni MMC coating to wear conditions, the wear result showed contrasting difference when compared with non-FSP treated cold-sprayed WC-Ni MMC coating. The SiO_2 abrasives used for wear test have size in range of 212- 300 µm. The carbides appearing in the FSP-treated cold-sprayed WC-Ni have square shape profile with sides in range of 0.3-1 µm while the nickel binder between carbides have width of 0.5- 1 µm. Such composite structure appears like alternate arrangement of hard carbides separated by soft nickel binder wherein hard reinforcing carbides provide hardness while tough nickel provides required stability against fluctuating stress. The structure appears to be compact, and can withstand stress fluctuations easily. When abrasives strike this composite, the thin nickel binder is less vulnerable to the attack, while hard, rigid reinforcing carbides offer strong resistance. The rolling abrasives tender less destructive effect on the composite compared to non FSP-treated WC-Ni MMC coatings. The attack on the nickel binder happens only when sharp corners of the abrasives are able to reach them However their depth of penetration is strongly restricted by the width and depth of the nickel binder. This is due to the presence of hard, rigid WC-12Co particles on sides as well as in the base of nickel binder.

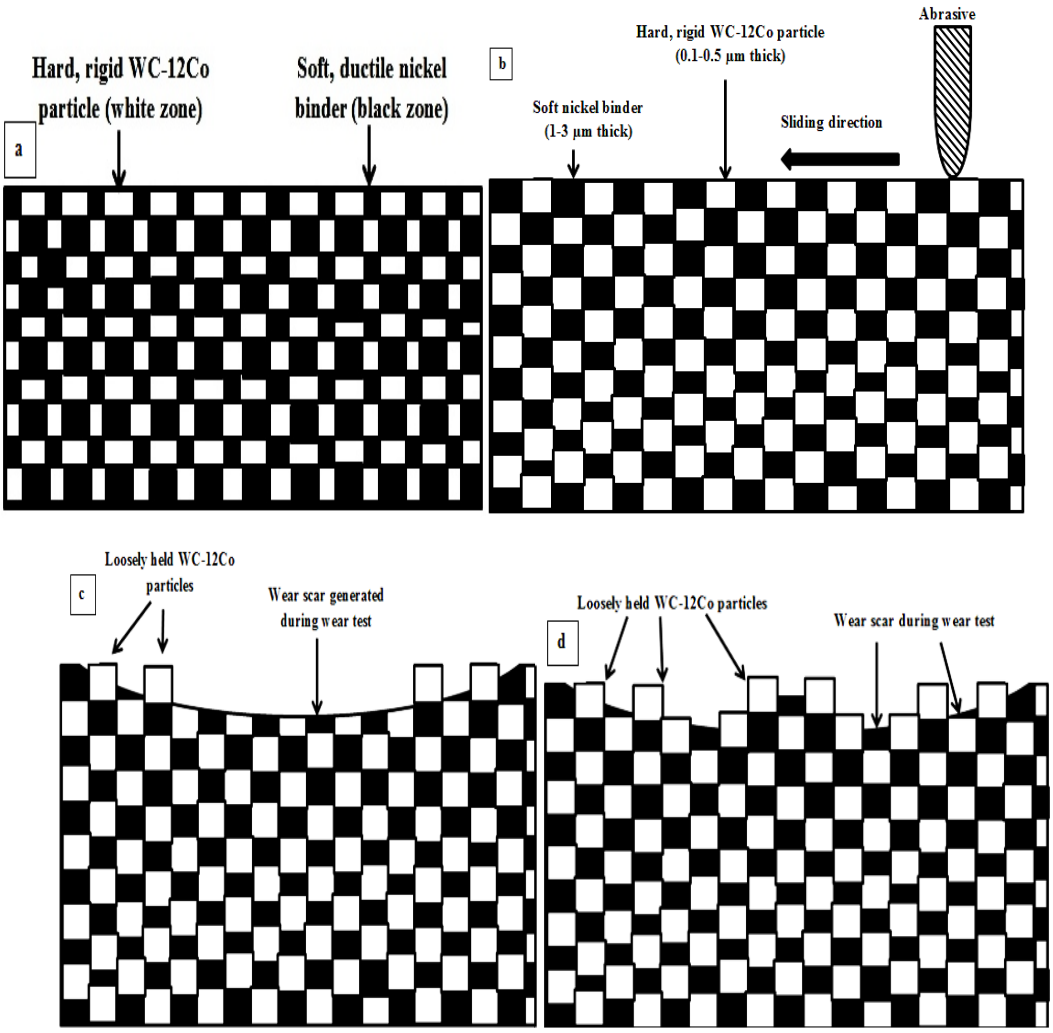

Figure 5.32. Schematic representation of (a) FSP-treated cold-sprayed WC-Ni MMC coating, (b) wear testing, (c) and (d) wear-tested FSP-treated cold-sprayed WC-Ni MMC coating.

The destructive attack of abrasives can happen if large size abrasives are used in the hopper. Such big abrasives are able to transfer large impact energy to the composite surface. Cracking may ensue and will propagate through soft ductile nickel binder. The FSP-treated cold-sprayed WC-Ni MMC coating has more compactness and rigidity compared to non-FSP treated coating. The limited nickel binder between carbides undergoes less plastic deformation during wear. Hence, the impact energy of abrasives may result in cracking or chipping-off of the carbides in the composite. So FSP-treated WC-Ni MMC coating under wear may show wear depression as indicated in Fig. 5.32 (c). However such uniform

removal of carbides is unrealistic and improbable due to its higher hardness compared to nickel as silica abrasive. In few cases, the soft nickel binder may crack or be scrapped-off by flowing abrasives while hard, rigid WC-12Co particles will be held by the limited nickel binder layer at its base (Fig. 5.32 (d)).

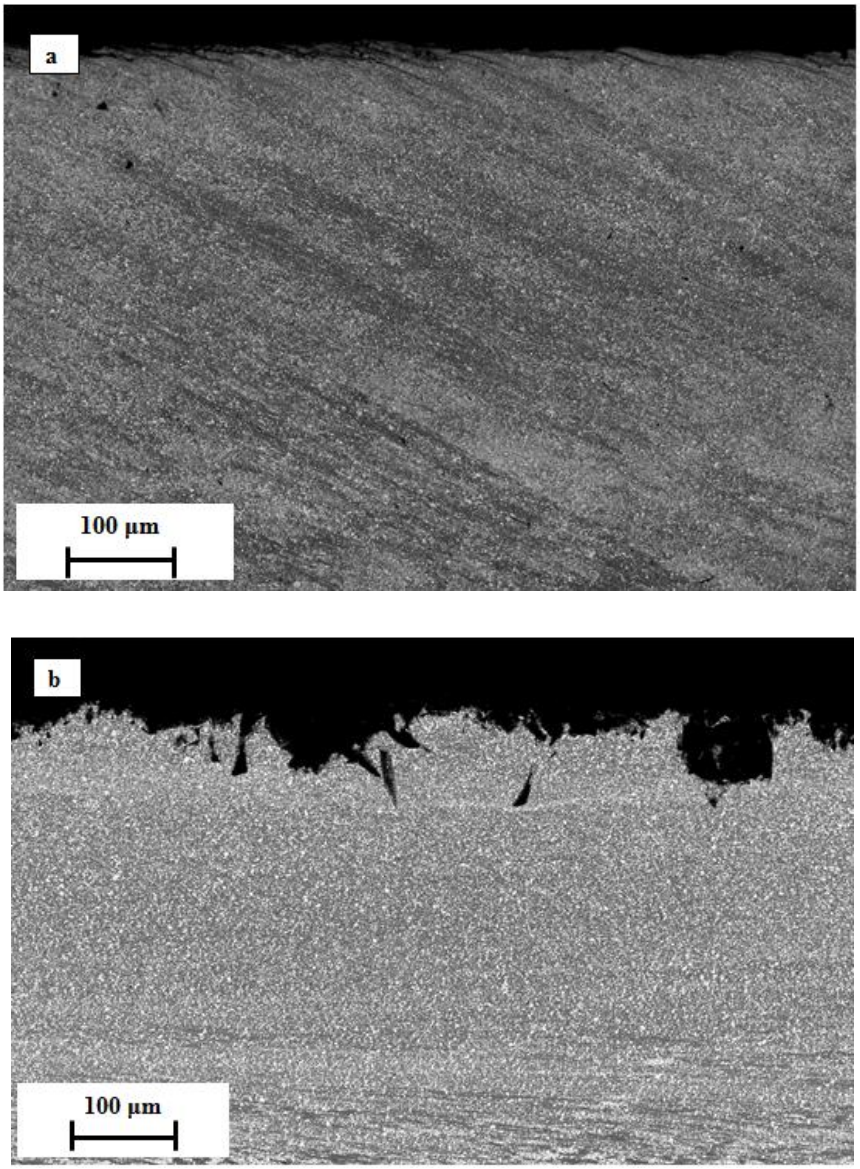

Figure 5.33. Cross-sectional SEM image of wear-tested FSP-treated cold-sprayed WC-Ni MMC coating showing presence of equiaxed and uniform distribution of individual carbides in the composite (a) with flow lines visible, (b) friction stir processed zone visible.

Compared to non-FSP treated cold-sprayed WC-Ni MMC coating, there is less tendency of formation of delaminated sheets in FSP-treated coatings. The main reason for this lies in improved casing of carbides with nickel binder (Fig. 5.34). The nickel binder surrounding individual carbides provide improved wetting of its surface which led to improved adhesive toughness of the composite coating. Also, it is seen that for smooth surface reinforcement with aspect ratio (l_o/r_o) =1, the binder around them are less stressed, hence higher stress is required for void nucleation. Thus, void nucleation tendency is lower for small size and simple shape reinforcement. It is found that particles with aspect ratio of 1 show higher strains to fracture [22, 23, 37]. Thus, high aspect ratio increases tendency to fracture and void nucleation due to the development of tensile hydrostatic stress around them, especially at the corners. Thus, it means that void nucleate easier for particles with sharp corners and edges and less is the tendency for smooth surface particles.

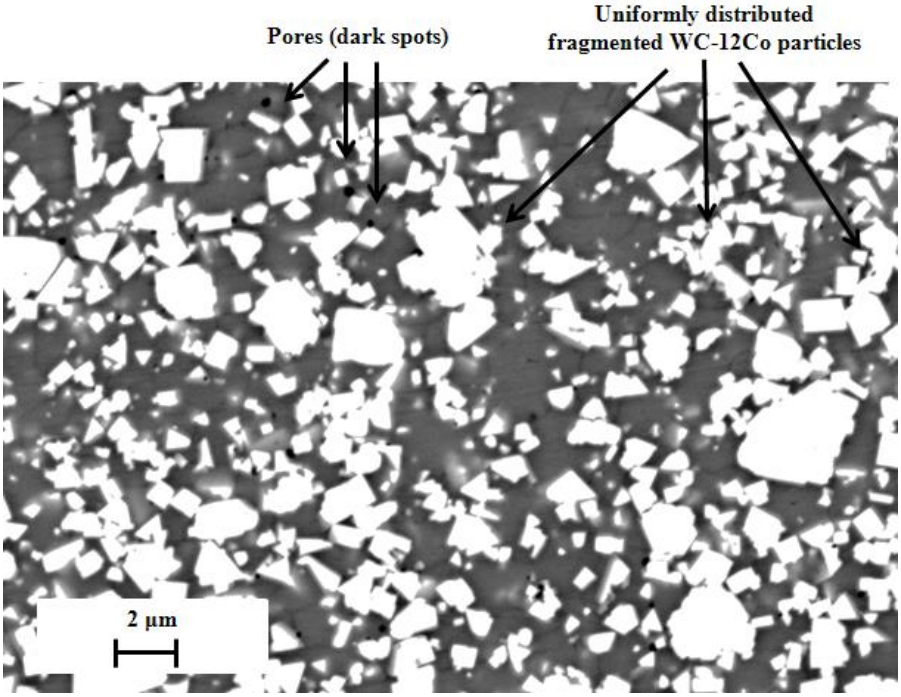

Figure 5.34. Cross-sectional BSE-SEM image of FSP-treated cold-sprayed WC-Ni MMC coating showing reduced content of pre-existing voids in the microstructure.

For HVOF-sprayed WC-Ni MMMC coating, the microstructure looks similar to the structure shown in Fig. 5.35. The white zones indicate the presence of hard, rigid WC-12Co carbides along with other hard oxides, carbides and compounds formed during spraying. The dark boundaries around the carbides indicate the presence of soft, ductile nickel binder. The nickel binder is also seen as widely scattered black islands in the composite (Fig. 5.36). The nickel binder as widely scattered islands in the HVOF-sprayed WC-Ni MMCs, act as vulnerable portion during wear and reduce the wear resistance of the composite coating. During wear, the continuous impact of the abrasives results in cracking of the surface. The fluctuating stress during wear result in easy crack generation at surface whose propagation is motivated by the presence of soft, nickel binder islands in the composite (Fig. 5.37).

The cause for cracking ensue from the rigidity and compactness attributed to the presence of hard phases in the surface. The increased hardness and rigidity combined with increased brittleness, and lower impact and fatigue strength of the MMC result in wear. Also, presence of residual stress during spraying further adds to the straining of the microstructure. This is clearly seen in Fig. 5.37 and 5.38 which show numerous subs-surface cracks oriented parallel to the surface and which nucleate from the coating surface. The opening of the voids under stress during wear is also clearly visible in image which firms the notion that void nucleation and crack propagation is easy in such microstructure.

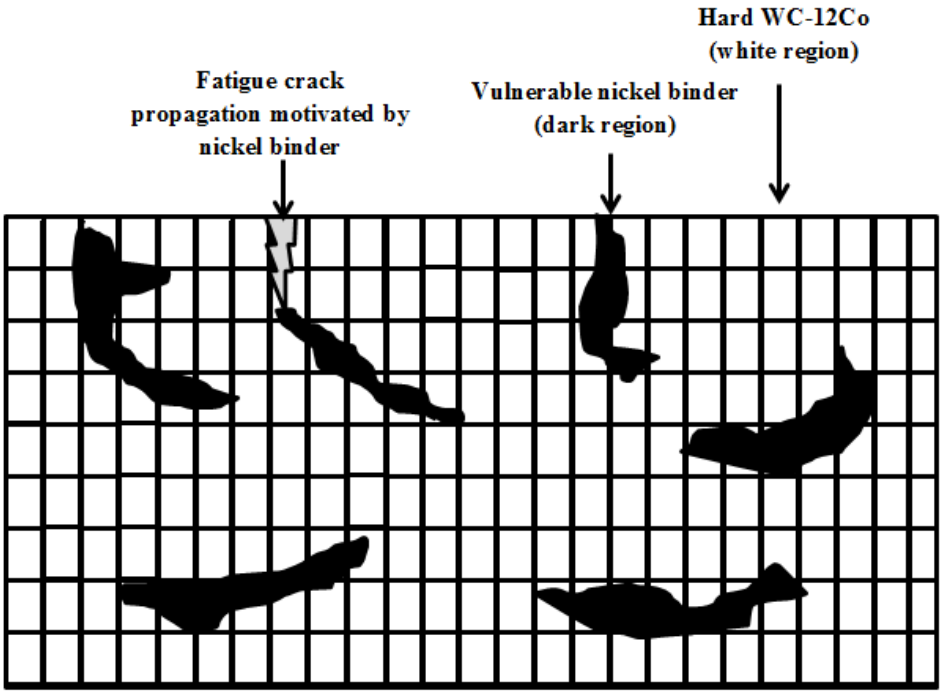

Figure 5.35. Schematic of HVOF-sprayed WC-Ni MMC coating showing islands of nickel scattered in WC-Ni MMC microstructure.

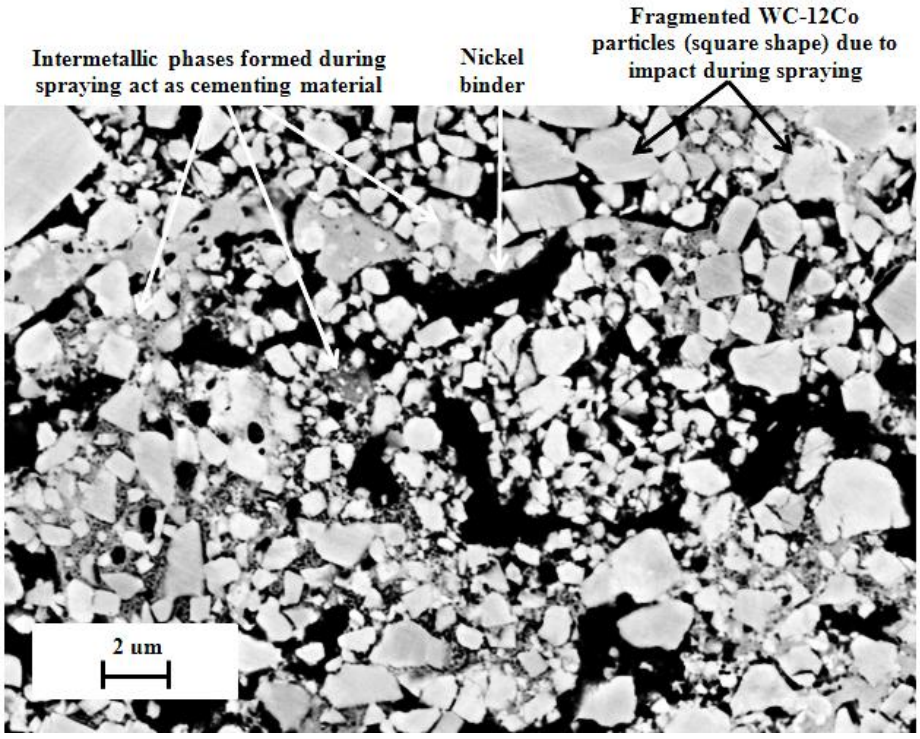

Figure 5.36. Cross-sectional BSE-SEM image of HVOF-sprayed WC-Ni MMC coating showing presence of numerous pre-existing voids in the microstructure.

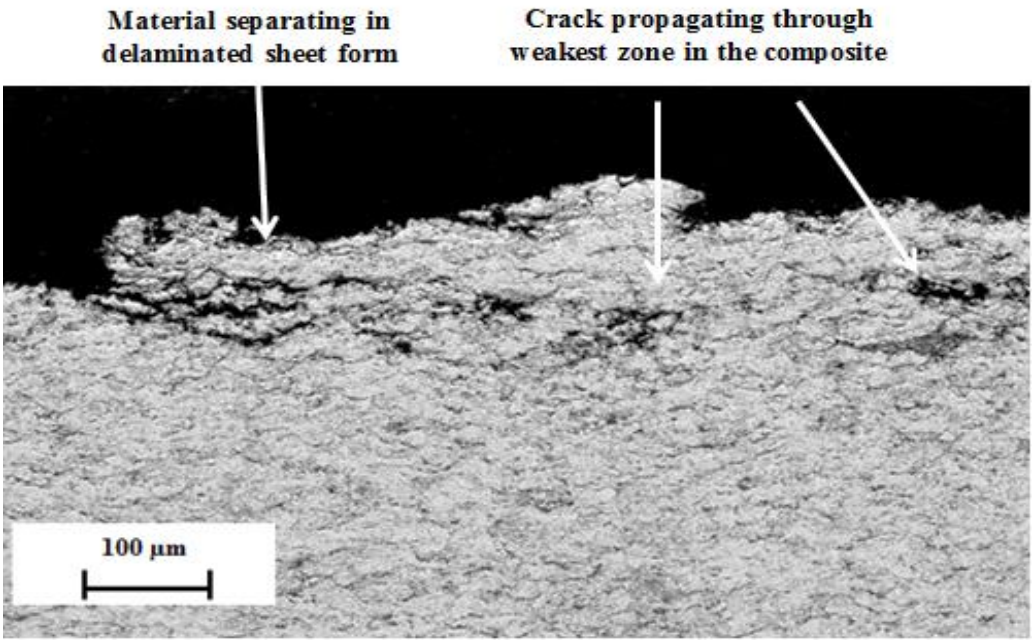

Figure 5.37. Cross-sectional BSE-SEM image of wear-tested HVOF-sprayed WC-Ni MMC coating showing presence of elongated voids and cracks oriented in sliding direction.

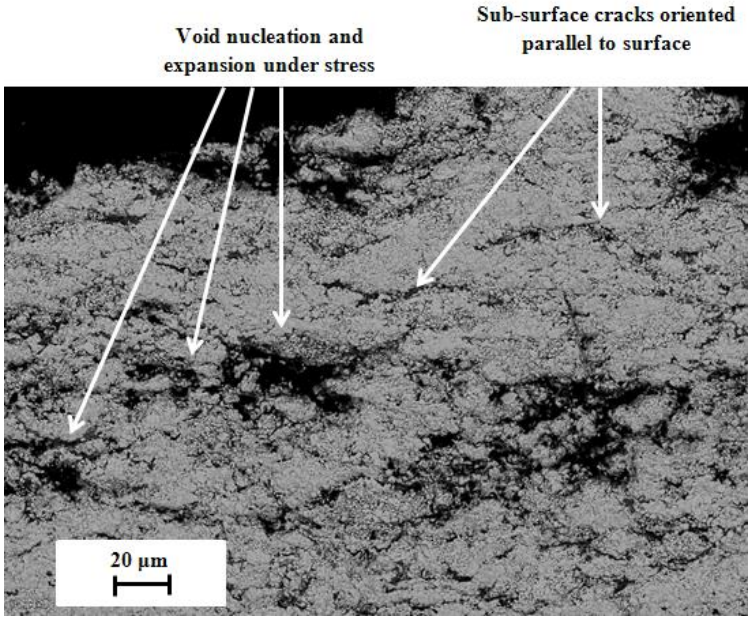

Figure 5.38. Cross-sectional BSE-SEM image of wear-tested HVOF-sprayed WC-Ni MMC coating showing presence of elongated voids and cracks oriented in sliding direction.

The FSP-treated HVOF-sprayed WC-Ni MMC coating can be represented in form of rectangular blocks juxtaposed next to each other (Fig. 5.39). Here, white blocks represent carbides, oxides and all the compounds present in composite while black boundary separating two blocks represent soft, ductile nickel binder. The notion behind such representation lies in fact that nickel binder is uniformly and homogenously distributed in the composite. Also, FSP treatment results in oxidation of some amount of nickel to NiO which further lowers content of soft nickel binder. The nickel binder in this composite appears as cementing agent instead of separate entity in microstructure like in HVOF-sprayed WC-Ni MMC coating (Fig. 5.40 and 5.41). A close look at cross-sectional image of the wear tested microstructure shows presence of scraping-off of composite, However scraping-off was localised. This is evident in Fig. 5.41, which shows that width of wear scar is limited compared to found in wear tested cold-sprayed and HVOF-sprayed WC-Ni MMC coating.

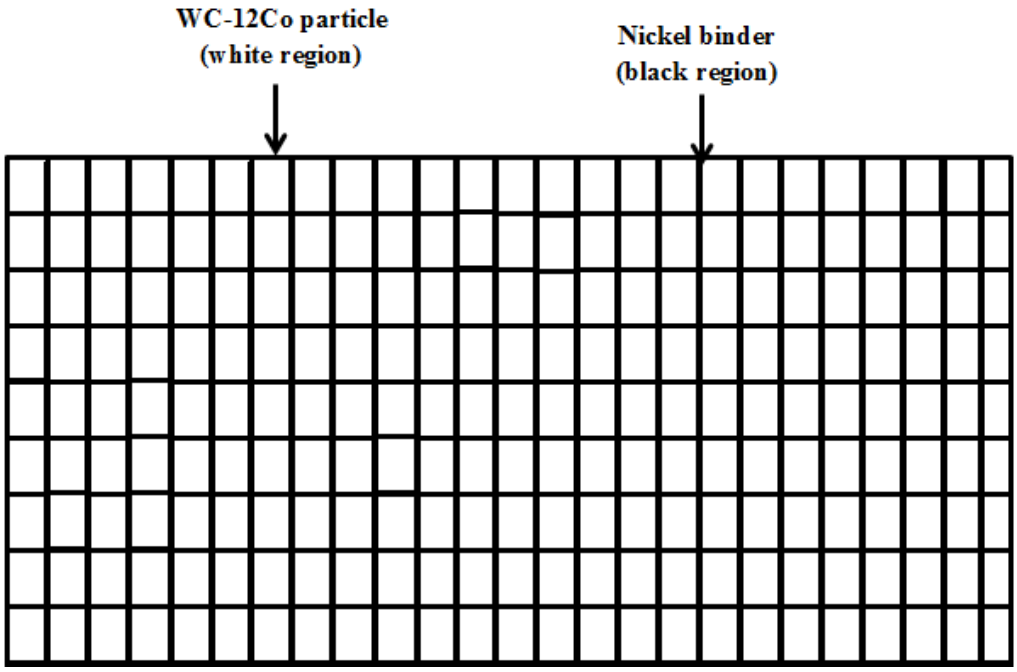

Figure 5.39. Schematic of FSP-treated HVOF-sprayed WC-Ni MMC coating showing islands of nickel scattered in WC-Ni MMC microstructure.

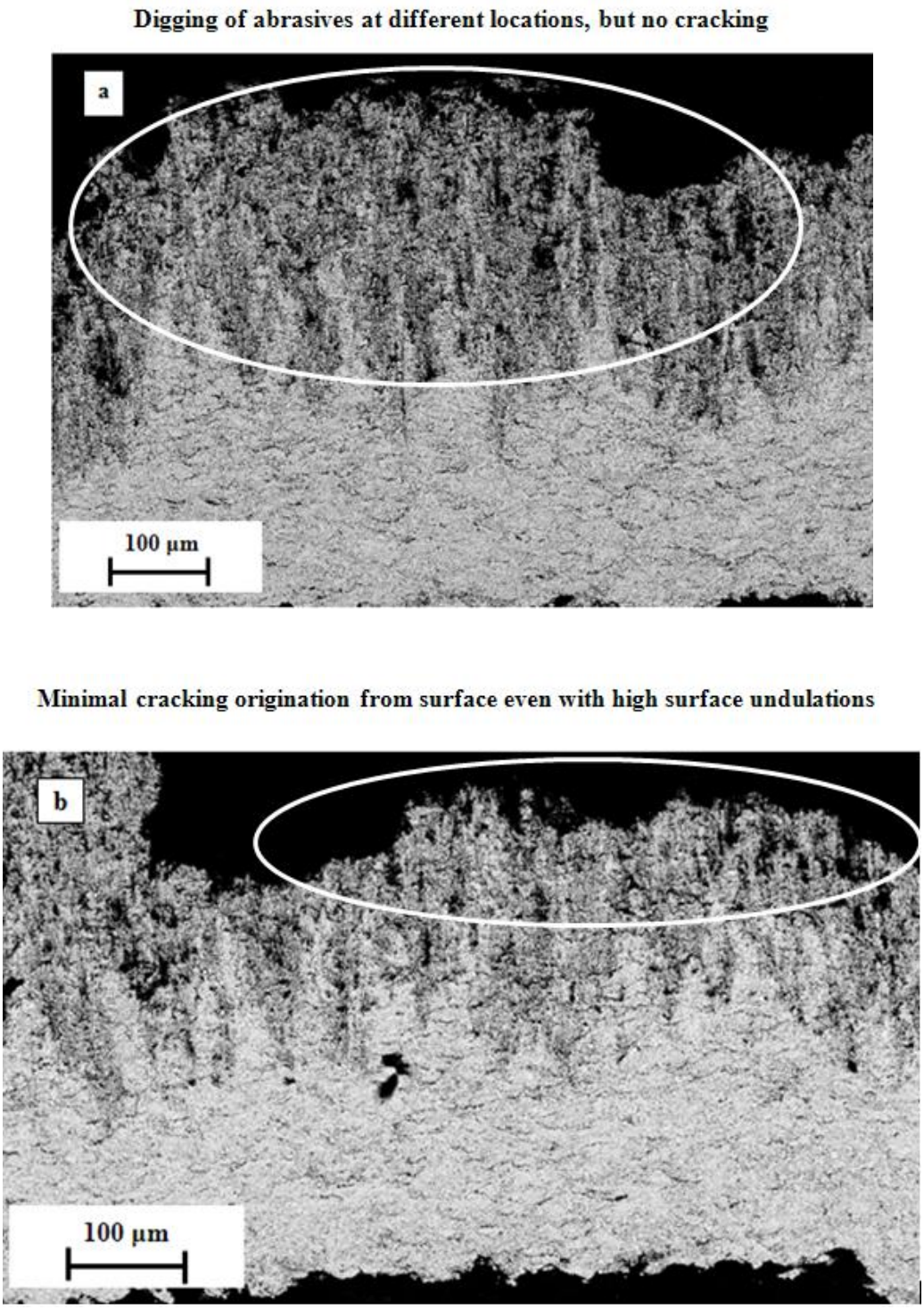

Figure 5.40. Cross-sectional BSE-SEM image of wear tested FSP-HVOF-sprayed WC-Ni MMC coating showing presence of (a) no sub-surface cracking and (b) limited sub-surface cracking, in the composite.

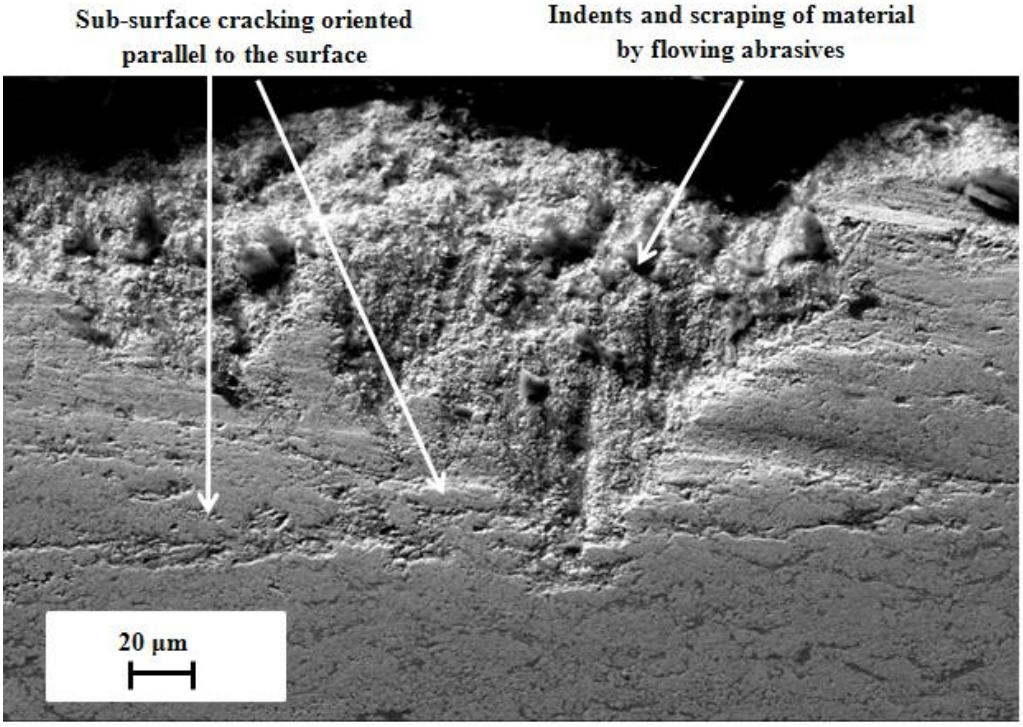

Figure 5.41. Cross-sectional SE-SEM image of wear tested FSP-treated HVOF-sprayed WC-Ni MMC coating showing presence of indents and subs-surface cracks.

The FSP treatment on the HVOF–sprayed coating generated thermal and mechanical stresses which contributed to uniform distribution of carbides and cementing binder. The vortex generated in material due to tool rotation was concentrated in a thin zone from the top surface (Fig. 5.42). Compared to the FSP-treated cold-sprayed WC-Ni MMC coating, the FSP-treated HVOF-sprayed WC-Ni MMC coating showed thin friction stir processed zone.

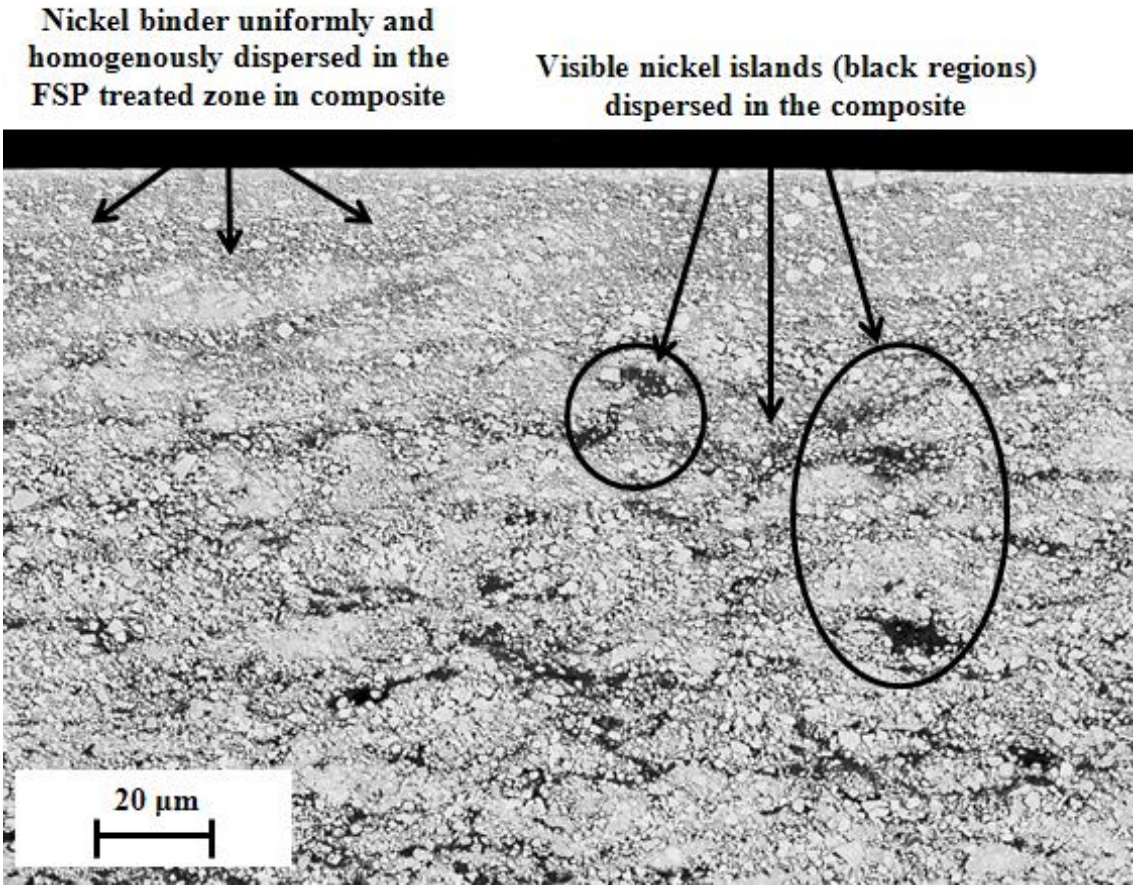

Figure 5.42. Cross-sectional SEM image of FSP-treated HVOF-sprayed WC-Ni MMC coating showing presence of homogenous and uniform microstructure in FSP-treated zone.

Since during HVOF spraying, there is breakage of bonds and fragmentation of agglomerated WC-12Co to individual WC-Co particles, so FSP treatment did not produce pronounced effect on carbides alike FSP-treated cold-sprayed WC-Ni MMC coatings. The absence or reduction in the porosity and cracked zones in the HVOF-sprayed WC-Ni MMC coating after FSP treatment indicates the fusion of pores and micro cracks due to the stresses generated during FSP treatment (Fig. 5.43). The friction stir processed zone showed uniform distribution of WC-12Co carbides in the composites. The distinctly visible nickel islands in HVOF-sprayed WC-Ni vanished to result in uniformly distributed nickel in FSP-treated HVOF-sprayed WC-Ni MMC coating Also, there was an indication of the increased

content of carbides per unit area in the FSP-treated HVOF-sprayed WC-Ni MMC coating compared to non-FSP-treated HVOF-sprayed WC-Ni MMC coating. The carbides being harder, contributed to an overall increase in the average hardness value of the coating in this zone. The toughness measurement made using Vickers indentation technique showed smaller indents with no cracking indicating improvement in adhesive toughness of the microstructure. The improvement in toughness was ascribed to the improved homogeneity in microstructure and reduction in microstructural flaws after FSP treatment. The uniform distribution of nickel binder contributed to enhanced wetting of carbides and collapsing of voids which improved adhesion between them. The uniformity also reduced variation in hardness and contributed to improved wear resistance of the MMC.

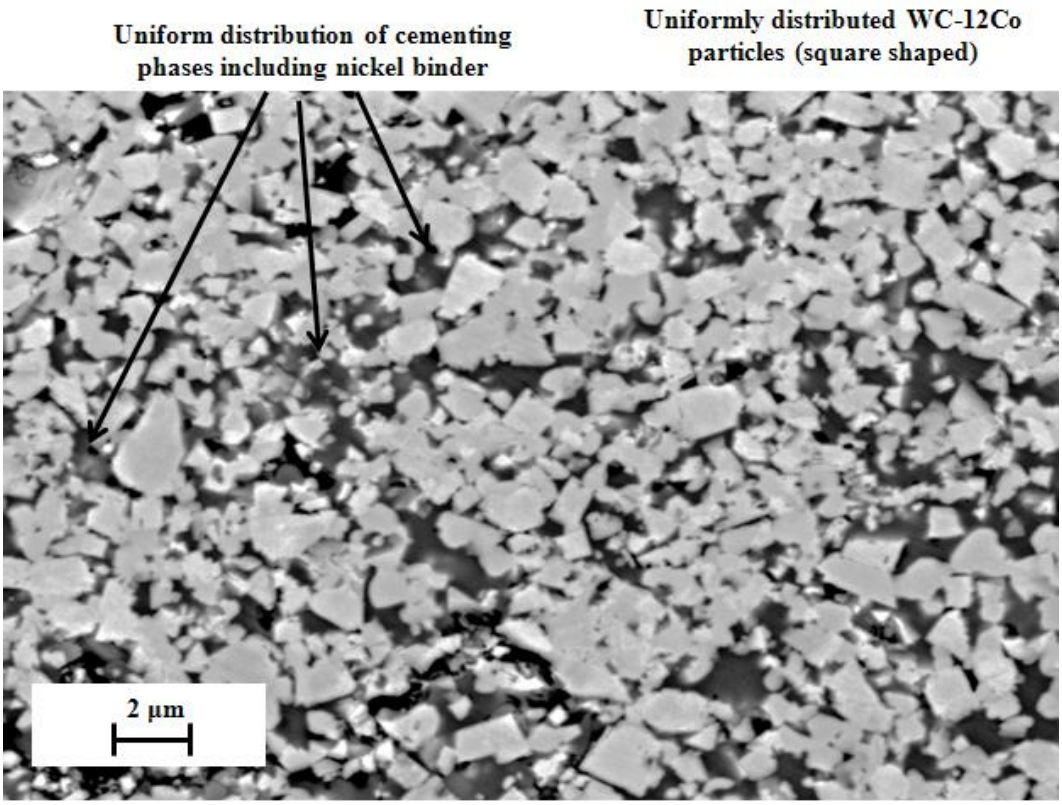

Figure 5.43. Cross-sectional BSE-SEM image of FSP-treated HVOF-sprayed WC-Ni MMC coating showing presence of nickel binder uniformly distributed in the microstructure.

Chapter 6. Conclusion

The cold-sprayed and HVOF-sprayed pure nickel and WC-Ni MMC coating were wear tested in dry abrasive wear test. The study involved optimization of wear rate for different WC-Ni MMC coatings with varying content of WC. Similarly, FSP-treated cold-sprayed and HVOF-sprayed WC-Ni MMC coatings after characterization were wear tested in similar wear conditions like as-sprayed coatings. The major deriving conclusion of this study was:

a. The mechanically blended WC-Ni mixture used for cold spraying of WC-Ni MMC coating showed non-homogenous distribution while transit through hose. This was assisted by density difference between nickel and WC-12Co powder. The mixture became homogenous as WC content was increased which also resulted in substantial induction of carbide content in MMC coating.
b. An investigation into wear mechanism of cold-sprayed WC-Ni MMC coating with varying content of WC-12Co was carried out. The wear changed from completely ductile behaviour combined with continuous delaminated sheet formation to fragmented thin wear sheets for WC-Ni MMC containing higher content of WC. The wear in all MMC seems to be influenced by void content. Void content is progressively reducing as constant of reinforcing WC-12Co particles are increasing. Sub-surface crack nucleation and propagation is motivated by presence of voids which accelerate for porous microstructure. Increased presence of carbides offered resistance to crack nucleation and propagation. The analyses of wear rate of WC-Ni MMC coatings indicated that lowering of mean free path resulted in increased carbide content which enhanced coating toughness during cold-spraying. This resulted in improved coating toughness with less void and crack nucleation followed by enhanced wear resistance.
c. The modified wear theory defined equation for wear rate values of WC-Ni MMC coating with WC- content varying from 10 to 52 vol. % only. For low content of WC, more coating wear rate values should be available to ascertain the defining equation.

d. Friction stir processing showed improved mechanical properties in thermal-sprayed WC-Ni MMC coating with change in tool rotational speed from 900 RPM to 1400 RPM. This was reflected in increased homogeneity, uniformity and better mechanical properties like hardness to name a few.
e. The wear results of FSP-treated thermal-sprayed WC-Ni MMC coating showed substantial improvement. The wear rate of cold-sprayed WC-Ni MMC coating containing lower content of WC was close to wear rate of HVOF-sprayed WC-Ni MMC with higher WC content. Similarly, wear rate of FSP-treated HVOF-sprayed WC-Ni MMC coating showed 80% fall. There was appreciable content of oxides and carbides in FSP-treated thermal-sprayed WC-Ni MMC coating indicating oxidation and decarburization during FSP treatment, However their deleterious effect by sub-sided by their uniform and homogenous distribution in the microstructure. The wear analyses of the wear-tested FSP-treated coatings indicated reduced surface and sub-surface cracking due to enhanced toughness. The vulnerable nickel binder was replaced by uniformly distributed micron size carbides which increased rigidity and compactness of the microstructure. Cracks if any were thin in width due to reduction in the width of nickel binder trapped between the carbides. This means that FSP treatment can show substantial improvement in mechanical properties of the thermal-sprayed coatings due to mechanical currents generated during treatment resulting in tough microstructure.

Chapter 7. Future works and recommendations

Considering that the research objectives mentioned in this study encompasses numerous aspects related to thermal spraying and FSP treatment, it was important to limit scope of the study. After observing positive outcomes from wear-tested FSP-treated thermal-sprayed WC-Ni MMC coating, it opened the scope of the study for future work. The following aspects have been strongly recommended from future work point of view:

a. The equation defining the behavior of increasing tungsten carbide content in low pressure cold-sprayed WC-Ni coating seem to be applicable only in the WC content of 11 to 52 vol. %. As shown by others papers, the wear of the metal matrix composite containing wear resistant reinforcing particles showed decreasing trend of wear rate with increasing reinforcement particle content in the composite. In our case, the fall was sudden and drastic at 4 vol.% WC in the WC-Ni coating. It means dry abrasive wear test to measure wear rate of different cold-sprayed WC-Ni coating with WC content less than 4 vol.% should be explored.
b. Seeing the success of dry abrasive wear test on FSP-treated cold-sprayed as well as HVOF-sprayed WC-Ni coating, the thermal sprayed WC-Ni coatings should be tested in wet abrasive wear test (ASTM B611).
c. The effect of varying number of passes of tool during friction stir processing of WC-Ni coatings on mechanical properties like hardness, toughness, depth of friction stir zone, porosity, wear resistance, should be checked. Similarly, effect of other friction stir processing parameters like tool travel velocity and axial load on tool, on mechanical properties of coatings should also be checked.
d. The cobalt and nickel in WC-Ni coating are corrosion prone. Also, leaching of cobalt between WC grains results in easy removal of WC in aqueous solution. Hence, corrosion rate of FSP-treated as well as non-FSP-treated cold-sprayed as well as HVOF-sprayed WC-Ni coating should be checked in alkaline as well as in acidic solutions.

e. After successful wear result for FSP-treated thermal sprayed WC-Ni coating, the effect of FSP treatment on wear and corrosion resistance of NiCrBSi, Cr_3C_2-NiCr, NiCr, TiO_2, Y_2O_3-X (where X is Cr, Ni, Co, or combination of these) should be tried.

Bibliography

1. I. Kovaříková, B. Szewczyková, P. Blaškovitš, E. Hodúlová, E. Lechovič, Study and characteristic of abrasive wear mechanisms. In: Materials Science and Technology [online]. - ISSN 1335-9053.
2. B. Bhushan, Modern Tribology Handbook, CRC press, 2000, pp. 1 – 156.
3. B. Bikramjit, Tribology of ceramics and composites: a material science perspective, Wiley, 2011, pp. 1 - 100
4. I. D. Marinescu, Tribology in Manufacturing Technology: Materials Forming, Machining and Tribology, Elsevier Inc. 2012, pp. 175 – 194.
5. A. Mishra, I. Finnie, Review of abrasive wear of materials, Transactions of ASME, 1982, 104, pp. 94 – 101.
6. ASTM G65-04, Standard Test Method for Measuring Abrasion Using the Dry Sand/Rubber Wheel Apparatus, West Conshohocken, USA, 2010
7. A. N. J. Stevenson, I.M. Hutchings, Development of the dry sand/ rubber wheel abrasion test, Wear, 1996, 195, pp. 232 - 240.
8. F. Borik, Using tests to define the influence of metallurgical variables on abrasion, Metallurgical Engineering Quarterly, 1972, 12, pp. 33 – 39.
9. P. A. Swanson, Comparison of laboratory abrasion tests and field tests, in A.W. Ruff and R.G. Bayer (eds.), Tribology: Wear test selection for Design and Application, ASTM STP 1199, ASTM, Philadelphia PA, 1993, pp. 80 – 99.
10. F. Borik, Rubber wheel abrasion test, SAE Transactions, 1970, 79, pp. 2145 - 2154.
11. E. Rabinowicz, L. A. Dunn, P. G. Russell, A study of wear under three body conditions, Wear, 1961, 4, pp. 345 – 355.
12. A. V. Levy, P. Chik, The effects of erodent composition and shape on the erosion of steel, 1983, Wear, 89, pp. 151 – 162.
13. I. Finnie, Some observations on the erosion of ductile metals, Wear, 1972, 19, pp. 81 – 90.

14. G. P. Tilly, Sand erosion of metals and plastics: brief review, Wear, 1969, 14, pp. 241 – 248.
15. J. Zahavi, G. F. Schmitt Jr., Solid particle erosion of polymeric coatings, Wear, 1981, 71, pp. 191 – 210.
16. J. Zahavi, G.F. Schmitt Jr., Solid particle erosion of reinforced composite materials, Wear, 1981, 71, pp. 179 – 190.
17. A. Mishra, I. Finnie, Correlations between two-body and three body abrasion and erosion of metals, Wear, 1981, 68, pp. 33 – 39.
18. R. Chattopadhyay, Surface Wear: Analysis, Treatment, and Prevention, Materials Park, Ohio: ASM International, 2001, pp. 143 – 199.
19. E. Toyserkani, A. Khajepour, S. Corbin, Laser Cladding: Introduction, CRC Press LLC, 2005, pp. 1 – 22.
20. B. A. Kushner, E. R. Novinski, Thermal Spray Coatings, Friction, Lubrication, and Wear Technology, ASM Handbook, ASM International, 1992, Vol. 18, pp. 829 – 833.
21. J. R. Davis, Handbook of Thermal Spray Technology, ASM International, 2004, p. 43 – 82.
22. N. P. Suh, An overview of the delamination theory of wear, Wear, 1977, 44, pp. 1 – 16.
23. S. Jahanmir, N. P. Suh, E. P. Abrahamson, Microscopic observations of the wear sheet formation by delamination, Wear, 1974, 28, pp. 235 – 249.
24. N. P. Suh, P. Sridharan, Relationship between the coefficient of friction and the wear rate of metals, Wear, 1975, 34, pp. 291 – 299.
25. G. Barbezat, A. R. Nicoll, A. Sickinger, Abrasion, erosion and scuffing resistance of carbide and oxide ceramic thermal sprayed coatings for different applications, Wear, 1993, 162- 164, pp. 529 – 537.
26. P. H. Shipway, J. J. Hogg, Dependence of microscale abrasion mechanism of WC-Co hardmetals on abrasive type, Wear, 2005, 259, pp. 44 – 51.
27. A. L. Zaitscv, Mechanisms of hard alloy wear in frictional processes with polymers and composite materials, Wear, 1993, 162 - 164, pp. 40 – 46.

28. P. Kulu, R. Tarbe, A. Vallinkivi, Abrasive wear of powder materials and coatings, Material Science, 2005, 11(3), pp. 230 – 234.
29. I. A. Ibrahim, F. A. Mohamed, E. J. Lavernia, Particulate reinforced metal matrix composites - a review, Journal of Material Science, 1991, 26, pp. 1137 – 1156.
30. S. Zhou, X. Dai, T. Zhang, Effect of binder metals in structure and properties of WC ceramic-metal composite coatings by laser–induction hybrid rapid cladding, Journal of Composite Materials, 2012, 0(0), pp. 1-11.
31. H. Holleck, Material selection for hard coatings, Journal of Vaccum Science and Technology A, 1986, 4(6), pp. 2661 - 2669.
32. C. N. Machio, G. Akdogan, M. J. Witcomb, S. Luyckx, Performance of WC-VC-Co thermal spray coatings in abrasion and slurry erosion tests, *Wear*, 2005, 258, pp. 434 – 442.
33. K. Jia, T. E. Fischer, B. Gallois, Microstructure, hardness and toughness of nanostructured and conventional WC-Co composites, Nanostructured Materials, 1998, 10(5), pp. 875 – 891.
34. A. J. Gant, M. G. Gee, B. Roebuck, Rotating wheel abrasion of WC/Co hardmetals, Wear, 2005, 258, pp. 178 – 188.
35. K. Jia, T. E. Fischer, Abrasion resistance of nanostructured and conventional cemented carbides, Wear, 1996, 200, pp. 206 – 214.
36. T. Sahraoui, N. -E. Fenineche, G. Montavon, C. Coddet, Structure and wear behavior of HVOF sprayed Cr_3C_2-NiCr and WC-Co coatings", Materials and Design , 2003, 24, pp. 309 – 313.
37. J. Llorca, A. Needleman, S. Suresh, An analysis of the effects of matrix void growth on deformation and ductility in metal-ceramic composites, Acta Metallurgica et Materialia, 1991, 39(10), pp. 2317 – 2335.
38. C. N. Machio, G. Akdogan, M. J. Witcomb, S. Luyckx, Performance of WC-VC-Co thermal spray coatings in abrasion and slurry erosion tests, Wear, 2005, 258, pp. 434 – 442.

39. D. A. Stewart, P. H. Shipway, D. G. McCartney, Abrasive wear behavior of conventional and nanocomposite HVOF-sprayed WC-Co coatings, Wear, 1999, 225-229, pp. 789 – 798.
40. K. Korpiola, High temperature oxidation of metal, alloy and cermet powders in HVOF spraying process, Doctoral Thesis, 2004, Helsinki University of Technology.
41. J. M. Guilemany, J. M. de Paco, J. Nutting, J. R. Miguel, Characterization of the W_2C phase formed during the high velocity oxygen fuel spraying of a WC + 12pct Co powder, Metallurgical and Materials Transactions-A, 1999, 30(A), pp. 1913 – 1921.
42. S. F. Wayne, S. Sampath, Structure/ property relationships in sintered and thermally sprayed WC-Co, Journal of Thermal Spray Technology, 1992, 1(4), pp. 307 – 315.
43. B. H. Kear, G. Skandan, R. K. Sadangi, Factors controlling decarburization in HVOF sprayed nano-WC/Co hardcoatings, Scripta Materialia, 2001, 44(8-9), pp. 1703 – 1707.
44. J. Stokes, L. Looney, Residual stress in HVOF thermally sprayed thick deposits, Surface and Coating Technology, 2004, 177 - 178, pp. 18 – 23.
45. O. Sarikaya, Effect of some parameters on microstructure and hardness of alumina coatings prepared by the air plasma spraying process, Surface and Coating Technology, 2005, 190, pp. 388 – 393.
46. J. M. Guilemany, V. V. Sobolev, J. Nutting, Z. Dong, J. A. Calero, Thermal interaction between WC-Co coating and Steel substrate in process of HVOF spraying, Scripta Metallurgica et Materialia, 1994, 31(7), pp. 915 – 920.
47. J. M. Guilemany, J. Nutting, Z. Dong, J. M. dePaco, The influence of WC-Co HVOF thermal spraying on the microstructure of an Al - 4% Cu alloy substrate, Scripta Metallurgica et Materialia, 1995, 33(7), pp. 1055 – 1062.
48. S. Fantassi, M. Vardelle, A. Vardelle, P. Fauchais, Influence of the velocity of Plasma-sprayed particles on splat formation, Journal of Thermal Spray Technology, 1993, 2(4), pp. 379 – 384.

49. J. Nerz, B. Krushner, A. Rotolico, Microstructural evaluation of Tungsten Carbide-cobalt coatings, Journal of Thermal Spray Technology, 1992, 1(2), pp. 147 – 152.
50. V. V. Sobolev, J. M. Guilemany, Formation of chemical inhomogeneity in the coating structure during high velocity oxy-fuel (HVOF) spraying, Material letters, 1995, 25, pp. 285 – 289.
51. V. V. Sobolev, J. M. Guilemany, Investigation of coating porosity formation during high velocity oxy-fuel (HVOF) spraying, Material letters, 1994, 18, pp. 304 – 308.
52. V. V. Sobolev, J. M. Guilemany, J. A. Calero, Thermal processes in HVOF sprayed WC-Co coating on a copper substrate, Journal of Thermal Spray Technology, 1998, 7(2), pp. 191 – 192.
53. L. P. Ward, B. Hinton, D. Gerrard, K. Short, Corroison behavior of modified HVOF sprayed WC based cermet coatings on stainless steel, Journal of Minerals and Materials Characterization and Engineering, 2011, 10(11), pp. 989 – 1005.
54. F. Gärtner, T. Stoltenhoff, T. Schmidt, H. Kreye, The cold spray process and its potential for industrial applications, Journal of Thermal Spray Technology, 2006, 15(2), pp. 223 – 232.
55. A. Papyrin, Cold spray technology, Advanced Materials and Processes, 2001, 159 (9), pp. 49 – 51.
56. T. Van Steenkiste, Evaluation of coatings produced via Kinetic and cold spray processes, Journal of Thermal Spray Technology, 2003, 13(2), pp. 274 – 282.
57. H. Assadi, F. Gärtner, T. Stoltenhoff, H. Kreye, Bonding mechanism in cold gas spraying, Acta Materialia, 2003, 51, pp. 4379 – 4394.
58. B. Jodoin, L. Ajdelsztajn, E. Sansoucy, A. Zúñiga, P. Richer, E. J. Lavernia, Effect of particle size, morphology and hardness of cold gas dynamic sprayed aluminum alloy coatings, Surface and Coating Technology, 2006, 201, pp. 3422 – 3429.

59. S. Dosta, M. Couto, J. M. Guilemany, Cold spray deposition of WC- 25 Co cermet onto Al7075-T6 and carbon steel substrates, Acta Materialia, 2013, 61(2), pp. 643 – 652.
60. H. -J. Kim, C. -H. Lee, S. Y. Hwang, Superhard nano WC-12% Co coating by cold spray deposition, Material Science and Engineering A - Structures, 2005, 391(1-2), pp. 243 – 248.
61. R. S. Lima, J. Karthikeyan, C. M. Kay, J. Lindermann, C. C. Berndt, Microstructural characteristics of cold-sprayed nano structured WC-Co coatings, Thin solid films, 2002, 416 (1-2), pp. 129 – 135.
62. H. -J. Kim, C. -H. Lee, S. Y. Hwang, Fabrication of WC-Co coatings by cold spray deposition, Surface and Coating Technology, 2005, 191 (2-3), pp. 335 – 340.
63. P. -H. Gao, C. -J. Li, G. -J. Yang, Y. -G. Li, C. -X. Li, Influence of substrate hardness on deposition behavior of single porous WC-12Co particle in cold spraying, Surface and Coating Technology, 2008, 203(3-4), pp. 384 – 390.
64. P. -H. Gao, C. -J. Li, G. -J. Yang, Y. -G. Li, C. -X. Li, Influence of substrate hardness transition on built-up of nanostructured WC-12Co by cold spraying, Applied Surface Science, 2010, 256, pp. 2263 – 2268.
65. C. J. Li, G. J. Yang, P. H. Gao, Y. Y. Ma, Y. Y. Wang, C. X. Li, Characterization of nano-structured WC-Co deposited by cold spraying, Journal of Thermal Spray Technology, 2007, 17(5-6), pp. 1011 – 1020.
66. A. S. M. Ang, C. C. Berndt, P. Cheang, Deposition effects of WC particle size on cold sprayed WC-Co coatings, Surface and Coating Technology, 2011, 205, pp. 3260 – 3267.
67. S. E. Tinashe, Conceptual design of Low Pressure Cold Gas Dynamic Spray (LPCGDS) System, Master of Science thesis, University of Witwatersrand, Johannesburg, 2010
68. J. Wang, J. Villafuerte, Low pressure cold spraying of tungsten carbide coatings, Advanced Materials and Processes, 2009, 167 (2), pp. 54 – 56.

69. E. Irissou, J. G. Legoux, B. Arsenault, C. Moreau, Investigation of Al-Al_2O_3 cold spray coating formation and properties, Journal of Thermal Spray Technology, 2007, 16(5-6), pp. 661 – 668.
70. L. Ajdelsztajn, B. Jodoin, J. M. Schoenung, Synthesis and mechanical properties of nanocrystalline Ni coatings produced by cold gas dynamic spraying, Surface and Coating Technology, 2006, 201, pp. 1166 – 1172.
71. N. M. Melendez, A. G. McDonald, Development of WC-based metal matrix composite coatings using low-pressure cold gas dynamic spraying, Surface and Coating Technology, 2013, 214, pp. 101 – 109.
72. L. Gil, M. A. Prato, M. H. Staia, Effect of post-heat treatment on the corrosion resistance of NiWCrBSi HVOF coatings in chloride solution, Journal of Thermal Spray Technology, 2000, 11(1), pp. 95 – 99.
73. M. Mittal, S. Prakash, S. K. Nath, Recrystallization of amorphous phases via post-coating heat-treatment of Plasma-sprayed hydroxyapatite coatings, Materials and Manufacturing Processes, 2012, 27, pp. 1001 – 1006.
74. M. Rodriguez, M. Staia, L. Gil, F. Arenas, A. Scagni, Effect of heat treatment on properties of Nickel hard surface alloy deposited by HVOF, Surface Engineering, 2000, 16(5), pp. 415 – 420.
75. P. Sudharshan Phani, P. Srinivas Rao, S. V. Joshi, G. Sundararajan, Effect of process parameters and heat treatments on properties of cold sprayed copper coatings, Journal of Thermal Spray Technology, 2007, 16 (3), pp. 425 – 434.
76. Friction stir welding, Azo Journal of Materials Online, Copy right: 2000 - 2013 Azom.com [Online], Available: http://www.azom.com/article.aspx?ArticleID=1170, 7 Jan. 2002, Accessed : 25 August 2013,
77. D. M. Rodrigues, A. Loureiro, C. Leitao, R. M. Leal, B. M. Chaparro, P. Vilaça, Influence of friction stir welding parameters and mechanical properties of AA 6016-T4 thin welds, Materials and Design, 2009, 30(6), pp. 1913 -1921.

78. V. Balasubramanian, Relationship between base metal properties and friction stir welding process parameters, Material Science and Engineering A - Structures, 2008, 480, pp. 397 – 403.
79. M. W. Mahoney, S. P. Lynch, Friction-stir Processing, DTIC document, 2006
80. R. S. Mishra, Z. Y. Ma, Friction stir welding and processing, Material Science and Engineering Reviews, 2005, 50, pp. 1 – 78.
81. L. E. Murr, G. Liu, J. C. McClure, Dynamic recrystallization in friction-stir welding of aluminium alloy 1100, Journal of Material Science letters, 1997, 16, pp. 1801 – 1803.
82. K. J. Hodder, H. Izadi, A. G. McDonald, A. P. Gerlich, Fabrication of aluminium-alumina metal matrix composite via cold gas dynamic spraying at low pressure followed by friction stir processing, Metallurgical and Materials Transactions - A, 2012, 556, pp. 114 – 121.
83. G. Faraji, P. Asadi, Characterization of AZ91/alumina nanocomposite produced by FSP, Material Science and Engineering A - Structures, 2011, 528, pp. 2431 – 2440.
84. M. Yoshiaki, F. Hidetoshi, Nanostructured thermally sprayed cemented carbide layer fabricated by friction stir processing, Transactions of JWRI, 2011, 40(1), pp. 35 – 39.
85. Y. Morisada, H. Fujii, T. Mizuno, G. Abe, T. Nagaoka, M. Fukusumi, Modification of thermally sprayed cemented carbide layer by friction stir processing, Surface and Coating Technology, 2010, 204, pp. 2459 – 2464.
86. T. G. Langdon, The physics of superplastic deformation, Material Science and Engineering A, 1991, 137, pp.1 – 11.
87. N. Chandra, Constitutive behavior of superplastic materials, International journal of non-linear mechanics, 2002, 37, pp. 461 – 484.
88. M. Kawasaki, T. G. Langdon, Grain boundary sliding in a superplastic zinc-Aluminum alloy processed using severe plastic deformation, Materials Transactions, 2008, 49(1), pp. 84 – 89.

89. J. Sieniawski, M. Motyka, Superplasticity in titanium alloys, Journal of achievement in Materials and Manufacturing engineering, 2007, 24 (1), 123 – 130.
90. K. A. Padmanabhan, Thermally assisted deformation of structural superplastics and nanostructured materials: A personal perspective, Sadhana, 2003, 28 (1 & 2), pp. 97 – 113.
91. J. S. Kim, J. H. Kim, Y. T. Lee, C. G. Park, C. S. Lee, Microstructural analysis on boundary sliding and its accommodation mode during superplastic deformation of Ti-6Al-4V alloy, Material Science and Engineering A, 1999, 263, pp. 272 – 280.
92. Y. Huang, Evolution of microstructure and texture during hot deformation of a commercially processed Supral100, Journal of Material Science Technology, 2012, 28(6), pp. 531 – 536.
93. J. J. Wlassich, A method to predict transitions in material behavior, 1995, PhD thesis, Massachusetts Institute of Technology.
94. I. Finnie, J. Wolak, Y. Kabil, Erosion of surfaces by solid particles, Wear, 1960, 3, pp. 87 – 103.
95. G. P. Tilly, Sand erosion of metals and plastics: a brief review, Wear, 1969, 14, pp. 241 – 248.
96. C. E. Smeltzer, M. E. Gulden, S. S. McElmury, W. A. Compton, Mechanisms of sand and dust erosion in gas turbine engines, U.S. Army Aviation Materiel Lab. Tech. Rep. 70 - 36, 1970.
97. D. A. Tuitt, Erosion tests of metallic coatings, Proc. 4th Int. Conf. on Rain Erosion, Meersburg, 1974.
98. I. M. Hutchings R. E. Winter, Particle erosion of ductile metals: a mechanism of material removal, Wear, 1974, 27, pp. 121 - 128.
99. I. M. Hutchings, R. E. Winter, The erosion of ductile metals by spherical particles, Journal of Physics D, 1975, 8, pp. 8 - 14.
100. I. M. Hutchings, The erosion of ductile metals by solid particles, Ph. D. dissertation, University of Cambridge, Great Britain, 1974.

101. Y. A. Tadolder, Influence of abrasive grain geometry on the solid particle erosion of metals, Tr. Tallin. Politekh. Inst., Ser. A, 1966, 237, pp. 15 - 22.
102. P. Ascarelli, Relation between the erosion by solid particles and the physical properties of metals, U.S. Army Materials and Mechanics Research Center Technical Report, 1971, 71-47.
103. I. M. Hutchings, Prediction of the resistance of metals to erosion by solid particles, Wear, 1975, 35, pp. 371 – 374.
104. J. H. Neilson, A. Gilchrist, Erosion by a stream of solid particles, Wear, 1968, II, pp. 111 – 122.
105. R. E. Winter, I. M. Hutchings, The role of adiabatic shear in solid particle erosion, Wear, 1975, 34, pp. 141 – 148.
106. T. Foley, A. Levy, The erosion of heat treated steels, Wear, 1983, 91, pp. 45 -64.
107. D. H. Graham, A. Ball, Particle erosion of candidate materials for hydraulic valves, Wear, 1989, 133, pp.125 – 132.
108. R. Bellman Jr., A. Levy, Erosion mechanism in ductile metals, Wear, 1981, 70, pp. 1 - 27.
109. K. Kato, Tribology of ceramics, Wear, 1990, 136, pp. 117 – 133.
110. A. V. Levy, Solid particle erosion behavior of steel as a function of microstructure, Wear, 1981, 68, pp. 269 – 287.
111. R. B. Waterhouse, D. B. Taylor, Fretting debris and delamination theory of wear, Wear, 1974, 29, pp. 337 – 344.
112. P. L. Hurricks, The occurrence of spherical particles in fretting, Wear, 1974, 27, pp. 319 – 328.
113. N. Omhae, T. Tsukizoe, The effect of slip amplitude on fretting, Wear, 1974, 27, pp. 281 – 294.
114. J. S. Halliday, W. Hirst, The fretting corrosion of mild steel, Proceedings of Royal Society of London A, 1956, 236, pp. 411.
115. H. Attia, A generalized fretting wear theory, Tribology International, 2009, 42, pp. 1380 - 1388.

116. G. Le Roy, J. D. Embury, G. Edwards, M. F. Ashby, A model of ductile fracture based on the nucleation and growth of voids, Acta Metallurgica, 1981, 29, pp. 1509 - 1522.
117. J. E. Merwin, K. L. Johnson, An analysis of plastic deformation in rolling contact, Proceedings of the Institution of Mechanical Engineers, 1963, 177 (25), pp. 676 – 690.
118. P. Heilman, D.A. Rigney, An energy based model of friction and its application to coated system, Wear, 1981, 72, pp. 195 – 217.
119. Y. P. Chiu, T. E. Tallian, J. I. McCool, An engineering model of spalling fatigue failure in rolling contact I. The subsurface model, Wear, 1971, 17, pp. 433 – 446.
120. J. M. Challen, P. L. B. Oxley, An explanation of the different regimes of friction and wear using asperity deformation models, Wear, 1979, 53, pp. 229 – 243.
121. N.P. Suh, An overview of the delamination theory of wear, Wear, 1977, 44, pp. 1 – 16.
122. T. Nagao, J. J. Pamies-Teixeira, N. P. Suh, Behaviour of medium carbon steel under combined fatigue and wear, Wear, 1977, 44, pp. 101 – 108.
123. K. Tanaka, T. Mori T. Nakamura, Cavity formation at the interface of a spherical inclusion in a plastically deformed matrix, Philosophical magazine, 1970, 21:70, pp. 267 – 279.
124. A. S. Argon, J. Im, R. Safoglu, Cavity formation from inclusions in ductile failure, Metallurgical Transaction A, 1975, 6A, pp. 825 – 837.
125. J. F. Archard, Contact and rubbing of flat surfaces, Journal of Applied Physics, 1953, 24(8), pp. 981 – 988.
126. K. L. Johnson, Contact mechanics and the wear of metals, Wear, 1995, 190, pp. 162 – 170.
127. A. R. Rosenfield, Criteria for ductile failure of two-phase alloys, International Materials Reviews, 1968, 13(1) pp. 29 - 40(12).
128. J. P. Hirth, D. A. Rigney, Crystal plasticity and the delamination theory of wear, Wear, 1976, 39, pp. 133 – 141.

129. A. W. Ruff, Deformation studies at sliding wear tracks in iron, Wear, 1976, 40, pp. 59 – 74.
130. J. Zhang, A. T. Alpas, Delamination wear in ductile materials containing second phase particles, 1993, A160, pp. 25 – 35.
131. F. A. McClintock, S. M. Kaplan, C. A. Berg, Ductile fracture by hole growth in shear bands, International Journal of Fracture Mechanics, 1966, 2(4), pp. 614 – 627.
132. I. R. Kramer, L. J. Demer, Effect of environment and mechanical properties of metals, Progress in Material Science, 1961, pp. 133 – 199.
133. I. S. Tuba, Elastic-plastic analysis of a flat plate with a circular rigid inclusion, Applied Science Research, 1965, 16, pp. 241 – 255.
134. J. Orr, D. K. Brown, Elasto-plastic solution for a cylindrical inclusion in plastic strain, Engineering fracture mechanics, 1974, 6, pp. 261 – 274.
135. R. B. Waterhouse, D. E. Taylor, Fretting debris and the delamination theory of wear, Wear, 1974, 29, pp. 337 – 344.
136. A. P. Green, Friction between unlubricated metals: A theoretical analysis of the junction model, Proceedings of Royal Society of London A, 1955, 228, pp. 191 – 206.
137. N. P. Suh, N. Saka, S. Jahanmir, Implications of the delamination theory on wear minimization, Wear, 1977, 44, pp. 127 – 134.
138. P. K. Gupta, N. H. Cook, Junction deformation models for asperities in sliding interaction, Wear, 1972, 20, pp. 73 – 87.
139. A. L. Zharin, G. P. Shpenkov, Macroscopic effects of delamination wear, Wear, 1979, 56, pp. 309 – 313.
140. M. V. Swain, Microscopic observations of abrasive wear of polycrystalline alumina, Wear, 1975, 35, pp.185 – 189.
141. S. Jahanmir, N. P. Suh, E. P. Abrahamson II, Microscopic observations of the wear sheet formation by delamination, Wear, 1974, 28, pp. 235 – 249.
142. A. D. Hearle, K. L. Johnson, Mode II stress intensity factors for a crack parallel to the surface of an elastic half-space subjected to a moving point

load, Journal of the Mechanics and Physics of Solids, 1985, 33(1), pp. 61 – 81.

143. D. R. Lesuer, G. J. Kay, M. M. LeBlanc, Modelling large strain, high rate deformation in metals, Third Biennial Tri-laboratory Engineering Conference, July 20, 2001, Modelling and Simulation, Pleasanton, CA, Nov. 3 - 5, 1999.
144. C. Luo, Modelling the behaviour of inclusions in plastic deformation of steels, Doctoral thesis, Royal Institute of technology, 2001.
145. J. D. Livingston, B. Chalmers, Multiple slip in bicrystal deformation, Acta Metallurgy, 1957, 5, pp. 322 – 327.
146. R. Hill, On discontinuous plastic states, with special reference to localized necking in thin sheets, Journal of the Mechanics and Physics of Solids, 1952, 1, pp. 19 – 30.
147. D.A. Hills, D.W. Ashelby, On the determination of stress intensification factors for a wearing half-space, Engineering fracture mechanics, 1980, 13, pp. 69 – 78.
148. J. R. Rice, D. M. Tracey, On the ductile enlargement of voids in triaxial stress fields, Journal of the Mechanics and Physics of Solids, 1969, 27, pp. 201 – 217.
149. P. Heilmann, W. A. T. Clark, D. A. Rigney, Orientation determination of subsurface cells generated by sliding, Acta Metallurgy, 1983, 31(8), pp. 1293 – 1305.
150. T. Akagaki, K. Kato, Plastic flow process of the surface layers in flow wear under boundary lubricated conditions, Wear, 1987, 117, pp. 179 – 196.
151. J. H. Dautzenberg, J. H. Zaat, Quantitative determination of deformation by sliding wear, Wear, 1973, 23, pp. 9 – 19.
152. K. L. Johnson, H. R. Shercliff, Shakedown of 2-dimensional asperities in sliding contact, International Journal of Mechanical Sciences, 1992, 34(5), pp. 375 – 394.

153. S. Jahanmir, E. P. Abrahamson II, N. P. Suh, Sliding wear resistance of metallic coated surfaces, Wear, 1976, 40, pp. 75 – 84.
154. H. Mughrabi, Some consequences of a surface and size effects in plastically deformed copper single crystals, Physica Status Solidi(b), 1971, 44, pp. 391 – 402.
155. J. A. Kirk, T. D. Swanson, Subsurface effects during sliding wear, Wear, 1975, 35, pp. 63 – 67.
156. V. D. Scott, H. Willman, Surface re-orientation caused on metals by abrasion-its nature, origin and relation to friction and wear, Proceedings of Royal Society of London- A, 1958, 247, pp. 353 – 371.
157. S. Jahanmir, N. P. Suh, Surface topography and integrity effects on sliding wear, Wear, 1977, 44, pp. 87 – 99.
158. D. R. Wheeler, D. H. Buckley, Texturing in metals as a result of sliding, Wear, 1975, 33, pp. 65 – 74.
159. I. L. Mogford, The deformation and fracture of two-phase materials, Metallurgical Reviews, 1967, 12, pp. 49 – 68.
160. T. R. Bates, K. C. Ludema, W. A. Braiard, A rheological mechanism of penetrative wear, 1974, Wear, 30, pp. 365 – 375.
161. E. Robinowicz, The determination of the compatibility of metals through static friction tests, A S L E Transactions, 1971, 14(3), pp. 198 – 205.
162. T. F. J. Quinn, The effect of hot-spot temperatures on unlubricated wear of steel, A SL E transactions, 1967, 10(2), pp.158 – 168.
163. A. N. Stroh, 1955, The formation of cracks in plastic flow II, Proceedings of Royal Society of London- A, 1955, 232, pp. 548 – 560.
164. A. N. Stroh, The formation of cracks as a result of plastic flow, Proceedings of Royal Society of London, 1954, 223, pp. 404 – 414.
165. J. S. Halliday, W. Hirst, The fretting corrosion of mild steel, Proceedings of Royal Society of London- A, 1956, 236, pp. 411 – 430.
166. A. F. Bower, K. L. Johnson, The influence of strain hardening on cumulative plastic deformation in rolling and sliding line contact, Journal of the Mechanics and Physics of Solids, 1989, 37(4), pp. 471 – 493.

167. M. A. Moore, R. C. D. Richardson, D. G. Attwood, The limiting strength of worn metal surfaces, Metallurgical transactions, 1972, 3, pp. 2485 – 2491.
168. A. P. Green, The plastic yielding of metal junctions due to combined shear and pressure, Journal of the Mechanics and Physics of solids, 1954, 2, pp. 197 – 211.
169. F. P. Bowden, A. J. W. Moore, D. Tabor, The ploughing and adhesion of sliding metals, Journal of Applied Physics, 1943, 14, pp. 80 – 91.
170. R. B. Waterhouse, The role of adhesion and delamination in the fretting wear of metallic materials, Wear, 1977, 45, pp. 355 – 364.
171. M. F. Ashby, Work hardening of dispersion-hardened crystals, Philosophical Magazine, 1966, 14:132, pp. 1157 – 1178.
172. A. T. Alpas, J. Zhang, Wear rate transitions in cast aluminium-silicon alloys reinforced with SiC particles, Scripta Metallurgica et Materialia, 1992, 26, pp. 505 – 509.
173. N. Saka, A. M. Eleiche, N. P. Suh, Wear of metals at high sliding speeds, Wear, 1977, 44, pp. 109 – 125.
174. J. J. Pamies-Teixeira, N. Saka, N. P. Suh, Wear of copper-based solutions, Wear, 1977, 44, pp. 65 – 75.
175. A. D. Sarkar, Wear of aluminium-silicon alloys, Wear, 1975, 31, pp. 331 – 343.
176. A. Kapoor, A. J. Franklin, Tribological layers and the wear of ductile materials, Wear, 2000, 245, pp. 204 – 215.
177. N. Saka, N. P. Suh, Delamination wear of dispersion-hardened alloys, Journal of Engineering for Industry, 1977, 99(2), pp. 289 – 294.
178. J. R. Fleming, N. P. Suh, Mechanics of crack propagation in delamination wear, Wear, 1977, 44, pp. 39 – 56.
179. K. E. Puttick, The shear component of ductile fracture, Philosophical Magazine, 1960, 5:55, pp. 759 – 762.

180. T. B. Cox, J. R. Low, An investigation of the plastic fracture of AISI 4340 and 18 Nickel-200 grade maraging steels, Metallurgical Transactions, 1974, 5(6), pp. 1457 – 1470.
181. I. E. French, P. F. Weinrich, The shear mode of ductile fracture in materials with few inclusions, Metallurgical Transactions A, 1976, 7A, pp. 1841 – 1845.
182. J. P. Fowler, M. J. Worswick, A. K. Pilkey, H. Nahme, Damage leading to ductile fracture under high strain-rate conditions, Metallurgical and materials transactions A, 2000, 31(3), pp. 831 – 844.
183. M. Kouzeli, A. Mortensen, Size dependent strengthening in particle reinforced aluminium, Acta Materialia, 2002, 50, pp. 39 – 51.
184. K. Jia, T. E. Fischer, Abrasion resistance of nanostructured and conventional cemented carbides, Wear, 1996, 200, pp. 206 – 214.
185. S. Luyckx, A. Love, The relationship between the abrasion resistance and the hardness of WC-Co alloys, The journal of the South African Institute of Mining and metallurgy, 2004, pp. 579 – 582.
186. S. Luyckx, A. Love, Empirical quantitative relationship among grain size, mean free path, contiguity and cobalt content in WC-Co hardmetal, Transactions of the Royal Society of South Africa, 2003, 58:2, pp. 145 – 148.
187. J. Llorca, A. Needleman, S. Suresh, An analysis of the effects of matrix void growth on deformation and ductility in metal-ceramic composites, Acta Metallurgica et Materialia, 1991, 39(10), pp. 2317 – 2335.
188. N. Chawla, Y. -L. Shen, Mechanical behaviour of particle reinforced metal matrix composites, Advanced Engineering Materials, 2001, 3(6), p: 357 – 370.
189. M. A. Zamzam, Abrasive wear of aluminum matrix composites, Metall, 1991, 45, p. 250 – 254.
190. N. Axén, K. -H. Zum Gahr, Abrasive wear of TiC-steel composite clad layers on tool steel, Wear, 1992, 157, pp.189 – 201.

191. N. Axén, A. Alahelisten, S. Jaconson, Abrasive wear of alumina fibre-reinforced aluminium, Wear, 1994, 173, pp. 95 – 104.
192. M. K. Surappa, S. V. Prasad, P. K. Rohatgi, Wear and abrasion of cast Al-alumina particle composites, Wear, 1982, 77, pp. 295 – 302.
193. W. Simm, S. Freti, Abrasive wear of multiphase materials, Wear, 1989, 129, pp. 105 – 121.
194. N. Axén, S. Jacobson, A model for the abrasive wear resistance of multiphase materials, Wear, 1994, 174, pp. 187 – 199.
195. N. Axén, S. Jacobson, Transitions in the abrasive wear resistance of fibre- and particle- reinforced aluminium, Wear, 1994, 178, pp. 1 – 7.
196. B. K. Yen, C. K. H. Dharan, A model for the abrasive wear of fibre-reinforced polymer composites, Wear, 1996, 195, pp. 123 – 127.
197. M. M. Khruschov, Principles of abrasive wear, Wear, 1974, 28, pp. 69 – 88.
198. M. M. Khruschov, M. A. Babichev, Resistance to abrasive wear of structurally heterogenous materials, Friction and Wear in Machinery, 1956, 12, pp. 5 - 24
199. W. M. Garrison Jr., Khruschov's rule and the abrasive wear resistance of multiphase solids, Wear, 1982, 82, pp. 213 – 220.
200. G. Y. Lee, C. K. H. Dharan, R.O. Ritchie, A physically-based abrasive wear model for composite materials, Wear, 2002, 252 (3-4), pp. 322 – 331.
201. ASTM C1327, Standard test method for Vickers Indentation Hardness of Advanced Ceramics, West Conshohocken, USA, 2008.
202. ASTM E384, Standard Test Method for Knoop and Vickers Hardness of Materials, West Conshohocken, USA, 2001.
203. A. Vasinonta, J. L. Beuth, Measurement of interfacial toughness in thermal barrier coating systems by indentation, Engineering Fracture Mechanics, 2001, 68(7), pp. 843 – 860.
204. S. Zhang, X. Zhang, Toughness evaluation of hard coatings and thin films, Thin Solid Films, 2012, 520, pp. 2375 – 2389.

205. C. B. Ponton, R. D. Rawlings, Vickers indentation fracture toughness test Part 2 Application and critical evaluation of standardised indentation toughness equations, Material Science and Technology, 1989, 5, 961 – 976.
206. G. R. Antis, P. Chintikul, B. R. Lawn, D. B. Marshall, A critical evaluation of indentation techniques for measuring fracture toughness: I, Direct crack measurements, Journal of the American Ceramic Society, 1981, 64 (9), 533 – 538.
207. E. Lopez Cantera, B. G. Mellor, Material Letters, 1998, 37, pp. 201 – 210.
208. J. K. Telford, A brief Introduction to Design of Experiments, John Hopkins APL Technical Digest, 2007, 27(3), pp. 224 - 232
209. J. F. Archard, Contact and Rubbing of Flat Surfaces, Journal of Applied Physics, 1953, 24, pp. 981 – 988.
210. A. G. Evans, D.E. Marshall, Wear mechanism in ceramics, in D. A. Rigney (ed.), Fundamental of friction and wear of materials, AS, Metals Park, OH, 1981, pp. 439 – 452
211. C. E. Smeltzer, M. E. Gulden, S. S. McElmury, W. A. Compton, Mechanisms of sand and dust erosion in gas turbine engines, U.S. Army Aviation Materiel Lab. Tech. Rep. 70 - 36, 1970.
212. A. J. Gant, M. J. Lee, Wear, 2001, 251, pp. 908-915
213. C.-J. Li, Y.-Y. Wang, G.-J. Yang, A. Ohmori, K.A. Khor, Material Science Technology, 2004, 20(9), pp. 1087-1096.
214. A. G. Barnett, J. C. van der Pols, A. J. Dobson, Regression to the mean: what it is and how to deal with it, International Journal of Epidemiology, 2005, 34, 215 – 220
215. J. Taylor, An Introduction to Error Analysis: The study of Uncertainties in Physical Measurements. second ed. University Science Books, Mill Valley, CA, 1997, p 165 – 169.
216. J. K. Telford, A brief Introduction to Design of Experiments, John Hopkins APL Technical Digest, 2007, 27(3), pp. 224 – 232

217. M. A. Irfan, V. Prakash, Dynamic deformation and fracture behavior of novel damage tolerant discontinuously reinforced aluminum composites, International Journal of Solids and Structures, 2000, 37, pp. 4477 – 4507.
218. T. Tsuchida, N. Morita, Formation of ternary carbide Co_6W_6C by mechanical activation assisted solid-state reaction, Journal of the European Ceramic Society, 2002, 22, pp. 2401 – 2407

Appendix 1. Wear theories calculation

Equal pressure theory mode

Wear rate of WC-Ni MMC as per equal pressure theory is given by [1]:

$$W_{\text{WC–Ni}} = V_{\text{WC–12Co}} \times W_{\text{WC–12Co}} + V_{Ni} \times W_{\text{Ni}} \quad (1)$$

Where,

$W_{\text{WC-Ni}}$ = Wear rate of cold-sprayed WC-Ni MMC coating,

$W_{\text{WC-12Co}}$ = Wear rate of cold-sprayed WC-12Co,

W_{Ni} = Wear rate of cold-sprayed Ni coating,

$V_{\text{WC-12Co}}$ = Volume content of WC-12Co in WC-Ni MMC coating,

V_{Ni} = Volume content of Ni in cold-sprayed WC-Ni MC coating.

For WC-Ni MMC coating fabricated from powder composition of 50 wt.% WC – 50 wt.% Ni, the coating composition is WC - 4 vol. % Ni

$$W_{\text{WC–Ni}} = V_{\text{WC–12Co}} \times W_{\text{WC–12Co}} + V_{Ni} \times W_{\text{Ni}}$$

$$W_{\text{WC–Ni}} = 0.04 \times 0.06 \times 10^{-6} + 0.96 \times 1232.94 \times 10^{-6}$$

$$W_{\text{WC–Ni}} = 1185 \times 10^{-6} \text{ mm}^3\text{/N-m}$$

For WC-Ni MMC coating fabricated from powder composition of 75 wt.% WC – 25 wt.% Ni, the coating composition is WC- 11 vol. % Ni

$$W_{\text{WC–Ni}} = 0.11 \times 0.06 \times 10^{-6} + 0.89 \times 1232.94 \times 10^{-6}$$

$$W_{\text{WC–Ni}} = 1093 \times 10^{-6} \text{ mm}^3\text{/N-m}$$

For WC-Ni MMC coating fabricated from powder composition of 92 wt.% WC – 8 wt.% Ni, the coating composition is WC- 58 vol. % Ni

$$W_{\text{WC–Ni}} = 0.42 \times 0.06 \times 10^{-6} + 0.58 \times 1232.94 \times 10^{-6}$$

$$W_{\text{WC–Ni}} = 711.3 \times 10^{-6} \text{ mm}^3\text{/N-m}$$

For WC-Ni MMC coating fabricated from powder composition of 96 wt.% WC – 4 wt.% Ni, the coating composition is WC- 48 vol. % Ni

$$W_{\text{WC–Ni}} = 0.52 \times 0.06 \times 10^{-6} + 0.48 \times 1232.94 \times 10^{-6}$$

$$W_{\text{WC–Ni}} = 595 \times 10^{-6} \text{ mm}^3\text{/N-m}$$

Equal Wear theory Model

Wear rate of WC-Ni MMC as per equal wear theory is given by [2]:

$$\frac{1}{W_{\text{WC–Ni}}} = \frac{V_{\text{WC–12Co}}}{W_{\text{WC–12Co}}} + \frac{V_{\text{Ni}}}{W_{\text{Ni}}} \quad (2)$$

For WC- 96 vol. % Ni MMC coating,

$$\frac{1}{W_{\text{WC–Ni}}} = \frac{V_{\text{WC–12Co}}}{W_{\text{WC–12Co}}} + \frac{V_{\text{Ni}}}{W_{\text{Ni}}}$$

$$\frac{1}{W_{\text{WC–Ni}}} = \frac{0.04}{0.06 \times 10^{-6}} + \frac{0.96}{1232 \times 10^{-6}}$$

$$W_{\text{WC–Ni}} = 1.544 \times 10^{-6} \text{ mm}^3\text{/N-m}$$

For WC- 89 vol. % Ni MMC coating,

$$\frac{1}{W_{\text{WC–Ni}}} = \frac{0.11}{0.06 \times 10^{-6}} + \frac{0.89}{1232 \times 10^{-6}}$$

$$W_{\text{WC–Ni}} = 0.53 \times 10^{-6} \text{ mm}^3\text{/N-m}$$

For WC- 58 vol. % Ni MMC coating,

$$\frac{1}{W_{\text{WC–Ni}}} = \frac{0.42}{0.06 \times 10^{-6}} + \frac{0.58}{1232 \times 10^{-6}}$$

$W_{WC-Ni} = 0.142 \times 10^{-6}$ mm^3/N-m

For WC- 48 vol. % Ni MMC coating,

$$\frac{1}{W_{WC-Ni}} = \frac{0.52}{0.06 \times 10^{-6}} + \frac{0.48}{1232 \times 10^{-6}}$$

$W_{WC-Ni} = 0.12 \times 10^{-6}$ mm^3/N-m

Modified wear theory model

The formula of wear rate as per modified wear theory model for WC-Ni MMC is given as [3]:

$$\frac{1}{W_{WC-Ni}} = \frac{V_{Ni}}{W_{Ni}} + \frac{(C \times V_{WC})}{W_{WC}} \quad (3)$$

Where,

C = Contribution coefficient.

Consider WC-Ni MMC coating fabricated from powder composition of 50 wt.% WC - 50 wt.% Ni. The composition of WC-Ni MMC coating is WC - 96.12 vol.% Ni. So on substituting the volume content and wear rate values in Eq.(3), we get:

$$\frac{1}{W_{WC-Ni}} = \frac{V_{Ni}}{W_{Ni}} + \frac{(C \times V_{WC})}{W_{WC}}$$

$$\frac{1}{112.975 \times 10^{-6}} = \frac{0.9612}{1244.18 \times 10^{-6}} + \frac{(C \times 0.0388)}{0.06 \times 10^{-6}}$$

This gives "C" = 12.5×10^{-3}

Now, this value of "C" is used to calculate wear rate of different WC-Ni MMC coating. For example, WC-Ni MMC coating fabricated from powder composition of 50 wt.% WC – 50 wt.% Ni gives coating composition as WC – 96 vol. % Ni. So wear rate of WC-Ni MMC using this "C" value is:

$$\frac{1}{W_{WC-Ni}} = \frac{0.96}{1244.18\times10^{-6}} + \frac{(0.0125\times0.04)}{0.06\times10^{-6}}$$

$$W_{WC-Ni} = 113\times10^{-6} \text{ mm}^3\text{/N-m}$$

For WC- 88.64 vol. % Ni MMC coating,

$$\frac{1}{W_{WC-Ni}} = \frac{0.8864}{1244.18\times10^{-6}} + \frac{(0.0125\times0.1164)}{0.06\times10^{-6}}$$

$$W_{WC-Ni} = 41\times10^{-6} \text{ mm}^3\text{/N-m}$$

For WC- 58 vol. % Ni MMC coating,

$$\frac{1}{W_{WC-Ni}} = \frac{0.58}{1244.18\times10^{-6}} + \frac{(0.0125\times0.42)}{0.06\times10^{-6}}$$

$$W_{WC-Ni} = 11.3\times10^{-6} \text{ mm}^3\text{/N-m}$$

For WC- 48 vol. % Ni MMC coating,

$$\frac{1}{W_{WC-Ni}} = \frac{0.48}{1244.18\times10^{-6}} + \frac{(0.0125\times0.52)}{0.06\times10^{-6}}$$

$$W_{WC-Ni} = 9.25\times10^{-6} \text{ mm}^3\text{/N-m}$$

Similarly, ‘C’ value for other powder compositions of WC-Ni MMC is as calculated below:

For WC- 88.64 vol. % Ni MMC coating, the ‘C’ value is:

$$\frac{1}{97.785\times10^{-6}} = \frac{0.8864}{1244.18\times10^{-6}} + \frac{(C\times0.136)}{0.06\times10^{-6}}$$

$C = 5.025 \times 10^{-3}$

For WC- 58 vol. % Ni MMC coating, the ‘C’ value is

$$\frac{1}{56.92\times10^{-6}} = \frac{0.5772}{1244.18\times10^{-6}} + \frac{(C\times0.423)}{0.06\times10^{-6}}$$

$C = 2.426 \times 10^{-3}$

For WC- 48 vol. % Ni MMC coating, the ‘C’ value is:

$$\frac{1}{20.147\times10^{-6}} = \frac{0.483}{1244.18\times10^{-6}} + \frac{(C\times0.517)}{0.06\times10^{-6}}$$

$C = 5.711 \times 10^{-3}$

For C = 5.025×10^{-3}, the wear rate values for different WC-Ni MMC coatings are as follows:

a) For WC- 96 vol. % Ni MMC coating,

$$\frac{1}{W_{\mathrm{WC-Ni}}} = \frac{0.96}{1244.18\times10^{-6}} + \frac{(0.005025\times0.04)}{0.06\times10^{-6}}$$

$$W_{\mathrm{WC-Ni}} = 249\times10^{-6}\ \mathrm{mm^3/N\text{-}m}$$

b) For WC- 88.64 vol. % Ni MMC coating,

$$\frac{1}{W_{\mathrm{WC-Ni}}} = \frac{0.8864}{1244.18\times10^{-6}} + \frac{(0.005025\times0.1164)}{0.06\times10^{-6}}$$

$$W_{\mathrm{WC-Ni}} = 97.8\times10^{-6}\ \mathrm{mm^3/N\text{-}m}$$

c) For WC- 58 vol. % Ni MMC coating,

$$\frac{1}{W_{WC-Ni}} = \frac{0.58}{1244.18\times10^{-6}} + \frac{(0.005025\times0.42)}{0.06\times10^{-6}}$$

$$W_{\mathrm{WC-Ni}} = 27.9\times10^{-6}\ \mathrm{mm^3/N\text{-}m}$$

d) For WC- 48 vol. % Ni MMC coating,

$$\frac{1}{W_{\mathrm{WC-Ni}}} = \frac{0.48}{1244.18\times10^{-6}} + \frac{(0.005025\times0.52)}{0.06\times10^{-6}}$$

$$W_{\mathrm{WC-Ni}} = 22.9\times10^{-6}\ \mathrm{mm^3/N\text{-}m}$$

For C= 2.426×10^{-3}, the wear rate values for different WC-Ni MMC coatings are:

a) For WC- 96 vol. % Ni MMC coating,

$$\frac{1}{W_{\mathrm{WC-Ni}}} = \frac{0.96}{1244.18\times10^{-6}} + \frac{(0.002426\times0.04)}{0.06\times10^{-6}}$$

$$W_{\mathrm{WC-Ni}} = 427\times10^{-6}\ \mathrm{mm^3/N\text{-}m}$$

b) For WC- 88.64 vol. % Ni MMC coating,

$$\frac{1}{W_{\mathrm{WC-Ni}}} = \frac{0.8864}{1244.18\times10^{-6}} + \frac{(0.002426\times0.1164)}{0.06\times10^{-6}}$$

$$W_{\mathrm{WC-Ni}} = 188\times10^{-6}\ \mathrm{mm^3/N\text{-}m}$$

c) For WC- 58 vol. % Ni MMC coating,

$$\frac{1}{W_{WC-Ni}} = \frac{0.58}{1244.18\times10^{-6}} + \frac{(0.002426\times0.42)}{0.06\times10^{-6}}$$

$$W_{WC-Ni} = 56.9\times10^{-6}\ \text{mm}^3\text{/N-m}$$

d) For WC- 48 vol. % Ni MMC coating,

$$\frac{1}{W_{WC-Ni}} = \frac{0.48}{1244.18\times10^{-6}} + \frac{(0.002426\times0.52)}{0.06\times10^{-6}}$$

$$W_{WC-Ni} = 47\times10^{-6}\ \text{mm}^3\text{/N-m}$$

For C = 5.711×10^{-3}, the wear rate values are:

a) For WC- 96 vol. % Ni MMC coating,

$$\frac{1}{W_{WC-Ni}} = \frac{0.96}{1244.18\times10^{-6}} + \frac{(0.005711\times0.04)}{0.06\times10^{-6}}$$

$$W_{WC-Ni} = 224\times10^{-6}\ \text{mm}^3\text{/N-m}$$

b) For WC- 88.64 vol. % Ni MMC coating,

$$\frac{1}{W_{WC-Ni}} = \frac{0.8864}{1244.18\times10^{-6}} + \frac{(0.005711\times0.1164)}{0.06\times10^{-6}}$$

$$W_{WC-Ni} = 86.8\times10^{-6}\ \text{mm}^3\text{/N-m}$$

c) For WC- 58 vol. % Ni MMC coating,

$$\frac{1}{W_{WC-Ni}} = \frac{0.58}{1244.18\times10^{-6}} + \frac{(0.005711\times0.42)}{0.06\times10^{-6}}$$

$$W_{WC-Ni} = 24.6\times10^{-6}\ \text{mm}^3\text{/N-m}$$

d) For WC- 48 vol. % Ni MMC coating,

$$\frac{1}{W_{WC-Ni}} = \frac{0.48}{1244.18\times10^{-6}} + \frac{(0.005711\times0.52)}{0.06\times10^{-6}}$$

$$W_{WC-Ni} = 20.2\times10^{-6}\ \text{mm}^3\text{/N-m}$$

The average of '*C*' values for all four WC-Ni MMC gives '*C*' value of 6.41×10^{-3}

For C = 6.41×10^{-3}, the wear rate of different WC-Ni MMC is:

a) For WC- 96 vol. % Ni MMC coating,

$$\frac{1}{W_{\text{WC–Ni}}} = \frac{0.96}{1244.18\times10^{-6}} + \frac{(0.00641\times0.04)}{0.06\times10^{-6}}$$

$$W_{\text{WC–Ni}} = 203\times10^{-6}\ \text{mm}^3\text{/N-m}$$

b) For WC- 88.64 vol. % Ni MMC coating,

$$\frac{1}{W_{WC-Ni}} = \frac{0.8864}{1244.18\times10^{-6}} + \frac{(0.00641\times0.1164)}{0.06\times10^{-6}}$$

$$W_{\text{WC–Ni}} = 77.8\times10^{-6}\ \text{mm}^3\text{/N-m}$$

c) For WC- 58 vol. % Ni MMC coating,

$$\frac{1}{W_{\text{WC–Ni}}} = \frac{0.58}{1244.18\times10^{-6}} + \frac{(0.00641\times0.42)}{0.06\times10^{-6}}$$

$$W_{\text{WC–Ni}} = 21.9\times10^{-6}\ \text{mm}^3\text{/N-m}$$

d) For WC- 48 vol. % Ni MMC coating,

$$\frac{1}{W_{\text{WC–Ni}}} = \frac{0.48}{1244.18\times10^{-6}} + \frac{(0.00641\times0.52)}{0.06\times10^{-6}}$$

$$W_{\text{WC–Ni}} = 18\times10^{-6}\ \text{mm}^3\text{/N-m}$$

The best value of 'C' considering Chauvenet's principle is 4.387×10^{-3}

For $C = 4.387 \times 10^{-3}$, the wear rate of different WC-Ni MMC is:

a) For WC- 96 vol. % Ni MMC coating,

$$\frac{1}{W_{\text{WC–Ni}}} = \frac{0.96}{1244.18\times10^{-6}} + \frac{(0.004387\times0.04)}{0.06\times10^{-6}}$$

$$W_{\text{WC–Ni}} = 277\times10^{-6}\ \text{mm}^3\text{/N-m}$$

b) For WC- 88.64 vol. % Ni MMC coating,

$$\frac{1}{W_{\text{WC–Ni}}} = \frac{0.8864}{1244.18\times10^{-6}} + \frac{(0.004387\times0.1164)}{0.06\times10^{-6}}$$

$$W_{\text{WC–Ni}} = 111\times10^{-6}\ \text{mm}^3\text{/N-m}$$

c) For WC- 58 vol. % Ni MMC coating,

$$\frac{1}{W_{\text{WC–Ni}}} = \frac{0.58}{1244.18\times10^{-6}} + \frac{(0.004387\times0.42)}{0.06\times10^{-6}}$$

$$W_{\text{WC–Ni}} = 31.9\times10^{-6}\ \text{mm}^3\text{/N-m}$$

d) For WC- 48 vol. % Ni MMC coating,

$$\frac{1}{W_{\text{WC–Ni}}} = \frac{0.48}{1244.18\times10^{-6}} + \frac{(0.004387\times0.52)}{0.06\times10^{-6}}$$

$$W_{\text{WC–Ni}} = 26.2\times10^{-6} \text{ mm}^3\text{/N-m}$$

The wear rate corresponding to different WC-Ni MMC coating using different "C" value is presented in Table 4.5.

References:

1. N. Axén, S. Jacobson, A model for the abrasive wear resistance of multiphase materials, Wear, 1994, 174, pp. 187 – 199.
2. M. M. Khruschov, Principles of abrasive wear, Wear, 1974, 28, pp. 69 – 88.
3. G. Y. Lee, C. K. H. Dharan, R.O. Ritchie, A physically-based abrasive wear model for composite materials, Wear, 2002, 252 (3-4), pp. 322 – 331.

Appendix 2. Calculation of clamping force to hold the coated sample during FSP treatment

To provide effective clamping of coated sample during FSP treatment, welding at base of the substrate is done. The length of the weld bead will decided on the basis of the minimum force to be exerted on them during FSP treatment

The substrate is mild steel, hence using appropriate filler material is necessary to avoid microstructural changes in substrate during welding. The filler metal rod used is mild steel (M.S.) with copper coating on them [1].

The rotating tool induces shear stress on welds at substrate base. Hence, maximum shear stress limit of weld material will decide its capacity to bear it.

The maximum (Permissible) shear stress on weld ($\varsigma_{max.}$) is given by [2]

$\zeta_{max.} = 0.5\ S_y = 0.5\ (372) = 186$ MPa (1)

Where,

S_y = Yield stress of weld bead material = 372MPa [1]

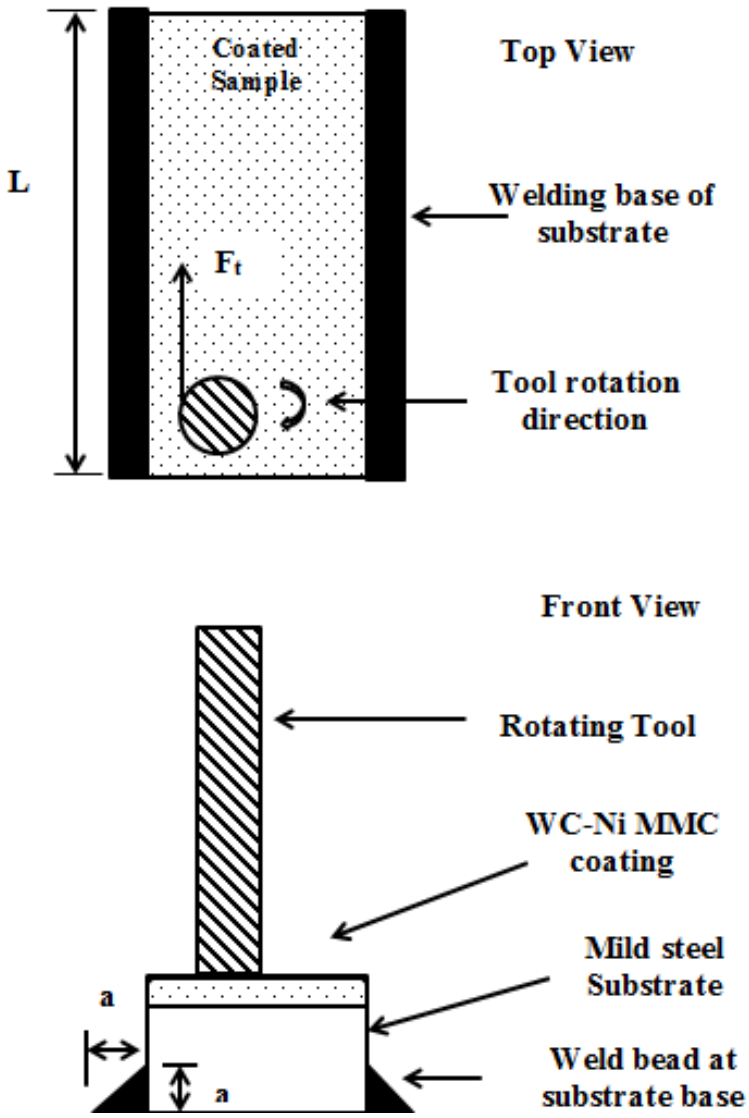

Figure 7.1. Depiction of weld bead at substrate base to provide effective clamping during FSP treatment of WC-Ni MMC coating

Now shear stress acting on each side weld bead (ζ) is given by

$$\zeta = \frac{F_t}{(2 \times 0.707 \times a \times L)} \quad (2)$$

Where,

F_t = Tangential force, N,

L = weld length, m,

a = weld bead width, m,

'2' is taken in base since tangential force is distributed between two welds provided on sides.

Now, tangential force due to rotating tool will induce in shear stress in weld bead.

Thus, $F_t = \mu N$ (3)

Where,

N= Normal force or vertical thrust force on tool, N

μ = coefficient of friction between tool and coating.

Usually normal force used is 1 kN.

As an extreme case, let F_t be 6-7 kN

Substitution of all the values in Eqn. (1), should give value of ζ. This value of ζ should be less than ζ_{max} to avoid fracturing of weld bead from substrate base. Usually, a = 3 mm, so only variable is L or weld length.

So to find least value of weld length (L) [2],

Let $\zeta = ,\zeta_{max.}$

So, $$L = \frac{F_t}{(2 \times 0.707 \times a \times \zeta)}$$

$$L = \frac{6 \times 10^3}{(2 \times 0.707 \times 3 \times 10^{-3} \times 186 \times 10^6)}$$

$L = 7.6\ mm$

Thus, minimum length of weld bead to be provided on each side of the substrate to provide effective clamping is 7.6mm.

References:

1. Mild steel welding wire, TIGSURE Inc., [Online] http://www.weldingwire.org/mild_steel_welding_wire.html, Accessed : 27 Aug. 2013
2. R.S. Khurmi, J. K. Gupta, Machine Design, Eurasia Publishing House (Pvt.) Ltd, India, 2005, 14th edition, pp. 341 – 376

Appendix 3. Maximum heat during FSP heat treatment

The heat generated in work piece during FSP treatment is sometimes responsible for failure of material. The limiting value of temperature during FSP treatment when operating on cold sprayed Nickel samples is as derived below:

Non-dimensional heat input, Q* [1]

$$Q^* = \frac{\sigma_G A_W \omega C_P f}{KU^2} \qquad (1)$$

Where,

$\sigma_{G=}$ Yield stress of nickel at 0.8 times of solidus temperature (T_s), MPa,

A_W = cross-sectional area of the FSP tool, m^2

C_p = Specific heat of the nickel coating, J/kg-ºC,

f = ratio of heat generated at work piece to heat generated in tool,

K = Thermal conductivity of the work piece, W/m-ºC,

ω = rotational speed of tool, rpm

U = Linear velocity of the tool on work piece, m/s

Now, "f" is ratio of heat generated at work piece to heat generated in tool [1]

$$f = \left[\frac{(K\rho C_P)_{Ni}}{(K\rho C_P)_{WC}} \right]^{0.5} \qquad (2)$$

The terms in the numerator are for pure Nickel coating while in denominator are for WC-10 wt. % Co tool. The parameters required for this ratio are as follows:

(a)For Pure Nickel, the properties are [2]:

Specific heat, C_p= 456 J/kg-ºC

Density, ρ= 8890 kg/m^3,

Thermal conductivity, K = 70 W/m-ºC

(b) Properties of pure WC [3, 4]:

C_p= 159.75 J/kg-ºC

ρ = 15800 kg/m^3,

K = 84.02 W/m-ºC

(c) Properties of Pure Co [5]:

C_p= 421 J/kg-ºC

ρ = 8900 kg/m^3,

K = 100 W/m-ºC

Case 1: FSP treatment on pure nickel coating.

Now the tool used for FSP treatment has composition of WC-10 wt.% Co which in vol.% will be WC-16.67 vol. % Co.

<u>Properties of WC-16.67 vol. % Co [6]</u>

Density, $\rho_{WC-Co} = \rho_{WC} \times V_{WC} + \rho_{Co} \times V_{Co}$

ρ_{WC-Co} = 0.8335 × 15800 kg/m^3 + 0.1667 ×8990 kg/m^3

ρ_{WC-Co} =14667.9 kg/m^3

Specific heat [6],

$$\rho_{\text{WC–Co}} \times (C_{\text{p}})_{\text{WC–Co}} = \rho_{\text{WC}} \times V_{\text{WC}} \times (C_{\text{p}})_{\text{WC}} + \rho_{\text{Co}} \times V_{\text{Co}} \times (C_{\text{p}})_{\text{Co}}$$

$\rho_{\text{WC–Co}} C_{\text{WC–Co}}$ = 0.8335 × 15800 kg/m^3 × 159.75 W/m-ºC

+ 0.1667 × 8990 kg/m^3×421 W/m-ºC

$\rho_{\text{WC–Co}} C_{\text{WC–Co}}$ = 2.7347 x 10^6

$C_{\text{WC–Co}}$ = 186.44 J /kg- ºC

Thermal Conductivity [6],

Upper limit: $K_{\text{WC–Co}} = V_{\text{WC}} \times K_{\text{WC}} + V_{\text{Co}} \times K_{\text{Co}}$

$K_{WC–Co}$ = 0.8335 x 82.02 W/m-ºC + .01667 x 100 W/m-ºC

$K_{WC–Co}$ = 85.03 W/m-ºC

Lower limit: $\dfrac{1}{K_{\text{WC–Co}}} = \dfrac{V_{\text{WC}}}{K_{\text{WC}}} + \dfrac{V_{\text{Co}}}{K_{\text{Co}}}$

$$\frac{1}{K_{\text{WC–Co}}} = \frac{0.8335}{82.02\text{W/m-}^{\text{o}}\text{C}} + \frac{0.1667}{100\text{W/m-}^{\text{o}}\text{C}}$$

$K_{\text{WC–Co}}$ = 84.5 W/m-ºC

Table 7.1. Properties of pure nickel and FSP tool

Ni coating	**WC-10 wt.% Co**
C_p= 456 J/kg-ºC	C_p = 186.44 J /kg- ºC
ρ= 8890 kg/m^3,	ρ_c =14667.9 kg/m^3
K = 70 W/m-ºC	Upper limit, K = 85.03 W/m-ºC Lower limit, K = 84.5 W/m-ºC

Substituting values in Eq. (2), we get

$$f = \left[\frac{(70\text{W/m-}^{o}\text{C} \times 8890\text{kg/m}^3 \times 456\text{J/kg-}^{o}\text{C})}{(85.03\text{W/m-}^{o}\text{C} \times 14667.9\text{kg/m}^3 \times 186.4\text{J/kg-}^{o}\text{C})} \right]^{0.5}$$

f = 1.1047 using upper limit of K and

= 1.10815 using lower limit of K

Now solidus temperature (T_s) for pure nickel is 1454ºC (1723K) or 2650ºF.

Now, 0.8 T_s = 1378K ≈1100 ºC.

Yield stress at 0.8 T_s from standard chart is given as [7]

$\sigma_G \approx 1\text{N/m}^2$

Now, non-dimensional heat input (Q*)

$$\text{Q*} = \frac{\sigma_G A_W \omega C_P f}{K v^2}$$

Where,

σ_G = 1N/m^2,

A_w = 1.226 x 10^{-4} m^2,

C_p= 456 J/kg-^{o}C,

K = 70 W/m-^{o}C

f = 1.1047,

ν = 33mm/min. = 0.55 x 10^{-3} m/sec.

Substituting values, we get,

$$Q^* = \frac{1\text{N/m}^2 \times 1.226 \times 10^{-4}\text{m}^2 \times 456\text{J/kg-}^o\text{C} \times 1400 \times 1.1047}{60 \times 70\text{W/m-}^o\text{C} \times (0.55 \times 10^{-3}\text{m/sec.})^2}$$

$Q^* = 68.054 \times 10^3$

Now, non-dimensional peak temperature (T*) is defined as [1]

$T^* = 0.151 \log_{10}(Q^*) + 0.097$ for $4 \times 10^2 < Q^* < 3.7 \times 10^5$ (3)

Substitution of values,

$T^* = 0.151 \log_{10}(68.054 \times 10^3) + 0.097$

$T^* = 0.83$

$$\text{Also, } T^* = \frac{T_P - T_A}{T_S - T_A} \quad (4)$$

Where, T_P = Peak temperature, K

T_A = ambient temperature, K,

Ts = Solidus temperature, K

Substituting values,

$$0.83 = \frac{T_P - 298K}{1723K - 298K}$$

T_P = 1476 K = 1203ºC.

Now, this is the limiting peak temperature which pure nickel coating can reach.

Relation between peak temperature and rotational speed [8]

$$\frac{T_P}{T_M} = K\left(\frac{\omega^2}{\upsilon \times 10^4}\right)^{\alpha} \quad (5)$$

Where,

T_P = Peak temperature reached during FSP operation, K

T_M = Melting point of work piece material, K

ω = rotational speed of tool, rpm

υ = travel velocity of tool on work piece, m/sec.

α, K = Constants.

Melting point of Nickel is 1454 ºC while ratio, T_P/T_M is 0.6 to 0.9.

α Varies between 0.04 - 0.06 while K varies between 0.65 - 0.75 [9].

Now, if travel velocity is kept constant while ω varied, it is clear that higher the ω, higher is T_P. So higher ω will result in higher torque and hence higher viscosity currents in the material during FSP treatment which will make coating unstable and coating will spall off due to this [10].

Now, value of T_p from Eq. (9) should not cross value given by Eq. (10). In fact, it should be as less as possible, usually $0.6T_M$. The ω value of 900- 1400 RPM resulted in melting of Inconel rods used as tool. So, it means, the temperature rise is really significant. So for pure nickel coatings, we should start with low rotational speed like 200 to 400 rpm and progressively increase till the coating will spall off. The value of ω just before coating spall off will be the final reading.

Case 2: FSP treatment to cold-sprayed and HVOF-sprayed WC-Ni MMC coating

Properties of WC-12wt.% Co:

ρ = 14213 kg/m^3

The WC-Co in volume percent is given by WC - 19.303 vol. % Co

$$\rho_{\text{WC–12Co}}(C_{\text{p}})_{\text{WC–12Co}} = V_{\text{WC}} \times (C_{\text{p}})_{\text{WC}} + V_{\text{Co}} \times \rho_{\text{Co}} \times (C_{\text{p}})_{\text{Co}}$$

$$\rho_c C_p = 0.807 \times 15800 \times 159.75 + 0.19303 \times 8900 \times 421$$

$$C_{\text{p}} = 194.2 \text{ J /kg- ºC}$$

Linear rule of mixture:

$$K_{\text{WC–Co}} = V_{\text{WC}} \times K_{\text{WC}} + V_{\text{Co}} \times K_{\text{Co}}$$

$$K_{\text{c}} = 0.807 \times 84.2\text{W/m-º C} + 0.19303 \times 100\text{W/m-º C}$$

$$K_{\text{c}} = 87.254 \text{ W/m-ºC}$$

Inverse rule of mixture [6]:

$$\frac{1}{K_{\text{WC–Co}}} = \frac{V_{\text{WC}}}{K_{\text{WC}}} + \frac{V_{\text{Co}}}{K_{\text{Co}}}$$

$$\frac{1}{K_{\text{C}}} = \frac{0.807}{84.2\text{W/m-º C}} + \frac{0.19303}{100\text{W/m-º C}}$$

$$K_{\text{C}} = 86.88 \text{ W/m-ºC}$$

Now, to find properties of WC-Ni MMC coating fabricated using cold spraying technique, we take volume content of both the constituents in composite. The WC-Ni content in the MMC coating is WC – 48 vol % Ni

Thus density of WC- 48 vol. % Ni coating is:

$$(\rho_{\text{WC–Ni}})_{\text{CS}} = \rho_{\text{WC}} \times V_{\text{WC}} + \rho_{\text{Ni}} \times V_{\text{Ni}}$$

$$= 14213\text{kg/m}^3 \times 0.52 + 8890\text{kg/m}^3 \times 0.48$$

$$(\rho_{WC-Ni})_{CS} = 11657.9\,\text{kg/m}^3$$

$$\frac{1}{(\rho_{\text{WC–Ni}})_{\text{CS}}} = \frac{V_{\text{WC}}}{\rho_{\text{WC}}} + \frac{V_{\text{Ni}}}{\rho_{\text{Ni}}}$$

$$= \frac{0.52}{14213\text{kg/m}^3} + \frac{0.48}{8890\text{kg/m}^3}$$

$$(\rho_{\text{WC–Ni}})_{\text{CS}} = 11041.2\text{kg/m}^3$$

Specific heat is given by:

$$\rho_{\text{WC–Ni}} \times (C_{\text{p}})_{\text{WC–Ni}} = \rho_{\text{WC}} \times V_{\text{WC}} \times (C_{\text{p}})_{\text{WC}} + \rho_{\text{Ni}} \times V_{\text{Ni}} \times (C_{\text{p}})_{\text{Ni}}$$

$$= 14213\text{kg/m}^3 \times 0.52 \times 194.2\text{W/m-}^{\text{o}}\text{C} + 8890\text{kg/m}^3 \times 0\ .48 \times 456\text{W/m-}^{\text{o}}\text{C}$$

Substituting value of $(\rho_{\text{WC–Ni}}) = 11657.9\text{kg/m}^3$,

$$(C_{\text{p}})_{\text{WC–Ni}} = 290\ \text{J /kg- }^{\text{o}}\text{C}$$

and

$$(C_{\text{p}})_{\text{WC–Ni}} = 306.23\ \text{J /kg- }^{\text{o}}\text{C}$$

$$(K_{\text{WC–Ni}})_{\text{CS}} = V_{\text{WC}} \times K_{\text{WC}} + V_{\text{Ni}} \times K_{\text{Ni}}$$

$$= 0.52 \times 86.88\text{W/m-}^{\text{o}}\text{C} + 0.48 \times 70\text{W/m-}^{\text{o}}\text{C}$$

$$(K_{WC-Ni})_{CS} = 78.78\text{W/m} - {}^{\circ}\text{C}$$

$$\frac{1}{(K_{\text{WC–Ni}})_{\text{CS}}} = \frac{V_{\text{WC}}}{K_{\text{WC}}} + \frac{V_{\text{Ni}}}{K_{\text{Ni}}}$$

$$= \frac{0.52}{86.88\text{W/m-}^{\text{o}}\text{C}} + \frac{0.48}{70\text{W/m-}^{\text{o}}\text{C}}$$

$(K_{\text{WC–Ni}})_{\text{CS}} = 77.86\text{W/m} - ^{\circ}\text{C}$

Similarly for HVOF-sprayed WC- Ni MMC coating, the coating composition is WC – 19 vol. % Ni

Density:

Linear rule of mixture [6]

$$(\rho_{\text{WC–Ni}})_{\text{HVOF}} = \rho_{\text{WC}} \times V_{\text{WC}} + \rho_{\text{Ni}} \times V_{\text{Ni}}$$

$$= 14213\text{kg/m}^3 \times 0.81 + 8890\text{kg/m}^3 \times 0.19$$

$$(\rho_{\text{WC–Ni}})_{\text{HVOF}} = 13201.63\text{kg/m}^3$$

Inverse rule of mixture

$$\frac{1}{(\rho_{\text{WC–Ni}})_{\text{HVOF}}} = \frac{V_{\text{WC}}}{\rho_{\text{WC}}} + \frac{V_{\text{Ni}}}{\rho_{\text{Ni}}}$$

$$= \frac{0.81}{14213\text{kg/m}^3} + \frac{0.19}{8890\text{kg/m}^3}$$

$$(\rho_{\text{WC–Ni}})_{\text{HVOF}} = 12761.2\text{kg/m}^3$$

Specific heat:

$$\rho_{\text{WC–Ni}} \times (C_{\text{p}})_{\text{WC–Ni}} = \rho_{\text{WC}} \times V_{\text{WC}} \times (C_{\text{p}})_{\text{WC}} + \rho_{\text{Ni}} \times V_{\text{Ni}} \times (C_{\text{p}})_{\text{Ni}}$$

$$= 14213\text{kg/m}^3 \times 0.81 \times 194.2\text{J/kg-}^{\circ}\text{C} + 8890\text{kg/m}^3 \times 0.19 \times 456\text{J/kg-}^{\circ}\text{C}$$

Substituting value of $(\rho_{\text{WC–Ni}}) = 13201.63\text{kg/m}^3$,

$(C_{\text{p}})_{\text{WC–Ni}} = 227.7$ J /Kg- $^{\circ}$C

and

$(C_p)_{WC-Ni} = 235.55$ J /Kg- ºC

Specific heat:

$$(K_{WC-Ni})_{HVOF} = V_{WC} \times K_{WC} + V_{Ni} \times K_{Ni}$$

$$= 0.81 \times 86.88 \text{W/m-}^{o}\text{C} + 0.19 \times 70 \text{W/m-}^{o}\text{C}$$

$$(K_{WC-Ni})_{HVOF} = 83.67 \text{W/m} - ^{\circ}\text{C}$$

$$\frac{1}{(K_{WC-Ni})_{HVOF}} = \frac{V_{WC}}{K_{WC}} + \frac{V_{Ni}}{K_{Ni}}$$

$$= \frac{0.81}{86.88 \text{W/m-}^{o}\text{C}} + \frac{0.19}{70 \text{W/m-}^{o}\text{C}}$$

$$(K_{WC-Ni})_{HVOF} = 83.07 \text{W/m} - ^{\circ}\text{C}$$

Substituting values in eqn.(8), we get

For HVOF-sprayed WC-Ni MMC

$$f = \left[\frac{(K\rho C_P)_{WC-Ni}}{(K\rho C_P)_{WC}} \right]^{0.5}$$

$$\left[\frac{(83.07 \text{W/m-}^{o}\text{C} \times 13201.63 \text{kg/m}^3 \times 235 \text{J/kg-}^{o}\text{C})}{(85.03 \text{W/m-}^{o}\text{C} \times 14667.9 \text{kg/m}^3 \times 186.44 \text{J/kg-}^{o}\text{C})} \right]^{0.5}$$

= 3.327

$$f = \left[\frac{(83.67 \text{W/m-}^{o}\text{C} \times 12761.2 \text{kg/m}^3 \times 227.7 \text{J/kg-}^{o}\text{C})}{(85.03 \text{W/m-}^{o}\text{C} \times 14667.9 \text{kg/m}^3 \times 186.44 \text{J/kg-}^{o}\text{C})} \right]^{0.5}$$

=3.232

For cold-sprayed WC-Ni MMC

$$\left[\frac{(78.78\text{W/m-}^{o}\text{C}\times 11041.2\text{kg/m}^{3}\times 290\text{J/kg-}^{o}\text{C})}{(85.03\text{W/m-}^{o}\text{C}\times 14667.9\text{kg/m}^{3}\times 186.44\text{J/kg-}^{o}\text{C})}\right]^{0.5}$$

=3.3

$$\left[\frac{(77.86\text{W/m-}^{o}\text{C}\times 11657.9\text{kg/m}^{3}\times 306.23\text{J/kg-}^{o}\text{C})}{(85.03\text{W/m-}^{o}\text{C}\times 14667.9\text{kg/m}^{3}\times 186.44\text{J/kg-}^{o}\text{C})}\right]^{0.5}$$

=3.456

The heat generation factor value is:

$$Q^{*} = \frac{\sigma_{G} A_{W} C_{P} \omega f}{KU^{2}}$$

$$Q^{*} = \frac{1\text{N/m}^{2}\times 1.226\times 10^{-4}\text{m}^{2}\times 235\text{J/Kg-}^{o}\text{C}\times 1400\times 3.327}{60\times 83.07\text{W/m-}^{o}\text{C}\times (0.55\times 10^{-3}\text{m/sec.})^{2}}$$

Q^{*} = 88807.9

$$Q^{*} = \frac{1\text{N/m}^{2}\times 1.226\times 10^{-4}\text{m}^{2}\times 227.7\text{J/Kg-}^{o}\text{C}\times 1400\times 3.232}{60\times 83.67\text{W/m-}^{o}\text{C}\times (0.55\times 10^{-3}\text{m/sec.})^{2}}$$

Q^{*} = 85432.17

$$Q^{*} = \frac{1\text{N/m}^{2}\times 1.226\times 10^{-4}\text{m}^{2}\times 290\text{J/Kg-}^{o}\text{C}\times 1400\times 3.3}{60\times 78.78\text{W/m-}^{o}\text{C}\times (0.55\times 10^{-3}\text{m/sec.})^{2}}$$

Q^{*} = 115560.7

$$Q^{*} = \frac{1\text{N/m}^{2}\times 1.226\times 10^{-4}\text{m}^{2}\times 306.23\text{J/Kg-}^{o}\text{C}\times 1400\times 3.456}{60\times 77.86\text{W/m-}^{o}\text{C}\times (0.55\times 10^{-3}\text{m/sec.})^{2}}$$

Q^{*} = 123470

Substituting value of Q^{*} in Eq. 8 and 9 gives the *T* value for cold-sprayed as well as HVOF-sprayed WC-Ni MMC in range of 2000 – 2100ºC.

References:

1. A. Arora, T. Debroy and H. K. D. H. Bhadeshia, Back of the envelope calculations in friction stir welding-velocities, peak temperature, torque and hardness, Acta Materialia, 2011, 59(5), pp: 2020-2028
2. Nickel Alloys.net [Online] Available: http://www.nickel-alloys.net/commercially_pure_nickel.html, Accessed : 24 August 2013
3. MEMS net, [Online] Available: http://www.memsnet.org/material/tungstencarbidewcbulk/, Accessed : 24 August 2013
4. F. Grønvold, S. Stølen, E. F. Westrum, A. K. Labban, B.Uhrenius, Heat capacity and thermodynamic proeprties of ditungsten carbide,W_2C_1-X from 10 to 1000 K, Thermochimica Acta, 1988, 129, pp. 115-125
5. Technical data for cobalt, Wolfram Research Inc., http://periodictable.com/Elements/027/data.html, Accessed : 26 Aug. 2013
6. A. Mortensen, Concise encyclopedia of composite materials, Elsevier, Dec. 2006, Second Edition, pp. 183-184
7. Nickel, Copy right: Special Metals, http://www.specialmetals.com/documents/Nickel%20200%20&%20201.pdf, Accessed : 24 Aug. 2013
8. T. Saeid, A. Abdollah-zadeh, H. Assadi, F. Malek Ghaini, Effect of friction stir welding speed on the microstructure and mechanical properties of a duplex stainless steel, Materials Science and Engineering A, 2008, 496 (1-2), pg: 262-268
9. Nagarajan Balasubramanian, Friction stir channeling: An innovative technique for Heat exchanger manufacturing, A Doctorate Dissertation, Missouri University of Science and technology, 2008,
10. R. Nandan, G. G. Roy, T. J. Lienert, T. Debroy, Three dimeniosnal heat and material flow during friction stir welding of mild steel, Acta Materialia, 2007, 55, pp. 883-895.